

LIMIT AND SHAKEDOWN ANALYSIS OF PLATES AND SHELLS INCLUDING UNCERTAINTIES

Von der Fakultät für Maschinenbau der
Technischen Universität Chemnitz
genehmigte

Dissertation

zur Erlangung des akademischen Grades
Doktoringenieur
(Dr.-Ing.)

vorgelegt

von MSc. Thanh Ngọc Trần
geboren am 03. Februar 1975
in Nam Dinh, Vietnam

eingereicht am 12. Dezember 2007

Gutachter:

Prof. Dr.-Ing. Reiner Kreißig

Prof. Dr.-Ing. Manfred Staat

Prof. Dr.-Ing. Christos Bisbos

Tag der Verteidigung: 12. März 2008

Trần, Thanh Ngọc

Limit and shakedown analysis of plates and shells including uncertainties

Dissertation an der Fakultät für Maschinenbau der Technischen Universität Chemnitz,
Institut für Mechanik und Thermodynamik, Chemnitz 2008

149 + vii Seiten
55 Abbildungen
28 Tabellen
162 Literaturzitate

Referat

The reliability analysis of plates and shells with respect to plastic collapse or to inadaptation is formulated on the basis of limit and shakedown theorems. The loading, the material strength and the shell thickness are considered as random variables. Based on a direct definition of the limit state function, the nonlinear problems may be efficiently solved by using the First and Second Order Reliability Methods (FORM/SORM). The sensitivity analyses in FORM/SORM can be based on the sensitivities of the deterministic shakedown problem. The problem of the reliability of structural systems is also handled by the application of a special barrier technique which permits to find all the design points corresponding to all the failure modes. The direct plasticity approach reduces considerably the necessary knowledge of uncertain input data, computing costs and the numerical error.

Die Zuverlässigkeitsanalyse von Platten und Schalen in Bezug auf plastischen Kollaps oder Nicht-Anpassung wird mit den Traglast- und Einspielsätzen formuliert. Die Lasten, die Werkstofffestigkeit und die Schalendicke werden als Zufallsvariablen betrachtet. Auf der Grundlage einer direkten Definition der Grenzzustandsfunktion kann die Berechnung der Versagenswahrscheinlichkeit effektiv mit den Zuverlässigkeitsmethoden erster und zweiter Ordnung (FROM/SORM) gelöst werden. Die Sensitivitätsanalysen in FORM/SORM lassen sich auf der Basis der Sensitivitäten des deterministischen Einspielpblems berechnen. Die Schwierigkeiten bei der Ermittlung der Zuverlässigkeit von strukturellen Systemen werden durch Anwendung einer speziellen Barrieremethode behoben, die es erlaubt, alle Auslegungspunkte zu allen Versagensmoden zu finden. Die Anwendung direkter Plastizitätsmethoden führt zu einer beträchtlichen Verringerung der notwendigen Kenntnis der unsicheren Eingangsdaten, des Berechnungsaufwandes und der numerischen Fehler.

Schlagworte:

Limit analysis, shakedown analysis, exact Ilyushin yield surface, nonlinear programming, first order reliability method, second order reliability method, design point

Archivierungsort:

<http://archiv.tu-chemnitz.de/pub/2008/0025>

ACKNOWLEDGEMENTS

This work has been carried out at the Biomechanics Laboratory, Aachen University of Applied Sciences, Campus Jülich. The author gratefully acknowledges the Deutscher Akademischer Austausch Dienst (DAAD) for a research fellowship award under the grant reference A/04/20207.

The author is indebted to Prof. Dr.-Ing. M. Staat who has been the constant source of caring and inspiration for his helpful guidance and encouragement. His commitment and assistance were limitless and this is greatly appreciated.

The author would like to express his deep gratitude to Prof. Dr.-Ing. R. Kreißig for giving him the permission to complete Doctorate of Engineering at the Chemnitz University of Technology and for kindly assistance and supervision.

The author would like to thank Prof. Dr.-Ing. C. Bisbos, Aristotle University of Thessaloniki, Greece for having kindly accepted to review this thesis.

The author is thankful to Dr.-Ing. Vũ Đức Khôi for help and advice, to Ms Wierskowski and Ms Dronia for their programming as part of their diploma theses in some parts of FEM source code. The author's thanks are also extended to Prof. Dr. rer. nat. Dr.-Ing. S. Sponagel and to the other colleagues at the Biomechanics Laboratory for their helpful assistance.

The author is immensely indebted to his father Trần Thanh Xuân and his mother Nguyễn Thị Hòa who have been the source of love and discipline for their inspiration and encouragement throughout the course of his education including this Doctorate.

Last but not least, the author is extremely grateful to his wife Mrs. Nguyễn Thị Thu Hà who has been the source of love, companionship and encouragement, to his daughters My and Ly who have been the source of joy and love.

TABLE OF CONTENTS

INTRODUCTION	1
1. FUNDAMENTALS	3
1.1 Basic concepts of plasticity.....	3
1.1.1 Elastic and rigid perfectly plastic materials	3
1.1.2 Fundamental principles in plasticity	4
1.1.3 Drucker's postulate	6
1.1.4 Yield criteria	7
1.1.5 Plastic dissipation function in local variables.....	8
1.2 Normalized shell quantities	9
1.2.1 Reference quantities.....	9
1.2.2 Stress quantities	9
1.2.3 Strain quantities	10
1.2.4 Stress-Strain relation.....	11
1.3 Exact Ilyushin yield surface.....	12
1.3.1 Derivation	12
1.3.2 Description of the exact Ilyushin yield surface	14
1.3.3 Reparameterization	16
1.3.4 Plastic dissipation function	18
1.3.5 Reformulation	19
2. MATHEMATICAL FORMULATIONS OF LIMIT AND SHAKEDOWN ANALYSIS IN GENERALIZED VARIABLES	21
2.1 Theory of limit analysis	22
2.1.1 Introduction.....	22
2.1.2 General theorems of limit analysis	23
2.2 Theory of shakedown analysis.....	24
2.2.1 Introduction.....	24
2.2.2 Definition of load domain.....	25
2.2.3 Fundamental of shakedown theorems.....	27
2.2.4 Separated shakedown limit	30
2.2.5 Unified shakedown limit.....	33

3. DETERMINISTIC LIMIT AND SHAKEDOWN PROGRAMMING.....	38
3.1 Finite element discretization.....	39
3.2 Kinematic algorithm	41
4. PROBABILISTIC LIMIT AND SHAKEDOWN PROGRAMMING.....	49
4.1 Basic concepts of probability theory	50
4.1.1 Sample space.....	50
4.1.2 Random variables	50
4.1.3 Moments	51
4.2 Reliability analysis.....	53
4.2.1 Failure function and probability	53
4.2.2 First- and Second-Order Reliability Method	55
4.3 Calculation of design point	58
4.4 Sensitivity of the limit state function.....	61
4.4.1 Mathematical sensitivity	62
4.4.2 Definition of the limit state function.....	63
4.4.3 First derivatives of the limit state function	65
4.4.4 Second derivatives of the limit state function.....	66
4.4.5 Special case of probabilistic shakedown analysis.....	70
5. MULTIMODE FAILURE AND THE IMPROVEMENT OF FORM/SORM RESULTS	72
5.1 Multimode failure	73
5.1.1 Bounds for the system probability of failure	73
5.1.2 First-order system reliability analysis.....	74
5.2 Solution technique	76
5.2.1 Basic idea of the method.....	76
5.2.2 Definition of the bulge	77
6. LIMIT AND SHAKEDOWN ANALYSIS OF DETERMINISTIC PROBLEMS	79
6.1 Limit analysis of a cylindrical pipe under complex loading.....	80
6.2 Limit and shakedown analysis of a thin-walled pipe subjected to internal pressure and axial force	82
6.3 Cylindrical shell under internal pressure and temperature change	84
6.4 Pipe-junction subjected to varying internal pressure and temperature	86
6.5 Grooved rectangular plate subjected to varying tension and bending	90
6.6 Square plate with a central circular hole.....	92
6.7 Elbow subjected to bending moment.....	97
6.8 Limit and shakedown analysis of pipe-elbow subjected to complex loads	103
6.9 Nozzle in the knuckle region of a torispherical head.....	109

7. PROBABILISTIC LIMIT AND SHAKEDOWN ANALYSIS OF STRUCTURES	115
7.1 Square plate with a central circular hole.....	115
7.2 Pipe-junction subjected to internal pressure	121
7.3 Limit analysis of cylindrical pipe under complex loading	123
7.4 Folding shell subjected to horizontal and vertical loads.....	129
8. SUMMARY	133
REFERENCES	136
APPENDIX: PROBABILITY DISTRIBUTIONS AND TRANSFORMATION TO THE STANDARD GAUSSIAN SPACE	146
1. Normal distribution.....	147
2. Log-Normal distribution	147
3. Exponential distribution.....	147
4. Uniform distribution	148
5. Gamma distribution	148
6. Weibull Distribution	149
7. Extreme Type I Distribution	149

INTRODUCTION

The present work aims at providing an effective numerical method for the limit and shakedown analysis (LISA) of general shell structures with the help of the finite element method. Both deterministic and probabilistic limit and shakedown analyses are presented. For deterministic problem, three failure modes of structure such as plastic collapse, low cycle fatigue and ratchetting are analysed based upon an upper bound approach. Probabilistic limit and shakedown analysis deals with uncertainties originating from the loads, material strength and thickness of the shell. Based on a direct definition of the limit state function, the calculation of the failure probability may be efficiently solved by using the First and Second Order Reliability Methods (FORM/SORM). Since the deterministic problem is a sub-routine of the probabilistic one, thus, even a small error in the deterministic model can lead to a big error in the reliability analysis because of the sensitivity of the failure probability. To this reason, a yield criterion which is exact for rigid-perfectly plastic material behaviour and is expressed in terms of stress resultants, namely the exact Ilyushin yield surface, will be applied instead of simplified ones (linear or quadratic approximations). The problem of reliability of structural systems (series systems) will also be handled by the application of a special technique which permits to find all the design points corresponding to all the failure modes. Studies show, in this case, that it improves considerably the FORM/SORM results.

The thesis consists of two parts: the theory part (chapters 1-5) and numerical part (chapters 6-7). Chapter 1 introduces some basic concepts of plasticity theory, including the fundamental principles and yield criteria. Based on the Love-Kirchhoff theory, several relations between physical and normalized values for plates and shells are presented. The derivation and description of the exact Ilyushin yield criterion is briefly summarized.

In chapter 2, we present the two fundamental theorems of limit and shakedown analysis, the static and kinematic theorems. Based on the original ones which were proposed by Melan and Koiter, an extension for lower and upper bound theorems in terms of generalized variables are proposed and formulated. A simple approach for the direct calculation of the shakedown limit as the minimum of incremental plasticity limit and alternating plasticity limit is also presented.

In chapter 3, a kinematic approach of limit and shakedown analysis, which is adopted for shell structures is developed (the deterministic LISA). Starting from a finite element discretization, a detailed kinematic algorithm in terms of generalized variables will

be formulated and introduced. A simple technique for overcoming numerical obstacles, such as the non-smooth and singular objective function, is also proposed.

Chapter 4 focuses on presenting a new algorithm of probabilistic limit and shakedown analysis for thin plates and shells, which is based on the kinematical approach. The loads and material strength as well as the thickness of the shell are to be considered as random variables. Many different kinds of distribution of basic variables are taken into consideration and performed with First and Second Order Reliability Methods (FORM/SORM) for calculation of the failure probability of the structure. In order to get the design point, a non-linear optimization was implemented, which is based on the Sequential Quadratic Programming (SQP). Non-linear sensitivity analyses are also performed for computing the Jacobian and the Hessian of the limit state function.

Chapter 5 presents a method to successively find the multiple design points of a component reliability problem, when they exist on the limit state surface. Each design point corresponds with an individual failure mode or mechanism. The FORM approximation is, then applied at each design point followed by a series system reliability analysis leading to improved estimates of the system failure probability.

In chapter 6, we aim at presenting various typical examples of deterministic limit and shakedown analyses to illustrate and validate the theoretical methods. Numerical results are tested against analytical solutions, experiments and several limit loads which have been calculated in literature with different numerical methods using shell or volume elements.

Numerical studies of limit and shakedown analysis for probabilistic problems are introduced in chapter 7. Uncertainties which originate from the loads, the strength of material and the thickness of the shell are all analyzed. For each test case, some existing analytical and numerical solutions found in literature are briefly represented and compared.

Finally chapter 8 contains some main conclusions and future perspectives.

1 FUNDAMENTALS

In the following, some theoretical foundations are stated, which are necessary for the developments in the subsequent chapters. We start with a brief introduction of plasticity theory, including the fundamental principles and yield criteria. Based on the Love-Kirchhoff theory, several relations between physical and normalized values for plates and shells are presented. The derivation and description of the exact Ilyushin yield criterion is summarized, which is closely related to the works of Burgoyne and Brennan [1993b], Seitzberger [2000]. For convenience, we will use only the concept of shells, instead of plates and shells.

1.1 Basic concepts of plasticity

1.1.1 Elastic and rigid perfectly plastic materials

Mechanical behaviour of rate intensities elastic-plastic, non-hardening solid body is idealized by the elastic perfectly plastic model. In this model, the material behaves elastically below the yield stress and will begin to yield if the stress intensity reaches the yield stress. Stresses are not allowed to become higher than this threshold. Furthermore, the elastic deformation can usually be disregarded when compared with the plastic deformation. This is equivalent to the rigid plastic material model. It can be proved that elastic characteristics do not affect the plastic collapse limit state and thus the application of the elastic perfectly plastic material model becomes same to that of the rigid perfectly plastic model for limit analysis.

In the geometrically linear theory the total strain ε_{ij} is assumed to be decomposed additively into an elastic or reversible part ε_{ij}^e and an irreversible part ε_{ij}^p . If some thermal effects occur, a thermal strain term ε_{ij}^θ should be added and thus

$$\varepsilon_{ij} = \varepsilon_{ij}^e + \varepsilon_{ij}^p + \varepsilon_{ij}^\theta. \quad (1.1)$$

The elastic part of the strain obeys Hooke's law, its relationship with stress is linear

$$\varepsilon_{ij}^e = C_{ijkl}^{-1} \sigma_{kl} \quad (1.2)$$

where C_{ijkl} , called the elastic constants, are components of a tensor of rank 4. For an isotropic material, this tensor is expressed in the form below

$$C_{ijkl} = \frac{\nu E}{(1+\nu)(1-2\nu)} \delta_{ij} \delta_{kl} + \frac{E}{2(1+\nu)} (\delta_{ik} \delta_{jl} + \delta_{il} \delta_{jk}) \quad (1.3)$$

where E denotes the Young's modulus and ν the Poisson ratio, $\delta_{\alpha\beta}$ ($\alpha, \beta = i, j, k, l$) the Kronecker delta. The inverse relationship of (1.2) can be written as

$$\sigma_{ij} = 2G\varepsilon_{ij}^e + \frac{2\nu}{(1-2\nu)} G \delta_{ij} \varepsilon_{kk}^e \quad (1.4)$$

where $G = \frac{E}{2(1+\nu)}$ is the shear modulus of elasticity.

The plastic strain rate obeys an associated flow law

$$\dot{\varepsilon}_{ij}^p = \dot{\lambda} \frac{\partial f}{\partial \sigma_{ij}} \quad (1.5)$$

where $\dot{\lambda}$ is a non-negative plastic multiplier and $f = f(\sigma_{ij})$ represents a time-independent yield surface such as

$$f(\sigma_{ij}) < 0 \quad \text{corresponds to elastic behaviour,} \quad (1.6a)$$

$$f(\sigma_{ij}) = 0 \quad \text{corresponds to appearance of plastic deformation,} \quad (1.6b)$$

$$f(\sigma_{ij}) > 0 \quad \text{corresponds to a region inaccessible for the material.} \quad (1.6c)$$

The definition of yield function means that the stress point cannot move outside the yield surface. Plastic flow can occur only when the stress point is on the yield surface and for elastic-perfectly plastic material the additional loading $\dot{\sigma}_{ij}$ can only move along the tangential direction.

1.1.2 Fundamental principles in plasticity

Consider a structure subjected to volume loads \bar{f}_i and surface loads \bar{t}_i . The stresses σ_{ij} are said to be in equilibrium if they satisfy the equations of internal equilibrium

$$\partial_j \sigma_{ij} + \bar{f}_i = 0 \quad \text{in } V \quad (1.7)$$

and the conditions of equilibrium at the surface of the body

$$t_i = n_j \sigma_{ij} = \bar{t}_i \quad \text{on } \partial V_\sigma. \quad (1.8)$$

Any stress field respecting conditions (1.7) and (1.8) is called a *statically admissible* field. Furthermore, if this stress field nowhere violates the yield criterion, $f(\sigma_{ij}) \leq 0$, it is called a *plastically admissible* or *licit* stress field.

The actual flow mechanism composed of the velocities \dot{u}_i and strain rate $\dot{\epsilon}_{ij}$ in the body which satisfy the compatibility and kinematical boundary conditions

$$\dot{\epsilon}_{ij} = \frac{1}{2}(\partial_j \dot{u}_i + \partial_i \dot{u}_j) \quad \text{in } V \quad (1.9)$$

$$\dot{u}_i = \dot{\bar{u}}_i \quad \text{on } \partial V_u. \quad (1.10)$$

Any mechanism $(\dot{u}_i, \dot{\epsilon}_{ij})$ respecting conditions (1.9) and (1.10) is called *kinematically admissible*. Furthermore, if this mechanism furnishes a non negative external power

$$W_E = \int_V \bar{f}_i \dot{u}_i dV + \int_{\partial V_\sigma} \bar{t}_i \dot{u}_i dA \geq 0 \quad (1.11)$$

then it is called a *licit* mechanism. A kinematically admissible strain and displacement field can be defined in a similar manner.

Principle of virtual power

One of the main tools in the mechanics of continua is the principle of virtual power, which states that *for an arbitrary set of infinitesimal virtual velocity variation $\delta \dot{u}_i$ that are kinematically admissible, the necessary and sufficient condition to make the stress field σ_{ij} equilibrium is to satisfy the following equation*

$$\int_V \sigma_{ij} \delta \dot{\epsilon}_{ij} dV = \int_V \bar{f}_i \delta \dot{u}_i dV + \int_{\partial V_\sigma} \bar{t}_i \delta \dot{u}_i dS. \quad (1.12)$$

Principle of complimentary virtual power

For an arbitrary set of infinitesimal virtual variations of the stress tensor $\delta \sigma_{ij}$ that are statically admissible, the necessary and sufficient condition to make the strain rate tensor $\dot{\epsilon}_{ij}$ and velocity vector \dot{u}_i compatible is to satisfy the following equation

$$\int_V \dot{\epsilon}_{ij} \delta \sigma_{ij} dV = \int_{\partial V_u} n_j \delta \sigma_{ij} \dot{\bar{u}}_i dS. \quad (1.13)$$

Equation of virtual power

From the two above principles, one can easily deduce that *for all strain rate tensors $\dot{\epsilon}_{ij}$ and velocity vectors \dot{u}_i that are kinematically admissible, and for all stresses σ_{ij} that are statically admissible we have the following virtual work equation*

$$\int_V \sigma_{ij} \dot{\epsilon}_{ij} dV = \int_V \bar{f}_i \dot{u}_i dV + \int_{\partial V_\sigma} \bar{t}_i \dot{u}_i dS + \int_{\partial V_u} n_j \sigma_{ij} \dot{\bar{u}}_i dS. \quad (1.14)$$

It is well known that the above variational principles are independent of the constitutive equation of the material.

1.1.3 Drucker's postulate

"Over the cycle of application and removal of the set of forces, the new work performed by the external agency on the changes in the displacements it produces is non-negative" [Martin, 1975].

This is expressed mathematically by the following inequality

$$\oint (\sigma_{ij} - \sigma_{ij}^0) d\varepsilon_{ij} \geq 0 \quad (1.15)$$

where \oint is the integral taken over a cycle of applying and removing the added stress set, σ_{ij} is the stress tensor on the yield surface satisfying the yield condition $f(\sigma_{ij}) = 0$, and σ_{ij}^0 is the plastically admissible stress tensor such that $f(\sigma_{ij}^0) \leq 0$. Starting from this postulate, we have the following important consequences [Lubliner, 2005]:

Principle of maximum energy dissipation

$$(\sigma_{ij} - \sigma_{ij}^0) \dot{\varepsilon}_{ij}^p \geq 0, \quad (1.16a)$$

or

$$\dot{\sigma}_{ij} \dot{\varepsilon}_{ij}^p \geq 0, \quad (1.16b)$$

sometimes known simply as Drucker's inequality. It is valid for both work-hardening and perfectly plastic materials.

Normality rule

From (1.16) one can deduce that the plastic strain rates tensor $\dot{\varepsilon}_{ij}^p$ must be normal to the yield surface at a smooth point or lie between adjacent normals at a corner (non-smooth point), see figure 1.1. In the case of having n intersected differentiable yield surfaces at a singular point, (1.5) should be replaced by:

$$\dot{\varepsilon}_{ij}^p = \sum_{k=1}^n \dot{\lambda}_k \frac{\partial f_k}{\partial \sigma_{ij}}. \quad (1.17)$$

Convexity of yield surface

It is clear from figure 1.1 that if there is any σ_{ij}^0 lying on the outside of the tangent, the inequality (1.16a) is violated. In other words, the entire elastic region must lie to one side of the tangent. As a result, the yield surface is convex.

The convexity of the yield surface has a very important role in plasticity. It permits the use of convex programming tools in limit and shakedown analysis. It should be noted that Drucker's postulate is quite independent of the basic laws of thermodynamics. It does not hold if internal structural changes occur or for temperature dependent behaviour [Kalisky, 1985]. Furthermore, the yield surface fails to be convex if there is an interaction between elastic and plastic deformations, i.e. if the elastic properties depend on the plastic deformation [Panagiotopoulos, 1985].

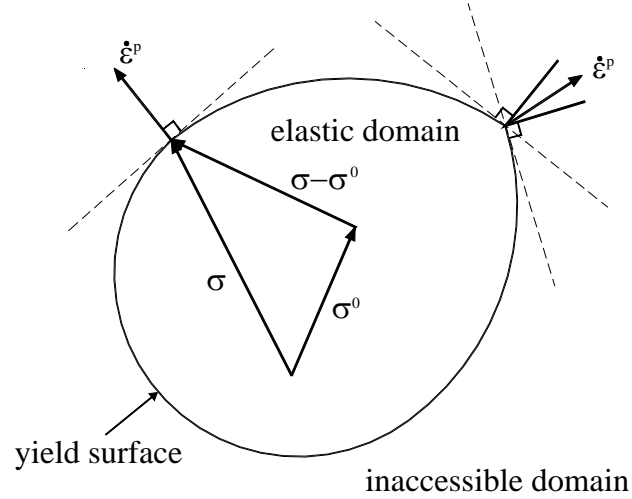


Figure 1.1 Normality rule

1.1.4 Yield criteria

The yield criterion defines the elastic limits of a material under a combined state of stress. The yield function f in stress space may be written with no loss of generality in terms of the stress deviator and the first invariant of stress, that is

$$f(\boldsymbol{\sigma}, \boldsymbol{\xi}) = f(\mathbf{s}, I_1, \boldsymbol{\xi}) \quad (1.18)$$

where $I_1 = \sigma_{kk} = \delta_{ij} \sigma_{ij}$ is the trace of σ_{ij} , $\boldsymbol{\xi}$ are internal variables which are determined experimentally and s_{ij} is the deviator defined as

$$s_{kl} = \sigma_{kl} - \frac{1}{3} I_1 \delta_{kl} = \left(\delta_{ik} \delta_{jl} - \frac{1}{3} \delta_{ij} \delta_{kl} \right) \sigma_{ij}. \quad (1.19)$$

Since the concept of plasticity was first applied to metals, in which the influence of mean stress on yielding is generally negligible [Bridgman, 1923 and 1952], the oldest and most commonly used yield criteria are those that are independent of I_1 . They are therefore formulated with s_{ij} using $J_1 = s_{kk} = 0$. We present here two most well-known yield criteria in plasticity.

Tresca criterion

The Tresca yield criterion is historically the oldest one; it embodies the assumption that plastic deformation occurs when the maximum shear stress over all planes attains a critical value, namely, the value of the current yield stress in shear, denoted k_T . This criterion may be represented by the yield function

$$f(\boldsymbol{\sigma}) = \text{Max}(|\sigma_1 - \sigma_2|, |\sigma_2 - \sigma_3|, |\sigma_3 - \sigma_1|) - 2k_T = 0 \quad (1.20)$$

where $k_T = \frac{\sigma_y}{2}$, σ_y is yield stress. It can also be expressed explicitly in terms of the invariants J_2 and J_3 of the stress deviator tensor as

$$f(J_2, J_3) = 4J_2^3 - 27J_3^2 - 36k_T^2J_2^2 + 96k_T^4J_2 - 64k_T^6 = 0. \quad (1.21)$$

Von Mises criterion

The von Mises criterion is known as the maximum-octahedral-shear-stress or maximum-distortional-energy criterion, which states, that yielding begins when the octahedral shearing stress reaches a critical value k_v such as

$$f(J_2) = J_2 - k_v^2 = 0 \quad (1.22)$$

where $k_v = \frac{\sigma_y}{\sqrt{3}}$. We may also formulate the von Mises yield criterion in the form of principal stresses

$$(\sigma_1 - \sigma_2)^2 + (\sigma_2 - \sigma_3)^2 + (\sigma_3 - \sigma_1)^2 = 6k_v^2. \quad (1.23)$$

The projection of the Tresca yield surface in the $(\sigma_1 - \sigma_3)(\sigma_2 - \sigma_3)$ -plane takes the form of an irregular hexagon, where the von Mises criterion is an ellipse. In the next section the von Mises criterion will be used to derive the so-called exact Ilyushin yield surface for the elastic-plastic analysis of shell-like structures.

1.1.5 Plastic dissipation function in local variables

The plastic dissipation function is defined by

$$D^p = \max(\sigma_{ij}^* \dot{\epsilon}_{ij}^p) = \sigma_{ij} \dot{\epsilon}_{ij}^p \quad (1.24)$$

where σ_{ij}^* is a plastically admissible stress tensor, i.e. satisfying $f(\sigma_{ij}^*) \leq 0$, σ_{ij} is the stress tensor satisfying yield condition $f(\sigma_{ij}) = 0$. The first equality of (1.24) is the definition, while the second one is due to the Drucker stability postulate: $(\sigma_{ij} - \sigma_{ij}^*) \dot{\epsilon}_{ij}^p \geq 0$. The plastic dissipation for the Mises criterion and associated flow rule is given by [Lubliner, 2005]

$$D^p(\dot{\varepsilon}_{ij}^p) = k_v \sqrt{2\dot{\varepsilon}_{ij}^p \dot{\varepsilon}_{ij}^p}. \quad (1.25)$$

1.2 Normalized shell quantities

1.2.1 Reference quantities

The representation of the exact Ilyushin yield surface and the description of its applications for the limit and shakedown analysis of shell structures are given in terms of normalized generalized stresses and strains. The membrane forces and bending moments are normalized with respect to the plastic limit loads in uniaxial tension and bending, respectively

$$N_0 = \sigma_y h, \quad M_0 = \sigma_y \frac{h^2}{4} \quad (1.26)$$

where σ_y and h are yield stress and shell thickness, respectively. Physical strain values are referred to the reference strain ε_0 . A convenient measure for ε_0 is given by

$$\varepsilon_0 = \sigma_y \frac{(1 - \nu^2)}{E}. \quad (1.27)$$

ε_0 corresponds to the elastic strain of an uniaxially stretched plate at the yield stress σ_y . For the sake of simplicity, the reference “curvature” κ_0 is defined as follows

$$\kappa_0 = \frac{4\varepsilon_0}{h}. \quad (1.28)$$

so that $N_0 \varepsilon_0 = M_0 \kappa_0$, [Burgoyne and Brennan 1993b], [Seitzberger, 2000]. This definition does not represent a kinematic relation.

A dimensionless thickness coordinate \bar{z} is used for through-thickness integrations. The relation between \bar{z} and the thickness coordinate s_3 is as follows

$$\bar{z} = \frac{s_3}{h}. \quad (1.29)$$

1.2.2 Stress quantities

Physical and normalized stress vectors for a state of plane stress are given by, respectively

$$\boldsymbol{\sigma} = \begin{pmatrix} \sigma_{11} \\ \sigma_{22} \\ \sigma_{12} \end{pmatrix} \quad \text{and} \quad \bar{\boldsymbol{\sigma}} = \frac{1}{\sigma_y} \begin{pmatrix} \sigma_{11} \\ \sigma_{22} \\ \sigma_{12} \end{pmatrix}. \quad (1.30)$$

From these, the normalized membrane force and bending moment vectors \mathbf{n} and \mathbf{m} can be obtained as follows

$$\begin{aligned}\mathbf{n} &= \frac{1}{N_0} \begin{pmatrix} N_{11} \\ N_{22} \\ N_{12} \end{pmatrix} = \frac{1}{N_0} \int_{-h/2}^{h/2} \boldsymbol{\sigma} ds_3 = \frac{1}{\sigma_y h} \int_{-1/2}^{1/2} \boldsymbol{\sigma} h d\bar{z} = \int_{-1/2}^{1/2} \bar{\boldsymbol{\sigma}} d\bar{z} \\ \mathbf{m} &= \frac{1}{M_0} \begin{pmatrix} M_{11} \\ M_{22} \\ M_{12} \end{pmatrix} = \frac{1}{M_0} \int_{-h/2}^{h/2} \boldsymbol{\sigma} s_3 ds_3 = \frac{4}{\sigma_y h^2} \int_{-1/2}^{1/2} \boldsymbol{\sigma} h^2 \bar{z} d\bar{z} = 4 \int_{-1/2}^{1/2} \bar{\boldsymbol{\sigma}} \bar{z} d\bar{z}\end{aligned}\quad (1.31)$$

where the terms $N_{\alpha\beta}$ and $M_{\alpha\beta}$, $(\alpha, \beta \in \{1, 2\})$ are the physical membrane force and bending moment components of the shell, respectively.

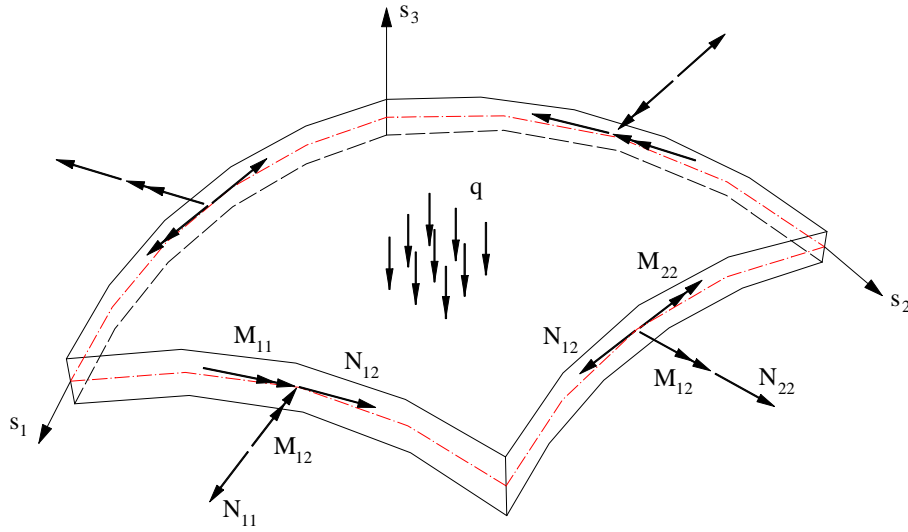


Figure 1.2 Static shell quantities

1.2.3 Strain quantities

The physical strain and curvature vectors

$$\boldsymbol{\varepsilon} = \begin{pmatrix} \varepsilon_{11} \\ \varepsilon_{22} \\ 2\varepsilon_{12} \end{pmatrix}, \quad \boldsymbol{\kappa} = \begin{pmatrix} \kappa_{11} \\ \kappa_{22} \\ 2\kappa_{12} \end{pmatrix} \quad (1.32)$$

are normalized with respect to the ε_0 and κ_0 , which gives

$$\mathbf{e} = \frac{1}{\varepsilon_0} \begin{pmatrix} \varepsilon_{11} \\ \varepsilon_{22} \\ 2\varepsilon_{12} \end{pmatrix}, \quad \mathbf{k} = \frac{1}{\kappa_0} \begin{pmatrix} \kappa_{11} \\ \kappa_{22} \\ 2\kappa_{12} \end{pmatrix}. \quad (1.33)$$

The Love-Kirchhoff assumptions state that the normals (i.e. the lines perpendicular to the shell's mid-plane) remain straight, unstretched and normal (i.e. they always make a

right angle to the mid-plane) after loading. These mean that the transversal shear strains in the thickness coordinate s_3 are negligible which is only valid for thin shells with small displacement u_3 ($u_3 \ll h$). Based on the Love-Kirchhoff hypothesis the physical strain vector can be written in the standard form as follows

$$\boldsymbol{\varepsilon}(s_3) = \bar{\boldsymbol{\varepsilon}} + s_3 \boldsymbol{\kappa} \quad (1.34)$$

where $\bar{\boldsymbol{\varepsilon}}$ and $\boldsymbol{\kappa}$ are physical mid-plane strain and curvature vectors ($s_3 = 0$). The relation between them and the displacements delivers

$$\begin{aligned} \bar{\varepsilon}_{11} &= \frac{\partial u_1}{\partial s_1}, \quad \bar{\varepsilon}_{22} = \frac{\partial u_2}{\partial s_2}, \quad 2\bar{\varepsilon}_{12} = \frac{\partial u_2}{\partial s_1} + \frac{\partial u_1}{\partial s_2} \\ \kappa_{11} &= \frac{\partial \theta_2}{\partial s_1}, \quad \kappa_{22} = -\frac{\partial \theta_1}{\partial s_2}, \quad 2\kappa_{12} = \frac{\partial \theta_2}{\partial s_2} - \frac{\partial \theta_1}{\partial s_1} \end{aligned} \quad (1.35)$$

with u_α, θ_α ($\alpha \in \{1,2\}$) being translations and rotations of the midplane, respectively. By the introduction of \bar{z} and ε_0 , (1.34) becomes

$$\frac{1}{\varepsilon_0} \boldsymbol{\varepsilon} = \frac{1}{\varepsilon_0} \bar{\boldsymbol{\varepsilon}} + \bar{z} \frac{4}{\kappa_0} \boldsymbol{\kappa}. \quad (1.36)$$

By using of (1.28), the Kirchhoff hypothesis may be written in normalized form as

$$\mathbf{e}(\bar{z}) = \bar{\mathbf{e}} + 4\bar{z}\mathbf{k}. \quad (1.37)$$

1.2.4 Stress-Strain relation

As will be shown in the subsequent chapters, it is convenient to group both the strain vectors and the curvature vectors as well as the section force and moment vectors into “engineering” vectors, as follows

$$\tilde{\boldsymbol{\varepsilon}} = \begin{pmatrix} \bar{\mathbf{e}} \\ \mathbf{k} \end{pmatrix}, \quad \tilde{\boldsymbol{\sigma}} = \begin{pmatrix} \mathbf{n} \\ \mathbf{m} \end{pmatrix}. \quad (1.38)$$

For an elasto-plastic material behaviour, the tangential stress-strain relations for a Kirchhoff shell may be written as

$$d\tilde{\boldsymbol{\sigma}} = \begin{pmatrix} d\mathbf{n} \\ d\mathbf{m} \end{pmatrix} = \begin{pmatrix} \mathbf{C} & \mathbf{B} \\ \mathbf{B} & \mathbf{D} \end{pmatrix} \begin{pmatrix} d\bar{\mathbf{e}} \\ d\mathbf{k} \end{pmatrix} = \begin{pmatrix} \mathbf{C} & \mathbf{B} \\ \mathbf{B} & \mathbf{D} \end{pmatrix} d\tilde{\boldsymbol{\varepsilon}} \quad (1.39)$$

where $\mathbf{B}, \mathbf{C}, \mathbf{D}$ are submatrices of the physical tangential stiffness matrix. For purely elastic material behaviour we have

$$\mathbf{B} = 0, \quad \mathbf{C} = \begin{pmatrix} 1 & \nu & 0 \\ \nu & 1 & 0 \\ 0 & 0 & \frac{1-\nu}{2} \end{pmatrix}, \quad \mathbf{D} = \frac{4}{3} \mathbf{C}. \quad (1.40)$$

1.3 Exact Ilyushin yield surface

In order to calculate the maximum collapse load of a shell, a criterion is needed to assess when the shell reaches a situation where the behaviour is governed by plasticity. Two approaches have been identified. It is possible to work either in terms of stresses (Moxham [1971], Little [1977]) which vary through the thickness, in which case a yield criterion such as the von Mises criterion is used, or in terms of stress resultants (Crisfield [1973], Frieze [1975]), when a more complex fully plasticity yield surface is needed. When dealing with stress resultants, it is of course important to identify a yield surface, which marks the limiting values of the stress resultants, beyond which the shell may not be loaded. In 1948 Ilyushin published the derivation of a stress resultant yield surface describing the case where a cross-section of a shell is fully plastified and thus reaches its load capacity. This yield surface, however, has not been used because the parametric form in which it was described by Ilyushin was not amenable to calculation. Some approximations have been used, e.g. a linear approximation proposed by Ilyushin himself, the Ivanov yield surface. A reparameterization of the exact Ilyushin yield surface for thin shells which produces a simpler (though still exact) form was presented by Burgoyne and Brennan [1993b]. Their work opens the way for the practical use of the exact Ilyushin yield surface in structural calculations.

1.3.1 Derivation of the exact Ilyushin yield surface

The derivation of the exact Ilyushin yield surface is based on the following assumptions

- perfectly plastic isotropic material behaviour obeying the von Mises yield criterion,
- validity of the normality rule for the plastic deformations,
- plane stress conditions in each material point,
- validity of the Kirchhoff hypothesis for both total and plastic strains.

At the limit state, each material point through the thickness has a plastic material behaviour. Thus both, the von Mises yield condition and the normality rule, are valid

$$f(\bar{\boldsymbol{\sigma}}) = \bar{\boldsymbol{\sigma}}^T \mathbf{P} \bar{\boldsymbol{\sigma}} - 1 = 0, \quad \mathbf{P} = \begin{pmatrix} 1 & -1/2 & 0 \\ -1/2 & 1 & 0 \\ 0 & 0 & 3 \end{pmatrix} \quad (1.41)$$

$$d\mathbf{e}^p = d\xi \frac{\partial f}{\partial \bar{\boldsymbol{\sigma}}} = 2d\xi \mathbf{P} \bar{\boldsymbol{\sigma}}. \quad (1.42)$$

From Eqs. (1.41) and (1.42) $\bar{\sigma}$ and $d\xi$ can be expressed as functions of $d\mathbf{e}^p$

$$\bar{\sigma}(d\mathbf{e}^p) = \frac{1}{2d\xi(d\mathbf{e}^p)} \mathbf{P}^{-1} d\mathbf{e}^p \quad (1.43)$$

$$d\xi(d\mathbf{e}^p) = \sqrt{\frac{1}{4} (d\mathbf{e}^p)^T \mathbf{P}^{-1} d\mathbf{e}^p} . \quad (1.44)$$

It is assumed that the plastic strain increment resultants obey the Kirchhoff hypothesis. From (1.37) we have

$$d\mathbf{e}^p(\bar{z}) = d\bar{\mathbf{e}}^p + 4\bar{z} d\mathbf{k}^p . \quad (1.45)$$

Substituting (1.45) into (1.44), which gives the consistency parameter

$$d\xi = \frac{1}{\sqrt{3}} \sqrt{P_\varepsilon + 2P_{\varepsilon\kappa}\bar{z} + P_\kappa\bar{z}^2} \quad (1.46)$$

with the incremental plastic strain resultant intensities

$$\begin{aligned} P_\varepsilon &= \frac{3}{4} (d\bar{\mathbf{e}}^p)^T \mathbf{P}^{-1} d\bar{\mathbf{e}}^p = \frac{3}{4} (d\tilde{\mathbf{e}}^p)^T \mathbf{P}_1 d\tilde{\mathbf{e}}^p \quad (\geq 0) \\ P_{\varepsilon\kappa} &= 3 (d\bar{\mathbf{e}}^p)^T \mathbf{P}^{-1} d\mathbf{k}^p = 3 (d\tilde{\mathbf{e}}^p)^T \mathbf{P}_2 d\tilde{\mathbf{e}}^p \\ P_\kappa &= 12 (d\mathbf{k}^p)^T \mathbf{P}^{-1} d\mathbf{k}^p = 12 (d\tilde{\mathbf{e}}^p)^T \mathbf{P}_3 d\tilde{\mathbf{e}}^p \quad (\geq 0) \end{aligned} \quad (1.47)$$

where

$$\mathbf{P}_1 = \begin{pmatrix} \mathbf{P}^{-1} & \mathbf{0} \\ \mathbf{0} & \mathbf{0} \end{pmatrix}, \quad \mathbf{P}_2 = \begin{pmatrix} \mathbf{0} & \mathbf{P}^{-1}/2 \\ \mathbf{P}^{-1}/2 & \mathbf{0} \end{pmatrix}, \quad \mathbf{P}_3 = \begin{pmatrix} \mathbf{0} & \mathbf{0} \\ \mathbf{0} & \mathbf{P}^{-1} \end{pmatrix} . \quad (1.48)$$

These incremental plastic strain resultant intensities are subject to the condition (by the Schwarz inequality)

$$P_\varepsilon P_\kappa \geq P_{\varepsilon\kappa}^2 \quad (1.49)$$

Substitution of Eqs. (1.45) and (1.46) in Eq. (1.43) gives

$$\bar{\sigma} = \frac{\sqrt{3}}{2} \frac{1}{\sqrt{P_\varepsilon + 2P_{\varepsilon\kappa}\bar{z} + P_\kappa\bar{z}^2}} \mathbf{P}^{-1} (d\bar{\mathbf{e}}^p + 4\bar{z} d\mathbf{k}^p) . \quad (1.50)$$

From Eqs. (1.31) and (1.50), the stress resultants may finally be written as

$$\tilde{\boldsymbol{\sigma}} = \begin{pmatrix} \mathbf{n} \\ \mathbf{m} \end{pmatrix} = \frac{3}{2} \begin{pmatrix} J_0 \mathbf{P}^{-1} & 4J_1 \mathbf{P}^{-1} \\ 4J_1 \mathbf{P}^{-1} & 16J_2 \mathbf{P}^{-1} \end{pmatrix} \begin{pmatrix} d\bar{\mathbf{e}}^p \\ d\mathbf{k}^p \end{pmatrix} = \frac{3}{2} \begin{pmatrix} J_0 \mathbf{P}^{-1} & 4J_1 \mathbf{P}^{-1} \\ 4J_1 \mathbf{P}^{-1} & 16J_2 \mathbf{P}^{-1} \end{pmatrix} d\tilde{\mathbf{e}}^p \quad (1.51)$$

where the integrals J_i (not to confuse with the invariants of the deviator) can be calculated as follows

$$J_i = \frac{1}{\sqrt{3}} \int_{-1/2}^{1/2} \frac{\bar{z}^i}{\sqrt{P_\varepsilon + 2P_{\varepsilon\kappa}\bar{z} + P_\kappa\bar{z}^2}} d\bar{z}. \quad (1.52)$$

Equation (1.51) can be regarded as a six-dimensional stress resultant yield surface for the limit that the shell is wholly plastic and thus in each point over the thickness the von Mises yield criterion and the normality rule are satisfied. If the direction of the plastic strain increment resultants is given, the stress resultants can be obtained from Eq. (1.51), provided the integrals J_i can be evaluated numerically.

1.3.2 Description of the exact Ilyushin yield surface

Corresponding to the quadratic strain resultant intensities, quadratic stress resultant intensities can also be defined

$$\begin{aligned} Q_t &= \mathbf{n}^T \mathbf{P} \mathbf{n} \quad (\geq 0) \\ Q_{tm} &= \mathbf{n}^T \mathbf{P} \mathbf{m} \\ Q_m &= \mathbf{m}^T \mathbf{P} \mathbf{m} \quad (\geq 0) \end{aligned} \quad (1.53)$$

From these, the surface (1.51) can be reduced to a surface in the three-dimensional Q-space as follows

$$\begin{pmatrix} Q_t \\ Q_{tm}/4 \\ Q_m/16 \end{pmatrix} = 3 \begin{pmatrix} J_0^2 & J_0 J_1 & J_1^2 \\ J_0 J_1 & (J_0 J_2 + J_1^2)/2 & J_1 J_2 \\ J_1^2 & J_1 J_2 & J_2^2 \end{pmatrix} \begin{pmatrix} P_\varepsilon \\ 2P_{\varepsilon\kappa} \\ P_\kappa \end{pmatrix}. \quad (1.54)$$

The surface is bounded by the condition that

$$Q_t Q_m \geq Q_{tm}^2 \quad (1.55)$$

which corresponds to $P_\varepsilon P_\kappa \geq P_{\varepsilon\kappa}^2$. Equation (1.54) describes a surface, which can be represented in parameter form as a function of two independent parameters. An implicit form of Eq. (1.54), i.e. $F = F(Q_t, Q_{tm}, Q_m) = 0$, however, can not be obtained. Ilyushin [1948] represented the surface in parameterized form, by introducing the two following parameters

$$\begin{aligned} \zeta &= \left(\frac{P_\varepsilon - P_{\varepsilon\kappa} + P_\kappa/4}{P_\varepsilon + P_{\varepsilon\kappa} + P_\kappa/4} \right)^{1/2}, \\ \mu &= \left(\frac{P_\varepsilon P_\kappa - P_{\varepsilon\kappa}^2}{P_\kappa (P_\varepsilon + P_{\varepsilon\kappa} + P_\kappa/4)} \right)^{1/2}. \end{aligned} \quad (1.56)$$

The resulting equations of the exact Ilyushin yield surface are

$$\begin{aligned}
Q_t &= \frac{1}{\Delta_1^2} (\mu^2 \psi^2 + \varphi^2) \\
Q_m &= \frac{2}{\Delta_1^3} (\mu^2 \Delta \psi^2 + \Delta \varphi^2 + \mu^2 \varphi \psi + \varphi \chi) \\
Q_m &= \frac{4}{\Delta_1^4} (\mu^2 \psi^2 (\mu^2 + \Delta^2) + \varphi^2 (4\mu^2 + \Delta^2) + 2\mu^2 \Delta \varphi \psi - 2\mu^2 \psi \chi + 2\Delta \varphi \chi + \chi^2)
\end{aligned} \tag{1.57}$$

where

$$\begin{aligned}
\varphi &= \zeta - 1 \\
\psi &= \left| \ln \frac{(1 + \sqrt{1 - \mu^2})}{\mu} \pm \ln \frac{(\zeta + \sqrt{\zeta^2 - \mu^2})}{\mu} \right| \\
\chi &= \left| \sqrt{1 - \mu^2} \pm \zeta \sqrt{\zeta^2 - \mu^2} \right| \\
\Delta_1 &= \sqrt{1 - \mu^2} \pm \sqrt{\zeta^2 - \mu^2} \\
\Delta &= \frac{1 - \zeta^2}{\Delta_1}
\end{aligned} \tag{1.58}$$

subject to the conditions

$$0 \leq \mu \leq 1, \quad \mu \leq \zeta \leq 1. \tag{1.59}$$

The boundary is given by $\mu = 0$. Ilyushin's original parameterization makes it necessary to divide the surface into four regions, known as the “in-plane dominant” and “bending dominant” regions, which are governed by different equations (due to the alternative signs). Since the lines of constant ζ and μ are virtually parallel in many cases and, a numerical algorithm based on these parameters will be ill-conditioned and numerically unstable [Burgoyne and Brennan, 1993b].

In his original paper Ilyushin proposed a linear approximation to his exact surface, which is usually referred to as Ilyushin yield surface

$$F_1 = Q_t + \frac{1}{\sqrt{3}} |Q_m| + Q_m = 1. \tag{1.60}$$

This crude approximation consists of two planes in the Q-space. It introduces a discontinuity at the line $Q_m = 0$. Figure 1.3 shows a graphical representation of the exact and the linear approximation of the yield surface in the Q-space. As can be seen, the surface is symmetric with respect to the $Q_t - Q_m$ plane. Thus, it can also be plotted in two-dimensional form as Q_m over $Q_t - Q_m$ without loss of clarity [Burgoyne and Brennan, 1993b], see figure 1.3.

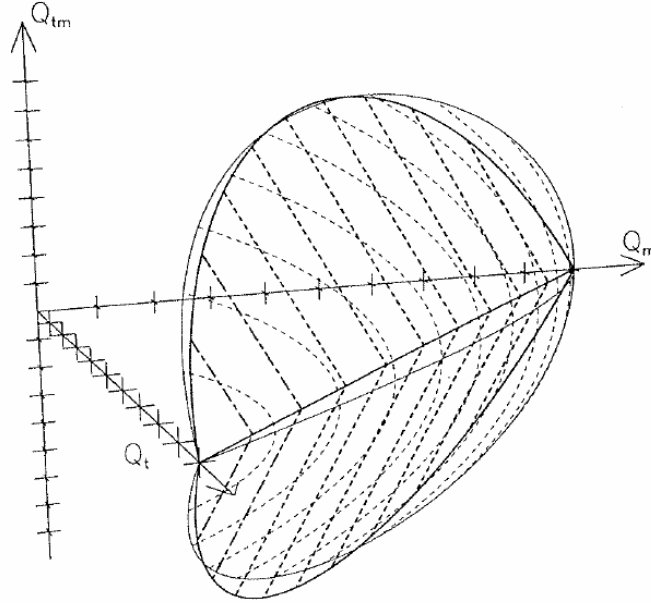


Figure 1.3 Exact and linear approximation of Ilyushin yield surfaces (from Burgoyne and Brennan, 1993b)

Ivanov [1967] proposed a quadratic approximation of the exact Ilyushin yield surface

$$F_2 = Q_t + \frac{Q_m}{2} + \sqrt{Q_m^2/4 + Q_{tm}^2} - \frac{1}{4} \left(\frac{Q_t Q_m - Q_{tm}^2}{Q_t + 0.48 Q_m} \right) = 1. \quad (1.61)$$

The Ivanov yield surface overcomes many of the difficulties associated with the approximate Ilyushin yield surface, it has no discontinuities in slope except one at $Q_t = 1$, where the exact surface also has a slope discontinuity, and always lies within 1% of the exact Ilyushin yield surface.

Further suggestions of approximate full plasticity yield surfaces, partly including the effect of transverse shear as well as hardening effects, can be found e.g. in [Robinson, 1971]. According to Robinson, the maximum error of the linear approximation is 6% on the safe side and 3,5% on the unsafe side. However, the error can increase up to approximately 10% according to [Preiss, 2000]. In structural reliability analyses such errors in the deterministic model are not acceptable because of the sensitivity of the failure probability.

1.3.3 Reparameterization

In order to avoid the difficulties arising with the parameterization of Ilyushin and open a possibility using the exact yield surface in practical computations, Burgoyne and Brennan [1993b] introduced the parameters

$$\nu = \frac{P_\varepsilon}{P_\kappa}, \quad \beta = -\frac{P_{\varepsilon\kappa}}{P_\kappa} \quad \text{and} \quad \gamma = \nu - \beta^2 \quad (1.62)$$

where β and γ are proposed as two independent parameters for the description of the yield surface. β has the physical meaning of being the position within the thickness of the shell, where the consistency parameter $d\xi$ in Eq. (1.46) is a minimum. With these parameters, the yield surface assumes the form

$$\begin{aligned} Q_t &= (\beta K_0 - K_1)^2 + \gamma K_0^2 \\ Q_m &= 4(\beta K_0 - K_1)(\beta K_1 - K_2) + 4\gamma K_0 K_1 \\ Q_m &= 16(\beta K_1 - K_2)^2 + 16\gamma K_1^2 \end{aligned} \quad (1.63)$$

where the integrals K_i are given by

$$K_i = \sqrt{3P_\kappa} J_i = \int_{-1/2}^{1/2} \frac{\bar{z}^i}{\sqrt{P_\varepsilon + 2P_{\varepsilon\kappa}\bar{z} + P_\kappa\bar{z}^2}} d\bar{z} \quad (1.64)$$

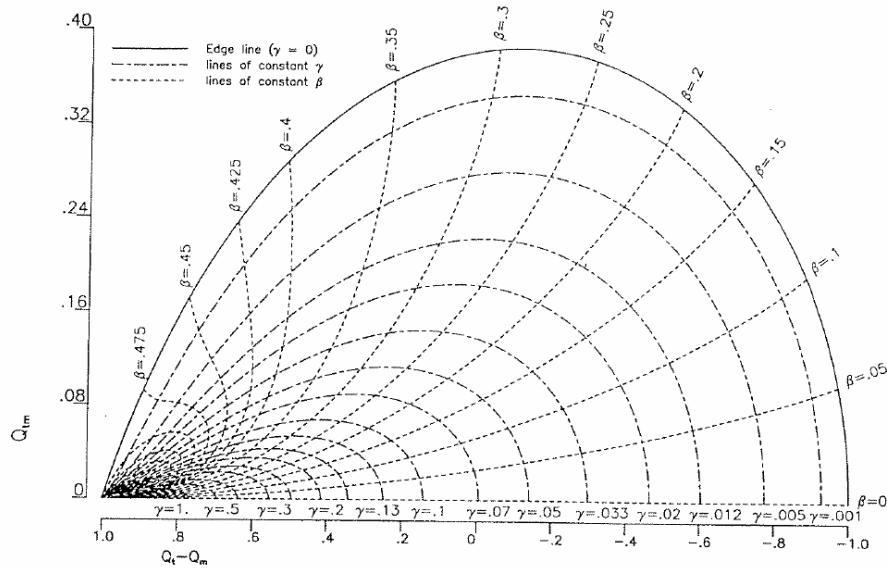


Figure 1.4 One half of the exact Ilyushin yield surface ($Q_m \leq 0$) constructed in terms of β and γ (from Burgoyne and Brennan, 1993b)

This yield surface is subject to the conditions

$$\begin{aligned} 0 &\leq \beta^2 \leq \nu \leq \infty, \\ 0 &\leq \gamma \leq \infty. \end{aligned} \quad (1.65)$$

The integrals K_i can be evaluated analytically giving

$$\begin{aligned}
K_0 &= \ln \left(\frac{\sqrt{(0.5 - \beta)^2 + \gamma} + (0.5 - \beta)}{\sqrt{(0.5 + \beta)^2 + \gamma} - (0.5 + \beta)} \right), \\
K_1 &= \sqrt{(0.5 - \beta)^2 + \gamma} - \sqrt{(0.5 + \beta)^2 + \gamma} + \beta K_0, \\
2K_2 &= (0.5 + \beta) \sqrt{(0.5 - \beta)^2 + \gamma} + (0.5 - \beta) \sqrt{(0.5 + \beta)^2 + \gamma} + 2\beta K_1 - \gamma K_0.
\end{aligned} \tag{1.66}$$

Figure 1.4 shows a two-dimensional representation of one half of the yield surface ($Q_m \leq 0$) in terms of the two parameters β and γ . This representation is the most convenient for calculations, since nowhere on the yield surface do lines of constant values of the two parameters become parallel.

1.3.4 Plastic dissipation function

The derivation and description of the exact Ilyushin yield surface presented above was performed with incremental strain quantities. For the evaluation of the power of internal forces, however, a description in terms of strain rate quantities is more convenient. It is to be noted that the state relations are not affected, if the strain rate quantities are used throughout in stead of the incremental strain quantities, provided the reference values ε_0 and κ_0 are replaced by reference strain and curvature rates $\dot{\varepsilon}_0$ and $\dot{\kappa}_0$, respectively. According to Eq. (1.34) a dimensionless generalized strain rate vector $\dot{\tilde{\mathbf{e}}}$ is defined

$$\dot{\tilde{\mathbf{e}}}^T = \begin{pmatrix} \dot{\tilde{\mathbf{e}}} & \dot{\mathbf{k}} \end{pmatrix} = \begin{pmatrix} \frac{1}{\dot{\varepsilon}_0} \dot{\tilde{\varepsilon}}_{11} & \frac{1}{\dot{\varepsilon}_0} \dot{\tilde{\varepsilon}}_{22} & \frac{1}{\dot{\varepsilon}_0} 2\dot{\tilde{\varepsilon}}_{12} & \frac{1}{\dot{\kappa}_0} \dot{\tilde{\kappa}}_{11} & \frac{1}{\dot{\kappa}_0} \dot{\tilde{\kappa}}_{22} & \frac{1}{\dot{\kappa}_0} 2\dot{\tilde{\kappa}}_{12} \end{pmatrix} \tag{1.67}$$

replacing the generalized strain increment vector $d\tilde{\mathbf{e}}$.

The plastic dissipation function for a shell structure may be written in the form

$$d^p = \frac{D^p}{N_0 \dot{\varepsilon}_0} = \begin{pmatrix} \mathbf{n} \\ \mathbf{m} \end{pmatrix}^T \begin{pmatrix} \dot{\tilde{\mathbf{e}}}^p \\ \dot{\tilde{\mathbf{k}}}^p \end{pmatrix} = \tilde{\boldsymbol{\sigma}}^T \dot{\tilde{\mathbf{e}}}^p \tag{1.68}$$

where D^p and d^p are the physical and normalized plastic dissipations per unit area of the mid-plane of the shell. With the six-dimensional representation of the exact Ilyushin yield surface Eq. (1.51) (written in rate form), d^p may be expressed as a function of the strain rate resultant quantities $\dot{\tilde{\mathbf{e}}}^p$

$$d^p(\dot{\tilde{\mathbf{e}}}^p) = \frac{3}{2} (\dot{\tilde{\mathbf{e}}}^p)^T \begin{pmatrix} J_0 \mathbf{P}^{-1} & 4J_1 \mathbf{P}^{-1} \\ 4J_1 \mathbf{P}^{-1} & 16J_2 \mathbf{P}^{-1} \end{pmatrix} \dot{\tilde{\mathbf{e}}}^p. \tag{1.69}$$

Analytical evaluation of this relation gives

$$d^p(\dot{\tilde{\mathbf{e}}}^p) = \frac{2}{\sqrt{3}} \int_{-1/2}^{1/2} \sqrt{P_\varepsilon + 2P_{\varepsilon\kappa} \bar{z} + P_\kappa \bar{z}^2} d\bar{z} \tag{1.70}$$

which finally may be written as [Seitzberger, 2000]

$$d^p = \begin{cases} 2\sqrt{\frac{P_\kappa}{3}} & \text{for } P_\kappa = 0 \quad (a) \\ \sqrt{\frac{P_\kappa}{3}} \left(\beta_1 \sqrt{\beta_1^2 + \gamma} + \beta_2 \sqrt{\beta_2^2 + \gamma} + \gamma K_0 \right) & \text{for } P_\kappa > 0 \quad (b) \end{cases} \quad (1.71)$$

where β_1 and β_2 are

$$\beta_1 = 0.5 - \beta \quad \text{and} \quad \beta_2 = 0.5 + \beta. \quad (1.72)$$

It is to be noted that the value of K_0 will become indefinite if both conditions $|\beta| \leq 0.5$ and $\gamma = 0$ are fulfilled. However, as long as γ is not exactly equal to zero, but to some small positive numbers, a “regularized” evaluation of K_0 may be obtained [Seitzberger, 2000]. Otherwise, in general, d^p is convex but not everywhere differentiable [Capsoni and Corradi, 1997]. In order to allow a direct non-linear, non-smooth, constrained optimization problem, as will be discussed later, a “smooth regularization method” will be used for overcoming the non-differentiability of the objective function. On the other hand, without the loss of generality, it is supposed that P_κ is always positive in order to have the expression of the plastic dissipation function as described in (1.71b). To this end it is necessary to add to γ and to P_κ a small positive number. Thus, in this case, Eq. (1.71) is amenable to a numerical evaluation for all values of $\tilde{\epsilon}^p$.

1.3.5 Reformulation

For our general purpose to deal with probabilistic problems, as will be discussed later, the yield limit σ_y and thickness h might be no longer constant but random variables, and then the reference quantities are also changed together with the different ‘realizations’ of random variables. Additionally, in reliability analysis, the sensitivities are required which contain first and second derivatives versus loading, material strength and thickness random variables. Thus some expressions of quantities which are necessary for analysis algorithm should be reformulated. Let us restrict ourselves to the case of homogeneous material and shells of constant thickness in which the yield limit σ_y and thickness h are the same at every Gaussian point of the structure. So we always can write

$$\sigma_y = Y\sigma_0, \quad h = Zh_0 \quad (1.73)$$

where σ_0, h_0 are constant reference values and Y, Z are random variables. By that way the normalized quantities in Eqs. (1.26), (1.27) and (1.28) assume the new form as follows

$$\tilde{N}_0 = \sigma_0 h_0 = \frac{\sigma_y h}{YZ} = \frac{N_0}{YZ} \quad (1.74a)$$

$$\tilde{M}_0 = \sigma_0 \frac{h_0^2}{4} = \frac{\sigma_y}{Y} \frac{h^2}{4Z^2} = \frac{M_0}{YZ^2} \quad (1.74b)$$

$$\tilde{\varepsilon}_0 = \frac{\sigma_0(1-\nu^2)}{E} = \frac{\sigma_y(1-\nu^2)}{YE} = \frac{\varepsilon_0}{Y} \quad (1.74c)$$

and

$$\tilde{\kappa}_0 = \frac{4\tilde{\varepsilon}_0}{h_0} = \frac{4Z\varepsilon_0}{Yh} = \frac{Z}{Y}\kappa_0. \quad (1.74d)$$

With the new normalized quantities, the new “engineering” strain and stress vectors are obtained

$$\hat{\mathbf{e}} = \begin{pmatrix} Y\bar{\mathbf{e}} \\ \frac{Y}{Z}\mathbf{k} \end{pmatrix}, \quad \hat{\mathbf{\sigma}} = \begin{pmatrix} YZ\mathbf{n} \\ YZ^2\mathbf{m} \end{pmatrix} \quad (1.75)$$

and the incremental plastic strain resultant intensities have the form

$$\begin{aligned} \hat{P}_\varepsilon &= \frac{3}{4}(\dot{\hat{\mathbf{e}}}^p)^T \mathbf{P}_1 \dot{\hat{\mathbf{e}}}^p = \frac{3}{4}(Y\dot{\hat{\mathbf{e}}}^p)^T \mathbf{P}_1 (Y\dot{\hat{\mathbf{e}}}^p) = Y^2 P_\varepsilon \quad (\geq 0) \\ \hat{P}_{\varepsilon\kappa} &= 3(\dot{\hat{\mathbf{e}}}^p)^T \mathbf{P}_2 \dot{\hat{\mathbf{e}}}^p = 3(Y\dot{\hat{\mathbf{e}}}^p)^T \mathbf{P}_2 \left(\frac{Y}{Z}\dot{\hat{\mathbf{e}}}^p\right) = \frac{Y^2}{Z} P_{\varepsilon\kappa} \\ \hat{P}_\kappa &= 12(\dot{\hat{\mathbf{e}}}^p)^T \mathbf{P}_3 \dot{\hat{\mathbf{e}}}^p = 12\left(\frac{Y}{Z}\dot{\hat{\mathbf{e}}}^p\right)^T \mathbf{P}_3 \left(\frac{Y}{Z}\dot{\hat{\mathbf{e}}}^p\right) = \frac{Y^2}{Z^2} P_\kappa \quad (\geq 0) \end{aligned} \quad (1.76)$$

Adapting the parameters ν, β, γ which were introduced in (1.62) with these new strain resultant intensities and then substitute them into (1.71), we obtain the new expression of the plastic dissipation function

$$D^p = \begin{cases} 2YZ\tilde{N}_0\tilde{\varepsilon}_0\sqrt{\frac{\hat{P}_\varepsilon}{3}} & \text{for } \hat{P}_\kappa = 0 \quad (a) \\ Y\tilde{N}_0\dot{\hat{\varepsilon}}_0\sqrt{\frac{\hat{P}_\kappa}{3}}\left(\beta_1\sqrt{\beta_1^2+\gamma}+\beta_2\sqrt{\beta_2^2+\gamma}+\gamma K_0\right) & \text{for } \hat{P}_\kappa > 0 \quad (b) \end{cases} \quad (1.77)$$

with the new β_1, β_2 and K_0 are

$$\beta_1 = \frac{Z}{2} - \beta, \quad \beta_2 = \frac{Z}{2} + \beta, \quad K_0 = \ln\left(\frac{\sqrt{\beta_1^2+\gamma}+\beta_1}{\sqrt{\beta_2^2+\gamma}-\beta_2}\right). \quad (1.78)$$

2 MATHEMATICAL FORMULATIONS OF LIMIT AND SHAKEDOWN ANALYSIS IN GENERALIZED VARIABLES

It is the objective of structural analysis to determine the load carrying capacity. In the early 20th century, it has been relatively easily defined by forcing the stress intensity at a certain point of the structure to attain the yield stress of the material. This implies that structural failure occurs before yielding. However, many materials, for example the majority of metals, exhibit distinct, plastic properties. Such materials can deform considerably without breaking, even after the stress intensity attains the yield stress. This implies that if the stress intensity reaches the critical (yield) value, the structure does not necessarily fail or deform extensively. To this case, in order to permit higher loads, elastic-plastic structural analysis becomes more general than the classical elastic one. Among the plasticity methods, Limit and Shakedown Analysis (LISA) seems to be the most powerful one. In Europe LISA has been developed as a direct plasticity method for the design and the safety analysis of severely loaded engineering structures, such as nuclear power plants and chemical plants, offshore structures etc. [Staat, 2002], [Staat and Heitzer, 2003a]. Annex B of the new European pressure vessel standard EN 13445-3 is based on LISA [European standard, 2005-06], [Taylor et al., 1999] thus indicating the industrial need for LISA software. All design codes are based on perfectly plastic models. The extension of LISA to hardening materials is no problem [Staat and Heitzer, 2002].

Based on the elastic-perfectly plastic or rigid-perfectly plastic models of material and considering the loads as monotonic and proportional, limit analysis evaluates the plastic collapse load or the largest load to which the structure would be subjected during its lifetime. Beyond this limit, the structure will fail due to global plastic flow. Limit analysis was pioneered approximately from the works of Kazincky in 1914 and Kist in 1917. The first complete formulations of both upper bound and lower bound theorems were established later by Drucker, Greenberg and Prager and the alternative formulation using rigid-plastic material was given by Hill in 1951. Since then, the applications of limit analysis theory in engineering have been widely reported, such as the works of Hodge [1959, 1961, 1963], Maier [1970], Prager [1972], Martin [1975], Lubliner [2005] and Capsoni and Corradi [1997].

However, in practice, the loads are generally time-dependent or may vary independently. Practical experience showed that in the case of variable repeated loads, not only can low-cycle fatigue cause structural failure below the plastic collapse load

calculated with limit analysis but also an accumulation of plastic deformations may occur, resulting in excessive deflections of the structure [König, 1987]. It may also happen that the structure comes back to its elastic behaviour after a certain time period. In this way, a new branch of plasticity, the theory of shakedown came to existence. The first static shakedown theorem was formulated by Bleich [1932] for a system of beam of ideal *I*-cross-sections. This static theorem was then extended by Melan [1936] to more the general case of a continuum. In an alternative way, Koiter [1960] developed a general kinematic shakedown theorem based on an analogy to limit analysis. He stated and proved the plastic analysis theorems, i.e. the limit analysis and the shakedown ones in the form used nowadays. Since then, large amount of work were reported in the literature, cf. Maier [1969, 1973], König [1966, 1969, 1972], Polizzotto et al. [1993a, b], Ponter et al. [1997a, 1997b, 2000], Nguyen Dang et al. [1976, 1990], Weichert et al. [1988, 2002], Staat et al. [1997, 2001, 2003b].

The theory of limit and shakedown analysis were established long time ago. However their numerical applications encountered some difficulties and were limited to some relatively simple structures. In the case of more complex structures, e.g. shell-like structures, a direct application of the limit and shakedown theorems is cumbersome if possible at all. The mathematical difficulties arising from the need to use a three-dimensional analysis are difficult to be overcome. In this case it is convenient to introduce some generalized, integrated variables, which are used to describe the static and kinematic quantities. Such an approach allows one to reduce complicated three-dimensional problems to simple plane or one-dimensional ones.

In this chapter, two fundamental theorems of limit and shakedown analysis are introduced, the static and kinematic theorems. Based on the original ones which were proposed by Melan and Koiter, an extension for lower and upper bound theorems in terms of generalized variables are proposed and formulated. A simple approach for direct calculation of the shakedown limit as the minimum of incremental plasticity limit and alternating plasticity limit, namely the unified shakedown limit method, is also presented.

2.1. Theory of limit analysis

2.1.1 Introduction

Let us consider a structure of volume V made of elastic-perfectly plastic or rigid-perfectly plastic material and subjected to external loading \mathbf{P} . The external loading \mathbf{P} consists of general body force $\bar{\mathbf{f}}$ in V and surface traction $\bar{\mathbf{t}}$ on ∂V_σ . We assume that all loads are applied in a monotonic and proportional way

$$\mathbf{P} = \alpha \mathbf{P}_0 \quad (2.1)$$

where $\mathbf{P}_0 = (\bar{\mathbf{f}}_0, \bar{\mathbf{t}}_0)$ denotes the nominal or initial load. If the value of α is sufficiently small, the body behaves elastically. As α increases and reaches a special value, the first point in the body reaches the plastic state. This state of stress is called elastic limit. Further

increase of α will lead to the expansion of plastic region in the body. The structure gradually forms a collapse mechanism. At limit state, the structure fails to support the applied load and collapses. If \mathbf{P}_0 represents the applied load, the value α_l corresponding to the plastic collapse state is called the safety factor of the structure or the limit load multiplier.

The theory of limit analysis offers a way to solve directly the problem of estimating the plastic collapse load, bypassing the spreading process of the plastic flow. The limit value of the load is estimated and at the same time the limit state of stress in the whole structure can be evaluated. The limit load and stresses so obtained are of great interest in practical engineering whenever the perfectly plastic model and small deformation assumption constitute a good approximation of the material.

2.1.2 General theorems of limit analysis

Lower bound theorem

Based on the variational principle of Hill for perfectly plastic material, also known as the *principle of maximum plastic work*, the lower bound theorem of limit analysis can be stated as follows

The exact limit load factor α_l is the largest one among all possible static solutions α_l^- corresponding to the set of all licit stress fields $\boldsymbol{\sigma}$, that is

$$\alpha_l^- \leq \alpha_l. \quad (2.2)$$

To prove this theorem the principle of virtual work and the property of convexity of the yield surface are used, [Hodge, 1959], [Prager, 1959], [Lubliner, 2005]. Then, the task of computing the limit load factor becomes a nonlinear optimization problem

$$\begin{aligned} \alpha_l &= \max \quad \alpha_l^- \\ \text{s.t.:} \quad &\begin{cases} L[\boldsymbol{\sigma}] + \alpha_l^- \mathbf{P}_0 = 0 & \text{(a)} \\ f(\boldsymbol{\sigma}) \leq 0 & \text{(b)} \end{cases} \end{aligned} \quad (2.3)$$

where Eq. (a) is equilibrium condition, L denotes a linear operator (usually differential one) and $f(\boldsymbol{\sigma})$ is the yield function. For the continuum we have $L[\boldsymbol{\sigma}] = \text{div} \boldsymbol{\sigma}$.

Upper bound theorem

The upper bound theorem can be demonstrated as

The actual limit load multiplier α_l is the smallest one of the set of all multipliers α_l^+ corresponding to the set of all licit velocity fields $\dot{\mathbf{u}}$

$$\alpha_l \leq \alpha_l^+ \quad (2.4)$$

where

$$\alpha_l^+ = W_{in}/W_{ex} \quad (a)$$

$$W_{in} = \int_V D^p(\dot{\boldsymbol{\varepsilon}}^p) dV \quad (b)$$

$$W_{ex} = \int_V \bar{\mathbf{f}}_0^T \dot{\mathbf{u}} dV + \int_{\partial V_\sigma} \bar{\mathbf{t}}_0^T \dot{\mathbf{u}} dS > 0 \quad (c)$$

$$\dot{\mathbf{u}} = \mathbf{0} \quad \text{on} \quad \partial V_u \quad (d)$$

with W_{in} and W_{ex} the total power of the internal deformation and the power of the external loads of the structure. The upper bound theorem permits us to estimate the limit load factor by solving the following optimization problem (written in a normalized form)

$$\begin{aligned} \alpha_l &= \min W_{in} \\ \text{s.t.:} \quad W_{ex} &= 1 \end{aligned} \quad (2.6)$$

2.2. Theory of shakedown analysis

2.2.1 Introduction

It has been understood in limit analysis considered above that the loading is simple, namely, monotonic and proportional mechanical load (self-equilibrium thermal load has no effect on classical limit analysis). In practice, however, structures are often subjected to the action of varying mechanical and thermal loading. These loads may be repeated (cyclic) or varying arbitrarily in certain domain. In this case, loads which are less than plastic collapse limit may cause the failure of the structure due to an excessive deformation or to a local break after a finite number of loading cycles.

Inelastic structures such as for example pressure vessels and pipelines subjected to variable repeated or cyclic loading may work in four different regimes, which are presented in the Bree-diagram (figure 2.1, [Bree, 1967]) together with the evolution of the structural response: elastic, shakedown (adaptation), inadapation (non-shakedown), and limit (ultimate) state. Since for the elastic regime there are no plastic effects at all, whereas for the adaptation regime the plastic effects are restricted to the initial loading cycles and then they are followed by asymptotically elastic behaviour, both regimes are considered as safe working ones and they constitute a foundation for the structural design. We do not consider elastic failure such as buckling or high cycle fatigue here. The inadapation phenomena such as low cycle fatigue and or ratchetting should be avoided since they lead to a rapid structural failure. At the limit load the structure loses instantaneously its load bearing capacity. Limit and shakedown analyses deal directly with the calculation of the load capacity or the maximum load intensities that the structure is able to support. The structural shakedown takes place due to development of permanent residual stresses which, imposed on the actual stresses shift them towards purely elastic behaviour. Residual stresses are a result of kinematically inadmissible plastic strains introduced to the structure by overloads. They clear out effects of all preceding smaller loads. They also avoid any plastic effects in the future provided that the loads are smaller than the initial overload.

Therefore, in limit and shakedown analyses the knowledge of the exact load history is not necessary. Only the maximum loads (limits) count and the envelopes should be taken into consideration.

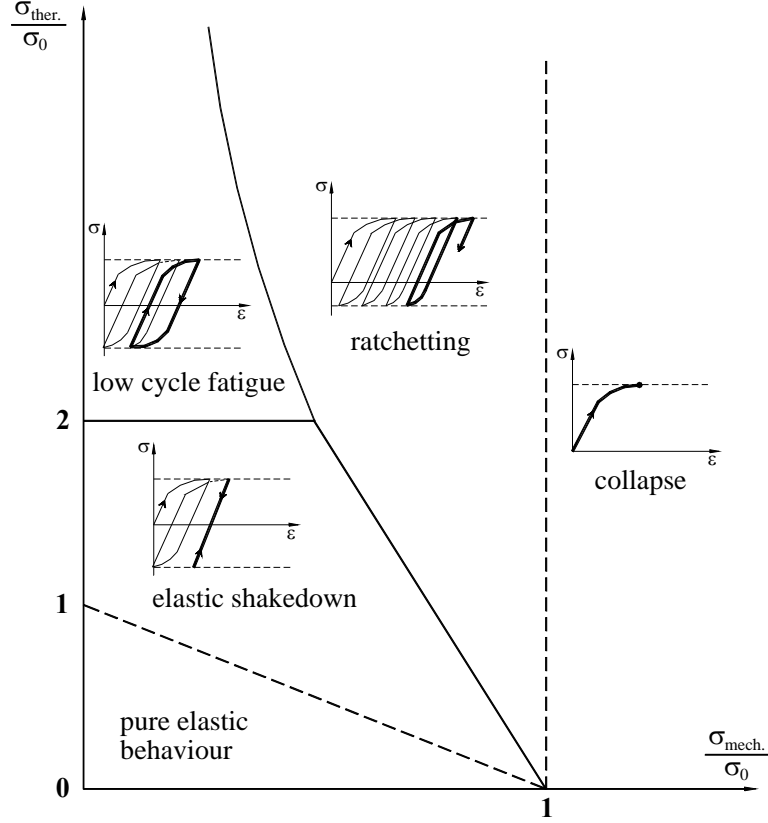


Figure 2.1 Bree-diagram of a pressurized thin wall tube under thermal and mechanical loads

Viewing the situations above, one can see that the first and second situations may not become dangerous but maximum exploitation of materials can only be attained in the adaptation or shakedown case. The maximum safe load is defined as the shakedown load avoiding low cycle fatigue and ratchetting. Thus, the main problem of shakedown theory is to investigate whether or not a structure made of certain material will shake down under the prescribed loads.

2.2.2 Definition of load domain

We study here the shakedown problem of a structure subjected to n time-dependent (thermal and mechanical) loads $\bar{P}_k^0(t)$ with time is denoted by t , each of them can vary independently within a given range

$$\bar{P}_k^0(t) \in I_k^0 = [\bar{P}_k^-, \bar{P}_k^+] = [\mu_k^-, \mu_k^+] P_k^0, \quad k = \overline{1, n}. \quad (2.7)$$

These loads form a convex polyhedral domain \mathcal{L} of n dimensions with $m = 2^n$ vertices in the load space as shown in figure 2.2 for two variable loads. This load domain can be represented in the following linear form

$$P(t) = \sum_{k=1}^n \mu_k(t) P_k^0 \quad (2.8)$$

where

$$\mu_k^- \leq \mu_k(t) \leq \mu_k^+, \quad k = \overline{1, n}. \quad (2.9)$$

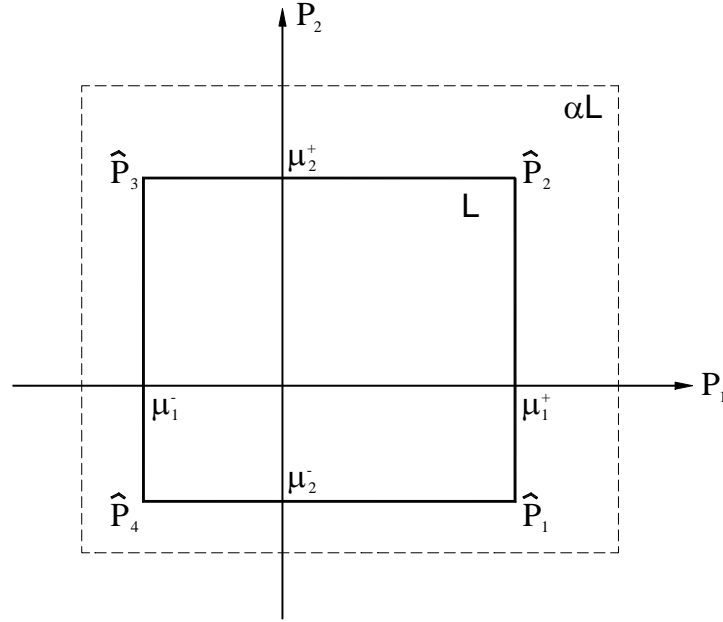


Figure 2.2 Two dimensional load domain \mathcal{L} and $\mathcal{L}' = \alpha \mathcal{L}$

In the case of shell structures, it is useful to describe this load domain in the generalized stress space. To this end, we use here the notion of a fictitious infinitely elastic structure which has the same geometry and elastic properties as the actual one. Let the cross-sections of the shell be identified by a vector-variable \mathbf{x} . The actual ‘engineering’ stress field in Eq. (1.75) in the elastic-plastic shell can be expressed in the following way

$$\hat{\boldsymbol{\sigma}}(\mathbf{x}, t) = \hat{\boldsymbol{\sigma}}^E(\mathbf{x}, t) + \bar{\boldsymbol{\rho}}(\mathbf{x}) \quad (2.10)$$

with the fictitious elastic generalized stress vector $\hat{\boldsymbol{\sigma}}^E(\mathbf{x}, t)$ is defined as that would appear in the fictitious infinitely elastic structure if this structure was subjected to the same loads as the actual one. This fictitious elastic generalized stress vector may be written in a form similar to (2.8)

$$\hat{\boldsymbol{\sigma}}^E(\mathbf{x}, t) = \sum_{k=1}^n \mu_k(t) \hat{\boldsymbol{\sigma}}^{Ek}(\mathbf{x}) \quad (2.11)$$

where $\hat{\boldsymbol{\sigma}}^{Ek}(\mathbf{x})$ denotes the generalized stress vector in the infinitely elastic (fictitious) structure when subjected to the unit load mode P_k^0 . $\bar{\mathbf{p}}(\mathbf{x})$ denotes a time-independent residual generalized stress field. This residual generalized stress field satisfies the homogeneous static equilibrium and boundary conditions (2.3.a) for $P = 0$.

Following (2.11), let us define a load domain $\mathcal{L}' = \alpha\mathcal{L}$ such that when subjected to \mathcal{L}' the fictitious elastic generalized stress vector $\hat{\boldsymbol{\sigma}}^E(\mathbf{x}, t)'$ of the structure under consideration is equal to $\hat{\boldsymbol{\sigma}}^E(\mathbf{x}, t)$ multiplied by a load factor α

$$\hat{\boldsymbol{\sigma}}^E(\mathbf{x}, t)' = \alpha \hat{\boldsymbol{\sigma}}^E(\mathbf{x}, t) = \alpha \sum_{k=1}^n \mu_k(t) \hat{\boldsymbol{\sigma}}^{Ek}(\mathbf{x}). \quad (2.12)$$

In shakedown analysis, the problem is to find the largest value of α which still guarantees elastic shakedown. This situation means that after some time t or some cycles of loading, plastic strain ceases to develop and the structure returns to elastic behaviour. One criterion for an elastic, perfectly plastic material to shake down elastically is that the plastic generalized strains and therefore the residual generalized stresses become stationary for given loads $P(t)$

$$\begin{aligned} \lim_{t \rightarrow \infty} \dot{\hat{\boldsymbol{\epsilon}}}^p(\mathbf{x}, t) &= 0, \\ \lim_{t \rightarrow \infty} \dot{\bar{\mathbf{p}}}(\mathbf{x}) &= 0, \quad \forall \mathbf{x} \in S \end{aligned} \quad (2.13)$$

where S denotes the middle surface of the shell. It is shown in this case, the total amount of plastic energy dissipated over any possible load path within the domain \mathcal{L}' must be finite

$$W_{in} = \tilde{N}_0 \tilde{\mathcal{E}}_0 \int_0^t \hat{\boldsymbol{\sigma}}^T \dot{\hat{\boldsymbol{\epsilon}}}^p dt < \infty. \quad (2.14)$$

The inequality (2.14) may be considered as an intuitive examination which verifies if a given structure is going to shake down. Indeed, most of the authors have formulated shakedown criteria in this way. However, it should be noted that such a concept leads to an approximate description: the total energy dissipated may be finite even if plastic strain increments appear at every load cycle but comprise a convergent series. Furthermore, boundedness of the total plastic work, without its maximum value being specified, seems to be sometimes too weak a requirement, for example when low cycle fatigue is considered.

2.2.3 Fundamental of shakedown theorems

Static shakedown theorem

The decomposition (2.10) is an extension of the classical formulae, which expresses

in terms of stresses. By comparing with the classical static shakedown criterion, which states for stress variables, one can easily see that the shakedown of a shell structure is equivalent to the existence of a time-independent residual generalized stress field $\bar{\mathbf{p}}(\mathbf{x})$ in structure such that it does not anywhere violate the yield criterion

$$f(\hat{\boldsymbol{\sigma}}(\mathbf{x}, t)) = f(\hat{\boldsymbol{\sigma}}^E(\mathbf{x}, t) + \bar{\mathbf{p}}(\mathbf{x})) \leq 0 \quad (2.15)$$

where f denotes the yield function in term of generalized variables. The following theorem shows that this is the necessary and sufficient condition for a structure to shake down

Theorem II.1:

1. *Shakedown occurs if there exists a time-independent residual generalized stress field $\bar{\mathbf{p}}(\mathbf{x})$, statically admissible, such that*

$$f(\hat{\boldsymbol{\sigma}}(\mathbf{x}, t)) = f(\hat{\boldsymbol{\sigma}}^E(\mathbf{x}, t) + \bar{\mathbf{p}}(\mathbf{x})) < 0. \quad (2.16)$$

2. *Shakedown will not occur if no $\bar{\mathbf{p}}(\mathbf{x})$ exists such that*

$$f(\hat{\boldsymbol{\sigma}}(\mathbf{x}, t)) = f(\hat{\boldsymbol{\sigma}}^E(\mathbf{x}, t) + \bar{\mathbf{p}}(\mathbf{x})) \leq 0. \quad (2.17)$$

Based on the above static theorem, we can find a permanent statically admissible residual generalized stress field in order to obtain a maximum load domain $\alpha\mathcal{L}$ that guarantees (2.17). The obtained shakedown load multiplier α^- is generally a lower bound. From the above static theorem, the shakedown problem can be seen as a mathematical maximization problem in nonlinear programming

$$\begin{aligned} \alpha^- &= \max \alpha \\ \text{s.t.: } &\begin{cases} L[\bar{\mathbf{p}}] = 0 & (a) \\ f(\alpha\hat{\boldsymbol{\sigma}}^E(\mathbf{x}, t) + \bar{\mathbf{p}}(\mathbf{x})) \leq 0 \quad \forall t & (b) \end{cases} \end{aligned} \quad (2.18)$$

Kinematic shakedown theorem

Using plastic strain field to formulate shakedown criterion, kinematic shakedown theorem is the counterpart of the static one. The theorem was given by Koiter [1960] and some of its applications in analysis of incremental collapse were derived by Gokhfeld [1980], Sawczuk [1969a, b]. The same as proposed by Koiter for plastic strain field, we introduce here an admissible cycle of plastic generalized strain field $\Delta\hat{\boldsymbol{\varepsilon}}^p$. The plastic generalized strain rate $\dot{\hat{\boldsymbol{\varepsilon}}}^p$ may not necessarily be compatible at each instant during the time cycle T but the plastic generalized strain accumulation over the cycle

$$\Delta \hat{\mathbf{e}}^p = \int_0^T \dot{\hat{\mathbf{e}}}^p dt \quad (2.19)$$

is required to be kinematically compatible such that

$$\Delta \hat{\mathbf{e}}^p = R[\dot{\mathbf{u}}(\mathbf{x})] \quad (2.20)$$

and

$$\int_0^T \int_S \tilde{N}_0 \dot{\hat{\mathbf{e}}}_0 (\hat{\mathbf{e}}^E)^T \dot{\hat{\mathbf{e}}}^p dt dS > 0 \quad (2.21)$$

where R is a linear, differential or algebraic operator, $\mathbf{u}(\mathbf{x})$ denotes the vector of displacements on the middle surface. The virtual power principle (1.14) permits us to write the external power in a more general form which contains the generalized variables

$$\int_0^T \left[\int_V (\bar{f}_i \dot{u}_i + \sigma_{ij}^\theta(\mathbf{x}, t) \dot{\varepsilon}_{ij}^p) dV + \int_{\partial V_\sigma} \bar{t}_i \dot{u}_i dS_\sigma \right] dt = \int_0^T \int_S \tilde{N}_0 \dot{\hat{\mathbf{e}}}_0 (\hat{\mathbf{e}}^E(\mathbf{x}, t))^T \dot{\hat{\mathbf{e}}}^p dS dt \quad (2.22)$$

where $\sigma_{ij}^\theta(\mathbf{x}, t)$ is a self-equilibrium thermal stress due to the temperature field $\theta(t)$. From Eq. (2.22), the following extension of Koiter theorem holds

Theorem II.2:

1. *Shakedown may happen if the following inequality is satisfied*

$$\int_0^T \int_S \tilde{N}_0 \dot{\hat{\mathbf{e}}}_0 (\hat{\mathbf{e}}^E(\mathbf{x}, t))^T \dot{\hat{\mathbf{e}}}^p dS dt \leq \int_0^T \int_S D^p(\dot{\hat{\mathbf{e}}}^p) dS dt. \quad (2.23)$$

2. *Shakedown can not happen when the following inequality holds*

$$\int_0^T \int_S \tilde{N}_0 \dot{\hat{\mathbf{e}}}_0 (\hat{\mathbf{e}}^E(\mathbf{x}, t))^T \dot{\hat{\mathbf{e}}}^p dS dt > \int_0^T \int_S D^p(\dot{\hat{\mathbf{e}}}^p) dS dt. \quad (2.24)$$

Based on the kinematic theorem, an upper bound of the shakedown limit load multiplier α^+ can be computed. The shakedown problem can be seen as a mathematical minimization problem in nonlinear programming

$$\begin{aligned} \alpha^+ = \min & \frac{\int_0^T \int_S D^p(\dot{\hat{\mathbf{e}}}^p) dS dt}{\int_0^T \int_S \tilde{N}_0 \dot{\hat{\mathbf{e}}}_0 (\hat{\mathbf{e}}^E(\mathbf{x}, t))^T \dot{\hat{\mathbf{e}}}^p dS dt} \\ \text{s.t: } & \begin{cases} \Delta \hat{\mathbf{e}}^p = \int_0^T \dot{\hat{\mathbf{e}}}^p dt \\ \Delta \hat{\mathbf{e}}^p = R[\dot{\mathbf{u}}(\mathbf{x})] \end{cases} \end{aligned} \quad (2.25)$$

In order to calculate the shakedown limit load multiplier, the two following methods can be applied: separated and unified methods. While the former analyses separately two different failure modes: incremental plasticity (ratchetting) and alternating plasticity, the latter analyses them simultaneously. Both methods deserve special attention due to their role in structural computation. In the following sections, from the original ones which state for local variables [König, 1987], an extension for generalized variables is presented.

2.2.4 Separated shakedown limit

As was mentioned above, incremental collapse and alternating plasticity may happen to combine. These inadapation modes can be defined precisely in the following way

Theorem II.3:

1. A perfect incremental collapse process (over a certain time interval $(0, T)$) is a process of plastic deformation $\bar{\epsilon}(\mathbf{x}, t)$ in which a kinematically admissible plastic generalized strain increment $\Delta\bar{\epsilon}(\mathbf{x}, t) = \bar{\epsilon}(\mathbf{x}, T) - \bar{\epsilon}(\mathbf{x}, 0)$ is attained in a proportional and monotonic way, namely

$$\begin{aligned}\Delta\bar{\epsilon} &= R[\dot{\mathbf{u}}(\mathbf{x})] \\ \dot{\bar{\epsilon}} &= \dot{\Lambda}(\mathbf{x}, t) \cdot \Delta\bar{\epsilon}(\mathbf{x}) \\ \dot{\Lambda}(\mathbf{x}, t) &\geq 0 \\ \Lambda(\mathbf{x}, 0) &= 0 \\ \Lambda(\mathbf{x}, T) &= 1\end{aligned}\tag{2.26}$$

2. An alternating plasticity process is any process of plastic deformation $\hat{\epsilon}(\mathbf{x}, t)$ within a certain time interval $(0, T)$ such that the total increment of the plastic generalized strain $\Delta\hat{\epsilon}(\mathbf{x})$ over this period is zero,

$$\Delta\hat{\epsilon}(\mathbf{x}) = \int_0^T \dot{\hat{\epsilon}}(\mathbf{x}, t) dt = 0.\tag{2.27}$$

The criteria of safety with respect to alternating plasticity or incremental collapse may be obtained by substituting the plastic strain history (2.26) or (2.27) into the shakedown condition (2.23).

From the above definitions (2.26) and (2.27), it is easy to see that any plastic generalized strain history $\hat{\epsilon}^p(\mathbf{x}, t)$, which leads to a kinematically admissible plastic generalized strain increment within a periodic interval $(0, T)$, can be decomposed into two components of perfectly incremental collapse and alternating plasticity

$$\hat{\epsilon}^p(\mathbf{x}, t) = \bar{\epsilon}(\mathbf{x}, t) + \hat{\epsilon}(\mathbf{x}, t).\tag{2.28}$$

2.2.4.1 Incremental collapse criterion

If the safety condition against any form of perfectly incremental collapse is considered, the plastic strain field is assumed by (2.26). Substituting (2.26) into (2.23), one obtains

$$W_{ex} = \int_0^T \int_S \tilde{N}_0 \dot{\hat{\epsilon}}_0^E(\mathbf{x}, t) \dot{\Lambda}(\mathbf{x}, t) \Delta \bar{\epsilon}(\mathbf{x}) dS dt \leq W_{in} = \int_0^T \int_S D^p(\dot{\Lambda} \Delta \bar{\epsilon}) dS dt. \quad (2.29)$$

By taking into account the properties of the dissipation function and the plastic strain history (2.26), we can write

$$W_{in} = \int_0^T \int_S D^p(\dot{\Lambda} \Delta \bar{\epsilon}) dS dt = \int_0^T \dot{\Lambda} \int_S D^p(\Delta \bar{\epsilon}) dS dt = \int_S D^p(\Delta \bar{\epsilon}) dS. \quad (2.30)$$

From the shakedown condition (2.29), the smallest upper bound of incremental limit could be attained when the external power W_{ex} assumes its maximum and the internal dissipation W_{in} takes its minimum. To this end, the function $\dot{\Lambda}(\mathbf{x}, t)$ is selected in such a way that $\dot{\Lambda}(\mathbf{x}, t) \neq 0$ only when the product $\hat{\epsilon}^E(\mathbf{x}, t) \Delta \bar{\epsilon}(\mathbf{x})$ takes its maximum possible value for a given load domain \mathcal{L} . In this case, the external power W_{ex} can be written as

$$W_{ex} = \int_0^T \int_S \tilde{N}_0 \dot{\hat{\epsilon}}_0^E(\mathbf{x}, t) \dot{\Lambda}(\mathbf{x}, t) \Delta \bar{\epsilon}(\mathbf{x}) dS dt = \int_S \tilde{N}_0 \dot{\hat{\epsilon}}_0^E(\mathbf{x}) \Delta \bar{\epsilon}(\mathbf{x}) dS \quad (2.31)$$

in which

$$\dot{\hat{\epsilon}}_0^E(\mathbf{x}) \Delta \bar{\epsilon}(\mathbf{x}) = \max \left(\hat{\epsilon}^E(\mathbf{x}, t) \Delta \bar{\epsilon}(\mathbf{x}) \right). \quad (2.32)$$

By this way, the safety condition against any form of perfectly incremental collapse thus has the form

$$\alpha \int_S \tilde{N}_0 \dot{\hat{\epsilon}}_0^E(\mathbf{x}) \Delta \bar{\epsilon}(\mathbf{x}) dS \leq \int_S D^p(\Delta \bar{\epsilon}) dS. \quad (2.33)$$

If the load variation domain is prescribed by (2.8), (2.9) and (2.11), namely n independently varying loads, the formulation (2.33) becomes

$$\alpha \int_S \sum_{k=1}^n \tilde{N}_0 \dot{\hat{\epsilon}}_0 \bar{\mu}_k \hat{\epsilon}^{Ek}(\mathbf{x}) \Delta \bar{\epsilon}(\mathbf{x}) dS \leq \int_S D^p(\Delta \bar{\epsilon}) dS \quad (2.34)$$

in which

$$\bar{\mu}_k = \begin{cases} \mu_k^+ & \text{if } \hat{\epsilon}^{Ek}(\mathbf{x}) \Delta \bar{\epsilon}(\mathbf{x}) \geq 0 \\ \mu_k^- & \text{if } \hat{\epsilon}^{Ek}(\mathbf{x}) \Delta \bar{\epsilon}(\mathbf{x}) < 0 \end{cases} \quad (2.35)$$

From condition (2.34), the shakedown load multiplier against incremental collapse α^+ can be formulated as a non-linear minimization problem

$$\alpha^+ = \min \left(\frac{W_{in}}{W_{ex}} \right) \quad (2.36)$$

or in normalized form

$$\begin{aligned} \alpha^+ &= \min W_{in} \\ s.t: \quad W_{ex} &= 1 \end{aligned} \quad (2.37)$$

2.2.4.2. Alternating plasticity criterion

If the safety condition against alternating plasticity is considered, the plastic strain field must be satisfied (2.27). The shakedown condition (2.24) in this case has the form

$$\alpha \int_0^T \int_S \tilde{N}_0 \dot{\tilde{\epsilon}}_0 \hat{\sigma}^E(\mathbf{x}, t) \dot{\hat{\epsilon}}(\mathbf{x}, t) dS dt \leq \int_0^T \int_S D^p(\dot{\hat{\epsilon}}) dS dt \quad (2.38)$$

with

$$\alpha > 1, \quad \int_0^T \dot{\hat{\epsilon}}(\mathbf{x}, t) dt = 0 \quad \text{for all } \mathbf{x} \in S. \quad (2.39)$$

Starting from the kinematic theorem and the last constraint in (2.39), the optimization problem leading to the most stringent limit condition can be established at each point \mathbf{x} separately. The global safety factor against alternating plasticity limit will be the *minimum* of local $\alpha(\mathbf{x})$ defined as

$$\begin{aligned} \frac{1}{\alpha(\mathbf{x})} &= \max_{\dot{\tilde{\epsilon}}_{ij}} \int_0^T \tilde{N}_0 \dot{\tilde{\epsilon}}_0 \hat{\sigma}^E(\mathbf{x}, t) \dot{\hat{\epsilon}}(\mathbf{x}, t) dt \\ s.t: \quad &\begin{cases} \int_0^T D^p(\dot{\hat{\epsilon}}) dt = 1 \\ \int_0^T \dot{\hat{\epsilon}}(\mathbf{x}, t) dt = 0 \end{cases} \end{aligned} \quad (2.40)$$

By solving this problem, the static shakedown condition against any form of alternating plasticity can be obtained

A given structure is safe against alternating plasticity if there exists a time-independent generalized stress field \mathbf{p} which, if superimposed on the envelope of elastic generalized stresses, does not violate the yield condition

$$f(\hat{\sigma}^E(\mathbf{x}, t) + \mathbf{p}) \leq 0. \quad (2.41)$$

It should be noted that the stress field \mathbf{p} in (2.41) is an arbitrary time-independent generalized stress field and not necessarily self-equilibrated as that in Melan's theorem (2.16) and (2.17). If we define a general stress response

$$\hat{\boldsymbol{\sigma}}^*(\mathbf{x}) = \sum_{k=1}^n (\bar{\mu}_k + \mu_k) \hat{\boldsymbol{\sigma}}^{Ek}(\mathbf{x}) \quad (2.42)$$

where $\hat{\boldsymbol{\sigma}}^{Ek}(\mathbf{x})$ is the elastic generalized stress field in the reference structure when subjected to the k-th load and

$$\bar{\mu}_k = \frac{\mu_k^+ + \mu_k^-}{2}, \quad |\mu_k| = \frac{\mu_k^+ - \mu_k^-}{2}. \quad (2.43)$$

In view of (2.40), the plastic shakedown load multiplier (lower bound) may be calculated as

$$\alpha = \min_{\mathbf{x}} \frac{1}{F(\hat{\boldsymbol{\sigma}}^*(\mathbf{x}) + \boldsymbol{\rho}(\mathbf{x}))} \quad (2.44)$$

where

$$f = F - 1. \quad (2.45)$$

The sign of μ_k must be chosen so that the value of function F is maximal. By considering the alternating characteristic of the stress corresponding to an alternating strain rate, the optimal time-independent generalized stress field $\boldsymbol{\rho}$ can be defined by

$$\boldsymbol{\rho} = - \sum_{k=1}^n \bar{\mu}_k \hat{\boldsymbol{\sigma}}^{Ek}. \quad (2.46)$$

Then the plastic shakedown limit load multiplier can be finally represented as

$$\alpha = \min_{\mathbf{x}} \frac{1}{F\left(\sum_{k=1}^n \mu_k \hat{\boldsymbol{\sigma}}^{Ek}(\mathbf{x})\right)} \quad (2.47)$$

where all the combinations of the signs \pm must be accounted for.

From equation (2.47) it can be shown that the constant loads have no influence on the plastic fatigue limit if these constant loads do not change the geometry and material properties. Kinematical strain hardening has also no influence on the alternating plasticity limit because it does not change the allowed stress variation. On the other hand, the alternating plasticity limit is proportional to the current material strength for an isotropic strain hardening material [Yan et al., 2003].

As counterparts of the static condition (2.40), a kinematic condition as well as an upper bound of the plastic shakedown load multiplier can be found, see Polizzotto [1993a, b] for further details.

2.2.5 Unified shakedown limit

In practical computation, in most cases it is impossible to apply lower and upper theorems to find directly the shakedown limit defined by the minimum of incremental

plasticity limit and alternating plasticity limit. The difficulty here is the presence of the time-dependent generalized stress field $\hat{\boldsymbol{\sigma}}^E(\mathbf{x}, t)$ in (2.16)÷(2.17) or the time integration in formulation (2.25). These obstacles can be overcome with the help of the following two convex-cycle theorems, introduced by König and Kleiber [1978].

Theorem II.4:

“Shakedown will happen over a given load domain \mathcal{L} if and only if it happens over the convex envelope of \mathcal{L} ”.

Theorem II.5:

“Shakedown will happen over any load path within a given load domain \mathcal{L} if it happens over a cyclic load path containing all vertices of \mathcal{L} ”.

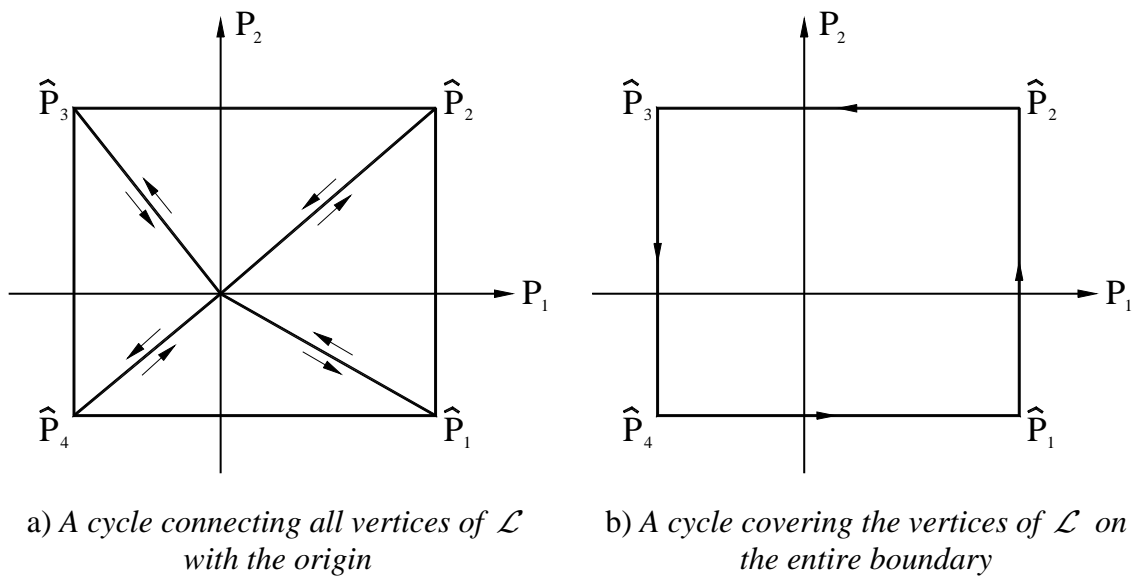


Figure 2.3 Critical cycles of load for shakedown analysis

These theorems, which hold for convex load domains and convex yield surfaces, permit us to consider one cyclic load path instead of all loading history. They allow us to examine only the stress and strain rate fields at every vertex of the given load domain instead of computing an integration over the time cycle. Based on these theorems, König and Kleiber suggested a load scheme as shown in figure 2.3.a for two independently varying loads. This scheme was applied in a simple step-by-step shakedown analysis by Borkowski and Kleiber [1980]. Another scheme (figure 2.3.b) was adopted later by Morelle [1984]. Extensions and implementations of these theorems can also be found in the works of Morelle [1989], Nguyen and Morelle [1990], Polizzotto [1991], Jospin [1992], Yan [1997].

Let us restrict ourselves to the case of a convex polyhedral load domain \mathcal{L} . The question is how to apply the above theorems to eliminate time-dependent elastic generalized stress field $\hat{\mathbf{\sigma}}^E(\mathbf{x}, t)$ and time integrations in the lower and upper shakedown theorems. In order to do so, let us consider a special load cycle $(0, T)$ passing through all vertices of the load domain \mathcal{L} such as

$$\mathbf{P}(\mathbf{x}, t) = \sum_{k=1}^m \mu(t - t_k) \hat{\mathbf{P}}_k(\mathbf{x}) \quad (2.48)$$

where $m = 2^n$ is the total number of vertices of \mathcal{L} , n is the total number of varying loads, $\delta(t_k)$ is the Dirac distribution with the property that

$$f(t_k) = \int_{-\infty}^{\infty} f(x) \delta(t - t_k) dx.$$

Intuitively it is understood by

$$\delta(t - t_k) = \begin{cases} \infty & \text{and } \int_{-\infty}^{\infty} \delta(x) dx = 1 \text{ if } t = t_k \\ 0 & \text{if } t \neq t_k \end{cases} \quad (2.49)$$

We define for eq. (2.48)

$$\mu(t - t_k) = \int_{-\infty}^{\infty} \delta[x - (t - t_k)] dx.$$

Over this load path, the generalized strain at any instant t is represented by

$$\hat{\mathbf{\epsilon}}(t) = \sum_k \mu(t - t_k) \dot{\hat{\mathbf{\epsilon}}}_k. \quad (2.50)$$

At each instant (or at each load vertex), the kinematical condition may not be satisfied, however the accumulated generalized strain over a load cycle

$$\Delta \hat{\mathbf{\epsilon}} = \sum_{k=1}^m \dot{\hat{\mathbf{\epsilon}}}_k \quad (2.51)$$

must be kinematically compatible.

Obviously, the Melan condition required in the whole load domain will be satisfied if and only if it is satisfied at all vertices (or the above special loading cycle) of the domain due to the convex property of load domain and yield function. This remark permits us to replace the time-dependent generalized stress field $\hat{\mathbf{\sigma}}^E(\mathbf{x}, t)$ by its values calculated only at load vertices. We have the following static shakedown theorem

Theorem II.6:

The necessary and sufficient condition for shakedown to occur is that there exists a permanent residual generalized stress field $\bar{\mathbf{p}}(\mathbf{x})$, statically admissible, such that

$$f\left(\hat{\boldsymbol{\sigma}}^E(\mathbf{x}, \hat{P}_k) + \bar{\mathbf{p}}(\mathbf{x})\right) \leq 0 \quad \forall k = \overline{1, m}. \quad (2.52)$$

The application of loading cycle (2.48) also leads to the elimination of time integration in kinematic shakedown condition as stated in the theorem hereafter

Theorem II.7:

The necessary and sufficient condition for shakedown to occur is that there exists a plastic accumulation mechanism $\dot{\hat{\boldsymbol{\varepsilon}}}_k$ such that

$$\begin{cases} \sum_{k=1}^m \int_S \tilde{N}_0 \dot{\hat{\boldsymbol{\varepsilon}}}_0 \left(\hat{\boldsymbol{\sigma}}^E(\mathbf{x}, \hat{P}_k) \right)^T \dot{\hat{\boldsymbol{\varepsilon}}}_k dS \leq \sum_{k=1}^m \int_S D^p(\dot{\hat{\boldsymbol{\varepsilon}}}_k) dS \\ \Delta \hat{\boldsymbol{\varepsilon}} = \sum_{k=1}^m \dot{\hat{\boldsymbol{\varepsilon}}}_k \\ \Delta \hat{\boldsymbol{\varepsilon}} = R[\dot{\mathbf{u}}(\mathbf{x})] \end{cases} \quad (2.53)$$

The bounds of shakedown limit load multiplier (2.18) and (2.25) now can be reformulated in simpler forms corresponding to the static theorem (2.52) and the kinematic theorem (2.53)

1. The lower bound

$$\begin{aligned} \alpha^- &= \max \alpha & (a) \\ \text{s.t.: } \begin{cases} L[\bar{\mathbf{p}}] = 0 & (b) \\ f\left(\alpha \hat{\boldsymbol{\sigma}}^E(\mathbf{x}, \hat{P}_k) + \bar{\mathbf{p}}(\mathbf{x})\right) \leq 0 \quad \forall k = \overline{1, m} & (c) \end{cases} & (2.54) \end{aligned}$$

2. The upper bound (in normalized form)

$$\begin{aligned} \alpha^+ &= \min \sum_{k=1}^m \int_S D^p(\dot{\hat{\boldsymbol{\varepsilon}}}_k) dS & (a) \\ \text{s.t.: } \begin{cases} \Delta \hat{\boldsymbol{\varepsilon}} = \sum_{k=1}^m \dot{\hat{\boldsymbol{\varepsilon}}}_k & (b) \\ \Delta \hat{\boldsymbol{\varepsilon}} = R[\dot{\mathbf{u}}(\mathbf{x})] & (c) \\ \sum_{k=1}^m \int_S \tilde{N}_0 \dot{\hat{\boldsymbol{\varepsilon}}}_0 \left(\hat{\boldsymbol{\sigma}}^E(\mathbf{x}, \hat{P}_k) \right)^T \dot{\hat{\boldsymbol{\varepsilon}}}_k dS = 1 & (d) \end{cases} & (2.55) \end{aligned}$$

Let us note that if there is only one load and this load does not vary then according to load domain definition (2.9) one has

$$\mu_1^- = \mu_1^+. \quad (2.56)$$

In this case it is easy to see that the above upper bound and lower bound reduce to the formulations of upper and lower bounds of limit load factor (2.3) and (2.6). This fact means that limit analysis can be considered as a special case of shakedown analysis.

3 DETERMINISTIC LIMIT AND SHAKEDOWN PROGRAMMING

Based on two theorems, the lower bound and upper bound theorems, different numerical methods for LISA which deal with both linear and non-linear programming were built to analyse complicated structures which analytical tools fail to deal with. In fact it is very cumbersome to use “step-by-step” procedures in solving the problem of limit and shakedown analysis. Direct procedures are thus necessary. With the help of the finite element method, the problem of finding the limit and shakedown load factors can be discretized and transformed into a problem of mathematical programming. In lower bound shakedown analysis, we calculate the interior approximation of the load domain, i.e. we determine the maximum load factor for shakedown. Alternatively, the exterior approximation of the load domain will be sought in upper bound analysis, i.e. we determine the minimum load factor for non-shakedown. Displacement finite elements work best with the upper bound approach in which kinematic conditions are satisfied. Users of the upper bound method sometimes state that the lower bound approach should be used with stress-based finite elements because otherwise the bounding character is lost. Actually, the minimum and maximum problems resulting from the lower bound and upper bound theorems are dual. Studies showed that they converge to the same load factor [Vu et al., 2004, 2007].

Being considered as a non-linear programming technique, the elastic compensation method modifies the Young's modulus of each element during an iterative linear-elastic finite element calculation in order to obtain an optimized statically admissible stress field. An upper bound and a pseudo-lower bound can be obtained after each iteration. In [Taylor et al., 1999], elastic compensation and the deviatoric map have been used for LISA of perfectly plastic shell structures by the finite element method. Recently many large-scale optimization methods have been developed for LISA with continuum finite elements in an European research project [Staat et al., 2003a]. The research showed that today LISA can achieve exact values of the carrying capacity under monotone and under cyclic loading for bounded linearly kinematic hardening material with the potential inclusion of continuum damage and moderately large deformations.

The elasto-plastic analysis of failure loads and failure modes for shell structures has been a problem of great interest to many designers. This can be achieved by performing a multi-layer analysis which requires the knowledge of the stress distribution through the thickness and thus requires extensive computing resources both of time and storage. The

more effective method is to deal with a single layer analysis which relates to stress resultants. However, in this case well-formulated finite element methods for the direct evaluation of shakedown limits are currently still rare due to the complexity of geometrical shape and the mathematical difficulties in the stress resultant yield criterion. Franco and Ponter [1997a, b] developed an approximate technique which is based on the reformulation of the kinematic shakedown theorem for an axisymmetric shell with piecewise linear yield conditions. Yan and Nguyen Dang [2000] proposed an approximate stress distribution through the thickness of the shell and simplified the von Mises criterion for generalized variables to get a yield condition in stress resultants. Bisbos and Papaioannou [2006], Bisbos and Pardalos [2007] formulated a lower bound shakedown analysis of steel shells as a specific mathematical optimization problem known as second-order cone programming by using the linear approximation of the exact Ilyushin yield surface (usually referred to as Ilyushin's generalized yield model)

In this chapter, we present a kinematic approach of limit and shakedown analysis, which is adopted for shell structures [Tran et al., 2007a, c, e]. The approach was initially proposed by Zhang [1995b] and further developed by Liu et al. [1997], Carvelli et al. [1999]. Vu [2001] applied this in conjunction with Newton's method to establish a numerical algorithm for dual shakedown limits. Starting from a finite element discretization, a detailed kinematic algorithm in terms of generalized variables will be formulated and introduced. A simple technique for overcoming numerical obstacles, such as non-smooth and singular objective functions, is also proposed.

3.1 Finite element discretization

By subdividing the whole middle surface S into elements S_e , the integration (2.33.a) becomes

$$\sum_{k=1}^m \sum_{e=1}^{ne} \int_{S_e} D^p(\dot{\mathbf{\epsilon}}_k) dS \quad (3.1)$$

where m is the number of vertices of the load domain \mathcal{L} and ne is the total number of elements. The two major numerical obstacles that appear here in dissipation function are

- the value of K_0 in the expression of the dissipation function $D^p(\dot{\mathbf{\epsilon}}_k)$ may become infinite in the case of $\gamma = 0$ (as mentioned in the first chapter).
- if the rigid or elastic perfectly plastic material model is adopted with the Ilyushin yield criterion, the objective function (3.1) is only differentiable in the plastified region of structures while powerful optimization methods require its gradient to be available everywhere.

Being considered as a special case of shakedown analysis, limit analysis based on kinematic formulation suffers from the same difficulty. Dealing with singular dissipation function in limit analysis, Andersen et al. [1995, 1998a, 1998b, 2000] introduced a

“smooth regularization method” by replacing the original dissipation function $D^p(\dot{\mathbf{\epsilon}}_k)$ by its disturbed one $D^p(\dot{\mathbf{\epsilon}}_k, \eta_0^2)$. In this function η_0 is a very small number and by that way all elements are seen as plastified or on the plastified verge. The technique is actually the whole-region regularization method mentioned in [Yan, 1997] and will be adopted here in our analysis.

In order to overcome the two obstacles above, we replace γ and the bending strain resultant intensity \hat{P}_κ in the expression of the dissipation function by the new ones $\gamma + \eta_0^2$ and $\hat{P}_\kappa + \eta_0^2$. By that way, the dissipation function is finite and differentiable everywhere, even in the non-plastified region. Furthermore, since the bending strain resultant intensity \hat{P}_κ is non-null, thus, the dissipation function now is

$$D^p(\dot{\mathbf{\epsilon}}_k, \eta_0^2) = Y\tilde{N}_0\dot{\tilde{\epsilon}}_0\sqrt{\frac{\hat{P}_\kappa}{3}}\left(\beta_1\sqrt{\beta_1^2 + \gamma} + \beta_2\sqrt{\beta_2^2 + \gamma} + \gamma K_0\right) \quad (3.2)$$

with $\beta_1, \beta_2, K_0, \gamma$ calculated by Eqs. (1.78) and (1.62). It is to be noted that, the quadratic strain resultant intensities now become

$$\begin{aligned} \hat{P}_\varepsilon &= \frac{3}{4}(\dot{\mathbf{\epsilon}}_k)^T \mathbf{P}_1 \dot{\mathbf{\epsilon}}_k \quad (\geq 0) \\ \hat{P}_{\varepsilon\kappa} &= 3(\dot{\mathbf{\epsilon}}_k)^T \mathbf{P}_2 \dot{\mathbf{\epsilon}}_k \\ \hat{P}_\kappa &= 12(\dot{\mathbf{\epsilon}}_k)^T \mathbf{P}_3 \dot{\mathbf{\epsilon}}_k + \eta_0^2 \quad (>0) \end{aligned} \quad (3.3)$$

where $\dot{\mathbf{\epsilon}}_k$ is the generalized strain rate vector corresponding to load vertex \hat{P}_k ,

$$\dot{\mathbf{\epsilon}}_k = \begin{bmatrix} \frac{1}{\dot{\tilde{\epsilon}}_0} \dot{\tilde{\epsilon}}_{11}^k & \frac{1}{\dot{\tilde{\epsilon}}_0} \dot{\tilde{\epsilon}}_{22}^k & \frac{1}{\dot{\tilde{\epsilon}}_0} 2\dot{\tilde{\epsilon}}_{12}^k & \frac{1}{\dot{\tilde{\kappa}}_0} \dot{\tilde{\kappa}}_{11}^k & \frac{1}{\dot{\tilde{\kappa}}_0} \dot{\tilde{\kappa}}_{22}^k & \frac{1}{\dot{\tilde{\kappa}}_0} 2\dot{\tilde{\kappa}}_{12}^k \end{bmatrix}^T. \quad (3.4)$$

It should be noted that the incompressibility condition, although it is true for plastic deformation of metal, introduces some numerical difficulties. Fortunately, by using plane stress or shell-type finite elements, this condition can be naturally achieved by adopting the Kirchhoff's hypothesis. This can reduce the computational cost in the optimization process.

The integrations $\int_{S_e} D^p(\dot{\mathbf{\epsilon}}_k) dS$ in objective function (3.1) are calculated by Gauss-

Legendre integration technique. From equations (3.1) and (3.2) one has

$$\begin{aligned} \sum_{k=1}^m \sum_{e=1}^{ne} \int_{S_e} D^p(\dot{\mathbf{\epsilon}}_k) dS &= \sum_{k=1}^m \sum_{e=1}^{ne} \int_{S_e} Y\tilde{N}_0\dot{\tilde{\epsilon}}_0\sqrt{\frac{\hat{P}_\kappa}{3}}\left(\beta_1\sqrt{\beta_1^2 + \gamma} + \beta_2\sqrt{\beta_2^2 + \gamma} + \gamma K_0\right) dS \\ &= \sum_{k=1}^m \sum_{i=1}^{NG} w_i Y\tilde{N}_0\dot{\tilde{\epsilon}}_0\sqrt{\frac{\hat{P}_\kappa}{3}}\left(\beta_1\sqrt{\beta_1^2 + \gamma} + \beta_2\sqrt{\beta_2^2 + \gamma} + \gamma K_0\right) \end{aligned} \quad (3.5)$$

where w_i is the weighting factor of the Gauss point i . The same integration technique is applied to evaluate external power (2.33.d)

$$\begin{aligned} \sum_{k=1}^m \int_S \tilde{N}_0 \dot{\tilde{\epsilon}}_0 \left(\hat{\sigma}^E(\mathbf{x}, \hat{P}_k) \right)^T \dot{\hat{\epsilon}}_k dS &= \sum_{k=1}^m \sum_{e=1}^{ne} \int_{S_e} \tilde{N}_0 \dot{\tilde{\epsilon}}_0 \left(\hat{\sigma}^E(\mathbf{x}, \hat{P}_k) \right)^T \dot{\hat{\epsilon}}_k dS \\ &= \sum_{k=1}^m \sum_{i=1}^{NG} w_i \tilde{N}_0 \dot{\tilde{\epsilon}}_0 \dot{\hat{\epsilon}}_{ik}^T \hat{\sigma}_{ik}^E \end{aligned} \quad (3.6)$$

where $\dot{\hat{\epsilon}}_{ik}$ denotes the plastic generalized strain rate vector corresponding to vertex k of the load domain and calculated at the Gauss point i in the structure. The compatible condition (2.33.c) is verified at each Gauss point i

$$\sum_{k=1}^m \dot{\hat{\epsilon}}_{ik} = \mathbf{B}_i \dot{\mathbf{u}} \quad (3.7)$$

with \mathbf{B}_i denotes the deformation matrix $\mathbf{B}(\mathbf{x})$ at Gauss point i .

From (3.5÷3.7) the shakedown limit load multiplier may be formulated as

$$\begin{aligned} \alpha^+ &= \min \sum_{k=1}^m \sum_{i=1}^{NG} w_i Y \tilde{N}_0 \dot{\tilde{\epsilon}}_0 \sqrt{\frac{\hat{P}_\kappa}{3}} \left(\beta_1 \sqrt{\beta_1^2 + \gamma} + \beta_2 \sqrt{\beta_2^2 + \gamma} + \gamma K_0 \right) \\ \text{s.t: } &\begin{cases} \sum_{k=1}^m \dot{\hat{\epsilon}}_{ik} = \mathbf{B}_i \dot{\mathbf{u}} & \forall i = \overline{1, NG} \\ \sum_{k=1}^m \sum_{i=1}^{NG} w_i \tilde{N}_0 \dot{\tilde{\epsilon}}_0 \dot{\hat{\epsilon}}_{ik}^T \hat{\sigma}_{ik}^E = 1 \end{cases} \end{aligned} \quad (3.8)$$

In the above formulation, for simplicity, the sums over all elements and over all Gauss points of one element (in the expressions of internal and external powers) are unified in the sum over all Gauss points of discretized structure. The total number of Gauss points in structure is $NG = ne \times ng$, where ng is the number of Gauss point on an element.

3.2 Kinematic algorithm

By restricting ourselves to polyhedral form of load domain, in this section we introduce a kinematic algorithm for limit and shakedown analysis of shell structures. To begin with, for the sake of simplicity, let us rewrite the upper bound limit (3.8) in a simpler form by introducing some new notations

- The new strain rate vector $\dot{\mathbf{e}}_{ik}$

$$\dot{\mathbf{e}}_{ik} = w_i \dot{\hat{\epsilon}}_{ik} \quad (3.9)$$

- The new fictitious elastic generalized stress field \mathbf{t}_{ik}

$$\mathbf{t}_{ik} = \tilde{N}_0 \dot{\tilde{\epsilon}}_0 \hat{\sigma}_{ik}^E \quad (3.10)$$

- The new deformation matrix $\hat{\mathbf{B}}_i$

$$\hat{\mathbf{B}}_i = w_i \mathbf{B}_i. \quad (3.11)$$

Following these definitions, the objective function in (3.8) becomes

$$\alpha^+ = \min \sum_{k=1}^m \sum_{i=1}^{NG} Y \tilde{N}_0 \dot{\tilde{\epsilon}}_0 \sqrt{\frac{\hat{P}_\kappa}{3}} \left(\beta_1 \sqrt{\beta_1^2 + \gamma} + \beta_2 \sqrt{\beta_2^2 + \gamma} + \gamma K_0 \right) \quad (3.12)$$

where β_1 , β_2 , γ , K_0 , \hat{P}_κ are calculated by Eqs. (1.72), (1.62), (1.66) and (3.3) in which the generalized strain vector $\dot{\tilde{\epsilon}}_{ik}$ is replaced by the rate $\dot{\epsilon}_{ik}$. It is to be noted that this replacing does not affect the value of β_1 , β_2 , γ , K_0 , but \hat{P}_κ .

By substituting (3.9)÷(3.12) into (3.8) one obtains a simplified version for upper bound of shakedown limit load

$$\begin{aligned} \alpha^+ = \min & \sum_{k=1}^m \sum_{i=1}^{NG} Y \tilde{N}_0 \dot{\tilde{\epsilon}}_0 \sqrt{\frac{\hat{P}_\kappa}{3}} \left(\beta_1 \sqrt{\beta_1^2 + \gamma} + \beta_2 \sqrt{\beta_2^2 + \gamma} + \gamma K_0 \right) \\ \text{s.t:} & \begin{cases} \sum_{k=1}^m \dot{\epsilon}_{ik} = \hat{\mathbf{B}}_i \dot{\mathbf{u}} & \forall i = \overline{1, NG} \\ \sum_{k=1}^m \sum_{i=1}^{NG} \dot{\epsilon}_{ik}^T \mathbf{t}_{ik} = 1 \end{cases} \end{aligned} \quad (3.13)$$

Dealing with the non-linear constrained optimization problem (3.13), the penalty method is used for satisfying the compatibility condition. To this purpose, let us write the penalty function as

$$F_p = \sum_{i=1}^{NG} \left\{ \sum_{k=1}^m \left(Y \tilde{N}_0 \dot{\tilde{\epsilon}}_0 \sqrt{\frac{\hat{P}_\kappa}{3}} \left(\beta_1 \sqrt{\beta_1^2 + \gamma} + \beta_2 \sqrt{\beta_2^2 + \gamma} + \gamma K_0 \right) \right) + \frac{c}{2} \left(\sum_{k=1}^m \dot{\epsilon}_{ik} - \hat{\mathbf{B}}_i \dot{\mathbf{u}} \right)^T \left(\sum_{k=1}^m \dot{\epsilon}_{ik} - \hat{\mathbf{B}}_i \dot{\mathbf{u}} \right) \right\} \quad (3.14)$$

where c is penalty parameter such that $c \gg 1$. This parameter c may be dependent on integration points or load vertices and c should be adjusted to fit different compatibility criteria. However, at this stage, for the sake of simplicity, c is let to be constant everywhere. Theoretically, when c goes to infinity we will recover related conditions.

Following (3.14) the modified kinematic formulation (3.13) becomes

$$\begin{aligned} \alpha^+ = \min & F_p & (a) \\ \text{s.t:} & & (3.15) \\ & \sum_{i=1}^{NG} \sum_{k=1}^m \dot{\epsilon}_{ik}^T \mathbf{t}_{ik} = 1 & (b) \end{aligned}$$

The corresponding Lagrange function of (3.15) is

$$F_{PL} = F_P - \lambda \left(\sum_{i=1}^{NG} \sum_{k=1}^m \dot{\mathbf{e}}_{ik}^T \mathbf{t}_{ik} - 1 \right). \quad (3.16)$$

Obviously, the normalization can be also treated by a penalty method, which may help to remove the Langrangian multiplier λ from our problem. However, the application of a penalty method to (3.15.b) leads to a system of equations which requires more effort and computer memory to solve. For this reason that λ is retained as variable and will be handled later on. The stationarity condition for the Lagrange function F_{PL} states that

$$\left\{ \begin{aligned} & \frac{\partial F_{PL}}{\partial \dot{\mathbf{e}}_{ik}} = Y \tilde{N}_0 \dot{\tilde{\mathbf{e}}}_0 \left(\frac{4\sqrt{3}}{\sqrt{\hat{P}_\kappa}} \left(\beta_1 \sqrt{\beta_1^2 + \gamma} + \beta_2 \sqrt{\beta_2^2 + \gamma} + \gamma K_0 \right) \mathbf{P}_3 \right. \\ & \quad \left. + \frac{4\sqrt{3}}{\sqrt{\hat{P}_\kappa}} \left(\sqrt{\beta_1^2 + \gamma} - \sqrt{\beta_2^2 + \gamma} \right) (\mathbf{P}_2 + 4\beta \mathbf{P}_3) \right) \dot{\mathbf{e}}_{ik} \\ & \quad \left. + \frac{\sqrt{3}}{2\sqrt{\hat{P}_\kappa}} K_0 (\mathbf{P}_1 + 8\beta \mathbf{P}_2 - 16(\gamma - \beta^2) \mathbf{P}_3) \right) \\ & \quad + c \left(\sum_{k=1}^m \dot{\mathbf{e}}_{ik} - \hat{\mathbf{B}}_i \dot{\mathbf{u}} \right) - \lambda \mathbf{t}_{ik} = \mathbf{0} \quad \forall i, k \quad (a) \\ & \frac{\partial F_{PL}}{\partial \dot{\mathbf{u}}} = -c \sum_{i=1}^{NG} \hat{\mathbf{B}}_i^T \left(\sum_{k=1}^m \dot{\mathbf{e}}_{ik} - \hat{\mathbf{B}}_i \dot{\mathbf{u}} \right) = \mathbf{0} \quad (b) \\ & \frac{\partial F_{PL}}{\partial \lambda} = \left(\sum_{i=1}^{NG} \sum_{k=1}^m \dot{\mathbf{e}}_{ik}^T \mathbf{t}_{ik} - 1 \right) = 0 \quad (c) \end{aligned} \right. \quad (3.17)$$

The first equation of (3.17) can be rewritten in the following form

$$Y \tilde{N}_0 \dot{\tilde{\mathbf{e}}}_0 \left(\begin{aligned} & 4\sqrt{3} \left(\beta_1 \sqrt{\beta_1^2 + \gamma} + \beta_2 \sqrt{\beta_2^2 + \gamma} + \gamma K_0 \right) \mathbf{P}_3 \\ & + 4\sqrt{3} \left(\sqrt{\beta_1^2 + \gamma} - \sqrt{\beta_2^2 + \gamma} \right) (\mathbf{P}_2 + 4\beta \mathbf{P}_3) \\ & + \frac{\sqrt{3}}{2} K_0 (\mathbf{P}_1 + 8\beta \mathbf{P}_2 - 16(\gamma - \beta^2) \mathbf{P}_3) \end{aligned} \right) \dot{\mathbf{e}}_{ik} + c \sqrt{\hat{P}_\kappa} \left(\sum_{k=1}^m \dot{\mathbf{e}}_{ik} - \hat{\mathbf{B}}_i \dot{\mathbf{u}} \right) - \lambda \sqrt{\hat{P}_\kappa} \mathbf{t}_{ik} = \mathbf{0}. \quad (3.18)$$

This form of stationary condition will help us reduce numerical difficulty in singular situation when $\sqrt{\hat{P}_\kappa} \rightarrow 0$. This means that (3.18) may be satisfied even when there is no plastic deformation and η_0 is set equal to zero while in the same conditions the equation (3.17.a) is indefinite. For convenience, let us rewrite Eqs. (3.18), (3.17.b) and (3.17.c) as follows

$$\begin{cases}
\mathbf{H}_{ik} \dot{\mathbf{e}}_{ik} + c\sqrt{\hat{P}_\kappa} \left(\sum_{k=1}^m \dot{\mathbf{e}}_{ik} - \hat{\mathbf{B}}_i \dot{\mathbf{u}} \right) - \lambda \sqrt{\hat{P}_\kappa} \mathbf{t}_{ik} = \mathbf{0} = \mathbf{f}_{ik} & (a) \\
\sum_{i=1}^{NG} \hat{\mathbf{B}}_i^T \left(\sum_{k=1}^m \dot{\mathbf{e}}_{ik} - \hat{\mathbf{B}}_i \dot{\mathbf{u}} \right) = \mathbf{0} = \sum_{i=1}^{NG} \mathbf{h}_i & (b) \\
\sum_{i=1}^{NG} \sum_{k=1}^m \dot{\mathbf{e}}_{ik}^T \mathbf{t}_{ik} - 1 = 0 & (c)
\end{cases} \quad (3.19)$$

where

$$\mathbf{H}_{ik} = Y\tilde{N}_0 \dot{\tilde{\mathbf{e}}}_0 \begin{pmatrix} 4\sqrt{3} \left(\beta_1 \sqrt{\beta_1^2 + \gamma} + \beta_2 \sqrt{\beta_2^2 + \gamma} + \gamma K_0 \right) \mathbf{P}_3 \\ + 4\sqrt{3} \left(\sqrt{\beta_1^2 + \gamma} - \sqrt{\beta_2^2 + \gamma} \right) (\mathbf{P}_2 + 4\beta \mathbf{P}_3) \\ + \frac{\sqrt{3}}{2} K_0 (\mathbf{P}_1 + 8\beta \mathbf{P}_2 - 16(\gamma - \beta^2) \mathbf{P}_3) \end{pmatrix} \quad (3.20)$$

By applying Newton-Raphson's method to solve the modified system (3.19) one gets

$$\begin{cases}
\mathbf{M}_{ik} d\dot{\mathbf{e}}_{ik} + c\sqrt{\hat{P}_\kappa} \left(\sum_{k=1}^m d\dot{\mathbf{e}}_{ik} - \hat{\mathbf{B}}_i d\dot{\mathbf{u}} \right) - d\lambda \sqrt{\hat{P}_\kappa} \mathbf{t}_{ik} = -\mathbf{f}_{ik} & (a) \\
\sum_{i=1}^{NG} \hat{\mathbf{B}}_i^T \left(\sum_{k=1}^m d\dot{\mathbf{e}}_{ik} - \hat{\mathbf{B}}_i d\dot{\mathbf{u}} \right) = -\sum_{i=1}^{NG} \mathbf{h}_i & (b) \\
\sum_{i=1}^{NG} \sum_{k=1}^m d\dot{\mathbf{e}}_{ik}^T \mathbf{t}_{ik} = -\sum_{i=1}^{NG} \sum_{k=1}^m \dot{\mathbf{e}}_{ik}^T \mathbf{t}_{ik} + 1 & (c)
\end{cases} \quad (3.21)$$

where

$$\mathbf{M}_{ik} = \mathbf{H}_{ik} + \mathbf{D}_{ik} + \frac{12}{\sqrt{\hat{P}_\kappa}} \left(c \left(\sum_{k=1}^m \dot{\mathbf{e}}_{ik} - \hat{\mathbf{B}}_i \dot{\mathbf{u}} \right) - \lambda \mathbf{t}_{ik} \right) \dot{\mathbf{e}}_{ik}^T \mathbf{P}_3 \quad (3.22)$$

with

$$\begin{aligned}
\mathbf{D}_{ik} = & Y\tilde{N}_0\dot{\tilde{\epsilon}}_0 \left(\begin{aligned} & \left(-\frac{48\sqrt{3}}{\hat{P}_\kappa} \left(\sqrt{\beta_1^2 + \gamma} - \sqrt{\beta_2^2 + \gamma} \right) \mathbf{P}_3 + \frac{24\sqrt{3}}{\hat{P}_\kappa} \left(\frac{\beta_1}{\sqrt{\beta_1^2 + \gamma}} + \frac{\beta_2}{\sqrt{\beta_2^2 + \gamma}} \right) \mathbf{A} \right) \dot{\mathbf{e}}_{ik} \dot{\mathbf{e}}_{ik}^T \mathbf{A} \\ & + \frac{3\sqrt{3}}{\hat{P}_\kappa} \left(\frac{1}{\sqrt{\beta_1^2 + \gamma}} - \frac{1}{\sqrt{\beta_2^2 + \gamma}} \right) \mathbf{B} - \frac{24\sqrt{3}}{\hat{P}_\kappa} K_0 \mathbf{P}_2 \end{aligned} \right) \\
& + \left(\begin{aligned} & \frac{3\sqrt{3}}{\hat{P}_\kappa} \left(\frac{1}{\sqrt{\beta_1^2 + \gamma}} - \frac{1}{\sqrt{\beta_2^2 + \gamma}} \right) \mathbf{A} \\ & + \frac{3\sqrt{3}}{8\hat{P}_\kappa} \left(\frac{1}{\sqrt{\beta_1^2 + \gamma} \left(\sqrt{\beta_1^2 + \gamma} + \beta_1 \right)} - \frac{1}{\sqrt{\beta_2^2 + \gamma} \left(\sqrt{\beta_2^2 + \gamma} - \beta_2 \right)} \right) \mathbf{B} \end{aligned} \right) \dot{\mathbf{e}}_{ik} \dot{\mathbf{e}}_{ik}^T \mathbf{B} \\
& - \frac{6\sqrt{3}}{\hat{P}_\kappa} K_0 \mathbf{P}_3 \dot{\mathbf{e}}_{ik} \dot{\mathbf{e}}_{ik}^T \mathbf{C}
\end{aligned} \right)
\end{aligned}$$

$$\begin{aligned}
\mathbf{A} &= \mathbf{P}_2 + 4\beta\mathbf{P}_3 \\
\mathbf{B} &= \mathbf{P}_1 + 8\beta\mathbf{P}_2 - 16(\gamma - \beta^2)\mathbf{P}_3 \\
\mathbf{C} &= \mathbf{P}_1 + 24\beta\mathbf{P}_2 - 16(\gamma - 5\beta^2)\mathbf{P}_3
\end{aligned} \tag{3.23}$$

In the system (3.21) $d\dot{\mathbf{e}}_{ik}$, $d\dot{\mathbf{u}}$ denote the incremental vectors of generalized strain rate and displacement respectively while $d\lambda$ denotes the incremental value of λ . By moving the last two terms in (3.21.a) to left-hand side and then, multiplying both sides with \mathbf{M}_{ik}^{-1} we get

$$d\dot{\mathbf{e}}_{ik} = -\mathbf{M}_{ik}^{-1}\mathbf{f}_{ik} - c\sqrt{\hat{P}_\kappa}\mathbf{M}_{ik}^{-1} \left(\sum_{k=1}^m d\dot{\mathbf{e}}_{ik} - \hat{\mathbf{B}}_i d\dot{\mathbf{u}} \right) + d\lambda\sqrt{\hat{P}_\kappa}\mathbf{M}_{ik}^{-1}\mathbf{t}_{ik}. \tag{3.24}$$

Writing (3.24) for $k = \overline{1, m}$ and summing them up, after some manipulations one has

$$\sum_k^m d\dot{\mathbf{e}}_{ik} = -\mathbf{E}_i^{-1} \sum_k^m \mathbf{M}_{ik}^{-1}\mathbf{f}_{ik} + c\mathbf{E}_i^{-1} \sum_k^m \sqrt{\hat{P}_\kappa}\mathbf{M}_{ik}^{-1}\hat{\mathbf{B}}_i d\dot{\mathbf{u}} + d\lambda\mathbf{E}_i^{-1} \sum_k^m \sqrt{\hat{P}_\kappa}\mathbf{M}_{ik}^{-1}\mathbf{t}_{ik} \tag{3.25}$$

where

$$\mathbf{E}_i = \mathbf{I}_i + c \sum_k^m \sqrt{\hat{P}_\kappa}\mathbf{M}_{ik}^{-1} \tag{3.26}$$

and \mathbf{I}_i is the identity matrix.

The substitution of (3.25) in (3.21.b) leads to

$$\sum_{i=1}^{NG} \hat{\mathbf{B}}_i^T \mathbf{K} \mathbf{B}_i d\dot{\mathbf{u}} = \sum_{i=1}^{NG} \mathbf{h}_i - \sum_{i=1}^{NG} \hat{\mathbf{B}}_i^T \mathbf{E}_i^{-1} \sum_k^m \mathbf{M}_{ik}^{-1} \mathbf{f}_{ik} + d\lambda \sum_{i=1}^{NG} \hat{\mathbf{B}}_i^T \mathbf{E}_i^{-1} \sum_k^m \sqrt{\hat{P}_\kappa} \mathbf{M}_{ik}^{-1} \mathbf{t}_{ik} \quad (3.27)$$

where

$$\mathbf{K} = \mathbf{I} - c \mathbf{E}_i^{-1} \sum_k^m \sqrt{\hat{P}_\kappa} \mathbf{M}_{ik}^{-1}. \quad (3.28)$$

Starting from the definition of \mathbf{E}_i , Eq. (3.26), we can further simplify (3.28) as

$$\mathbf{K} = \mathbf{I} - c \mathbf{E}_i^{-1} \sum_k^m \sqrt{\hat{P}_\kappa} \mathbf{M}_{ik}^{-1} = \mathbf{I} - \mathbf{E}_i^{-1} (\mathbf{E}_i - \mathbf{I}) = \mathbf{E}_i^{-1}. \quad (3.29)$$

By introducing (3.29) in (3.27) and take into account Eqs. (3.21.a), (3.21.b), one has the following system

$$\mathbf{S} d\dot{\mathbf{u}} = -\mathbf{S} \dot{\mathbf{u}} + \mathbf{f}_1 + \mathbf{f}_2 (\lambda + d\lambda) \quad (3.30)$$

where

$$\begin{cases} \mathbf{S} = \sum_{i=1}^{NG} \hat{\mathbf{B}}_i^T \mathbf{E}_i^{-1} \hat{\mathbf{B}}_i & (a) \\ \mathbf{f}_1 = \sum_{i=1}^{NG} \hat{\mathbf{B}}_i^T \mathbf{E}_i^{-1} \sum_{k=1}^m \mathbf{M}_{ik}^{-1} (\mathbf{M}_{ik} - \mathbf{H}_{ik}) \dot{\mathbf{e}}_{ik} & (b) \\ \mathbf{f}_2 = \sum_{i=1}^{NG} \hat{\mathbf{B}}_i^T \mathbf{E}_i^{-1} \sum_k^m \sqrt{\hat{P}_\kappa} \mathbf{M}_{ik}^{-1} \mathbf{t}_{ik} & (c) \end{cases} \quad (3.31)$$

The system (3.30) with the last two terms on the right-hand side may be interpreted as the linear system arising in purely elastic computations with the global stiffness matrix \mathbf{S} and applied force vector $[\mathbf{f}_1 + \mathbf{f}_2 (\lambda + d\lambda)]$. The matrix \mathbf{E}_i^{-1} plays the role of the elastic matrix at the Gauss point i while the vector

$$\mathbf{f} = \mathbf{f}_1 + \mathbf{f}_2 (\lambda + d\lambda) \quad (3.32)$$

can be considered as the vector of nodal forces applied on the structure. A difficulty arises here in the system (3.30) due to a non-symmetry of the matrix \mathbf{S} . In order to reduce the computational costs, one can make the matrix \mathbf{E}_i^{-1} symmetric by

$$\mathbf{E}_i^{-1} = \frac{1}{2} (\mathbf{E}_i^{-1} + (\mathbf{E}_i^{-1})^T). \quad (3.33)$$

From (3.30), (3.25), and (3.24) and after some manipulations we get the incremental vectors of displacement and strain rate as

$$\begin{cases} d\dot{\mathbf{u}} = d\dot{\mathbf{u}}_1 + d\dot{\mathbf{u}}_2 (\lambda + d\lambda) & (a) \\ d\dot{\mathbf{e}}_{ik} = (d\dot{\mathbf{e}}_{ik})_1 + (d\dot{\mathbf{e}}_{ik})_2 (\lambda + d\lambda) & (b) \end{cases} \quad (3.34)$$

where

$$\begin{cases} d\dot{\mathbf{u}}_1 = -\dot{\mathbf{u}} + \mathbf{S}^{-1}\mathbf{f}_1 \\ d\dot{\mathbf{u}}_2 = \mathbf{S}^{-1}\mathbf{f}_2 \\ (d\dot{\mathbf{e}}_{ik})_1 = c\sqrt{\hat{P}_\kappa}\mathbf{M}_{ik}^{-1}\mathbf{E}_i^{-1}\left(\sum_k^m \mathbf{M}_{ik}^{-1}\mathbf{H}_{ik}\dot{\mathbf{e}}_{ik} + \hat{\mathbf{B}}_i d\dot{\mathbf{u}}_1 - \left(\sum_{k=1}^m \dot{\mathbf{e}}_{ik} - \hat{\mathbf{B}}_i \dot{\mathbf{u}}\right)\right) - \mathbf{M}_{ik}^{-1}\mathbf{H}_{ik}\dot{\mathbf{e}}_{ik} \\ (d\dot{\mathbf{e}}_{ik})_2 = -c\sqrt{\hat{P}_\kappa}\mathbf{M}_{ik}^{-1}\mathbf{E}_i^{-1}\left(-\hat{\mathbf{B}}_i d\dot{\mathbf{u}}_2 + \sum_k^m \sqrt{\hat{P}_\kappa}\mathbf{M}_{ik}^{-1}\mathbf{t}_{ik}\right) + \sqrt{\hat{P}_\kappa}\mathbf{M}_{ik}^{-1}\mathbf{t}_{ik} \end{cases} \quad (3.35)$$

The vectors $d\dot{\mathbf{u}}$, $d\dot{\mathbf{e}}_{ik}$ are actually Newton's directions which assure that a suitable step along them will lead to a decrease of the objective function.

In order to compute $(d\lambda + \lambda)$ we substitute (3.34.b) into (3.21.c) and have

$$(\lambda + d\lambda) = \left[\frac{1 - \sum_{i=1}^{NG} \sum_{k=1}^m \mathbf{t}_{ik}^T (\dot{\mathbf{e}}_{ik} + (d\dot{\mathbf{e}}_{ik})_1)}{\sum_{i=1}^{NG} \sum_{k=1}^m \mathbf{t}_{ik}^T (d\dot{\mathbf{e}}_{ik})_2} \right]. \quad (3.36)$$

Based on (3.34) we can update the displacement vector $\dot{\mathbf{u}}$ and the global generalized strain rate vector $\dot{\mathbf{e}}$

$$\dot{\mathbf{e}} = [\dot{\mathbf{e}}_{11} \quad \dots \quad \dot{\mathbf{e}}_{ik} \quad \dots \quad \dot{\mathbf{e}}_{NG,m}]^T. \quad (3.37)$$

The new vectors of $\dot{\mathbf{u}}$ and $\dot{\mathbf{e}}$ tend to satisfy (3.17.b) and (3.18) simultaneously. By forcing them to fulfil (3.17.c) we get Lagrange multiplier λ updated as $(d\lambda + \lambda)$ in (3.36). Iterating these steps may drive us to a stable set of $\dot{\mathbf{u}}$, $\dot{\mathbf{e}}$, λ satisfying all conditions (3.17.b), and (3.17.c) and (3.18). Details of the iterative algorithm are presented hereafter.

• Step 1: Initialize displacement and strain rate vectors: $\dot{\mathbf{u}}^0$ and $\dot{\mathbf{e}}^0$ such that the normalized condition (3.17.c) is satisfied

$$\sum_{i=1}^{NG} \sum_{k=1}^m \mathbf{t}_{ik}^T \dot{\mathbf{e}}_{ik}^0 = 1. \quad (3.38)$$

Normally the fictitious solution must be computed first in order to define the load domain \mathcal{L} in terms of the fictitious elastic generalized stress $\hat{\boldsymbol{\sigma}}_{ik}^E$. Hence $\dot{\mathbf{u}}^0$ and $\dot{\mathbf{e}}^0$ may assume fictitious values (after being normalized) for their initialization. Set up initial values for the penalty parameter c and for η_0 . Set up convergence criteria, maximum number of iterations.

• Step 2: Calculate \mathbf{S} , \mathbf{f}_1 and \mathbf{f}_2 from (3.31) at current values of $\dot{\mathbf{u}}$ and $\dot{\mathbf{e}}$

• Step 3: Calculate $(d\lambda + \lambda)$, $d\dot{\mathbf{u}}$, $d\dot{\mathbf{e}}_{ik}$ from Eqs. (3.34) and (3.36)

• Step 4: Perform a line search to find Λ_s such that

$$F_p(\dot{\mathbf{u}} + \Lambda_s d\dot{\mathbf{u}}, \dot{\mathbf{e}} + \Lambda_s d\dot{\mathbf{e}}) \rightarrow \min. \quad (3.39)$$

Update displacement, strain rate and λ as

$$\begin{aligned} \dot{\mathbf{u}} &= \dot{\mathbf{u}} + \Lambda_s d\dot{\mathbf{u}} & (a) \\ \dot{\mathbf{e}}_{ik} &= \dot{\mathbf{e}}_{ik} + \Lambda_s d\dot{\mathbf{e}}_{ik} & (b) \\ \lambda &= \lambda + d\lambda & (c) \end{aligned} \quad (3.40)$$

As was shown above, it is costly to get the analytical form of the derivatives of the objective function. Thus, a line search without using the derivatives is recommended here, e.g. the Golden section method.

• Step 5: Check convergence criteria: if they are all satisfied go to step 6 otherwise repeat steps 2, 3 and 4.

• Step 6: Stop

The algorithm can fail due to some reasons: failure in computing the inverse matrix \mathbf{S}^{-1} or unsuccessful initialization step, which after some iterations results in an unexpected form

$$\sum_{i=1}^{NG} \sum_{k=1}^m \mathbf{t}_{ik}^T \dot{\mathbf{e}}_{ik}^0 = 0$$

or the maximum number of iterations is insufficient to get a convergent solution. If those obstacles do not exist, a solution set $(\dot{\mathbf{u}}, \bar{\mathbf{e}}, \bar{\lambda})$ can be found as proved in [Vu, 2001].

4 PROBABILISTIC LIMIT AND SHAKEDOWN PROGRAMMING

The traditional approach to safety assessment and design is based on a deterministic model which invariably involves a large safety factor usually assigned from heuristic and somewhat arbitrary decisions. This approach has almost certainly been reinforced by the very large extent to which structural engineering design is codified and the lack of feedback about the actual performance of the structure. Use of large safety factors can lead to the view that “absolute” safety can be achieved. Absolute safety is, of course, undesirable if not unobtainable, since it could only be approached by deploying infinite resources. Moreover, these safety factors do not provide any information regarding the probability that would lead to the loss of structural integrity.

The realistic evaluation of structural performance can be conducted only if the uncertainty of the actual load-carrying capacity of the structure is taken into consideration. Uncertainty may originate from random fluctuations of significant physical properties, from limited information and from model idealizations of unknown credibility. Structural reliability analysis deals with all these uncertainties in a rational way. Reliability assessment of structures requires on the one hand mechanical models and analysis procedures that are capable of modeling limit states accurately. On the other hand, full coverage of the present random variables is also necessary for a meaningful reliability assessment.

Present structural reliability analysis is typically based on the limit state of initial or local failure. This may be defined by first yield or by some member failure if the structure can be designed on an element basis. However, this gives quite pessimistic reliability estimates, because virtually all structures are redundant or statically undetermined. Progressive member failures of such systems reduce redundancy until finally the statically determined system fails. This system approach is not defined in an obvious way for a finite element representation of a structure. The more effective method of structural reliability analysis is probabilistic limit and shakedown analyses, which is based on the direct computation of the load-carrying capacity or the safety margin.

The aim of this chapter is to present a new algorithm of probabilistic limit and shakedown analysis for thin plates and shells, which is based on the kinematic approach [Tran et al., 2007b, d, 2008]. The loading, material as well as the thickness of the shell are to be considered as random variables. Many different kinds of distribution of basic variables are taken into consideration and performed with First and Second Order

Reliability Methods (FORM/SORM) for calculation of the failure probability of the structure. In order to get the design point, a non-linear optimization was implemented, which is based on the Sequential Quadratic Programming (SQP). Non-linear sensitivity analyses are also performed for computing the Jacobian and the Hessian of the limit state function.

4.1 Basic concepts of probability theory

4.1.1 Sample space

A standard way of determining the yield stress of a material such as steel is to perform a number of simple tensile tests with specimens made from the material in question. By each test a value for the yield stress is determined but this value will probably be different from test to test. Therefore, in this connection, the yield stress must be taken as an uncertain quantity and it is in accordance with this point of view said to be random quantity. The set of all possible outcomes of such tests is called the *sample space*. The sample space for the yield stress is the set of all positive real numbers and is continuous.

A subset of sample space is called an *event*. An event is the set of sample points. If it contains no sample points, it is called an impossible event.

4.1.2 Random variables

An event can be identified through the value of a function called a *random variable*. A random variable is a function which maps events ω in the sample space Ω into the real line R . Usually a random variable is denoted by a capital letter X

$$X : \Omega \rightarrow R. \quad (4.1)$$

A random variable can be continuous or discrete. The values of $X = x(\omega)$ are called *realizations* of X and denoted by x . The space of event Ω is characterized by a *probability measure* P , which satisfies the properties of a normed, non-negative and σ -additive measure

- 1) $0 \leq P(A) \leq 1$,
- 2) $P(\Omega) = 1, P(\emptyset) = 0$,
- 3) $P(A \cup B) = P(A) + P(B)$ if $A \cap B = \emptyset$.

A family $\{X_i\}_i$ of random variables with $X_i : \Omega \rightarrow R$ is called stochastically independent or independent for short, if for every choice of a subset $A_i \subset R$ the event $\{X_i \in A_i\}_i$ are independent of each other.

The *cumulative probability distribution function* (CDF) of the random X is defined as follows

$$F(x) = P(X < x). \quad (4.2)$$

This means, that the value of F at x is the probability of the event, that the random variable X has a realization lower than x . A random variable is characterized by its CDF. We summarize the most important characteristics of distribution functions

- 1) $F(x)$ is non-decreasing and continuous
- 2) $\lim_{x \rightarrow \infty} F(x) = 1, \quad \lim_{x \rightarrow -\infty} F(x) = 0, \quad P(a < X < b) = F(b) - F(a).$

For the continuous random variable, it is often useful to use the derivative probability function. This function is called the *probability density function* (PDF) $f : R \rightarrow R$. We have

$$F(x) = \int_{-\infty}^x f(t)dt. \quad (4.3)$$

The probability density function has the properties

- 1) $P(a \leq X \leq b) = \int_a^b f(t)dt,$
- 2) $f(x) \geq 0,$
- 3) $\int_{-\infty}^{\infty} f(t)dt = 1.$

The appendix summarizes the most important distribution functions, densities and further details. The following distributions play a special role in structural reliability analysis.

Normal distribution and standard normal distribution ($\sigma = 1, \mu = 0$) with the respective densities

$$f(x) = \frac{1}{\sqrt{2\pi}\sigma^2} e^{-(x-\mu)^2/2\sigma^2} \quad \text{and} \quad f(x) = \frac{1}{\sqrt{2\pi}} e^{-0.5x^2}. \quad (4.4)$$

4.1.3 Moments

Let X be a continuous random variable. Then its probabilistic characteristics are described by the cumulative distribution function F . However, in many applications, the form of F is not known in all details. It is therefore useful to have an approximate description of a random variable by its most important features. In the following it is assumed that all the random variables are continuous.

The *expected value* $E[X]$ of X with the density f is defined as

$$E[X] = \int_{-\infty}^{\infty} xf(x)dx. \quad (4.5)$$

The expected value is also called the ensemble average, the *mean* or the *first moment* of X and the symbol μ is often used for it. The following simple rules for the expectation hold

- 1) $E[a] = a, \quad a \in R,$
- 2) $E[X + Y] = E[X] + E[Y], \quad E[\lambda X] = \lambda E[X], \quad \lambda \in R,$
- 3) $E[XY] = E[X]E[Y]$ if and only if X and Y are independent.

The n^{th} central moment of X is defined by $E[(X - \mu)^n]$. The second central moment of X is called the *variance* of X and is denoted by σ^2 or $Var[X]$

$$Var[X] = \sigma^2 = E[(X - \mu)^2] = E[X^2] - \mu^2. \quad (4.6)$$

The variance reflects the expected deviation of a realization x from the expected value $E[X]$. The positive square root of the variance, $\sigma[X]$, is called *standard deviation* of X .

The concept of random variable has been used only in one-dimensional sense. This definition can easily be extended to a vector valued random variable $\mathbf{X} : \Omega \rightarrow R^n$ called a *random vector*. The *joint cumulative distribution function* for the random vector \mathbf{X} is defined as

$$F(\mathbf{X}) = P\left(\bigcap_{i=1}^n (X_i \leq x_i)\right) = \int_{-\infty}^{x_1} \dots \int_{-\infty}^{x_n} f(t_1, \dots, t_n) dt_1 \dots dt_n. \quad (4.7)$$

The *mixed central moment* of random variables is defined as

$$\Sigma_{ij} = Cov[X_i, X_j] = E[(X_i - \mu_i)(X_j - \mu_j)] = E[X_i X_j] - \mu_i \mu_j \quad (4.8)$$

is called *covariance* of random variables (written with random vector components X_i and X_j). The *covariance matrix* Σ_{ij} is symmetric semi-definite. The ratio

$$\rho_{ij} = \frac{Cov[X_i, X_j]}{\sigma_i \sigma_j} \quad (4.9)$$

where σ_i, σ_j are the standard deviations of the random variables X_i and X_j , is called the *correlation coefficient*. It can be used as a measure of mutual linear dependence between a pair of random variables. It can be shown that $-1 \leq \rho_{ij} \leq 1$. Two random variables X_i and X_j are said to be uncorrelated if $Cov[X_i, X_j] = 0$ (or $\rho_{ij} = 0$) holds. Therefore, independent random variables are uncorrelated but not vice versa. In the appendix the expectations and variances of the most important distribution functions for structural reliability analysis are listed.

4.2 Reliability analysis

The behavior of a structure is influenced by various typically uncertain parameters (loading type, loading magnitude, dimensions, or material data, ...). Data with random fluctuations in time and space is adequately described by stochastic processes and fields. Typical examples of engineering interest are earthquake ground motion, sea waves, wind turbulence, imperfections. The probabilistic characteristics of the processes are known from various available measurements and investigation in the past. In engineering mechanics, the available probabilistic characteristics of random quantities affecting the loading of the mechanical system often cannot be utilized directly to account for the randomness of the structural response due to its complexity. In structural response calculations a distinction is made between the involved structural model properties which are either considered as being deterministic or stochastic.

The principles of reliability analysis have been applied to a very large class of problems, ranging from the design of control systems for complex nuclear and chemical plants to the design of specific mechanical and structural components, as well as more generally in the field of aero-space industries. Reliability analysis should not, however, be thought of as an isolated discipline as it is closely related to the theory of statistics and probability and to such fields as operations research, systems engineering, quality control engineering and statistical acceptance testing.

4.2.1 Failure function and probability

In reliability based structural analysis all probabilistic characteristics are modelled as random variables. These so-called physical basic random variables are collected in a vector $\mathbf{X} = (X_1, X_1, \dots, X_n)$ where n is the number of stochastic variables. The deterministic safety margin M is based on the comparison of a structural resistance (threshold) R and loading S (which is usually an invariant measure of local stress at a hot spot or in a representative cross-section). With R, S functions of \mathbf{X} the structure fails for any realization with non-positive *failure function* or *limit state function* $g(\mathbf{X})$, i.e.

$$g(\mathbf{X}) = R(\mathbf{X}) - S(\mathbf{X}) \begin{cases} < 0 & \text{for failure} \\ = 0 & \text{for limit state} \\ > 0 & \text{for safe structure} \end{cases} \quad (4.10)$$

The limit state $g(\mathbf{X}) = 0$ defines the limit state hyper-surface ∂F which separates the failure region $F = \{\mathbf{x} \mid g(\mathbf{X}) < 0\}$ from safe region. Figure 4.1 shows the densities of two random variables R, S which are generally unknown or difficult to establish. The failure probability P_f is the probability that $g(\mathbf{X})$ is non-positive, i.e.

$$P_f = P(g(\mathbf{X}) \leq 0) = \int_F f_{\mathbf{X}}(\mathbf{x}) d\mathbf{x} \quad (4.11)$$

where $f_x(\mathbf{x})$ is the n -dimensional joint probability density function. Usually, it is not possible to calculate P_f analytically. In special cases, where the basic variables are jointly Gaussian distributed and the failure surface is a hyperplane, it can be shown that

$$P_f = \Phi(-\beta_c) \quad (4.12)$$

where β_c is the second moment reliability index defined as the mean of M divided by the standard deviation of M . $\Phi(\cdot)$ is the standard Gaussian distribution function.

The concept of a reliability index which is invariant with respect to the formulation of the failure function was proposed by Hasofer and Lind [1974]. It is defined as the shortest distance from origin to the failure surface ∂F in the standardised and uncorrelated \mathbf{u} -space (figure 4.2), i.e.

$$\beta_{HL} = \min_{g(\mathbf{u})=0} \sqrt{\mathbf{u}^T \mathbf{u}}. \quad (4.13)$$

For the general cases, there are several approximate methods to compute the failure probability P_f . Direct Monte Carlo Simulation (MCS) becomes increasingly expensive with the increase of the structural reliability but it is independent on the dimension n of the space of basis variables. Acceptable failure probabilities might be in the range of 10^{-4} to 10^{-6} . They are even much lower in nuclear reactor technology. For a validation that the failure probability P_f is less than an accepted limit P_c , the sample size required for direct MCS must be at least $P_c/10$ leading to a minimum sample size in the range of 10^{-5} to 10^{-7} . Such a large number exceeds particularly for complex FE-models, available resources by far. The numerical effort can be reduced considerably by variance reduction methods like Importance Sampling and by Response Surface Methods (RSM). However, the most effective analysis is based on First- and Second-Order Reliability Methods (FORM/SORM) if gradient information is available [Gollwitzer et al., 1988]. However the numerical effort of FORM/SORM increases with the dimension n .

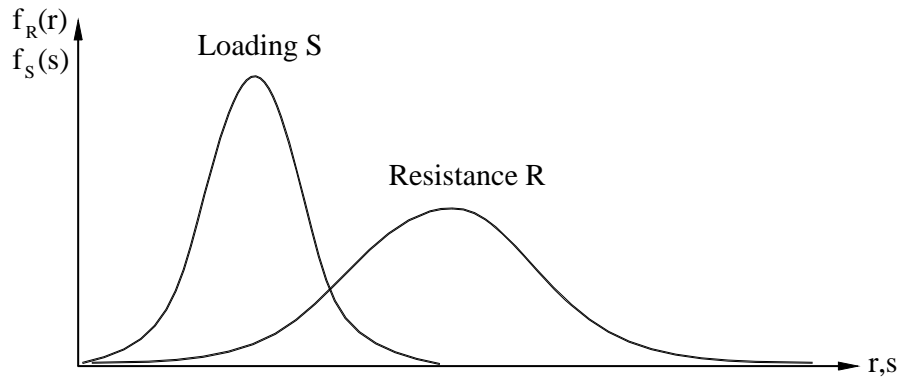


Figure 4.1 Density functions of R, S presenting on one axis

4.2.2 First- and Second-Order Reliability Method

First- and Second-Order Reliability Methods (FORM/SORM) are efficient means and standard methods of numerical probability calculations for multiple random variables. These methods have only become popular since the advent of inexpensive computing. They are often confused with other so-called first order methods that may rely on assumptions of normality and/or small numbers of random variables to achieve closed-form solutions. FORM/SORM, on the other hand, can deal with random variables having arbitrary probability distributions and can estimate reliability results for large numbers of random variables.

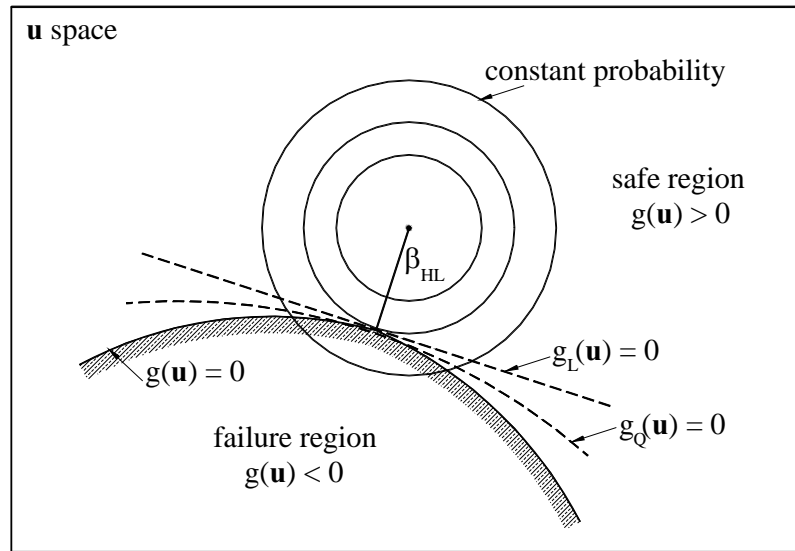


Figure 4.2 Domain based on linear and quadratic approximations in \mathbf{u} space

FORM/SORM are analytical probability integration methods. Therefore, the defined problem has to fulfill the necessary analytical requirements (e.g. FORM/SORM apply to problems, where the set of basic variables are continuous). Because of the large computational effort of MCS due to small failure probabilities, any effective analysis is based on FORM/SORM [Hohenbichler et al., 1987], in which the numerical effort depends on the number of stochastic variables but not on P_f (contrary to MCS). Practical experience with FORM/SORM algorithm indicates that their estimates usually provide satisfactory reliability measure. Especially in the case of small failure probability (large reliability), FORM/SORM are extremely efficient compared with the MCS method regarding the requirement of computer time, such as the Central Processing Unit (CPU). The failure probability is computed in three steps

- Transformation: The physical space \mathbf{x} of uncertain parameters, \mathbf{X} , is transformed into a new n -dimensional space, \mathbf{u} , consisting of independent standard Gaussian variables \mathbf{U} ($\mu = 0, \sigma = 1$). Such a transformation is always possible for continuous random variables. The appendix provides a description of some independent random variables,

equations to map them into the standard Gaussian space. By this transformation, the original limit state function $g(\mathbf{x})=0$ is mapped into the new limit state function $g(\mathbf{u})=0$ in the \mathbf{u} space. This transformation is exact and not an approximation [Bjerager, 1991].

- Computation of design point: The design point or β_{HL} -point, which is the point on the limit state surface having the shortest distance to the origin in the \mathbf{u} space, is determined by an appropriate non-linear optimization algorithm. More details of this algorithm will be discussed in next section.
- Approximating the limit state surface and calculation of the failure probability: The limit state surface $g(\mathbf{u})=0$ is approximated by a tangential hypersurface at the design point. This corresponds to an approximating hyperplane $g_L(\mathbf{u})=0$ (linear or first-order) or hyperparaboloid $g_Q(\mathbf{u})=0$ (quadratic or second-order), respectively. The failure probability P_f is thus approximated by $P(g_L(\mathbf{u}) < 0)$ in FORM or $P(g_Q(\mathbf{u}) < 0)$ in SORM.

4.2.2.1 First-Order Reliability Method (FORM)

Consider a tangential linearization at the design point \mathbf{u}_0 on the limit state surface $g(\mathbf{u})=0$, which is given by

$$g_L(\mathbf{u}) = \mathbf{a}^T (\mathbf{u} - \mathbf{u}_0) = \mathbf{a}^T \mathbf{u} + \beta_{HL} \quad (4.14)$$

where \mathbf{a} is the vector of direction cosines and can be obtained from

$$\mathbf{a} = \frac{\nabla g(\mathbf{u}_0)}{\|\nabla g(\mathbf{u}_0)\|}. \quad (4.15)$$

Here $g_L(\mathbf{u})=0$ is the Hesse normal form of the tangential hypersurface to the limit state function at the design point. If the failure function is not strictly non-linear, the probability of failure P_f can be determined with good accuracy by

$$P_{f,I} = \Phi(-\beta_{HL}) = \frac{1}{\sqrt{2\pi}} \int_{-\infty}^{-\beta_{HL}} e^{-0.5z^2} dz \quad (4.16)$$

where β_{HL} is calculated from (4.13). The first-order reliability index can be defined as following

$$\beta_I = \beta_{HL} = -\Phi^{-1}(P_{f,I}). \quad (4.17)$$

Consider a small vector $\boldsymbol{\varepsilon}$ which can be interpreted as an error appearing in the calculation of the design point (i.e. \mathbf{u}_0 is replaced by $\mathbf{u}_0 + \boldsymbol{\varepsilon}$). The resulting disturbance of the reliability index $\beta_{HL}(\boldsymbol{\varepsilon})$ can be calculated as follows [Rackwitz, 2004]

$$\beta_{HL}(\boldsymbol{\varepsilon}) = -\Phi^{-1}(P_{f,I}(\mathbf{u}_0 + \boldsymbol{\varepsilon})) \approx \mathbf{a}^T \boldsymbol{\varepsilon} + \beta_{HL}, \quad (4.18)$$

and therefore

$$\begin{aligned} \left. \frac{\partial \beta_{HL}(\boldsymbol{\varepsilon})}{\partial \varepsilon_i} \right|_{\varepsilon_i \rightarrow 0} &= a_i, \\ \left. \frac{\partial P_{f,I}(\boldsymbol{\varepsilon})}{\partial \varepsilon_i} \right|_{\varepsilon_i \rightarrow 0} &= -\varphi(-\beta_{HL}) a_i. \end{aligned} \quad (4.19)$$

Obviously, a_i represents the sensitivities of β_{HL} and $P_{f,I}$ versus the changes of the mean value of $u_{0,i}$.

4.2.2.2 Second-Order Reliability Method (SORM)

Various methods have been suggested to improve the accuracy of FORM calculations and to give a rough estimate of the approximation quality [Madsen et al., 1986], [Fiessler et al., 1979]. The general idea is to approximate the limit state surface by a quadratic hypersurface rather than by a hyperplane. The main curvatures of the quadratic hypersurface at the design point are equal to those of the limit state surface. This leads to the so-called Second-Order Reliability Methods (SORM). Using all $n-1$ main curvatures κ_j , the failure probability is calculated as a three term approximation suggested by Tvedt [1983] as

$$P_{f,II} = S_1 + S_2 + S_3 \quad (4.20a)$$

$$S_1 = \Phi(-\beta_{HL}) \prod_{j=1}^{n-1} (1 - \beta_{HL} \kappa_j)^{-1/2} \quad (4.20b)$$

$$S_2 = [\beta_{HL} \Phi(-\beta_{HL}) - \phi(\beta_{HL})] \left\{ \prod_{j=1}^{n-1} (1 - \beta_{HL} \kappa_j)^{-1/2} - \prod_{j=1}^{n-1} (1 - (\beta_{HL} + 1) \kappa_j)^{-1/2} \right\} \quad (4.20c)$$

$$S_3 = (\beta_{HL} + 1) [\beta_{HL} \Phi(-\beta_{HL}) - \phi(\beta_{HL})] \left\{ \prod_{j=1}^{n-1} (1 - \beta_{HL} \kappa_j)^{-1/2} - \operatorname{Re} \left[\prod_{j=1}^{n-1} (1 - (\beta_{HL} + i) \kappa_j)^{-1/2} \right] \right\} \quad (4.20d)$$

where $i = \sqrt{-1}$, $\operatorname{Re}[\cdot]$ represents the real part of the complex argument and $\phi(\cdot)$ is the standard Gaussian PDF. S_1 is an asymptotic approximation of P_f being exact for $\beta_{HL} \rightarrow \infty$, S_2 and S_3 are correction terms.

The curvatures κ_j are obtained in the following way. First, the co-ordinate system of the standard normalized \mathbf{u} space is rotated, so that the design point becomes part of the last axis of the rotated normal \mathbf{y} space. In other words, the last basic vector of the \mathbf{y} space coincides with the design point position vector in the normalized \mathbf{u} space. This is achieved through the following transformation

$$\mathbf{Y} = \mathbf{D}^T \mathbf{U} \quad (4.21)$$

and, provided that $\mathbf{D}^{-1} = \mathbf{D}^T$

$$\mathbf{U} = \mathbf{D} \mathbf{Y}. \quad (4.22)$$

Defining \mathbf{H}_{y_0} as the matrix of second derivatives of the limit state function in \mathbf{y} space at the design point \mathbf{y}_0 , the curvatures are obtained as solutions of a characteristic equation

$$\det \left(\mathbf{H}_y \left(\frac{\partial g(\mathbf{y}_0)}{\partial y_n} \right)^{-1} - \kappa \mathbf{I} \right) = 0 \quad (4.23)$$

where \mathbf{I} is the identity matrix. The second-order reliability index can be defined as following

$$\beta_{II} = -\Phi^{-1}(P_{f,II}) \quad (4.24)$$

It should be noted that β_I has a geometric meaning but β_{II} has no such interpretation. The open source code of FORM/SORM is available in [Wierskowski, 2005].

4.3 Calculation of design point

In order to apply FORM/SORM, the design point must be identified. This leads to a non-linear constrained optimization problem as follows [Heitzer, 1999]

$$\begin{aligned} \text{minimize: } f(\mathbf{u}) &= \frac{1}{2} \mathbf{u}^T \mathbf{u} \\ \text{s.t. } g(\mathbf{u}) &\leq 0 \end{aligned} \quad (4.25)$$

where a coefficient $\frac{1}{2}$ is added for technical reasons. Many algorithms have been suggested to deal with this problem. Staat et al. [2003] and Bjerager [1989] got good results in probabilistic limit analyses with Rackwitz's simple gradient search algorithm, which is based on a linearization of the limit state function at each step. However, this algorithm is only guaranteed to converge towards a locally most likely failure point in each sequence of points on the failure surface if the safe region is quasi-convex or concave (see section 7.4).

A more general algorithm is the Sequential Quadratic Programming (SQP). This method has proved to be suitable for tasks in the area of the reliability theory [Rackwitz, 2004]. Due to the complex shape of the limit state surface, SQP becomes an efficient tool for solving non-linear optimization problems and shall be introduced for this reason here in short statements. More details can be found in the literature, e.g Schittkowski [1983a, 1983b, 1988, 2004], Bazaraa et al. [1993]. Example of applying SQP in reliability analysis can be found in [Dronia, 2005].

The SQP method, also known as successive or recursive quadratic programming, employs Newton's method (or quasi-Newton methods) to solve the KKT conditions for the

original problem directly. As a result, the accompanying subproblem turns out to be the minimization of a quadratic approximation to the Lagrangian function optimized over a linear approximation to the constraints. Consider the inequality constrained nonlinear optimization problem

$$\begin{aligned} & \text{minimize: } f(\mathbf{x}) \\ & \text{s.t. } g_i(\mathbf{x}) \leq 0 \quad i \in I \end{aligned} \quad (4.26)$$

where \mathbf{x} is an n -dimensional parameter vector containing the design variables. For this case, given an iterate $(\mathbf{x}_k, \boldsymbol{\lambda}_k)$, where $\boldsymbol{\lambda}_k \geq 0$ is the Lagrange multiplier estimating for the inequality constraints. Define $\nabla^2 L(\mathbf{x}_k) = \nabla^2 f(\mathbf{x}_k) + \sum_{i \in I} \lambda_{ki} \nabla^2 g_i(\mathbf{x}_k)$ to be the usual Hessian of the Lagrangian at \mathbf{x}_k . Then a quadratic programming subproblem of the form

$$\begin{aligned} & \text{minimize: } f(\mathbf{x}_k) + \nabla f(\mathbf{x}_k)^T \mathbf{d} + \frac{1}{2} \mathbf{d}^T \nabla^2 L(\mathbf{x}_k) \mathbf{d} \\ & \text{s.t. } g_i(\mathbf{x}_k) + \nabla g_i(\mathbf{x}_k)^T \mathbf{d} \leq 0 \quad i \in I \end{aligned} \quad (4.27)$$

is formulated and must be solved in each iteration. Let \mathbf{d}_k be the optimal solution, $\boldsymbol{\lambda}_{k+1}$ the corresponding multiplier of this subproblem, then the new iterate is obtained by

$$\begin{pmatrix} \mathbf{x}_{k+1} \\ \boldsymbol{\lambda}_{k+1} \end{pmatrix} = \begin{pmatrix} \mathbf{x}_k \\ \boldsymbol{\lambda}_k \end{pmatrix} + \alpha_k \begin{pmatrix} \mathbf{d}_k \\ \boldsymbol{\lambda}_{k+1} - \boldsymbol{\lambda}_k \end{pmatrix} \quad (4.28)$$

where $\alpha_k \in (0, 1]$ is a suitable step length parameter. Since $\nabla^2 L(\mathbf{x}_k)$ might not be positive definite, it can be replaced by a positive definite approximation \mathbf{B}_k , which is known as BFGS update [Powell, 1978]

$$\mathbf{B}_{k+1} = \mathbf{B}_k - \frac{\mathbf{B}_k \mathbf{p}_k \mathbf{p}_k^T \mathbf{B}_k}{\mathbf{p}_k^T \mathbf{B}_k \mathbf{p}_k} + \frac{\mathbf{s}_k \mathbf{s}_k^T}{\mathbf{s}_k^T \mathbf{p}_k} \quad (4.29)$$

with

$$\begin{aligned} \mathbf{p}_k &= \mathbf{x}_{k+1} - \mathbf{x}_k \\ \mathbf{s}_k &= \theta \mathbf{q}_k + (1 - \theta) \mathbf{B}_k \mathbf{p}_k \\ \mathbf{q}_k &= \nabla L(\mathbf{x}_{k+1}, \boldsymbol{\lambda}_{k+1}) - \nabla L(\mathbf{x}_k, \boldsymbol{\lambda}_{k+1}) \\ \theta &= \begin{cases} 1 & \text{when } \mathbf{p}_k^T \mathbf{q}_k \geq 0.2 \mathbf{p}_k^T \mathbf{B}_k \mathbf{p}_k \\ 0.8 \frac{\mathbf{p}_k^T \mathbf{B}_k \mathbf{p}_k}{\mathbf{p}_k^T \mathbf{B}_k \mathbf{p}_k - \mathbf{p}_k^T \mathbf{q}_k} & \text{otherwise} \end{cases} \end{aligned} \quad (4.30)$$

To ensure global convergence of the SQP method and avoid the Maratos effect, a certain irregularity leading to infinite cycles, we have to select a suitable steplength ξ_k subject to the augmented Lagrangian merit function $\psi(\xi)$ [Schittkowski, 1983a]

$$\psi(\xi) = f(\mathbf{x} + \xi \mathbf{d}) + \sum_{i \in I_1} \left(\lambda_i g_i(\mathbf{x} + \xi \mathbf{d}) + \frac{1}{2} r_i g_i(\mathbf{x} + \xi \mathbf{d})^2 \right) + \frac{1}{2} \sum_{i \in I_2} \frac{\lambda_i^2}{r_i} \quad (4.31)$$

where $I_1 = \{i \in I : g_i(\mathbf{x}) \leq \lambda_i / r_i\}$ and $I_2 = I \setminus I_1$, $r_i \geq 1$ is the penalty parameter. In order to get the value of penalty parameter, two positive constants $\bar{r} > 1$, $\bar{\varepsilon} < 1$ should be chosen. Then at each iteration, together with the search direction \mathbf{d}_k , two additional variables

$$\delta_k = \min \left\{ \frac{\mathbf{d}_k^T \mathbf{B}_k \mathbf{d}_k}{\|\mathbf{d}_k\|^2}, \delta_{k-1} \right\} \quad \text{and} \quad \varepsilon_k = \begin{cases} \frac{\|\mathbf{d}_k\|^2}{\|\lambda_{k+1} - \lambda_k\|}, & \text{when } \lambda_{k+1} \neq \lambda_k \\ \bar{\varepsilon}, & \text{otherwise} \end{cases} \quad (4.32)$$

with $\delta_0 = 1$ and a small positive number j_k , which satisfies the inequality

$$\frac{1}{\bar{r}^j} < \frac{1}{4} \varepsilon_k \delta_k \left(1 - \frac{1}{4} \delta_k \right), \text{ i.e. } j_k = \min \left\{ j \in N, j > \frac{\ln \frac{16}{\varepsilon_k \delta_k (4 - \delta_k)}}{\ln \bar{r}} \right\} \quad (4.33)$$

must be identified. The penalty parameter r_i^k at iteration k can be obtained from

$$r_i^k = \max \{ r_i^{k-1}, \bar{r}^{j_k} \} \quad (4.34)$$

with $r_0 = \bar{r}$. The step length ξ_k can be chosen by a separate algorithm, which should take the curvature of the merit function into account. If ξ_k is too small, the resulting step sizes might become too small leading to a higher number of outer iteration. On the other hand, a large value close to one requires too many function calls during the line search. Thus we need some kind of compromise which is obtained by applying first a polynomial interpolation. Rackwitz [2004] proposed a simple line search, which is based on a quadratic interpolation minimization algorithm

$$\xi_k = \frac{\nabla \psi(0)}{2(\psi(0) + \nabla \psi(0) - \psi(1))} \geq \gamma > 0 \quad (4.35)$$

where

$$\nabla \psi(0) = \nabla f(\mathbf{x})^T \mathbf{d} + \sum_{i \in I_1} \left(\lambda_i \nabla g_i(\mathbf{x})^T \mathbf{d} + r_i g_i(\mathbf{x}) \nabla g_i(\mathbf{x})^T \mathbf{d} \right) \quad (4.36)$$

and γ is a small positive number, which ensures that the value of ξ_k is not too small. This algorithm is very useful in reliability analysis, because it allows to reduce the number of deterministic loop in an iteration to two, for $\xi = 0$ and $\xi = 1$, and thus considerably reduce the computational cost.

Applying SQP method for solving the optimization problem (4.25), the quadratic programming sub-problem (4.27) at iteration k becomes

$$\begin{aligned}
&\text{minimize: } f(\mathbf{u}_k) + \nabla f(\mathbf{u}_k)^T \mathbf{d}_k + \frac{1}{2} \mathbf{d}_k^T \nabla^2 f(\mathbf{u}_k) \mathbf{d}_k \\
&\text{s.t. } g(\mathbf{u}_k) + \nabla g(\mathbf{u}_k)^T \mathbf{d}_k \leq 0
\end{aligned} \tag{4.37}$$

with $\nabla f(\mathbf{u}_k) = \mathbf{u}_k$ and $\nabla^2 f(\mathbf{u}_k) = \mathbf{I}$. The Karush-Kuhn-Tucker conditions for this problem are

$$\begin{cases} \nabla L(\mathbf{u}_k, \lambda_k) = \nabla f(\mathbf{u}_k) + \mathbf{d}_k + \lambda_k \nabla g(\mathbf{u}_k) = 0 \\ g(\mathbf{u}_k) + \nabla g(\mathbf{u}_k)^T \mathbf{d}_k = 0 \end{cases} \tag{4.38}$$

Applying Newton's method for solving these equations leads to the system

$$\begin{bmatrix} \mathbf{B}_k & \nabla g(\mathbf{u}_k) \\ \nabla g(\mathbf{u}_k)^T & 0 \end{bmatrix} \begin{pmatrix} \mathbf{d}_k \\ \lambda_{k+1} \end{pmatrix} = - \begin{pmatrix} \nabla f(\mathbf{u}_k) \\ g(\mathbf{u}_k) \end{pmatrix} \tag{4.39}$$

with the solutions

$$\begin{aligned}
\lambda_{k+1} &= - \frac{\nabla g(\mathbf{u}_k)^T \mathbf{B}_k^{-1} \nabla f(\mathbf{u}_k) - g(\mathbf{u}_k)}{\nabla g(\mathbf{u}_k)^T \mathbf{B}_k^{-1} \nabla g(\mathbf{u}_k)} \\
\mathbf{d}_k &= -\mathbf{B}_k^{-1} \nabla g(\mathbf{u}_k) \lambda_{k+1} - \mathbf{B}_k^{-1} \nabla f(\mathbf{u}_k)
\end{aligned} \tag{4.40}$$

as the Lagrange multiplier and search direction for the next iteration. If $\mathbf{d}_k = 0$ then \mathbf{u}_k together with the Lagrange multiplier λ_{k+1} yields the optimal solution for the problem (4.25), i.e. the design point is actually found. The calculation of the necessary derivatives are considered as the sensitivity analysis and will be discussed in the next section.

4.4 Sensitivity of the limit state function

The reliability analysis described above can be carried out now with the help of a probabilistic limit and shakedown analysis. From the results of the finite element analysis, the necessary derivatives of the limit state function based shakedown analysis can be determined analytically. This represents a considerable reduction of computing time comparing with the other methods, e.g. the difference approximation, and makes such an efficient and cost-saving calculation of the reliability of the structure. Contrary to the numerical calculation, the analytical calculation is faster and more exact. The necessary data for the calculation of the derivatives are available after the execution of the deterministic shakedown analysis since they are based on the limit load factor α_{lim} .

The derivatives must be calculated firstly at each iteration in the physical \mathbf{x} space. Then it is transferred into the standard Gaussian \mathbf{u} space by using the chain rule

$$\begin{aligned}
\nabla_u g(\mathbf{u}) &= \nabla_u g(\mathbf{x}) = \nabla_x g(\mathbf{x}) \nabla_u \mathbf{x} \\
\nabla_u^2 g(\mathbf{u}) &= \nabla_u (\nabla_x g(\mathbf{x}) \nabla_u \mathbf{x}) = (\nabla_u \mathbf{x})^T \nabla_x^2 g(\mathbf{x}) \nabla_u \mathbf{x} + \nabla_x g(\mathbf{x}) \nabla_u^2 \mathbf{x}
\end{aligned} \tag{4.41}$$

The calculation of the derivatives in the physical \mathbf{x} space is based on a sensitivity analysis. Sensitivity arises prominently in microeconomic theory, where optimality

condition provide the basic for analysis. It is interested primarily not in finding an optimal solution, but rather in how the solution is affected by changes in the problem data. By this way, sensitivity analysis becomes widely in engineering, especially in reliability analysis of the structures, where the data defining problem are random variables.

4.4.1 Mathematical sensitivity

Consider a constraint optimization problem P is defined as follows

$$\begin{aligned} &\text{minimize: } f(\mathbf{x}) \\ &\text{s.t. } h_i(\mathbf{x}) = 0 \quad i \in I \end{aligned} \quad (4.42)$$

Suppose that $f, h_i : R^n \rightarrow R$ are twice continuously differentiable and I is some index set. In many applications the objective function f as well as the constraint functions h_i may depend on other parameters. Consider the following pertubation problem $P(\boldsymbol{\varepsilon})$ of the original problem $P(\mathbf{0})$

$$\begin{aligned} &\text{minimize: } f(\mathbf{x}, \boldsymbol{\varepsilon}) \\ &\text{s.t. } h_i(\mathbf{x}, \boldsymbol{\varepsilon}) = 0 \quad i \in I, \boldsymbol{\varepsilon} \in R^m \end{aligned} \quad (4.43)$$

The perturbations $\boldsymbol{\varepsilon}$ can be interpreted in two ways: as a random error or as aspecific change in the parameters defining the problem functions. The optimal solution $\mathbf{x}^*(\boldsymbol{\varepsilon})$ of the problem $P(\boldsymbol{\varepsilon})$ with the Lagrange multipliers $\boldsymbol{\lambda}^*$ fulfills the following first order Karush-Kuhn-Tucker conditions

$$\begin{aligned} \nabla L(\mathbf{x}^*, \boldsymbol{\lambda}^*, \boldsymbol{\varepsilon}) &= \nabla f(\mathbf{x}^*, \boldsymbol{\varepsilon}) - \sum_{i \in I} \lambda_i^* \nabla h_i(\mathbf{x}^*, \boldsymbol{\varepsilon}) = 0 \\ h_i(\mathbf{x}^*, \boldsymbol{\varepsilon}) &= 0 \quad i \in I \end{aligned} \quad (4.44)$$

If f has a continuous and nonsingular gradient matrix $\nabla_{\mathbf{x}} f(\mathbf{x}, \boldsymbol{\varepsilon})$ in an open set containing $(\mathbf{x}^*, \boldsymbol{\varepsilon})$, the implicit function theorem implies the existence of a unique differentiable local solution $(\mathbf{x}^*(\boldsymbol{\varepsilon}), \boldsymbol{\lambda}^*(\boldsymbol{\varepsilon}))$ of the problem $P(\boldsymbol{\varepsilon})$. Let $\boldsymbol{\varepsilon} = \mathbf{0}$ then the conditions are fulfilled in a local solution $\mathbf{x}^*(\mathbf{0})$ of the problem $P(\mathbf{0})$. We defined the *optimal value function* $f^*(\boldsymbol{\varepsilon})$ and the optimal value Lagrangian $L^*(\boldsymbol{\varepsilon})$ as follows

$$\begin{aligned} f^*(\boldsymbol{\varepsilon}) &\equiv f(\mathbf{x}^*(\boldsymbol{\varepsilon}), \boldsymbol{\varepsilon}) \\ L^*(\boldsymbol{\varepsilon}) &\equiv L(\mathbf{x}^*(\boldsymbol{\varepsilon}), \boldsymbol{\lambda}^*(\boldsymbol{\varepsilon}), \boldsymbol{\varepsilon}) \end{aligned} \quad (4.45)$$

Theorem [Fiacco, 1983]

If the linear independence condition and the second order sufficient condition of the problem $P(\boldsymbol{\varepsilon})$ are satisfied, and if the problem functions are twice continuously differentiable in $(\mathbf{x}, \boldsymbol{\varepsilon})$ near $(\mathbf{x}^*, \mathbf{0})$ then, in a neighborhood of $\boldsymbol{\varepsilon} = \mathbf{0}$, we have

$$f^*(\boldsymbol{\varepsilon}) = L^*(\boldsymbol{\varepsilon}) \quad (4.46a)$$

$$\frac{d}{d\boldsymbol{\varepsilon}} f^*(\boldsymbol{\varepsilon}) = \frac{\partial}{\partial \boldsymbol{\varepsilon}} f(\mathbf{x}^*(\boldsymbol{\varepsilon}), \boldsymbol{\varepsilon}) - \sum_{i \in I} \lambda_i^*(\boldsymbol{\varepsilon}) \frac{\partial}{\partial \boldsymbol{\varepsilon}} h_i(\mathbf{x}^*(\boldsymbol{\varepsilon}), \boldsymbol{\varepsilon}) \quad (4.46b)$$

$$\begin{aligned} \frac{d^2}{d\boldsymbol{\varepsilon}^2} f^*(\boldsymbol{\varepsilon}) = & \frac{\partial^2 L(\mathbf{x}^*(\boldsymbol{\varepsilon}), \boldsymbol{\lambda}^*(\boldsymbol{\varepsilon}), \boldsymbol{\varepsilon})}{\partial \mathbf{x} \partial \boldsymbol{\varepsilon}} \frac{d}{d\boldsymbol{\varepsilon}} \mathbf{x}^*(\boldsymbol{\varepsilon}) \\ & - \sum_{i \in I} \left(\frac{\partial h_i(\mathbf{x}^*(\boldsymbol{\varepsilon}), \boldsymbol{\varepsilon})}{\partial \boldsymbol{\varepsilon}} \right)^T \frac{\partial \lambda_i^*(\boldsymbol{\varepsilon})}{\partial \boldsymbol{\varepsilon}} + \frac{\partial^2 L(\mathbf{x}^*(\boldsymbol{\varepsilon}), \boldsymbol{\lambda}^*(\boldsymbol{\varepsilon}), \boldsymbol{\varepsilon})}{\partial \boldsymbol{\varepsilon}^2} \end{aligned} \quad (4.46c)$$

and

$$\begin{bmatrix} \nabla_{\mathbf{x}}^2 L & -\nabla_{\mathbf{x}} \mathbf{h}^T \\ -\nabla_{\mathbf{x}} \mathbf{h} & \mathbf{0} \end{bmatrix} \begin{Bmatrix} \nabla_{\boldsymbol{\varepsilon}} \mathbf{x} \\ \nabla_{\boldsymbol{\varepsilon}} \boldsymbol{\lambda} \end{Bmatrix} = \begin{Bmatrix} -\nabla_{\boldsymbol{\varepsilon} \mathbf{x}}^2 L \\ \nabla_{\boldsymbol{\varepsilon}} \mathbf{h} \end{Bmatrix} \quad (4.46d)$$

where $\mathbf{h} = [h_1, h_2, \dots]^T$. The sensitivity analyses (4.46) provide a quantitative measure of the first- and second-order change in the optimal value function of $P(\boldsymbol{\varepsilon})$. It should be noted that the value of the optimal value function and its gradient can be calculated once the optimal solutions $(\mathbf{x}^*(\boldsymbol{\varepsilon}), \boldsymbol{\lambda}^*(\boldsymbol{\varepsilon}))$ have been determined. However, for the general problem, the value of Hessian matrix of the optimal value function requires the determination of both the optimal solutions and its first derivatives.

4.4.2 Definition of the limit state function

As mentioned above, the limit state function contains the parameters of structural resistance R and loading S . If we defined the limit load factor α_{lim} as follows

$$\alpha_{\text{lim}} = \frac{P_{\text{lim}}}{P} \quad (4.47)$$

where P_{lim}, P are limit load and actual load of the structure. For the sake of simplicity, the limit state function g can be normalized with the actual load P and then becomes

$$g = \alpha_{\text{lim}} - 1 \quad (4.48)$$

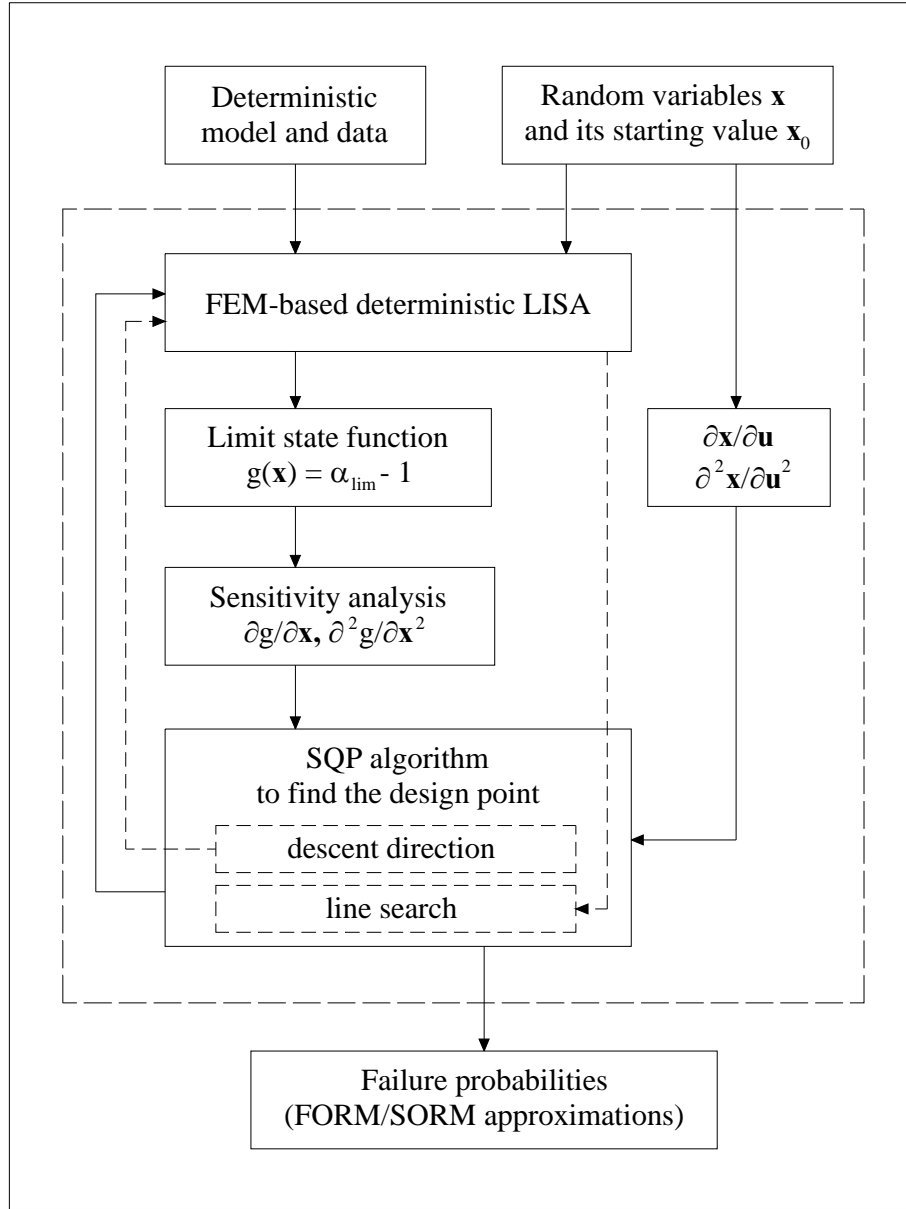


Figure 4.3 Flowchart of the probabilistic limit and shakedown analysis

From previous chapter, the shakedown load factor can be calculated by the non-linear programming (3.15)

$$\begin{aligned}
 \alpha_{\text{lim}} &= \min_{\dot{\mathbf{e}}_{ik}, \mathbf{u}} (F_P) \\
 s.t : \quad & \left(\sum_{i=1}^{NG} \sum_{k=1}^m \dot{\mathbf{e}}_{ik}^T \mathbf{t}_{ik} - 1 \right) = 0
 \end{aligned} \tag{4.49}$$

with

$$\begin{aligned}
F_P &= \sum_{i=1}^{NG} \left\{ \sum_{k=1}^m \left(Y \tilde{N}_0 \dot{\tilde{\epsilon}}_0 \sqrt{\frac{\hat{P}_\kappa}{3}} \left(\beta_1 \sqrt{\beta_1^2 + \gamma} + \beta_2 \sqrt{\beta_2^2 + \gamma} + \gamma K_0 \right) \right) \right. \\
&\quad \left. + \frac{c}{2} \left(\sum_{k=1}^m \dot{\mathbf{e}}_{ik} - \hat{\mathbf{B}}_i \dot{\mathbf{u}} \right)^T \left(\sum_{k=1}^m \dot{\mathbf{e}}_{ik} - \hat{\mathbf{B}}_i \dot{\mathbf{u}} \right) \right\} \\
&= \sum_{i=1}^{NG} \left\{ \sum_{k=1}^m (Y \eta_{ik}) + \frac{c}{2} \left(\sum_{k=1}^m \dot{\mathbf{e}}_{ik} - \hat{\mathbf{B}}_i \dot{\mathbf{u}} \right)^T \left(\sum_{k=1}^m \dot{\mathbf{e}}_{ik} - \hat{\mathbf{B}}_i \dot{\mathbf{u}} \right) \right\}
\end{aligned} \tag{4.50}$$

with

$$\eta_{ik} = \tilde{N}_0 \dot{\tilde{\epsilon}}_0 \sqrt{\frac{\hat{P}_\kappa}{3}} \left(\beta_1 \sqrt{\beta_1^2 + \gamma} + \beta_2 \sqrt{\beta_2^2 + \gamma} + \gamma K_0 \right). \tag{4.51}$$

It can be seen that the limit state function is the function of yield stress variable Y , thickness variable Z and load variables. The shakedown range obtained from (4.49) is linear function of the yield stress variable Y (see 4.4.4). In the case of heterogeneous material, we will obtain at different Gaussian points i eventually different yield stress variables Y_i . Then the limit state function is no more a linear function of these variables. The actual load P is defined in n components by using the concept of a constant referent load P^0 as follows

$$\begin{aligned}
P^0 &= P_1^0 + P_2^0 + \dots + P_n^0 \\
P &= x_1 P_1^0 + x_2 P_2^0 + \dots + x_n P_n^0
\end{aligned} \tag{4.52}$$

where x_j is the realization of the j^{th} basic load variable X_j ($j = 1, n$). The corresponding actual stress field can also be described in the same way

$$\hat{\boldsymbol{\sigma}} = x_1 \hat{\boldsymbol{\sigma}}_1^0 + x_2 \hat{\boldsymbol{\sigma}}_2^0 + \dots + x_n \hat{\boldsymbol{\sigma}}_n^0. \tag{4.53}$$

From (3.10) and (4.53), the corresponding normalized stress fields are obtained

$$\mathbf{t} = \tilde{N}_0 \dot{\tilde{\epsilon}}_0 \hat{\boldsymbol{\sigma}} = \tilde{N}_0 \dot{\tilde{\epsilon}}_0 \left[x_1 \hat{\boldsymbol{\sigma}}_1^0 + x_2 \hat{\boldsymbol{\sigma}}_2^0 + \dots + x_n \hat{\boldsymbol{\sigma}}_n^0 \right] = x_1 \mathbf{t}_1 + x_2 \mathbf{t}_2 + \dots + x_n \mathbf{t}_n \tag{4.54}$$

or

$$\mathbf{t} = \sum_{j=1}^n x_j \mathbf{t}_j. \tag{4.55}$$

4.4.3 First derivatives of the limit state function

With the nonlinear programming (4.51), the Lagrange function becomes

$$\begin{aligned}
F_{PL} &= F_P - \lambda \left(\sum_{i=1}^{NG} \sum_{k=1}^m \dot{\mathbf{e}}_{ik}^T \mathbf{t}_{ik} - 1 \right) \\
&= \sum_{i=1}^{NG} \left\{ \sum_{k=1}^m (Y \eta_{ik}) + \frac{c}{2} \left(\sum_{k=1}^m \dot{\mathbf{e}}_{ik} - \hat{\mathbf{B}}_i \dot{\mathbf{u}} \right)^T \left(\sum_{k=1}^m \dot{\mathbf{e}}_{ik} - \hat{\mathbf{B}}_i \dot{\mathbf{u}} \right) \right\} - \lambda \left(\sum_{i=1}^{NG} \sum_{k=1}^m \dot{\mathbf{e}}_{ik}^T \mathbf{t}_{ik} - 1 \right)
\end{aligned} \quad (4.56)$$

In order to get the sensitivity of the limit state function, one require is that the derivatives of the limit load factor α_{lim} must be available. Let $(\dot{\mathbf{e}}_{ik}^*, \mathbf{u}^*, \lambda^*)$ are the solutions of the optimization problem. At optimal point, the first derivative of the limit load factor α_{lim} versus j^{th} load variable X_j can be calculated as follows

$$\frac{\partial \alpha_{lim}}{\partial X_j} = \frac{\partial F_{PL}}{\partial X_j} \bigg|_{(\dot{\mathbf{e}}_{ik}^*, \mathbf{u}^*, \lambda^*)} = -\lambda \sum_{i=1}^{NG} \sum_{k=1}^m \dot{\mathbf{e}}_{ik}^T \frac{\partial \mathbf{t}_{ik}}{\partial X_j} \bigg|_{(\dot{\mathbf{e}}_{ik}^*, \lambda^*)} = -\lambda \sum_{i=1}^{NG} \sum_{k=1}^m \dot{\mathbf{e}}_{ik}^T \mathbf{t}_{ik,j} \bigg|_{(\dot{\mathbf{e}}_{ik}^*, \lambda^*)} \quad (4.57)$$

where $\mathbf{t}_{ik,j}$ is the stress vector at Gaussian point i and load vertex k due to the j^{th} load case. The derivatives of the limit load factor α_{lim} versus yield stress variable Y and thickness variable Z can be determined in the same way and have the form

$$\frac{\partial \alpha_{lim}}{\partial Y} = \frac{\partial F_{PL}}{\partial Y} \bigg|_{(\dot{\mathbf{e}}_{ik}^*, \mathbf{u}^*, \lambda^*)} = \frac{\partial}{\partial Y} \left(\sum_{i=1}^{NG} \sum_{k=1}^m Y \eta_{ik} \right) \bigg|_{(\dot{\mathbf{e}}_{ik}^*)} = \sum_{i=1}^{NG} \sum_{k=1}^m \eta_{ik}^* = \frac{\alpha_{lim}}{Y} \quad (4.58)$$

$$\begin{aligned}
\frac{\partial \alpha_{lim}}{\partial Z} &= \frac{\partial F_{PL}}{\partial Z} \bigg|_{(\dot{\mathbf{e}}_{ik}^*, \mathbf{u}^*, \lambda^*)} = \frac{\partial}{\partial Z} \left(\sum_{i=1}^{NG} \sum_{k=1}^m \left(Y \tilde{N}_0 \tilde{\epsilon}_0 \sqrt{\frac{\hat{P}_k}{3}} \left(\beta_1 \sqrt{\beta_1^2 + \gamma} + \beta_2 \sqrt{\beta_2^2 + \gamma} + \gamma K_0 \right) \right) \right) \bigg|_{\dot{\mathbf{e}}_{ik}^*} \\
&= \sum_{i=1}^{NG} \sum_{k=1}^m \left(Y \tilde{N}_0 \tilde{\epsilon}_0 \sqrt{\frac{\hat{P}_k}{3}} \left(\sqrt{\beta_1^2 + \gamma} + \sqrt{\beta_2^2 + \gamma} \right) \right) \bigg|_{\dot{\mathbf{e}}_{ik}^*}
\end{aligned} \quad (4.59)$$

4.4.4 Second derivatives of the limit state function

In SORM algorithm, as discussed above, the Hessian matrix which summarizes second partial derivatives of the limit state function is needed. They can be obtained from a directly analytical derivation of the first derivatives. Consider first the derivatives of α_{lim} versus load variables. Taking the derivatives of (4.57) versus X_l , one gets

$$\begin{aligned}
\frac{\partial^2 \alpha_{lim}}{\partial X_l \partial X_j} &= \frac{\partial}{\partial X_l} \left(-\lambda \sum_{i=1}^{NG} \sum_{k=1}^m \dot{\mathbf{e}}_{ik}^T \mathbf{t}_{ik,j} \right) \bigg|_{(\dot{\mathbf{e}}_{ik}^*, \lambda^*)} \\
&= -\frac{\partial \lambda}{\partial X_l} \sum_{i=1}^{NG} \sum_{k=1}^m \dot{\mathbf{e}}_{ik}^T \mathbf{t}_{ik,j} \bigg|_{(\dot{\mathbf{e}}_{ik}^*, \lambda^*)} - \lambda \sum_{i=1}^{NG} \sum_{k=1}^m \mathbf{t}_{ik,j}^T \frac{\partial \dot{\mathbf{e}}_{ik}}{\partial X_l} \bigg|_{(\dot{\mathbf{e}}_{ik}^*, \lambda^*)}
\end{aligned} \quad (4.60)$$

It can be seen that the derivative $\partial^2 \alpha_{\text{lim}} / \partial X_j^2$ is a special case of (4.60) when $l \equiv j$. To complete the calculation in (4.60) the derivatives of λ and $\dot{\mathbf{e}}_{ik}$ versus X_l are also needed. Since the Karush-Kuhn-Tucker conditions and the strict complementary slackness hold at the optimal point, it follows that

$$\frac{\partial F_{PL}}{\partial \dot{\mathbf{e}}_{ik}} = \frac{1}{\sqrt{\hat{P}_k}} \mathbf{H}_{ik} \dot{\mathbf{e}}_{ik} + c \left(\sum_{k=1}^m \dot{\mathbf{e}}_{ik} - \hat{\mathbf{B}}_i \dot{\mathbf{u}} \right) - \lambda \mathbf{t}_{ik} = \mathbf{0} \quad \forall i, k \quad (4.61a)$$

$$\frac{\partial F_{PL}}{\partial \dot{\mathbf{u}}} = -c \sum_{i=1}^{NG} \hat{\mathbf{B}}_i^T \left(\sum_{k=1}^m \dot{\mathbf{e}}_{ik} - \hat{\mathbf{B}}_i \dot{\mathbf{u}} \right) = \mathbf{0} \quad (4.61b)$$

$$\sum_{i=1}^{NG} \sum_{k=1}^m \dot{\mathbf{e}}_{ik}^T \mathbf{t}_{ik} - 1 = 0. \quad (4.61c)$$

Since this relation $\left(\sum_{k=1}^m \dot{\mathbf{e}}_{ik} - \hat{\mathbf{B}}_i \dot{\mathbf{u}} \right) = \mathbf{0}$ holds at optimal point, then we can delete it in equation (4.61a) and equation (4.61b) is automatically fulfilled. According to implicit function theorem, by taking derivative of (4.61a, c) versus X_l and using the chain rule for two variables $\dot{\mathbf{e}}_{ik}$, λ one gets

$$\mathbf{G}_{ik} \frac{\partial \dot{\mathbf{e}}_{ik}}{\partial X_l} - \mathbf{t}_{ik} \frac{\partial \lambda}{\partial X_l} - \lambda \mathbf{t}_{ik,l} = \mathbf{0} \quad \forall i, k \quad (4.62a)$$

$$\sum_{i=1}^{NG} \sum_{k=1}^m \mathbf{t}_{ik}^T \frac{\partial \dot{\mathbf{e}}_{ik}}{\partial X_l} = - \sum_{i=1}^{NG} \sum_{k=1}^m \dot{\mathbf{e}}_{ik}^T \frac{\partial \mathbf{t}_{ik}}{\partial X_l} \quad (4.62b)$$

with

$$\mathbf{G}_{ik} = \frac{\partial^2 F_{PL}}{\partial \dot{\mathbf{e}}_{ik}^2} = - \frac{12}{\sqrt{\hat{P}_k^3}} \mathbf{H}_{ik} \dot{\mathbf{e}}_{ik} \dot{\mathbf{e}}_{ik}^T \mathbf{P}_3 + \frac{1}{\sqrt{\hat{P}_k}} (\mathbf{H}_{ik} + \mathbf{D}_{ik}) \quad (4.63)$$

with $\mathbf{H}_{ik}, \mathbf{D}_{ik}, \mathbf{P}_3$ are obtained from (3.20), (3.23) and (1.49).

At the optimal point, \mathbf{G}_{ik} must be positive definite due to the second order sufficiency condition, thus it is invertible. Referring to (4.57) the equation (4.62b) can be written as follows

$$\sum_{i=1}^{NG} \sum_{k=1}^m \mathbf{t}_{ik}^T \frac{\partial \dot{\mathbf{e}}_{ik}}{\partial X_l} = \frac{1}{\lambda} \frac{\partial \alpha_{\text{lim}}}{\partial X_l}. \quad (4.64)$$

From (4.62a) we obtain the derivative of $\dot{\mathbf{e}}_{ik}$ versus X_l

$$\frac{\partial \dot{\mathbf{e}}_{ik}}{\partial X_l} = \mathbf{G}_{ik}^{-1} \mathbf{t}_{ik} \frac{\partial \lambda}{\partial X_l} + \lambda \mathbf{G}_{ik}^{-1} \mathbf{t}_{ik,l}. \quad (4.65)$$

Substituting (4.65) into (4.64) and after some manipulations we obtain as well the derivative of λ versus X_l

$$\frac{\partial \lambda}{\partial X_l} = \frac{\frac{1}{\lambda} \frac{\partial \alpha_{\text{lim}}}{\partial X_l} - \lambda \sum_{i=1}^{NG} \sum_{k=1}^m \mathbf{t}_{ik}^T \mathbf{G}_{ik}^{-1} \mathbf{t}_{ik,l}}{\sum_{i=1}^{NG} \sum_{k=1}^m \mathbf{t}_{ik}^T \mathbf{G}_{ik}^{-1} \mathbf{t}_{ik}}. \quad (4.66)$$

Analogously, by taking derivatives of (4.58) versus X_j, Y and referring to (4.57) one has

$$\frac{\partial^2 \alpha_{\text{lim}}}{\partial X_j \partial Y} = \frac{\partial}{\partial X_j} \left(\frac{\alpha_{\text{lim}}}{Y} \right) \bigg|_{(\mathbf{e}_{ik}^*, \lambda^*)} = \frac{1}{Y} \frac{\partial \alpha_{\text{lim}}}{\partial X_j} \bigg|_{(\mathbf{e}_{ik}^*, \lambda^*)} = -\frac{\lambda}{Y} \sum_{i=1}^{NG} \sum_{k=1}^m \dot{\mathbf{e}}_{ik}^T \mathbf{t}_{ik,j} \bigg|_{(\mathbf{e}_{ik}^*, \lambda^*)} \quad (4.67)$$

$$\frac{\partial^2 \alpha_{\text{lim}}}{\partial Y^2} = \frac{\partial}{\partial Y} \left(\frac{\alpha_{\text{lim}}}{Y} \right) \bigg|_{\mathbf{e}_{ik}^*} = \left(\frac{1}{Y} \frac{\partial \alpha_{\text{lim}}}{\partial Y} - \frac{\alpha_{\text{lim}}}{Y^2} \right) \bigg|_{\mathbf{e}_{ik}^*} = \left(\frac{1}{Y} \frac{\alpha_{\text{lim}}}{Y} - \frac{\alpha_{\text{lim}}}{Y^2} \right) \bigg|_{\mathbf{e}_{ik}^*} = 0. \quad (4.68)$$

It is obvious from (4.68) that for the case of homogeneous material the shakedown load factor is actually a linear function of yield stress, i.e. the optimisation variables $\dot{\mathbf{e}}_{ik}$, $\dot{\mathbf{u}}$ are independent of Y . Moreover, the Lagrange multiplier λ is as well a linear function of Y . These can be proved by taking derivatives of (4.61a, c) versus Y , it follows that

$$\mathbf{G}_{ik} \frac{\partial \dot{\mathbf{e}}_{ik}}{\partial Y} - \mathbf{t}_{ik} \frac{\partial \lambda}{\partial Y} + \frac{\mathbf{H}_{ik} \dot{\mathbf{e}}_{ik}}{Y \sqrt{\hat{P}_k}} = \mathbf{0} \quad \forall i, k \quad (4.69a)$$

$$\sum_{i=1}^{NG} \sum_{k=1}^m \mathbf{t}_{ik}^T \frac{\partial \dot{\mathbf{e}}_{ik}}{\partial Y} = 0. \quad (4.69b)$$

Substituting (4.69a) into (4.69b) with referring to the relation (4.61a) and after some manipulations we obtain

$$\frac{\partial \lambda}{\partial Y} = \frac{\lambda}{Y}, \quad \frac{\partial \dot{\mathbf{e}}_{ik}}{\partial Y} = 0. \quad (4.70)$$

The second derivatives of α_{lim} versus thickness variable Z are also necessary. Since $\dot{\mathbf{e}}_{ik}$ and λ are functions of Z , from (4.59) and (4.57) one has

$$\begin{aligned} \frac{\partial^2 \alpha_{\text{lim}}}{\partial Z^2} = & \left\{ \sum_{i=1}^{NG} \sum_{k=1}^m \left(\frac{\partial \dot{\mathbf{e}}_{ik}}{\partial Z} \right)^T \frac{\partial}{\partial \dot{\mathbf{e}}_{ik}} \left(Y \tilde{N}_0 \tilde{\varepsilon}_0 \sqrt{\frac{\hat{P}_k}{3}} \left(\sqrt{\beta_1^2 + \gamma} + \sqrt{\beta_2^2 + \gamma} \right) \right) \right\} \bigg|_{\mathbf{e}_{ik}^*} \\ & + \frac{\partial}{\partial Z} \left\{ \sum_{i=1}^{NG} \sum_{k=1}^m \left(Y \tilde{N}_0 \tilde{\varepsilon}_0 \sqrt{\frac{\hat{P}_k}{3}} \left(\sqrt{\beta_1^2 + \gamma} + \sqrt{\beta_2^2 + \gamma} \right) \right) \right\} \bigg|_{\mathbf{e}_{ik}^*} \end{aligned} \quad (4.71)$$

$$\begin{aligned}
\frac{\partial^2 \alpha_{\text{lim}}}{\partial X_j \partial Z} &= \frac{\partial}{\partial Z} \left(-\lambda \sum_{i=1}^{NG} \sum_{k=1}^m \dot{\mathbf{e}}_{ik}^T \mathbf{t}_{ik,j} \right) \bigg|_{(\dot{\mathbf{e}}_{ik}^*, \lambda^*)} \\
&= -\frac{\partial \lambda}{\partial Z} \sum_{i=1}^{NG} \sum_{k=1}^m \dot{\mathbf{e}}_{ik}^T \mathbf{t}_{ik,j} \bigg|_{(\dot{\mathbf{e}}_{ik}^*, \lambda^*)} - \lambda \sum_{i=1}^{NG} \sum_{k=1}^m \mathbf{t}_{ik,j}^T \frac{\partial \dot{\mathbf{e}}_{ik}}{\partial Z} \bigg|_{(\dot{\mathbf{e}}_{ik}^*, \lambda^*)}
\end{aligned} \tag{4.72}$$

$$\begin{aligned}
\frac{\partial^2 \alpha_{\text{lim}}}{\partial Y \partial Z} &= \frac{\partial}{\partial Y} \left(\sum_{i=1}^{NG} \sum_{k=1}^m \left(Y \tilde{N}_0 \tilde{\varepsilon}_0 \sqrt{\frac{\hat{P}_k}{3}} \left(\sqrt{\beta_1^2 + \gamma} + \sqrt{\beta_2^2 + \gamma} \right) \right) \right) \bigg|_{\dot{\mathbf{e}}_{ik}^*} \\
&= \sum_{i=1}^{NG} \sum_{k=1}^m \left(\tilde{N}_0 \tilde{\varepsilon}_0 \sqrt{\frac{\hat{P}_k}{3}} \left(\sqrt{\beta_1^2 + \gamma} + \sqrt{\beta_2^2 + \gamma} \right) \right) \bigg|_{\dot{\mathbf{e}}_{ik}^*}
\end{aligned} \tag{4.73}$$

The first term in (4.71) can be simplified by

$$\begin{aligned}
&\frac{\partial}{\partial \dot{\mathbf{e}}_{ik}} \left(Y \tilde{N}_0 \tilde{\varepsilon}_0 \sqrt{\frac{\hat{P}_k}{3}} \left(\sqrt{\beta_1^2 + \gamma} + \sqrt{\beta_2^2 + \gamma} \right) \right) \\
&= \frac{\sqrt{3}}{4\sqrt{\hat{P}_k}} Y \tilde{N}_0 \tilde{\varepsilon}_0 \left\{ 16 \left(\sqrt{\beta_1^2 + \gamma} + \sqrt{\beta_2^2 + \gamma} \right) \mathbf{P}_3 + 8 \left(\frac{\beta_1}{\sqrt{\beta_1^2 + \gamma}} - \frac{\beta_2}{\sqrt{\beta_2^2 + \gamma}} \right) \mathbf{A} \right. \\
&\quad \left. + \left(\frac{1}{\sqrt{\beta_1^2 + \gamma}} + \frac{1}{\sqrt{\beta_2^2 + \gamma}} \right) \mathbf{B} \right\} \dot{\mathbf{e}}_{ik}
\end{aligned} \tag{4.74}$$

with \mathbf{P}_3 , \mathbf{A} , \mathbf{B} are given by (1.49) and (3.23). The second term in (4.71) can be rewritten as follows

$$\begin{aligned}
&\frac{\partial}{\partial Z} \left\{ \sum_{i=1}^{NG} \sum_{k=1}^m \left(Y \tilde{N}_0 \tilde{\varepsilon}_0 \sqrt{\frac{\hat{P}_k}{3}} \left(\sqrt{\beta_1^2 + \gamma} + \sqrt{\beta_2^2 + \gamma} \right) \right) \right\} \\
&= \sum_{i=1}^{NG} \sum_{k=1}^m \left(Y \tilde{N}_0 \tilde{\varepsilon}_0 \sqrt{\frac{\hat{P}_k}{3}} \left(\frac{\beta_1}{2\sqrt{\beta_1^2 + \gamma}} + \frac{\beta_2}{2\sqrt{\beta_2^2 + \gamma}} \right) \right)
\end{aligned} \tag{4.75}$$

In order to complete (4.71), the derivatives of λ and $\dot{\mathbf{e}}_{ik}$ versus Z are needed. By taking derivatives of (4.61a, c) versus Z and using the chain rule for two variables $\dot{\mathbf{e}}_{ik}$, λ , one has

$$\mathbf{G}_{ik} \frac{\partial \dot{\mathbf{e}}_{ik}}{\partial Z} - \mathbf{t}_{ik} \frac{\partial \lambda}{\partial Z} + \frac{1}{\sqrt{\hat{P}_k}} \frac{\partial \mathbf{H}_{ik}}{\partial Z} \dot{\mathbf{e}}_{ik} = \mathbf{0} \quad \forall i, k \tag{4.76a}$$

$$\sum_{i=1}^{NG} \sum_{k=1}^m \mathbf{t}_{ik}^T \frac{\partial \dot{\mathbf{e}}_{ik}}{\partial Z} = 0 \tag{4.76b}$$

Referring to (3.20) and after some manipulations we obtain

$$\frac{\partial \mathbf{H}_{ik}}{\partial Z} = Y\tilde{N}_0\tilde{\varepsilon}_0 \left(\begin{array}{l} 4\sqrt{3} \left(\sqrt{\beta_1^2 + \gamma} + \sqrt{\beta_2^2 + \gamma} \right) \mathbf{P}_3 \\ + 2\sqrt{3} \left(\frac{\beta_1}{\sqrt{\beta_1^2 + \gamma}} - \frac{\beta_2}{\sqrt{\beta_2^2 + \gamma}} \right) \mathbf{A} \\ + \frac{\sqrt{3}}{4} \left(\frac{1}{\sqrt{\beta_1^2 + \gamma}} + \frac{1}{\sqrt{\beta_2^2 + \gamma}} \right) \mathbf{B} \end{array} \right) \quad (4.77)$$

From (4.76a) we obtain the derivative of $\dot{\mathbf{e}}_{ik}$ versus Z

$$\frac{\partial \dot{\mathbf{e}}_{ik}}{\partial Z} = \mathbf{G}_{ik}^{-1} \mathbf{t}_{ik} \frac{\partial \lambda}{\partial Z} - \frac{1}{\sqrt{\hat{P}_\kappa}} \mathbf{G}_{ik}^{-1} \frac{\partial \mathbf{H}_{ik}}{\partial Z} \dot{\mathbf{e}}_{ik} \quad (4.78)$$

Substituting (4.78) into (4.76b) one gets

$$\frac{\partial \lambda}{\partial Z} = \frac{\sum_{i=1}^{NG} \sum_{k=1}^m \frac{1}{\sqrt{\hat{P}_\kappa}} \mathbf{t}_{ik}^T \mathbf{G}_{ik}^{-1} \frac{\partial \mathbf{H}_{ik}}{\partial Z} \dot{\mathbf{e}}_{ik}}{\sum_{i=1}^{NG} \sum_{k=1}^m \mathbf{t}_{ik}^T \mathbf{G}_{ik}^{-1} \mathbf{t}_{ik}}. \quad (4.79)$$

4.4.5 Special case of probabilistic shakedown analysis

Consider a special case of probabilistic shakedown analysis, where P is a stochastic one-parameter load, i.e. with a reference load P^0 we have $P = xP^0$ and $\mathbf{t}_{ik} = x\mathbf{t}_{ik}^0$ where \mathbf{t}_{ik}^0 is the stress vector due to referent load P^0 . Otherwise we have as well

$$\frac{\partial \mathbf{t}_{ik}}{\partial X} = \frac{\mathbf{t}_{ik}}{X}. \quad (4.80)$$

In this case, the non-linear optimisation (4.49) becomes

$$\begin{aligned} \alpha_{\text{lim}} &= \min_{\dot{\mathbf{e}}_{ik}, \mathbf{u}} (F_P) \\ s.t : \quad & \left(\sum_{i=1}^{NG} \sum_{k=1}^m \dot{\mathbf{e}}_{ik}^T x \mathbf{t}_{ik}^0 - 1 \right) = 0 \end{aligned} \quad (4.81)$$

If we now define a new strain vector $\dot{\hat{\mathbf{e}}}_{ik} = x\dot{\mathbf{e}}_{ik}$ and new displacement vector $\hat{\mathbf{u}} = x\mathbf{u}$, then (4.81) can be rewritten as follows

$$\begin{aligned} \alpha_{\text{lim}} &= \min_{\dot{\hat{\mathbf{e}}}_{ik}, \hat{\mathbf{u}}} (F_P) \\ s.t : \quad & \left(\sum_{i=1}^{NG} \sum_{k=1}^m \dot{\hat{\mathbf{e}}}_{ik}^T \mathbf{t}_{ik}^0 - 1 \right) = 0 \end{aligned} \quad (4.82)$$

with

$$F_P = \sum_{i=1}^{NG} \left\{ \sum_{k=1}^m \left(\frac{Y}{X} \eta_{ik} \right) + \frac{c}{2} \left(\sum_{k=1}^m \dot{\mathbf{e}}_{ik} - \hat{\mathbf{B}}_i \hat{\mathbf{u}} \right)^T \left(\sum_{k=1}^m \dot{\mathbf{e}}_{ik} - \hat{\mathbf{B}}_i \hat{\mathbf{u}} \right) \right\}. \quad (4.83)$$

Since the constraint is now no longer depended on the load variable X , it follows that

$$\frac{\partial \alpha_{\text{lim}}}{\partial X} = \frac{\partial F_{PL}}{\partial X} \bigg|_{(\hat{\mathbf{e}}_{ik}^*, \hat{\mathbf{u}}^*, \lambda^*)} = \sum_{i=1}^{NG} \sum_{k=1}^m \left(-\frac{Y}{X^2} \eta_{ik} \right) \bigg|_{\dot{\mathbf{e}}_{ik}^*} = -\frac{\alpha_{\text{lim}}}{X} \quad (4.84)$$

$$\frac{\partial^2 \alpha_{\text{lim}}}{\partial X^2} = -\frac{\partial}{\partial X} \left(\frac{\alpha_{\text{lim}}}{X} \right) = -\frac{1}{X} \frac{\partial \alpha_{\text{lim}}}{\partial X} + \frac{\alpha_{\text{lim}}}{X^2} = \frac{1}{X} \frac{\alpha_{\text{lim}}}{X} + \frac{\alpha_{\text{lim}}}{X^2} = \frac{2\alpha_{\text{lim}}}{X^2} \quad (4.85)$$

$$\frac{\partial^2 \alpha_{\text{lim}}}{\partial Y \partial X} = -\frac{\partial}{\partial Y} \left(\frac{\alpha_{\text{lim}}}{X} \right) = -\frac{1}{X} \frac{\partial \alpha_{\text{lim}}}{\partial Y} = -\frac{\alpha_{\text{lim}}}{XY} \quad (4.86)$$

$$\frac{\partial^2 \alpha_{\text{lim}}}{\partial Z \partial X} = -\frac{\partial}{\partial Z} \left(\frac{\alpha_{\text{lim}}}{X} \right) = -\frac{1}{X} \frac{\partial \alpha_{\text{lim}}}{\partial Z}. \quad (4.87)$$

These above derivatives can also be easily obtained by using the same procedure as applied for the material variable Y . By this way, it is easy to prove that

$$\frac{\partial \lambda}{\partial X} = -\frac{\lambda}{X}, \quad \frac{\partial \dot{\mathbf{e}}_{ik}}{\partial X} = 0, \text{ and then we find again the above expressions finally.}$$

The flowchart in figure 4.3 contains the logical connections of the main analysis steps as they have been implemented in our finite element code based probabilistic limit and shakedown analysis. In each probabilistic iteration, i.e. the iteration for finding the design point, two deterministic loops are required, the first one provides information for sensitivity analysis and the second one for the simple line search algorithm, as mentioned in (4.35).

5 MULTIMODE FAILURE AND THE IMPROVEMENT OF FORM/SORM RESULTS

In the previous chapter, the concept of reliability has mainly been concerned with individual structural elements and failure mechanisms. The reliability of a real structure is usually much more difficult to evaluate since more than one element (member) can fail and because there is the possibility of more than one failure mode for the system. In this case, analysis of the structural system is required to evaluate the safety of the structure as a whole [Ditlevsen and Bjerager, 1986]. To handle problems of this kind, the real structure is sometimes modelled by an equivalent system in such a way that all relevant failure modes can be treated [Thoft-Christensen and Baker, 1982]. Structural systems can generally be characterized as series or parallel systems or some combination of the two [Madsen et al., 1986]. In series system, the formation of any individual failure mode or mechanism is defined as system failure. For example, in statically determinate or rigid-plastic structures, formation of a collapse mechanism will result in failure of the total system and therefore they can be modelled as series system with each element of the series being a failure mechanism. In parallel system, failure in a single element will not result in failure of the system, because the remaining elements may be able to sustain the external loads by redistributing of the loads. A typical example of a parallel system is a statically indeterminate structures. Failure of such structures will always require that more than one element fails before the structure loses integrity and fails.

The non-linear optimization algorithm which was developed in section 4.3 is globally convergent [Tran et al., 2007b, d], i.e., the sequence is guaranteed to converge to a minimum-distance point on the limit state surface, provided that the limit state function is continuous and differentiable. However, as with any non-convex optimisation problem, it is not guaranteed that the solution point will be the global minimum-distance point when the system has more than one failure mode (multimode failure or multiple design points). This chapter aims at presenting a method to successively find the multiple design points of a component reliability problem, when they exist on the limit state surface. Each design point corresponds with an individual failure mode or mechanism. FORM and SORM approximations are applied at each design point followed by a series system reliability analysis to lead to improved estimates of the system failure probability.

5.1 Multimode failure

5.1.1 Bounds for the system probability of failure

In the previous chapter, a probabilistic algorithm was developed to identify the failure mode and to evaluate the failure probability of an elasto-plastic shell structure. In structural analysis, it is rather an exception to deal with a problem where the failure of a structure can be satisfactorily defined by one limit state equation only. Thus, the identified mode is only one of many modes that can occur, and the probability of the mode occurring may or may not provide a good estimate of the system probability of failure. If there are m failure mechanisms and the limit state surface is respectively described by m equations

$$g_i(\mathbf{X}) = g_i(X_1, \dots, X_n) = 0, \quad i = 1, m \quad (5.1)$$

and if we denote the failure due to the i th mode as the random event E_i

$$E_i = \{\mathbf{x} \mid g_i(\mathbf{X}) \leq 0\} \quad (5.2)$$

then the probability that the system fails is the probability that any failure mechanism occurs. It means that

$$P_f = P(E_1 \cup E_2 \cup \dots \cup E_m) = P\left(\bigcup_{i=1}^m E_i\right). \quad (5.3)$$

If the joint probability density function of the failure events $f_E(\mathbf{e})$ is known, then the system probability of failure can be calculated by the n -dimensional integral

$$P_f = P\left(\bigcup_{i=1}^m E_i\right) = \int_{-\infty}^0 \dots \int_{-\infty}^0 f_E(e_1, \dots, e_m) de_1 \dots de_m. \quad (5.4)$$

Several techniques such as simulation methods or reducing the dimension of the original integral (e.g. [Dunnet et al., 1955], [Rackwitz, 1978], [Hohenbichler, 1981]) exist for evaluation of equation (5.4). However, in general, evaluation of the system probability of failure through direct integration may not be feasible, even if an expression exists for the joint density function of failure modes and all failure modes have been identified. In this case, bounds relieve the necessity of evaluating the m -dimensional integral either analytically, numerically or through Monte Carlo simulation [Ramachandran, 1984], [Melchers, 1987]. Several first-order bounds exist (e.g., [Cornell, 1967]) which only require knowledge of the individual probabilities of failure resulting directly from the axioms of the probability theory. Unfortunately, these bounds may be quite wide for structural reliability application [Grimmelt and Schueller, 1982]. Closer or second-order bounds can be given in term of the individual failure probabilities and the joint failure probabilities between any two modes. If we denote the individual failure probabilities P_i as

$$P_i = P[g_i(\mathbf{X}) \leq 0], \quad i = 1, m \quad (5.5)$$

then, the bounds of the system probability of failure for a series system are [Ditlevsen, 1979]

$$P_1 + \sum_{i=2}^m \max \left\{ P_i - \sum_{j=1}^{i-1} P_{ij}, 0 \right\} \leq P_f \leq \sum_{i=1}^m P_i - \sum_{i=2}^m \max_{j < i} P_{ij} \quad (5.6)$$

with the notation P_{ij} has been used for the joint failure probability

$$P_{ij} = P[g_i(\mathbf{X}) \leq 0, g_j(\mathbf{X}) \leq 0]. \quad (5.7)$$

Since not all couples of the random events E_i are taken into account in equation (5.6) the ordering of the modes will have an effect on the bounds. Practical experience suggested that ordering the failure modes according to decreasing values P_i may correspond to the better bounds. In structural reliability, these bounds are frequently used and are considered sufficiently accurate for most structural systems [Grimmelt and Schueller, 1982]. Next section will present the calculation of these second-order bounds based on the first-order system reliability analysis. Another bounds can, of course, be derived which include the joint probabilities of failure of any three failure modes. It appears, however, that for practical problems this improvement is small compared to the improvement in using second-order bounds instead of first-order bounds [Hohenbichler and Rackwitz, 1983].

5.1.2 First-order system reliability analysis

In a first-order system reliability analysis, the failure set is approximated by the polyhedral set bounded by the tangent hyper-planes at the design points. Each design point corresponds to a failure mode and they are the points on the limit state surface that have smallest distances to the origin in a standard normal space. We denote the design points in standard normal space as u_i^* , $i = 1, 2, \dots, m$ and associated with each design point, we define the distance $\beta_{HLi} = \|u_i^*\|$, which is the corresponding reliability index. The individual probabilities of failure P_i are determined as

$$P_i = \Phi(-\beta_{HLi}). \quad (5.8)$$

The first-order approximation to P_{ij} is obtained by approximating the joint failure set by the set bounded by the tangent hyper-planes at the design points for the two failure modes. Figure 5.1 presents the projection of the limit state surface for the two failure modes on the plane containing the origin and the two design points \mathbf{u}_i^* and \mathbf{u}_j^* . The joint failure probability P_{ij} is thus calculated as

$$P_{ij} = \Phi(-\beta_{HLi}, -\beta_{HLj}; \rho_{ij}) = \int_{-\infty}^{-\beta_{HLi}} \int_{-\infty}^{-\beta_{HLj}} \varphi(x, y; \rho_{ij}) dx dy \quad (5.9)$$

with the correlation coefficient between two failure modes ρ_{ij} are

$$\rho_{ij} = \cos \nu_{ij} = \frac{(\mathbf{u}_i^*)^T \mathbf{u}_j^*}{\beta_{HLi} \beta_{HLj}} \quad (5.10)$$

and $\varphi(x, y; \rho)$ is the probability density function for a bivariate normal vector with zero mean values, unit variances and correlation coefficient ρ

$$\varphi(x, y; \rho) = \frac{1}{2\pi\sqrt{1-\rho^2}} \exp\left[-\frac{1}{2} \frac{x^2 + y^2 - 2\rho xy}{1-\rho^2}\right]. \quad (5.11)$$

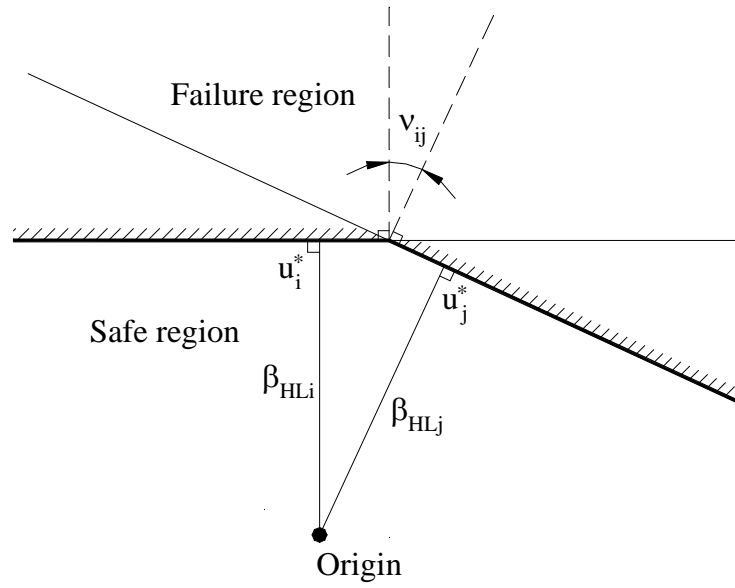


Figure 5.1 Geometrical illustration of first-order system failure set

Substituting the density function in (5.9) by the corresponding cumulative distribution function $\Phi(x, y; \rho)$, which gives

$$\begin{aligned} P_{ij} &= \Phi(-\beta_{HLi}, -\beta_{HLj}; 0) + \int_0^{\rho_{ij}} \frac{\partial \Phi(-\beta_{HLi}, -\beta_{HLj}; z)}{\partial \rho} dz \\ &= \Phi(-\beta_{HLi})\Phi(-\beta_{HLj}) + \int_0^{\rho_{ij}} \varphi(-\beta_{HLi}, -\beta_{HLj}; z) dz \end{aligned} \quad (5.12)$$

Numerical techniques are available for evaluating the joint failure probability in equation (5.12), e.g. Newton-Codes method. Simple bounds on the joint failure probability, which is based on geometrical illustration of multimode failure system can also be given, thus avoiding any numerical integration [Madsen et al., 1986]. It should be noted that the bounds (5.6) still estimate a solution of the generally unknown region which respect to the exact value of the probability of failure. If we do not know where the values of the

probabilities are placed with respect to the exact values, we can not confirm that the bounds given above estimate the probability of failure. They bound some approximation and we can only more-or-less reasonably expect that the approximation is close to the exact result and the bounds remain meaningful.

5.2 Solution technique

As discussed above, a real structure may have several failure modes or failure mechanisms and the existence of multiple failure modes (or multiple design points) may cause the following problems in FORM and SORM. That is, the optimization algorithm which was developed in section 4.3 may converge to a local design point. In that case, the FORM/SORM solution will miss the region of dominant contribution to the failure probability integral and, thus, has large error. Even if the global design point is found, the neighborhoods of the local design points may also have significant contribution to the failure probability integral. Approximating the limit state surface only at the global design point will lose these contributions.

In this section, a simple method is presented for finding the multiple design points of a reliability analysis problem, when they exist on the limit state surface. The method was developed by [Der Kiureghian and Dakessian, 1998]. Once all the design points are known, the failure probability of series system is calculated by using first-order system reliability method and second-order bounds as presented above.

5.2.1 Basic idea of the method

In optimization theory, one method often suggested to find the global and local solutions is to repeat the analysis with different starting points and hope that all optimal points will be found. Unfortunately, it is possible for all trials to converge to the same point even when the other optimal points exist. A more effective method is to construct “barriers” around previously found solutions, thus forcing the algorithm to seek a new solution. In our problem to find the points which have the minimum distances from origin, the “barriers” around found solutions can be construct by moving the limit state surface in the neighborhood of them away from the origin. Supposing that the first design point \mathbf{u}_1^* is already found by the non-linear optimization algorithm in section 4.3. We construct a “barrier” for this point by adding a ‘bulge’ to the limit state surface. Thus, the limit state function for the deformed surface is

$$g_1(\mathbf{u}) = g(\mathbf{u}) + B_1(\mathbf{u}) \quad (5.13)$$

where $B_1(\mathbf{u})$ defines the bulge fitted at \mathbf{u}_1^* . Solving the optimisation problem with the new limit state function $g_1(\mathbf{u})$ leads to a second design point \mathbf{u}_2^* . In order to seek the third solution point \mathbf{u}_3^* , a bulge $B_2(\mathbf{u})$ is now added at \mathbf{u}_2^* resulting in the limit state function

$g_2(\mathbf{u}) = g_1(\mathbf{u}) + B_2(\mathbf{u}) = g(\mathbf{u}) + B_1(\mathbf{u}) + B_2(\mathbf{u})$. Repeating the process until all design points are found. The limit state function for finding the m -th design point thus, is

$$g_{m-1}(\mathbf{u}) = g(\mathbf{u}) + \sum_{i=1}^{m-1} B_i(\mathbf{u}) \quad (5.14)$$

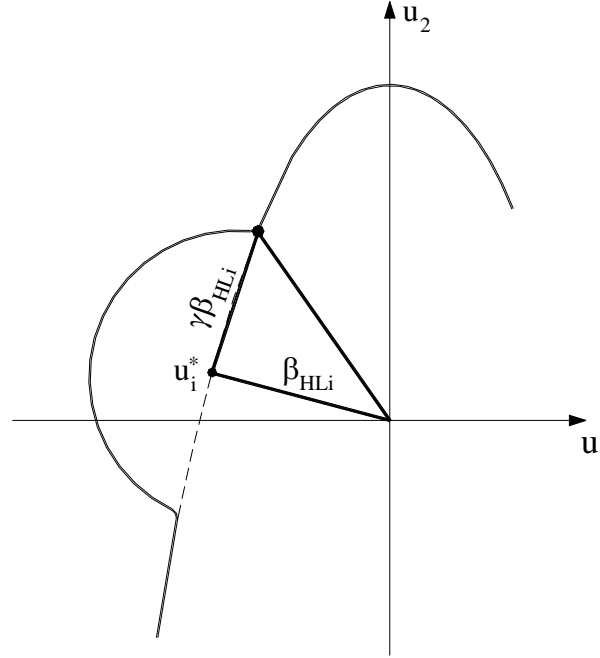


Figure 5.2 Definition of a bulge at design point \mathbf{u}_i^*

As is shown in the figure 5.2, it is possible for the optimisation algorithm to converge to the points located at the feet of the bulge, which are actually the spurious minimum-distance points. However, practical experience showed that this occurs only when there is no other genuine design point. Thus, convergence to a spurious point usually means that no other genuine design point exists [Der Kiureghian and Dakessian, 1998]. This nature can be used as the stopping criterion of the algorithm.

5.2.2 Definition of the bulge

The derivation of a bulge $B_i(\mathbf{u})$ at a design point \mathbf{u}_i^* is based on the following requirements

- $B_i(\mathbf{u})$ must be positive in the neighborhood of \mathbf{u}_i^* (in order to move the limit state surface away from the origin) and zero elsewhere.
- The bulge should have a strong outward curvature at its feet in order to make the search algorithm converging to an existing genuine design point rather than to its feet.
- $B_i(\mathbf{u})$ must be continuous and differentiable since the optimization algorithm requires a continuous and differentiable limit state function.

Basing on the above considerations, Der Kiureghian and Dakessian proposed a spherical shape of the bulge as follows

$$B_i(\mathbf{u}) = \begin{cases} s_i \left(r_i^2 - \|\mathbf{u} - \mathbf{u}_i^*\|^2 \right)^2 & \text{if } \|\mathbf{u} - \mathbf{u}_i^*\| \leq r_i \\ 0 & \text{elsewhere} \end{cases} \quad (5.15)$$

where $r_i = \gamma \beta_{HLi}$ is the radius of the bulge. The parameter γ should be chosen carefully since a small γ is conservative but may produce insufficient curvature at the foot of the bulge, whereas a large one may result in a bulge that conceals other significant design points. The scale factor s_i governs the height of the bulge and, thus, the distance by which the limit state surface in the neighborhood of \mathbf{u}_i^* is moved away from the origin. It must be chosen large enough to assure a strong outward curvature at the food of the bulge. Suppose we want to move the design point \mathbf{u}_i^* away from the origin by the amount $\delta \beta_{HLi}$, where $0 < \delta < \gamma$. Since the slope of the limit state surface at \mathbf{u}_i^* is $\|\nabla g(\mathbf{u}_i^*)\|$, it is seen that the necessary height of the bulge at that point is $\delta \beta_{HLi} \|\nabla g(\mathbf{u}_i^*)\|$. From equation (5.15), it follows that

$$s_i = \frac{\delta \beta_{HLi} \|\nabla g(\mathbf{u}_i^*)\|}{\left[(\gamma \beta_{HLi})^2 - (\delta \beta_{HLi})^2 \right]^2}. \quad (5.16)$$

The definition of the bulge at each design point in term of β_{HLi} , $\|\nabla g(\mathbf{u}_i^*)\|$ and two parameters γ , δ is complete through the two equations (5.15) and (5.16). To complete the method one needs to know whether a newly found design point is genuine or spurious. This is easily solved by calculating its distances from previously found design points. If any one of these distances is smaller than or equal to the radius of the corresponding bulge, then the newly found design point is at the foot of this bulge and, therefore, is spurious. Convergence to a spurious design point usually means that no more genuine design points exist. However, in order to make sure that this is the case, one may wish to add a new bulge at this spurious design point and continue the search. Of course, the spurious design points are not included in the reliability calculations.

6 LIMIT AND SHAKEDOWN ANALYSIS OF DETERMINISTIC PROBLEMS

The deterministic and probabilistic shakedown optimizations described in the above chapters is programmed and implemented in the finite element package Code_Aster, a free open source computing software [Code_Aster 7.3, 2003]. The 3-node triangular and 4-node quadrangular isoparametric flat shell elements, which are based on the Kirchhoff's hypothesis, were applied. Although the flat shell elements may fail to satisfy the basic convergence properties that should be expected from sound finite element procedures in general, they can produce reasonably accurate approximations [Chapelle and Bathe, 2003]. The presented shakedown method applies also to more effective shell elements that work with generalized variables. But currently only flat elements are available in Code_Aster. The finite element discretisations were realized by the personal pre- and post-processor GiD [GiD 7.2, 2002].

Nine examples are presented below for the sake of evaluation the algorithm, including both plate and shell structures. The structures under consideration can be subjected to mechanical and thermal loads and are made of elastic-perfectly plastic material. In each numerical test, some existing analytical, numerical and experimental solutions found in literature are briefly represented and compared. Perfectly plastic LISA methods cover two mandatory design checks of the new European pressure vessel standard [European standard, 2005-06], [Taylor et al., 1999].

- *GP check*: Limit analysis with the Tresca yield function and a typical safety factor of 1.5 can be used to exclude plastic collapse under monotonic loading by gross plastic deformation. In practice the non-smooth Tresca function is replaced by the von Mises function so that an additional safety factor of $\frac{2}{\sqrt{3}} = 1.1547$ is effective in pipes and cylindrical pressure vessels. The total safety factor is $\sqrt{3} = 1.732$, [Vu et al., 2007].
- *PD check*: Shakedown analysis with the von Mises yield function may be used without a safety factor to exclude incremental collapse by ratcheting under cyclic loading.

With respect to pressure vessel design it can be concluded that shakedown analysis is decisive if the shakedown load is less than $\frac{1}{\sqrt{3}} = 0.57735$ –times the limit load. If only the safety factor 1.5 is applied in the GP check then the PD check is decisive if the shakedown load is less than 0.6 –times the limit load. The present shakedown analysis includes also the AP check against failure by alternating plasticity. However, this check is not mandatory.

6.1 Limit analysis of a cylindrical pipe under complex loading

Consider an example of a cylindrical pipe under complex loading, which was examined by Yan [1997], Vu [2001] and [Larson et al., 1975]. The pipe is subjected to bending and torsion moments M_b , M_t as well as internal pressure p and axial tension F (figure 6.1). We denote here L the length, r the mean radius and h the thickness of the pipe.

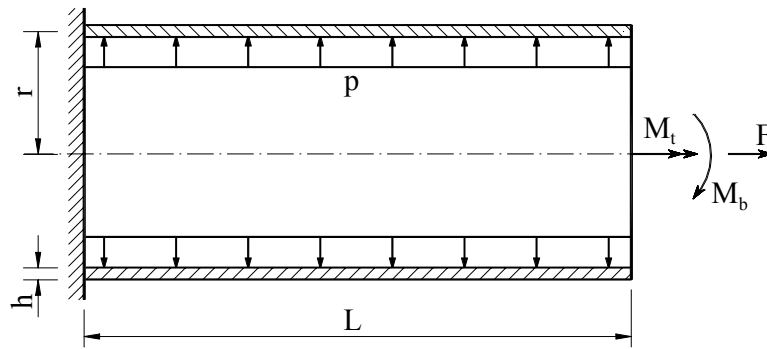


Figure 6.1 Cylindrical pipe under complex loading

Firstly, consider the pipe under pure bending. The analytic solution of plastic collapse limit may be easily obtained by Bernoulli's theory

$$M_{bl} = \sigma_y \eta_{pl} W_{el} = 4\sigma_y h \left(r^2 + \frac{h^2}{12} \right) \quad (6.1)$$

where σ_y denotes the material yield stress, M_{bl} is the maximum bending moment we can apply on the pipe while other loads are removed.

If only torsion moment is applied on the pipe, the plastic collapse limit is then

$$M_{tl} = \frac{2}{\sqrt{3}} \pi r^2 h \sigma_y. \quad (6.2)$$

Furthermore if bending moment, internal pressure and axial tension apply at the same time on a thin-walled pipe, the following analytical solution may be used

$$m = \frac{\sqrt{4-3n_\phi^2}}{2} \cos \left[\frac{n_\phi - 2n_x}{\sqrt{4-3n_\phi^2}} \frac{\pi}{2} \right] \quad (6.3)$$

in which m, n_ϕ, n_x are the normalized quantities

$$\begin{aligned} m &= M/M_l, \quad M_l = 4r^2 h \sigma_y \\ n_\phi &= p/p_l, \quad p_l = \sigma_y h/r \\ n_x &= F/F_l, \quad F_l = 2\pi \sigma_y r h \end{aligned} \quad (6.4)$$

The formulations (6.1÷6.4) are taken from Yan [1997]. If axial tension is caused by only internal pressure (the pipe has closed ends), it is easy to find that $n_x = n_\phi / 2$ and the formulation (6.3) now becomes

$$m = \frac{\sqrt{4-3n_\phi^2}}{2}. \quad (6.5)$$

In our numerical analysis the whole pipe is discretized by 300 quadrangular flat 4-node shell elements as shown in figure 6.2. The following geometrical and physical parameters are adopted: $L = 2700\text{mm}$, $r = 300\text{mm}$, $h = 60\text{mm}$, $\sigma_y = 160\text{MPa}$.

If only a bending moment is applied with its limit value $M_b = M_{bl} = 3467.52 \text{ kNm}$ (formula 6.1), the limit load factor is 1.010. In this case, the numerical error is 1% compared with the analytical solution. On the other hand, if only torsion moment is applied with its limit value $M_t = M_{tl} = 3134.24 \text{ kNm}$ (formula 6.2), the limit load factor is 1.0053, and the numerical error is only 0.53% compared with the analytical solution.



Figure 6.2 FE-mesh of cylindrical pipe

When the two loads (bending moment and internal pressure) are applied, the limit load factor can be estimated by using (6.5). The interaction diagram (figure 6.3) presents both numerical and analytical results. It is observed that the numerical solution agrees very

well with the analytical one: the maximum numerical error is less than 1%.

On the other hand, if only axial tension is applied, the limit load factor is 1.0015. In this case, numerical error is only 0.15% compared with the analytical solution.

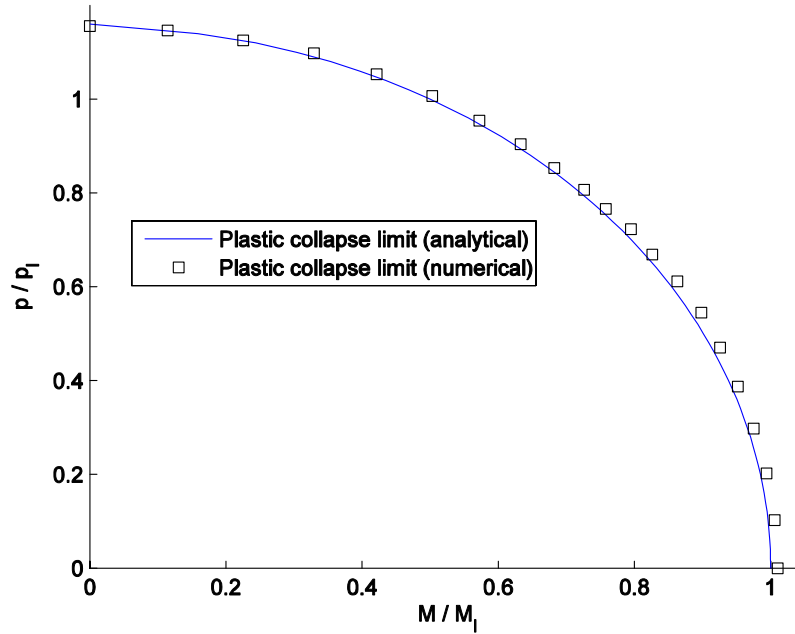


Figure 6.3 Cylindrical pipe under bending and internal pressure

6.2 Limit and shakedown analysis of a thin-walled pipe subjected to internal pressure and axial force

In this example, a thin-walled pipe with thickness h and mean radius r as shown in figure 6.4 is considered. The pipe is subjected to internal pressure p together with axial force F . This problem was investigated analytically by Cocks and Leckie [1988] using the Tresca yield criterion and by Yan [1997] using the von Mises yield criterion.

When both internal pressure and axial force increase monotonically and proportionally, the plastic collapse limit can be computed by using the condition:

$$\frac{p^2}{p_l^2} + \frac{F^2}{F_l^2} - \frac{p}{p_l} \frac{F}{F_l} = 1 \quad (6.6)$$

where $p_l = \beta \frac{\sigma_y h}{r}$, $F_l = 2\pi r h \sigma_y$ with $\beta = 1$ for a long pipe without the end constraining effect.

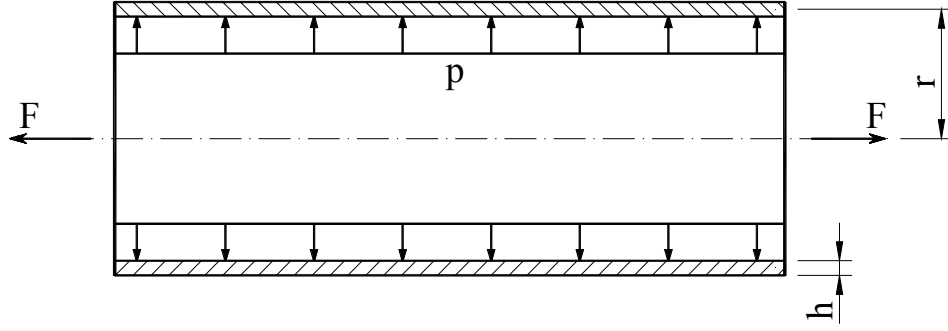


Figure 6.4 Thin-walled pipe

If internal pressure remains constant while axial force varies within the range $[-F, F]$, the shakedown limit can be computed by using the following condition:

$$\frac{p^2}{p_l^2} + \frac{F^2}{F_l^2} + \frac{p}{p_l} \frac{F}{F_l} = 1. \quad (6.7)$$

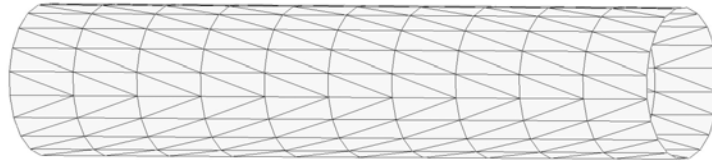


Figure 6.5 FE-mesh of the pipe

Note that (6.6) and (6.7) were found by using the von Mises yield criterion [Yan 1997]. On the other hand, if the Tresca yield criterion is used, the shakedown range is limited by the condition [Cocks and Leckie 1988]:

$$\frac{p}{p_l} = 1 - \frac{F}{F_l}. \quad (6.8)$$

In our numerical analysis the whole pipe is discretized by 400 3-node triangular flat shell elements as shown in figure 6.5 with the following geometrical properties and material yield stress: $r = 300$ mm, $h = 10$ mm, $L = 2700$ mm, $\sigma_y = 116$ MPa.

The interaction diagram for limit and shakedown analysis with normalized pressure p/p_l and normalized axial force F/F_l is plotted in figure 6.6. Analytical solutions are computed by using the formulations (6.6) and (6.7). In all cases, the diagram shows good agreements between numerical and analytical solutions. The numerical error is less than 1%.

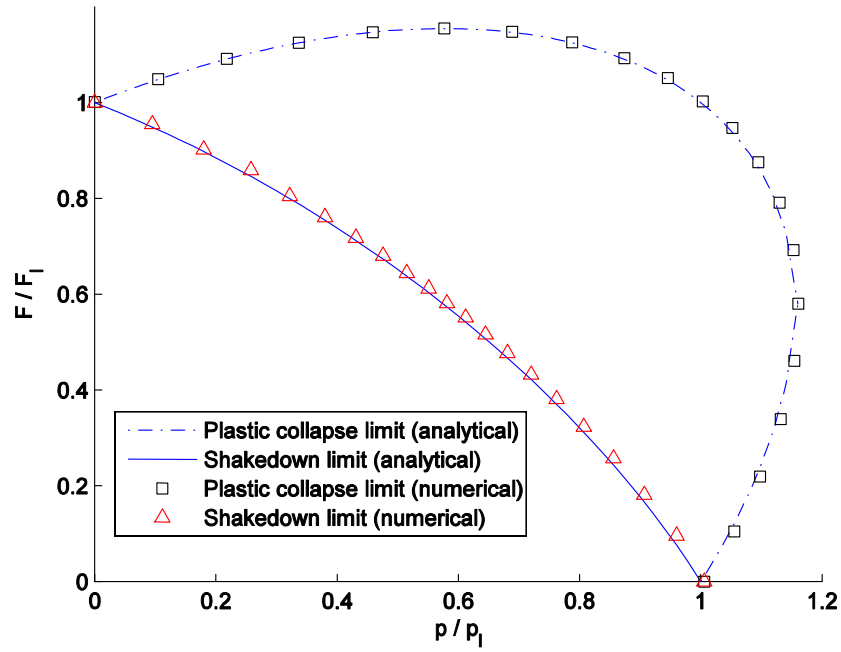


Figure 6.6 Interaction diagram

6.3 Cylindrical shell under internal pressure and temperature change

In this continuous well-known example, consider an axially restrained cylindrical shell of mean radius r and thickness h . The shell is subjected to a constant internal pressure p and a uniformly or linearly distributed temperature T which may vary within a certain range. Numerical analysis is carried out by using 200 quadrangular flat 4-node shell elements as presented in figure 6.7. The following material properties and geometrical data are adopted: $\sigma_y = 116.2$ MPa, $E = 151000$ MPa, $\nu = 0.3$, $\alpha_T = 1.0 \times 10^{-5} \text{ } ^\circ\text{C}^{-1}$, $r = 500$ mm, $h = 10$ mm in which E is Young's modulus, α_T is the coefficient of thermal expansion and σ_y is the yield limit. Two following cases are examined

Uniformly distributed temperature

This problem was examined by Zhang [1995b] and Vu [2001]. The inner and outer temperature are the same $T_i = T_u = T$ and vary within the range $[T_0, T_0 + \Delta T]$. Omitting the failure caused by axial instability, the shakedown load can be computed by using the following condition [Zhang, 1995b]

$$s_p^2 + s_T^2 = 1$$

$$s_p = \frac{\sqrt{3}pr}{2\sigma_y h}, \quad s_T = \frac{E\alpha_T \Delta T}{2\sigma_y} \quad (6.9)$$

In the case of $\Delta T = 0$ the analytical solution leads to $p_{sd} = 2.684 \text{ MPa}$. On the other hand, when only temperature applies $p = 0$, it results in $\Delta T_{sd} = 102.605 \text{ }^{\circ}\text{C}$.

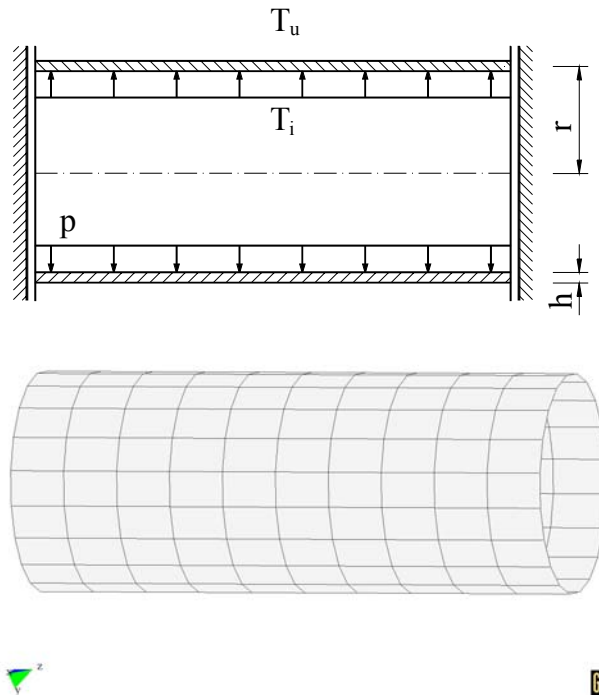


Figure 6.7 FE-mesh and geometrical dimensions

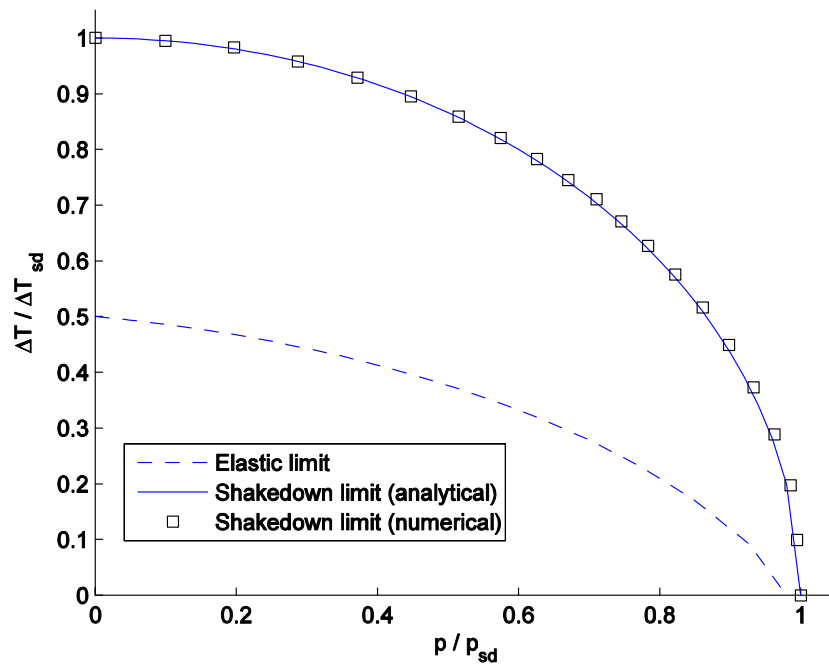


Figure 6.8 Interaction diagram (uniformly distributed temperature)

Numerical results with normalized loads $(p_{sd}, \Delta T_{sd})$ are presented in the interaction diagram, figure 6.8. It can be shown that these results agree well with the analytical

approximation. The maximum error is less than 1%. It is noted that the collapse mode at shakedown limit is alternating plasticity in the axial direction of the pipe only when pressure is absent and purely incremental plasticity in the other cases.

Linearly distributed temperature

This case was investigated by Heitzer [1999] when the temperature field is linearly distributed between inner and outer wall of the shell. The inner temperature T_i may vary within the range $[0, T_0]$ while the outer one is set to zero $T_u = 0$.

In the case of $p = 0$ shakedown analysis gives the shakedown load $T_{sd} = 136.248 \text{ } ^\circ\text{C}$. Numerical results with normalized loads (p_{sd}, T_{sd}) are presented in the interaction diagram, figure 6.9. It can be shown that the collapse mode at shakedown limit is alternating plasticity when pressure is small and purely incremental plasticity when pressure becomes bigger.

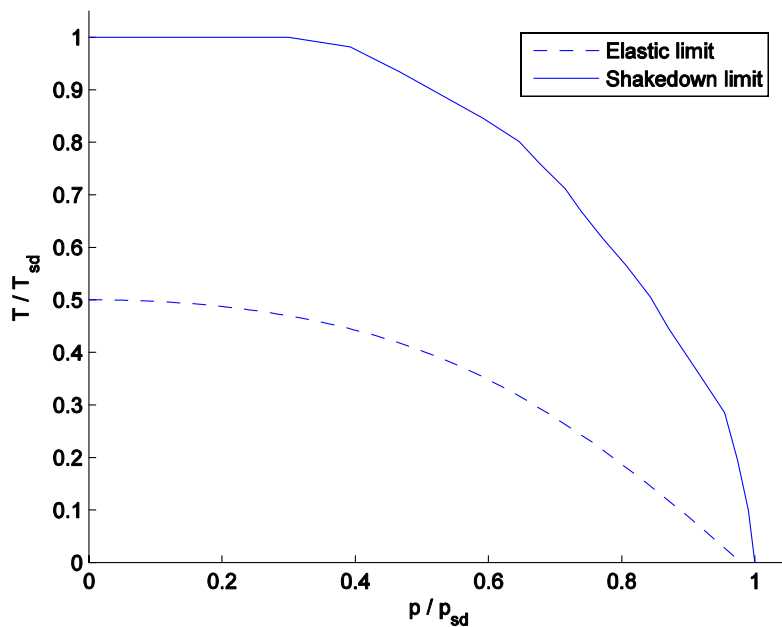


Figure 6.9 Interaction diagram (linearly distributed temperature)

6.4 Pipe-junction subjected to varying internal pressure and temperature

Thermal loading is known to have a great effect on the shakedown or inadaptation behaviour of structures. In this example a pipe-junction subjected to internal pressure p and temperature loads is examined. The supposed temperature field T is a linearly distributed function through the thickness with outer value T_u and inner value $T_i = 0$. The essential dimensions are chosen as follows

Internal diameter of the pipe $D = 39 \text{ mm}$.

Internal diameter of the junction $d = 15 \text{ mm}$.

Thickness of the pipe and junction $s = t = 3.44$ mm.

In the work of Heitzer and Staat [1999], which is based on the lower bound approach, 125 solid 27-node hexahedron elements were used to model one fourth of the structure due to its symmetry. Analogously, the problem was analyzed by Vu [2001] with a primal-dual shakedown algorithm using 720 solid 20-node hexahedron elements. In our analysis, numerical computations are carried out by using 800 flat 4-noded shell elements as presented in figure 6.10. The following material properties are adopted: $\sigma_y = 160$ MPa, $E = 210000$ MPa, $\nu = 0.3$ with the coefficient of thermal expansion $\alpha_T = 1.0 \times 10^{-5} \text{ } ^\circ\text{C}^{-1}$.

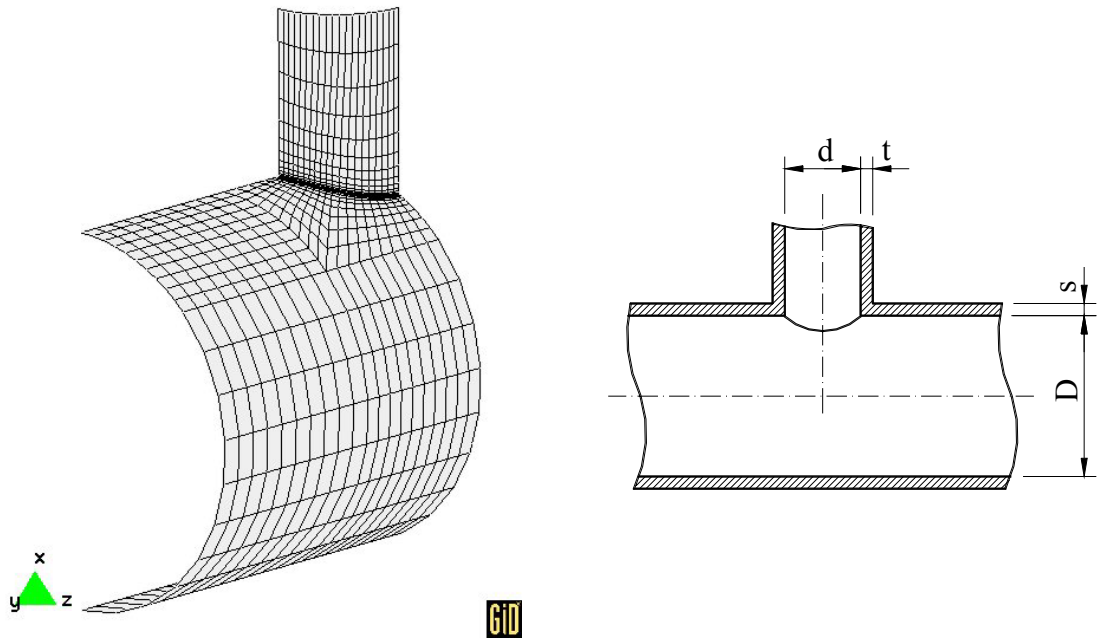


Figure 6.10 FE-mesh and geometrical dimensions

Pipe-junction under internal pressure

For the sake of comparison, consider firstly the case of having only mechanical load. Numerical limit analysis leads to the plastic collapse pressure $p_l = 0.145\sigma_y = 23.2$ MPa compared with other results (table 6.1). The convergence property of this solution presented in figure 6.11 shows that the limit load factor becomes stationary after only five iteration steps.

In the case of shakedown analysis, the internal pressure may vary within range $[0, p_0]$. Numerical analysis gives the shakedown load $p_{sd} = 0.10267\sigma_y = 16.43$ MPa compared with other known solutions (table 6.2). It is noted that in this case the structure fails due to the alternating plasticity. Convergence analysis of the optimization algorithm shows that the shakedown load factor becomes stationary also after five iteration steps.

Table 6.1: Limit analysis of pipe-junction

	Limit load normalized with σ_y	Nature of solution	Source
Staat and Heitzer	0.134	lower bound	[Heitzer, 1999]
AD-Merkblatt B9	0.136	German design rules	[Heitzer, 1999]
Vu	0.14424	lower bound	[Vu, 2001]
Vu	0.14434	upper bound	[Vu, 2001]
SAMCEF	0.161	step by step method	[Vu, 2001]
Vu	0.141	double elastic slope method	[Vu, 2001]
Present	0.145	upper bound	-

Table 6.2: Shakedown analysis of pipe-junction

	Shakedown load normalized with σ_y	Nature of solution	Source
Staat and Heitzer	0.0952	lower bound	[Heitzer, 1999]
Vu	0.10983	lower bound	[Vu, 2001]
Vu	0.11044	upper bound	[Vu, 2001]
Present	0.10267	upper bound	-

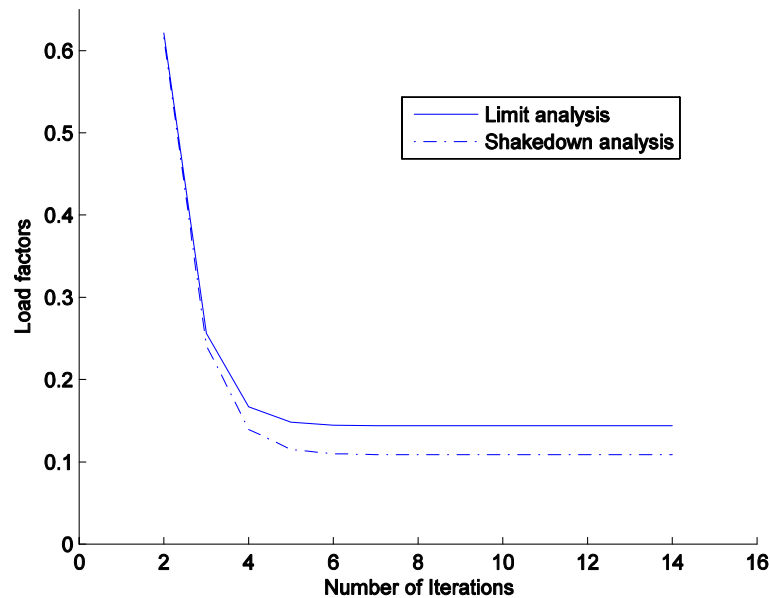


Figure 6.11 Convergence of limit and shakedown load factors

Pipe-junction under temperature change

Consider the case of only thermal load being applied, where T_u may vary within the range $[0, T_0]$. Numerical analysis gives the shakedown load $T_{sd} = 93.5086^\circ\text{C}$. It is also noted that in this case the structure fails due to the alternating plasticity.

Pipe-junction under internal pressure and temperature

For this case, two loading ranges are examined

1) The pressure and temperature vary simultaneously and dependently (one-parameter loads)

$$\begin{aligned} 0 \leq p \leq \mu p_0 \\ 0 \leq T_u \leq \mu T_0, \quad 0 \leq \mu \leq 1 \end{aligned} \quad (6.10)$$

2) The pressure and temperature vary independently (two-parameter loads)

$$\begin{aligned} 0 \leq p \leq \mu_1 p_0, \quad 0 \leq \mu_1 \leq 1 \\ 0 \leq T_u \leq \mu_2 T_0, \quad 0 \leq \mu_2 \leq 1 \end{aligned} \quad (6.11)$$

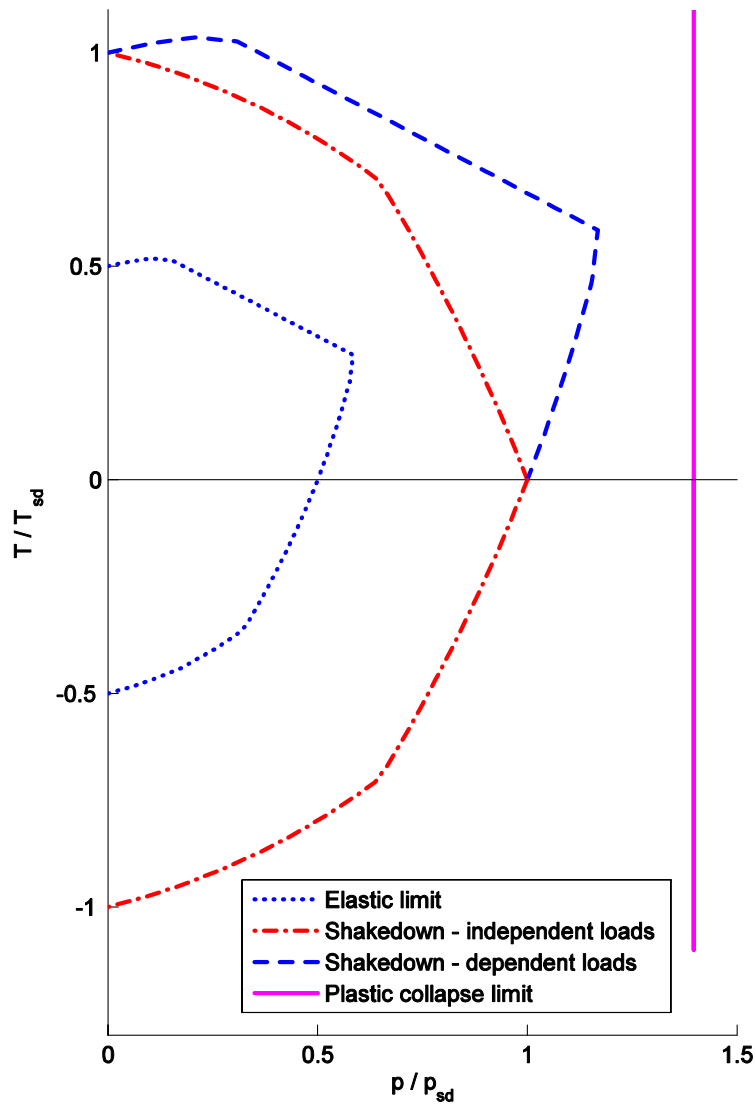


Figure 6.12 Interaction diagram of pipe-junction^

In order to get the general solutions, both positive and negative temperatures $T_0 \geq 0$ and $T_0 \leq 0$ are included. Numerical results are presented in figure 6.12.

From the interaction diagram it can be shown that a thermal load has no effect on the limit load of the pipe-junction. In the case of two-parameter loads, the shakedown loads are symmetric via pressure load axis, i.e. they are the same for both positive and negative ranges of the outer temperature, while the elastic limits are not. Otherwise the elastic limits and shakedown loads become bigger when the loads vary simultaneously and dependently (one-parameter loads) with the temperature varying in the positive range, but they are identical when the temperature is in the negative range. In all cases, the shakedown limit is twice the elastic limit which indicates that inadaptation will occur due to alternating plasticity. In this case the shakedown check is not mandatory although this leads to a design which is prone to LCF. Staat et al. [2005] have discussed this example demonstrating that twice the elastic limit is a PD check which should be used with great case or better avoided at all because it is an AP check and it may be not safe for independently varying loads.

6.5 Grooved rectangular plate subjected to varying tension and bending

In order to examine the limit and shakedown loads of thin plates, we consider firstly a grooved rectangular plate subjected to in-plane tension p_N and bending p_M (figure 6.13). The load domain is defined by

$$\begin{aligned} p_M &\in [0, \sigma_y] \\ p_N &\in [0, \sigma_y] \end{aligned} \quad (6.12)$$

where σ_y denotes the material yield stress.

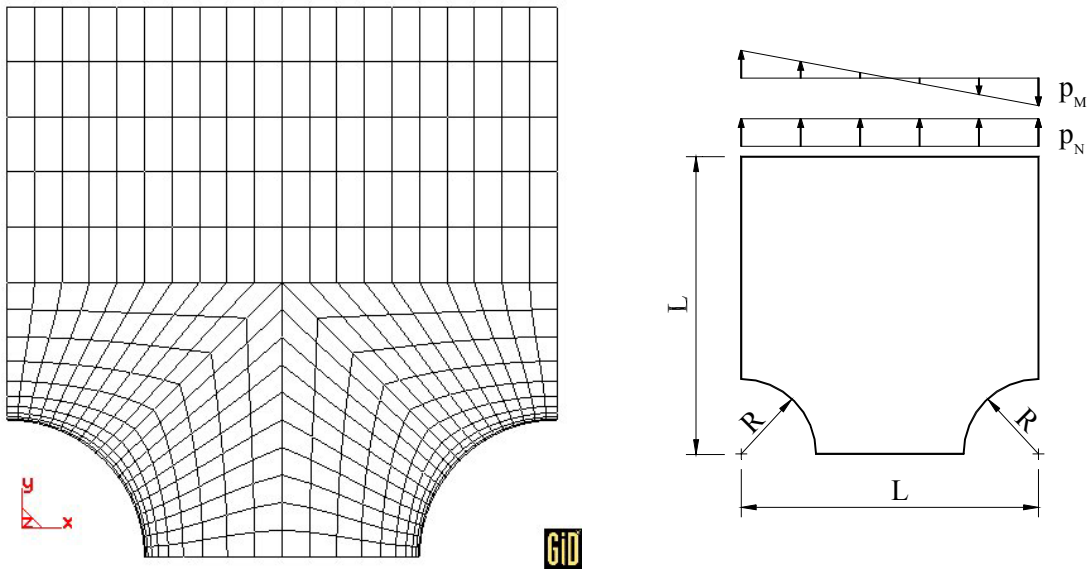


Figure 6.13 FE-mesh and geometrical dimensions

Limit analysis of the structure was studied by Prager and Hodge [1951], Casciaro and Cascini [1982] and Yan [1997] for pure tension load $p_N \neq 0$, $p_M = 0$. Heitzer [1999] and Vu [2001] investigated the problem for the more complicated case with $p_N \neq 0$, $p_M \neq 0$. In the present analysis, the structure is modelled by 300 quadrangular flat 4-node shell elements as shown in figure 6.13. The following geometrical and material properties are chosen: $R = 250 \text{ mm}$, $L = 4R$, $h = 50 \text{ mm}$, $E = 21000 \text{ MPa}$, $\nu = 0.3$, $\sigma_y = 116.2 \text{ MPa}$.

Consider the case of constant pure tension $p_N = \sigma_y$, $p_M = 0$. The plastic collapse load factor is presented in table 6.3 together with known solutions for comparison. It can be shown that our solution is well accordant with the others, which used volume finite elements basing on plane stress assumption.

Table 6.3: Limit analysis ($p_N = \sigma_y$, $p_M = 0$)

	Plane stress	Plane strain	Nature of solution	Yield criterion
Prager	0.500	0.630÷0.695	analytical	Tresca
Casciaro	0.568	0.699	numerical	von Mises
Yan	0.500÷0.577	0.727÷0.800	analytical	von Mises
Yan	0.558	0.769	numerical	von Mises
Vu	0.557	0.799÷0.802	numerical	von Mises
Present	0.572	-	numerical	von Mises

For the case of having both the in-plane tension and bending, limit and shakedown analysis are implemented. Figure 6.14 shows the evolutions of limit and shakedown load factors. In the case of limit analysis, the upper bound converges rapidly to the solution $\alpha_l = 0.30498$. Numerical result gives the shakedown load factor $\alpha_{sd} = 0.23624$ compared with upper bound factor of 0.23494 obtained by Vu [2001].

The interaction diagram of the plate in figure 6.15 shows three limit lines: the plastic collapse limit, shakedown limit and elastic limit. It is observed that, in almost cases, inadaptation will occur due to alternating plasticity. These results agree well with the solutions of Vu [2001] and Heitzer [1999].

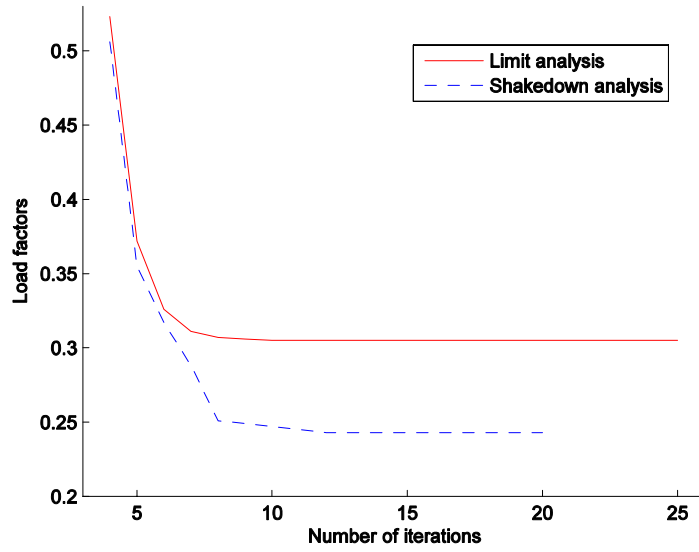


Figure 6.14 Limit and shakedown analysis $p_N \in [0, \sigma_y]$, $p_M \in [0, \sigma_y]$

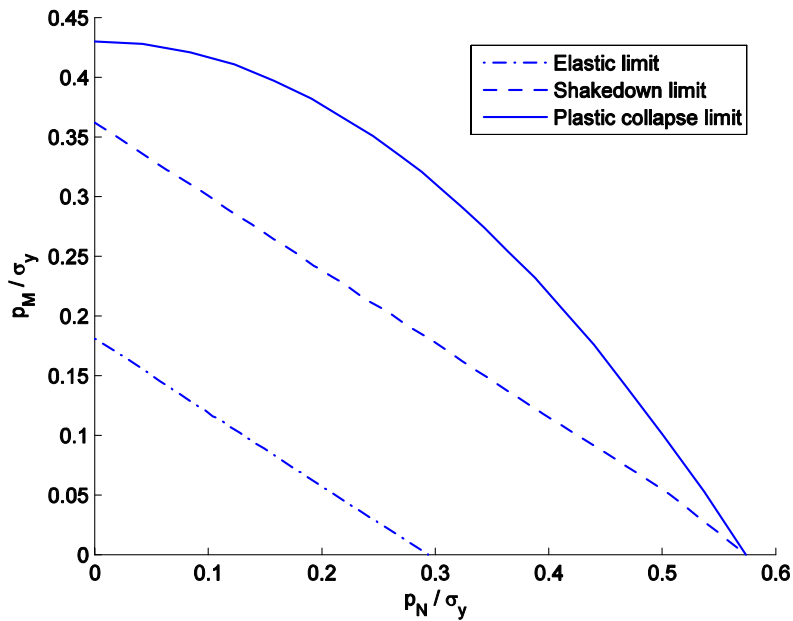


Figure 6.15 Interaction diagram of grooved rectangular plate

6.6 Square plate with a central circular hole

In this continuous well-known example, a square plate with central circular hole subjected to two loads p_1 and p_2 which can vary dependently or independently is considered. The limit load of the problem was examined analytically by Gaydon and McCrum [1954] by using plane stress hypothesis and von Mises yield criterion. Numerical limit and shakedown analyses were also investigated by some authors, e.g. Heitzer [1999], Vu [2001] for different ratios R/L to evaluate the elastic-plastic behaviour of the structure.

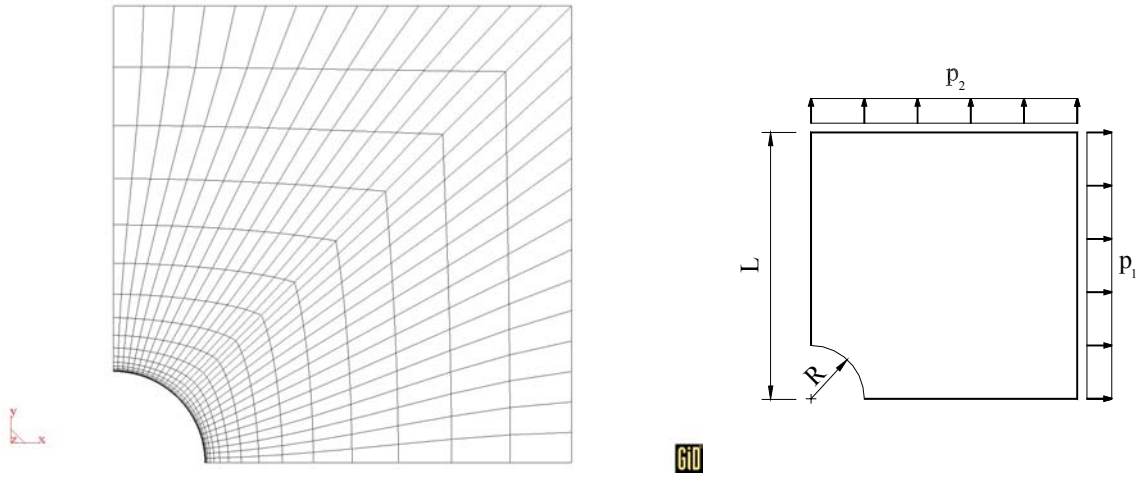


Figure 6.16 FE-mesh and geometrical dimensions

In our analysis, due to the symmetry, one fourth of the plate is discretized by 600 quadrangular flat 4-node shell elements as shown in figure 6.16. The following material properties are chosen: $E = 21000 \text{ MPa}$, $\nu = 0.3$, $\sigma_y = 116.2 \text{ MPa}$. The two cases: one and two applied loads are examined.

One applied load

In this case one load is set to zero and the other one can vary within a range $p_2 = 0, p_1 \in [0, \sigma_y]$. With $0 < R/L \leq 0.204$, the exact plastic collapse limit is found since in this range the lower and the upper bound are coincident

$$p_{\lim} = (1 - R/L)\sigma_y. \quad (6.13)$$

As example, the exact collapse limit load in the case of $R/L = 0.2$ is $p_{\lim} = 0.8\sigma_y$. Our numerical solution obtained in this case is $0.80149\sigma_y$. Based on an elastic analysis, the alternating (plastic fatigue) limit can be estimated by using formula (2.47). The numerical results obtained by our unified shakedown algorithm represent the minimum between the alternating limit and the incremental limit. For $R/L = 0.2$, the collapse mode is alternating plasticity. Our obtained alternating limit is $0.59904\sigma_y$ and the unified shakedown algorithm gives $0.60332\sigma_y$. The small gap between them may be caused by the use of the quadratic approximation of exact Ilyushin yield surface in the calculation of alternating plasticity, while the exact one was used in the unified shakedown analysis. The convergence property of these solutions presented in figure 6.17 shows that the limit and shakedown load factor become stationary after seven iteration steps.

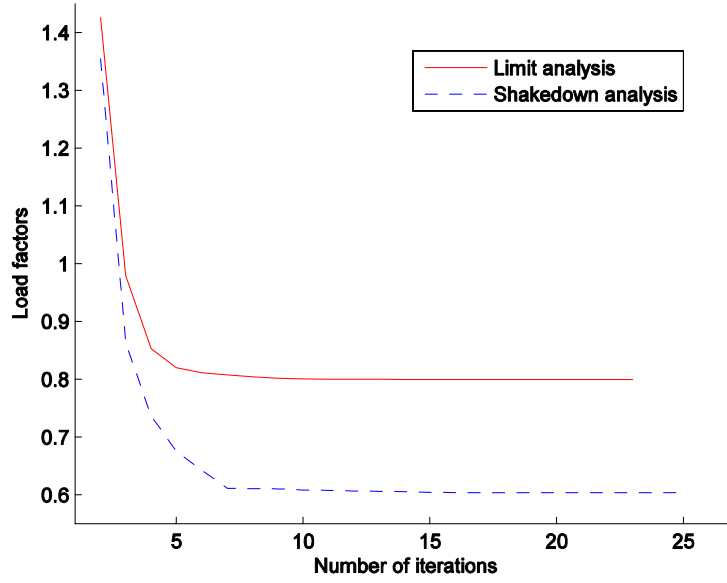


Figure 6.17 Limit and shakedown analysis $p_1 \in [0, \sigma_y]$, $p_2 = 0$

In order to examine the geometrical effect of the circular hole, various values of ratio R/L were also considered. The obtained numerical results are introduced in table 6.4, compared with the solutions of Heitzer [1999], which are obtained by lower bound algorithm. It can be shown that our solutions agree well with those of Heitzer.

Table 6.4: Limit and shakedown analysis $p_1 \in [0, \sigma_y]$, $p_2 = 0$

R/L	Shakedown load factors (Heitzer)	Limit load factors (Heitzer)	Shakedown load factors (present)	Limit load factors (present)
0.1	0.671	0.8951	0.6546	0.90172
0.2	0.6157	0.7879	0.60332	0.80149
0.3	0.5212	0.691	0.52012	0.70221
0.4	0.4361	0.572	0.43367	0.59139
0.5	0.3302	0.4409	0.31600	0.40117
0.6	0.2104	0.2556	0.21323	0.24249
0.7	0.1327	0.1378	0.12378	0.12541
0.8	0.0557	0.0565	0.05225	0.05227
0.9	0.0191	0.0193	0.01226	0.01226

Two applied loads

For this case, exact value of the plastic collapse limit load are known in the range $0.483 < R/L \leq 1$ where analytical lower bound coincides with upper one:

$$p_{\lim} = \frac{2}{\sqrt{3}} \sin\left(\alpha - \frac{\pi}{6}\right) \sigma_y, \quad \frac{1}{(R/L)^2} = \frac{\sqrt{3}}{2 \cos(\alpha)} e^{\sqrt{3}\left(\alpha - \frac{\pi}{6}\right)} \quad (6.14)$$

Details about the upper and lower bounds within the range $0 \leq R/L < 0.483$ can be found in the work of Gaydon and McCrum [1954]. Numerical limit load factors for different values of R/L are introduced in tables 6.5, compared with analytical results [Gaydon and McCrum, 1954] and numerical results of Vu [2001], which are obtained by a dual algorithm.

Table 6.5: Limit analysis $p_1 = p_2 = \sigma_y$

R/L	Lower bound (analytical)	Upper bound (analytical)	Lower bound (Khoi [2001])	Upper bound (Khoi [2001])	Present
0.1	0.97063	0.99215	0.97082	0.97104	0.96951
0.2	0.89425	0.92376	0.89374	0.89472	0.89404
0.3	0.79122	0.80829	0.79075	0.79125	0.79167
0.4	0.67602	0.69048	0.67585	0.67592	0.67814
0.5	0.55682	0.55682	0.55666	0.55679	0.56133
0.6	0.43801	0.43801	0.43791	0.43819	0.44109
0.7	0.32195	0.32195	0.32196	0.32221	0.32504
0.8	0.20991	0.20991	0.21010	0.21016	0.21285
0.9	0.10249	0.10249	0.10264	0.10267	0.10457

Table 6.6: Shakedown analysis $p_1 \in [0, \sigma_y], p_2 \in [0, \sigma_y]$, two-parameter loads

R/L	Alternating limit (Khoi [2001])	Lower bound (Khoi [2001])	Upper bound (Khoi [2001])	Present
0.1	0.49082	0.49082	0.49086	0.48718
0.2	0.43384	0.43384	0.43390	0.43136
0.3	0.36128	0.36128	0.36131	0.35575
0.4	0.27635	0.27635	0.27638	0.27300
0.5	0.19442	0.19442	0.19445	0.19052
0.6	0.12360	0.12360	0.12364	0.12102
0.7	0.06763	0.06763	0.06765	0.06940
0.8	0.02903	0.02903	0.02905	0.02772
0.9	0.00709	0.00709	0.00710	0.00640

In the case of shakedown analysis three loading ranges are examined including both positive and negative loads $p_2 \geq 0$ and $p_2 \leq 0$.

- 1) Two loads vary simultaneously and dependently (one-parameter loads)

$$\begin{aligned}
 0 \leq p_1 \leq \mu \sigma_y, \quad 0 \leq \mu \leq 1 \\
 0 \leq p_2 \leq \mu \sigma_y, \text{ or } 0 \geq p_2 \geq -\mu \sigma_y
 \end{aligned} \tag{6.15}$$

- 2) Two loads vary independently (two-parameter loads)

$$\begin{aligned}
0 \leq p_1 \leq \mu_1 \sigma_y, \quad 0 \leq \mu_1 \leq 1 \\
0 \leq p_2 \leq \mu_2 \sigma_y, \quad 0 \leq \mu_2 \leq 1
\end{aligned}
\tag{6.16}$$

3) Two loads vary independently (two-parameter loads)

$$\begin{aligned}
0 \leq p_1 \leq \mu_1 \sigma_y, \quad 0 \leq \mu_1 \leq 1 \\
0 \geq p_2 \geq -\mu_2 \sigma_y, \quad 0 \leq \mu_2 \leq 1
\end{aligned}
\tag{6.17}$$

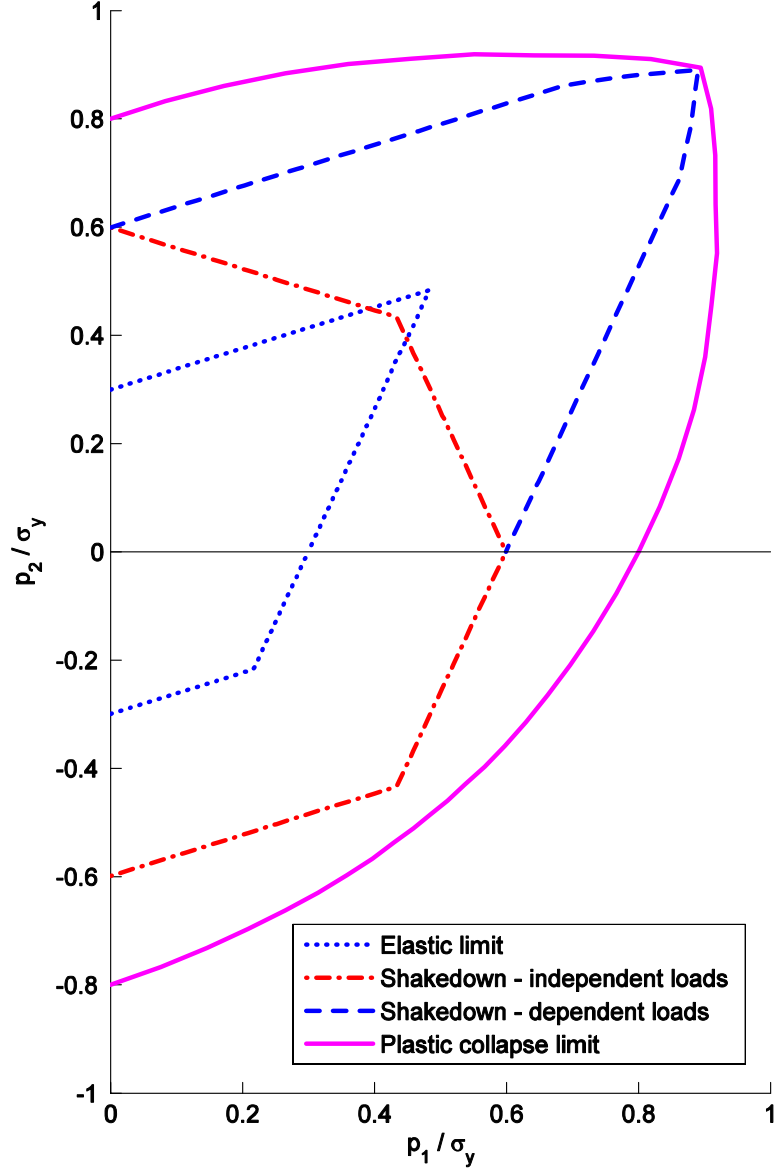


Figure 6.18 Interaction diagram of a square plate with a central hole, $R/L = 0.2$

For the sake of comparison, consider first the two-parameter load case with positive load ranges. Numerical shakedown load factors for different values of R/L are introduced in tables 6.6, compared with numerical results of Vu [2001], which are obtained by a primal-dual algorithm.

Figure 6.18 presents both the numerical limit and shakedown analyses for the case of $R/L = 0.2$. From this interaction diagram it can be shown that, in the case of two-parameter loads, the shakedown loads are symmetric via p_1/σ_y -axis, i.e. they are the same for both positive and negative ranges of p_2 , while the elastic limits are not. Otherwise the elastic limits and shakedown loads become bigger when the loads vary simultaneously and dependently (one-parameter loads) with one load varies in the positive range, but they are identical when this load is in the negative range. It is also noted that when one load varies within the negative range, the collapse mode is purely alternating plasticity.

6.7 Elbow subjected to bending moment

The pipe bends are a problem of great interest to many designers. They have a complex response to in-plane and out-of-plane bending moments. When an external moment is applied to one of its ends, the cross section tends to deform significantly both in and out of its own plane. The moment-end rotation curves show a defined limit load behaviour for the closing mode of in-plane bending but not for the opening mode [Chattopadhyay et al., 2000], [Diem, 1994]. This difference can be explained as an effect of large displacements. Due to their curved geometry, the stresses and strains are much higher than those present in a straight pipe of the same size and material, under the same loading conditions. For this reason, pipe bends are considered as critical components of a piping system. In addition, the variation of the limit moment with the change of the internal pressure has been of great interest and has been studied numerically, analytically and experimentally [Kusmaul et al., 1995], [Yan, 1996, 1997], [Shalaby et al., 1998a, b], [Mourad et al., 2002], [Chattopadhyay et al., 1999, 2000], [Fanous et al., 2005], [Tran et al., 2007a,e]. However, the examination of shakedown limit is still rare.

Consider an 90° elbow with mean radius r , bend radius of curvature R and thickness h . One of its ends is supposed clamped and the other one is subjected to an in-plane closing moment M_I or out-of-plane bending moment M_{II} as shown in figure 6.19. The curvature factor is defined as follow

$$\lambda = \frac{Rh}{r^2} \quad (6.18)$$

Generally, $\lambda \leq 0.5$ corresponds to a highly-curved pipe, while $\lambda \rightarrow \infty$ corresponds to a straight pipe. In order to evaluate the model different values of λ within the range $[0.1, 1.2]$ are examined. Our model for elastic-plastic analysis is meshed by 700 quadrangular flat 4-node shell elements as shown in figure 6.19. The following material properties are chosen: $E = 208000$ MPa, $\nu = 0.3$, $\sigma_y = 250$ MPa.

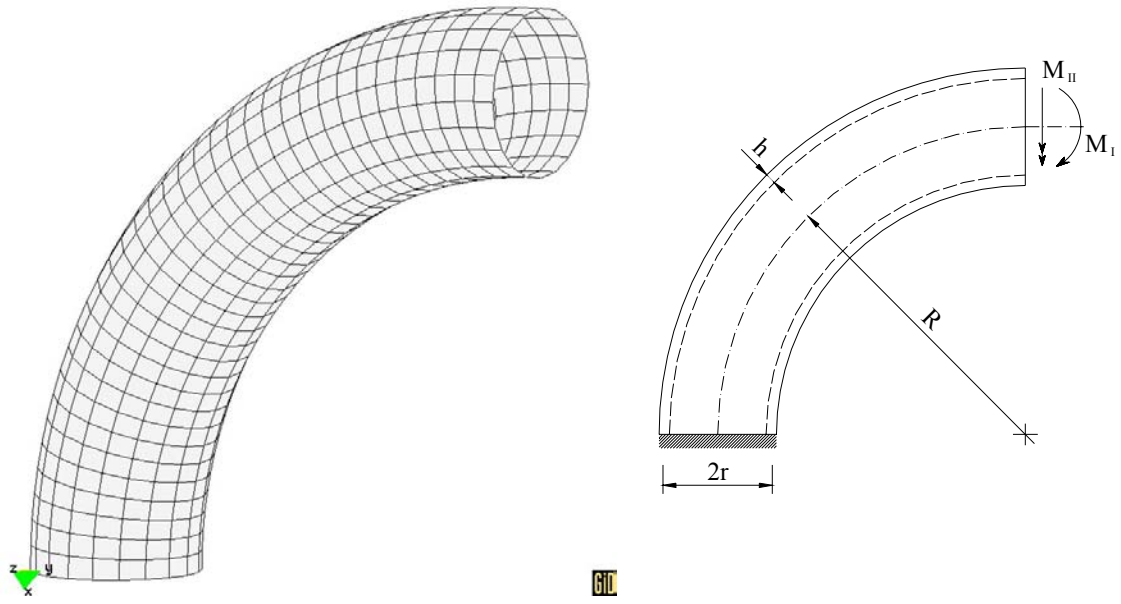


Figure 6.19 FE-mesh and geometrical dimensions

Elbow under in-plane closing bending moment

We define the limit load factor as follows

$$\alpha_I = M_I^e / M_I^s \quad (6.19)$$

in which M_I^e is in-plane limit moment of elbow, M_I^s is the limit moment of the straight pipe, which has the same radius as the elbow. For a straight thin-walled pipe, M_I^s is determined as (see formular 6.4)

$$M_I^s = 4hr^2\sigma_y. \quad (6.20)$$

For this kind of pipe bend, some analytical solutions are available in the literature

1) *Based on small displacement analysis and perfectly plastic material behavior*

• Calladine's and Yan's solutions

By using an elastic solution of Clark and Reissner [1951] and the criterion of Hodge [1954], which is a kind of sandwich approximation of Mises' criterion in the case of a cylindrical shell, Calladine [1974] proposed a lower bound solution for an infinite highly-curved pipe ($\lambda \leq 0.5$)

$$\alpha_I^C = 0.9346\lambda^{2/3}. \quad (6.21a)$$

This solution is considered in the literature to come close to the experimental limit load factor [Bolt and Greenstreet, 1972], [Goodall, 1978a, b], [Griffiths, 1979]. According

to Yan [1996, 1997], it is a good approximation when $\lambda < 0.7$. For a slightly-curved pipe ($\lambda \geq 0.7$), he proposed an approximate solution which is validated by numerical analysis

$$\alpha_I^Y = \cos\left(\frac{\pi}{6\lambda}\right). \quad (6.21b)$$

• Desquines's solution

In the framework of his PhD thesis, Desquines et al. [1997] proposed a more general analytical solution as a lower bound, which can be applied for any value of λ

$$\alpha_I^{De} = \frac{1}{\sqrt{1 + \frac{0.3015}{\lambda^2}}}. \quad (6.22)$$

• Spence and Findlay's solution

In order to get an analytical solution for the limit load of an elbow, Spence and Findlay [1973] already developed two theoretical approaches. The first one utilises a linear elastic analysis to estimate limit loads as similar to Calladine. The second one is to manipulate the results of a creep analysis of bends to give an approximate solution of the limit load. They result with $\lambda < 1.45$

$$\alpha_I^{SF} = 0.8\lambda^{0.6}, \quad \lambda < 1.45, \quad (6.23a)$$

$$\alpha_I^{SF} = 1, \quad \lambda > 1.45. \quad (6.23b)$$

2) Based on large displacement analysis

• Goodall's solution

Goodall [1978a] proposed the maximum load-carrying capacity of the elbow subjected to closing bending moment as

$$\alpha_I^G = \frac{1.04\lambda^{2/3}}{1 + \beta} \quad (6.24)$$

where

$$\beta = \frac{4\sqrt{3(1-\nu^2)}r\sigma_y}{\pi Eh} \left[2 + \frac{(3\lambda)^{2/3}}{3} \right]. \quad (6.25)$$

• Touboul's solution

Based on the experimental study at CEA DMT, Touboul et al. [1989] proposed the following equations of collapse moments of elbows

$$\text{Closing collapse: } \alpha_I^T = 0.715\lambda^{2/3}, \quad (6.26a)$$

$$\text{Opening collapse: } \alpha_I^T = 0.722\lambda^{1/3}. \quad (6.26b)$$

• Drubay's solution

Drubay et al [1995] proposed another closing mode collapse moments of elbows as

$$\alpha_I^{Dr} = 0.769\lambda^{2/3}. \quad (6.27)$$

Our numerical results are introduced in table 6.7 and figure 6.20, compared with these above analytical solutions and a numerical solution of Yan [1997]. It is shown that our solutions compare well with the other analytical solutions, which are based on small displacement theory, but are bigger than those which are based on large displacement theory. They converge as an upper bound of Calladine's solution and lower bound of Desquines's solution.

Elbow under out-of-plane bending moment

We define the limit load factor for this case as follows

$$\alpha_{II} = M_{II}^e / M_{II}^t \quad (6.28)$$

where M_{II}^e is out-of-plane limit moment of the elbow, M_{II}^t is the torsion limit moment of the axle which has the same radius as the elbow and determined by

$$M_{II}^t = \frac{2}{\sqrt{3}} \pi h r^2 \sigma_y. \quad (6.29)$$

By this definition, Yan [1996, 1997] proposed an analytical solution for the elbow subjected to out-of-plane bending moment

$$\alpha_{II}^Y = 1.1\lambda^{0.6}, \quad \lambda < 0.5, \quad (6.30)$$

$$\alpha_{II}^Y = 0.9\lambda^{1/3}, \quad 0.5 \leq \lambda \leq 1.4. \quad (6.31)$$

Numerical results are introduced in table 6.8 and figure 6.21, compared with the analytical solution of Yan [1997]. It is shown that our solutions compare well with the analytical solution outside the range $0.4 \leq \lambda \leq 0.7$.

Table 6.7: Limit load factors of an elbow under in-plane closing bending moment

λ	Calladine (6.21a)	Yan (6.21b)	Desquines (6.22)	Spence- Findlay (6.23)	Goodall (6.24)	Touboul (6.26)	Drubay (6.27)	Present
0.100	0.2013	-	0.1791	0.2001	0.1489	0.154	0.1657	0.2155
0.200	0.3196	-	0.3422	0.3046	0.2817	0.2445	0.263	0.3279
0.250	0.3709	-	0.4144	0.3482	0.3401	0.2838	0.3052	0.3900
0.300	0.4188	-	0.4794	0.3885	0.3947	0.3204	0.3446	0.4614
0.363	0.4756	-	0.5515	0.4355	0.4593	0.3638	0.3913	0.5200
0.400	0.5074	-	0.5888	0.4617	0.4955	0.3882	0.4175	0.5589
0.500	0.5887	-	0.6732	0.5278	0.5879	0.4504	0.4844	0.6260
0.600	0.6648	-	0.7377	0.5888	0.6741	0.5087	0.5471	0.6930
0.650	0.7013	-	0.7639	0.6178	0.7153	0.5365	0.577	0.7227
0.700	0.7368	0.7330	0.7868	0.6458	0.7554	0.5637	0.6063	0.7494
0.750	-	0.7660	0.8069	0.6732	0.7945	0.5902	0.6348	0.7773
0.800	-	0.7933	0.8244	0.6998	0.8327	0.6162	0.6627	0.7974
0.903	-	0.8365	0.8544	0.7525	0.909	0.668	0.7184	0.8341
1.000	-	0.8660	0.8765	0.8000	0.9782	0.715	0.769	0.8617
1.200	-	0.9063	0.9093	0.8925	1.1138	0.8074	0.8684	0.9006

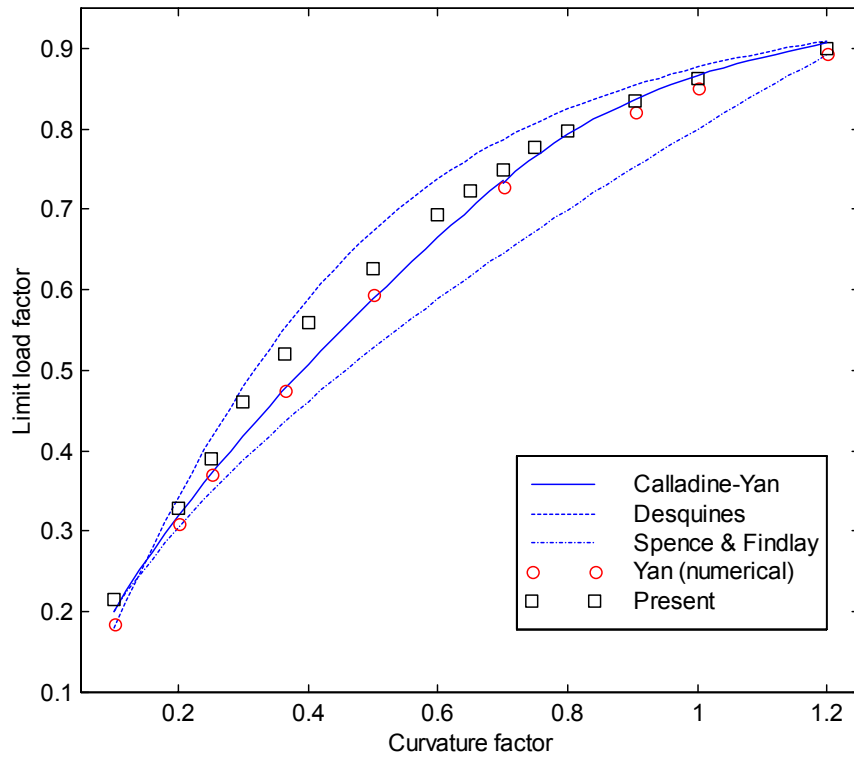


Figure 6.20 Limit load factors of an elbow under in-plane closing bending moment

Table 6.8: Limit load factors of an elbow under out-of-plane bending moment

λ	Yan (6.30)	Yan (6.31)	Present
0.100	0.2763	-	0.2476
0.200	0.4188	-	0.4047
0.250	0.4788	-	0.4709
0.300	0.5341	-	0.5244
0.363	0.5989	-	0.5675
0.400	0.6348	-	0.6063
0.450	0.6813	-	0.6337
0.500	0.7257	0.7143	0.6575
0.550	-	0.7374	0.6924
0.600	-	0.7591	0.7245
0.650	-	0.7796	0.7539
0.700	-	0.7991	0.7808
0.750	-	0.8177	0.8053
0.800	-	0.8355	0.8276
0.903	-	0.8699	0.8674
1.000	-	0.9000	0.8984
1.200	-	0.9564	0.9467

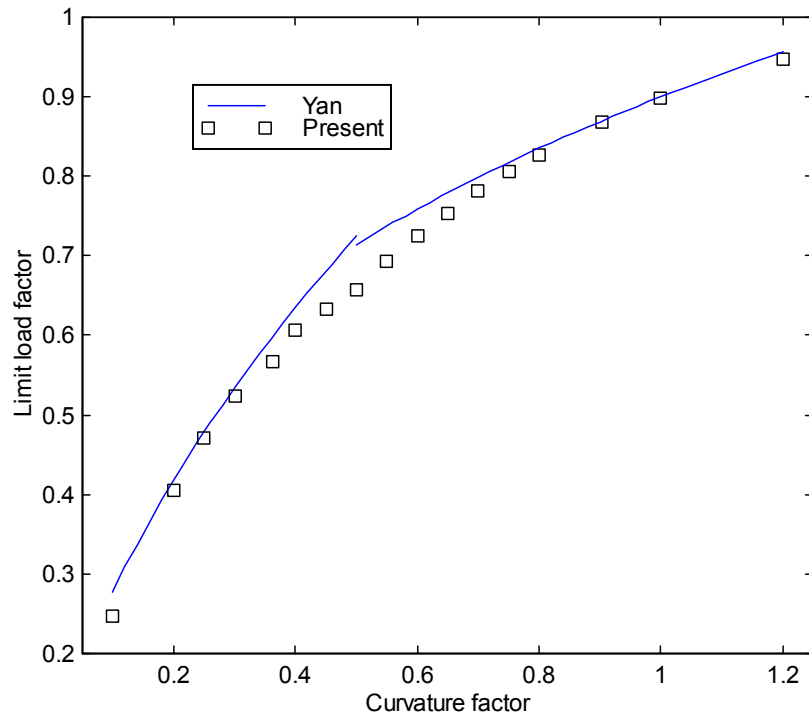


Figure 6.21 Limit load factors of an elbow under out-of-plane bending moment

6.8 Limit and shakedown analysis of pipe-elbow subjected to complex loads

In this continuous example of pipe bends a system of two straight pipes connected to the ends of an elbow is considered. This pipe-elbow can be subjected to internal pressure p , axial force F_p , transversal forces F and bending moments M_I , M_{II} as shown in figure 6.22. One of its ends is clamped and the other one is free. In the case of transversal forces, the two pipe ends are free. In order to evaluate the model, some sub-problems are examined [Tran et al., 2007c].

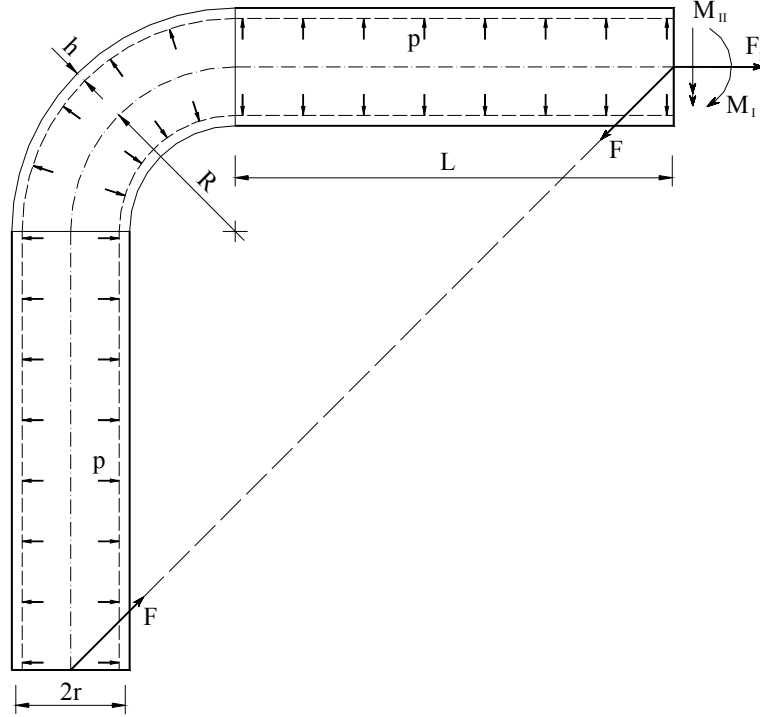


Figure 6.22 Pipe-elbow subjected to complex loads

Pipe-elbow under transverse forces F

This is an experimental model presented in [Diem, 1994], [Kussmaul et al., 1995]. The geometrical data and material properties are chosen as: $h = 30.5 \text{ mm}$, mean radius $r = 229.25 \text{ mm}$, $R = 900 \text{ mm}$, $L = 5100 \text{ mm}$ (curvature factor $\lambda = 0.522$), $E = 208000 \text{ MPa}$, $\nu = 0.3$, $\sigma_y = 387 \text{ MPa}$.

In this case, the structure can be considered as being subjected to the in-plane closing bending moment which is determined by

$$M = F \left[\frac{1}{\sqrt{2}} (L - R) + R \right]. \quad (6.32)$$

For this reason the available analytical solution in the literature can be applied to calculate the limit load F_l . In the analysis, due to the symmetry, one fourth of the structure is modelled by 300 quadrangular flat 4-node shell elements as shown in figure 6.23. Table

6.9 shows the comparison of the numerical result. It is seen that the present result is compatible with the result of Goodall [1978] but higher than that of Diem [1994], Kussmaul et al. [1995] and Calladine [1974]. This is due to two reasons: the stiffening effect of connecting straight pipes and not taking into account the nonlinear geometrical effect in the present method. It was noted by Griffiths [1979] that the effect of connecting straight pipes can increase the limit load up to 33% with respect to Calladine's solution.

Table 6.9: Limit load F_l of the pipe-elbow under transverse force (kN)

Diem [1994]	Goodall eq. (6.24)	Touboul eq. (6.26)	Drubay eq. (6.27)	Calladine eq. (6.21)	Desquines (6.22)	Spence & Findlay (6.23)	Present
exp.	large displacements			small displacements			LISA
372	403.26	297.22	319.67	387.45	441.79	347.29	404.83

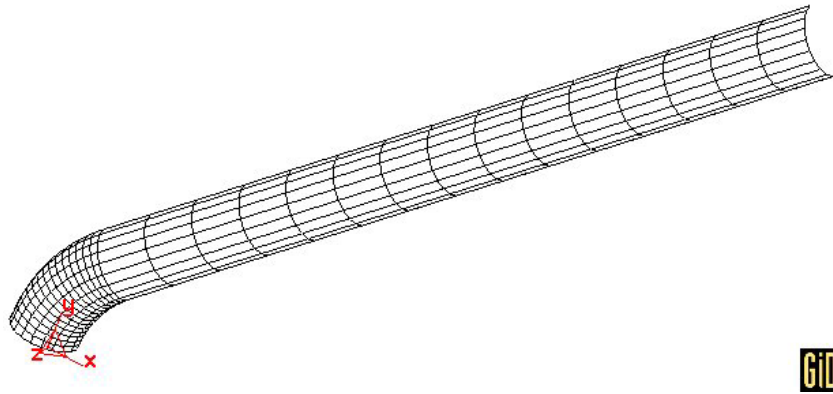


Figure 6.23 FE-mesh of a pipe-elbow subjected to transversal forces

Pipe-elbow under in-plane closing bending moment and internal pressure

A pipe-elbow is often subjected to combined internal pressure and bending moment during service, which may vary independently in the range $[0, p_0]$ and $[-M_0, M_0]$, respectively. It is now well known that the internal pressure has a significant effect on the limit load of a pipe-elbow. In all the foregoing analytical equations, the effect of internal pressure is not taken into account. Goodall [1978b] was the first to propose the closed-form equation of the limit load of pipe-elbows under combined internal pressure and in-plane bending moment by the small displacement analysis. The proposed equation was

$$\alpha_l^G = 1.04\lambda^{2/3} \left(1 - \frac{pr}{2h\sigma_y} \right)^{1/3}. \quad (6.33)$$

From (6.33), it can be seen that the internal pressure reduces the limit moment. Based on nonlinear finite element analyses and twice the elastic slope method, Chattopadhyay [1999, 2000] investigated various sizes of pipe-elbows subjected to

combined internal pressure and in-plane bending moment. He proposed another analytical solution for the pipe-elbow which takes the strain-hardening of the material into account by

$$\text{Closing collapse: } \alpha_l^C = 1.122\lambda^{2/3} + 0.175\frac{\alpha_p}{\lambda} - 0.508\alpha_p^2 \quad (6.34a)$$

$$\text{Opening collapse: } \alpha_l^C = 1.047\lambda^{1/3} + 0.124\frac{\alpha_p}{\lambda^{1.2}} - 0.568\alpha_p^2 \quad (6.34b)$$

$$\text{Applicability: } 0.24 \leq \lambda \leq 0.6 \text{ and } 0 \leq \alpha_p \leq 1.0$$

where $\alpha_p = pr/h\sigma_y$ is the normalized pressure. In our numerical analysis one half of the pipe-elbow is meshed by using 640 quadrangular 4-node flat shell elements as shown in figure 6.24. The following geometrical data and material properties are adopted: $h = 40$ and 45 mm , $r = 250 \text{ mm}$, $R = 750 \text{ mm}$, $L = 1500 \text{ mm}$ (curvature factor $\lambda = 0.480$ and $\lambda = 0.540$), $E = 203000 \text{ MPa}$, $\nu = 0.3$, $\sigma_y = 270 \text{ MPa}$, $\sigma_u = 513 \text{ MPa}$. The elastic data is only needed for the calculation of the elastic limit. Closed-end condition of the pipe-elbow is simulated by applying an axial force of intensity $p\pi r^2$ at the end of connecting straight pipe.

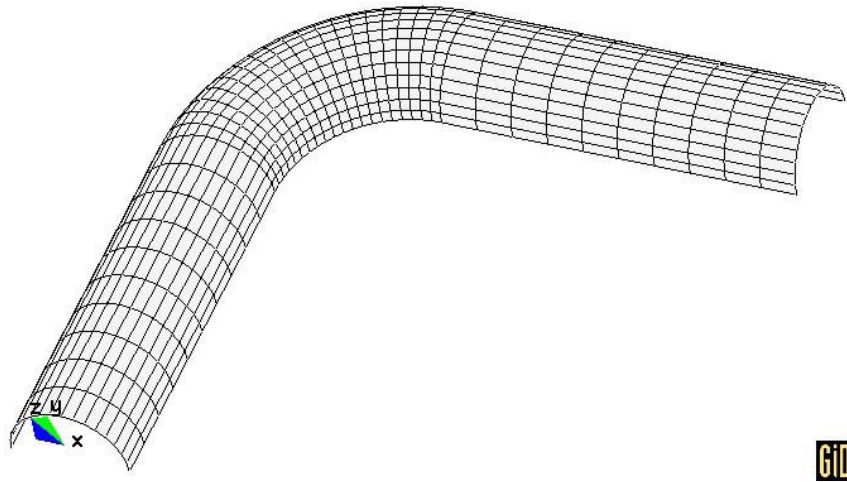


Figure 6.24 FE-mesh of pipe-elbow under internal pressure and in-plane bending

Figure 6.25 shows the effect of internal pressure on the limit moment of the pipe-elbow. It can be seen that the limit moment decreases when the pressure increases, as presented by Fanous et al. [2005]. Our solutions agree well with those of Goodall [1978b] but not with those of [Chattopadhyay, 2000]. This is due to the omission of geometrical non-linearity and strain-hardening of the material by the present method and in Goodall's analysis. Hence, the analysis of the pipe-elbow without the large displacement effect gives a conservative and acceptable result [Fanous et al., 2005].

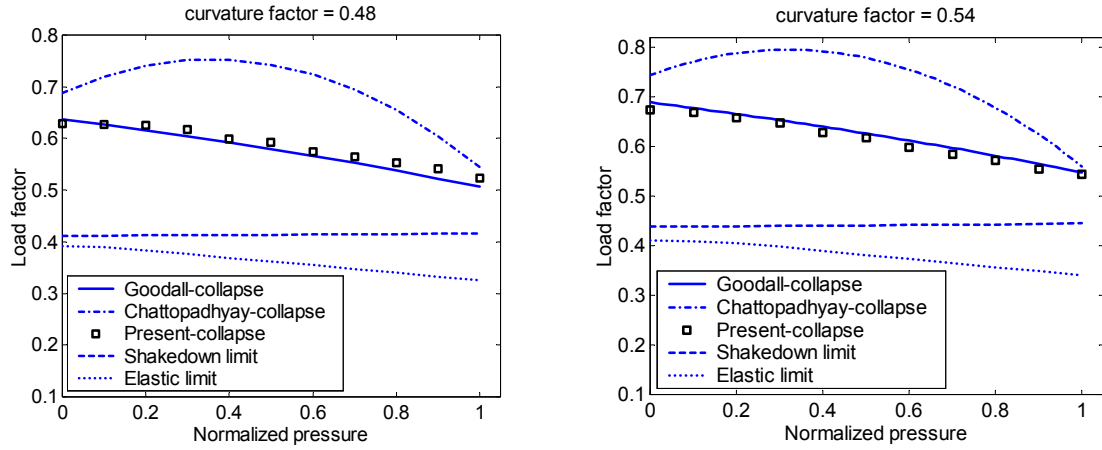


Figure 6.25 Effect of internal pressure on in-plane limit moments

Contrary to the case of limit analysis, internal pressure has a very little effect on the shakedown limit moment. For small pressure the shakedown limit is between 57.7% and 66.7% of the plastic collapse load. This small shakedown loads limits the benefit of the strengthening effect of the geometrical non-linear analysis in [Chattopadhyay et al, 2000]. At low pressure also the difference between the elastic limit and the shakedown load is small so that fatigue and ratchetting could be of concern. The allowance of cyclic loading up to the shakedown limit without any safety factor may only be acceptable in connection with a planned monitoring and maintenance program.

Pipe-elbow under out-of-plane bending moment and internal pressure

This pipe-elbow analyzed by Mourad and Younan [2002], Fanous et al. [2005] is considered. The curvature factor of the pipe bend is 0.1615, the mean radius $r = 203.2$ mm, the bend radius $R = 609.6$ mm, and the thickness $h = 10.94$ mm. The length of two straight pipes is four times the diameter $L = 1625.6$ mm in order to reduce the effect of the pipe ends on the response of the elbow [Fanous et al., 2005]. Both internal pressure and bending moment can vary independently in the range $[0, p_0]$ and $[-M_0, M_0]$, respectively.

In our analysis, the model is discretised by 1500 quadrangular flat 4-node shell elements as shown in figure 6.26. An axial force is applied at the end of connecting straight pipe to account for the closed-end condition. The material model used is perfectly plastic stainless steel 304 which has an Young's modulus $E = 193743$ MPa, a yield stress $\sigma_y = 272$ MPa and Poisson's ratio $\nu = 0.47$.

The applied internal pressure effects the plastic collapse limit moment. Our numerical results are presented in figure 6.27, compared with three plastic collapse limit solutions of Fanous et al. [2005], which are obtained by R-Node (redistribution of nodes), Iterative R-Node and plastic analysis methods. It is shown that these results compare well with those of Fanous et al. [2005]. The plastic collapse limit moment decreases when

pressure increases noticeably above 4 MPa . The thesis [Rahman, 2006] demonstrates that the existing cyclic plasticity models (Chaboche, Ohno-Wang, and Abdel Karim-Ohno) are not capable of simulating straight and elbow pipe ratchetting responses satisfactorily when the model parameters are determined from material level responses. The direct shakedown analysis gives robust predictions of shakedown limits on the basis of restricted information about the material, [Staat and Heitzer, 2002]. Figure 6.27 shows that large pressure (greater than 9 MPa) reduces the shakedown limit moment considerably. But smaller pressure has no effect in contrast to the elastic limit. With respect to the design code the same comments apply as for figure 6.25.

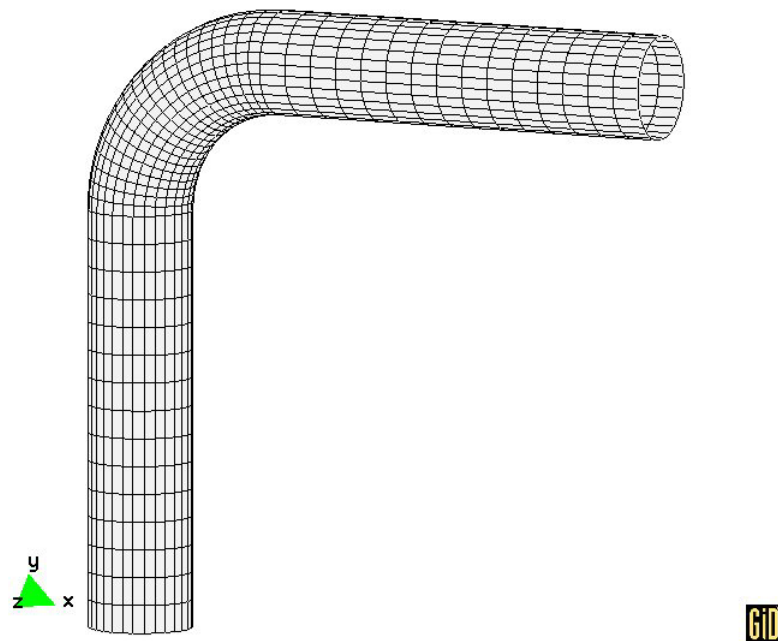


Figure 6.26 FE-mesh of pipe-elbow under internal pressure and out-of-plane bending

For both pipe-elbows no PD check has been published which could be used to verify the calculated shakedown limits. The shakedown analysis of pipe bends in [Abdalla et al., 2006] is a non-mandatory AP check. In order to show the convergence property of the algorithm, convergence analysis and the influences of optimisation parameters such as the penalty parameter c and η^2 were included for the reference loads $M = 225.97$ kNm and $p = 6.895$ MPa . Figure 6.28 demonstrates that the direct plasticity methods are extremely effective. Shakedown analysis converges in only three iterations which each needs approximately the computing time of a linear elastic analysis. This is an important saving compared to the analysis of a large number of plastic cycles and makes limit and shakedown analysis a first candidate for structural optimization or reliability analysis [Tran et al., 2007d]. It is shown in figures 6.29-6.30 that the parameters η^2 and c have very little

influence on the both solutions in the ranges of $\eta^2 \in [10^{-12}, 10^{-28}]$ and $c \in [10^8, 10^{17}]$. The numerical results remain virtually constant over these intervals.

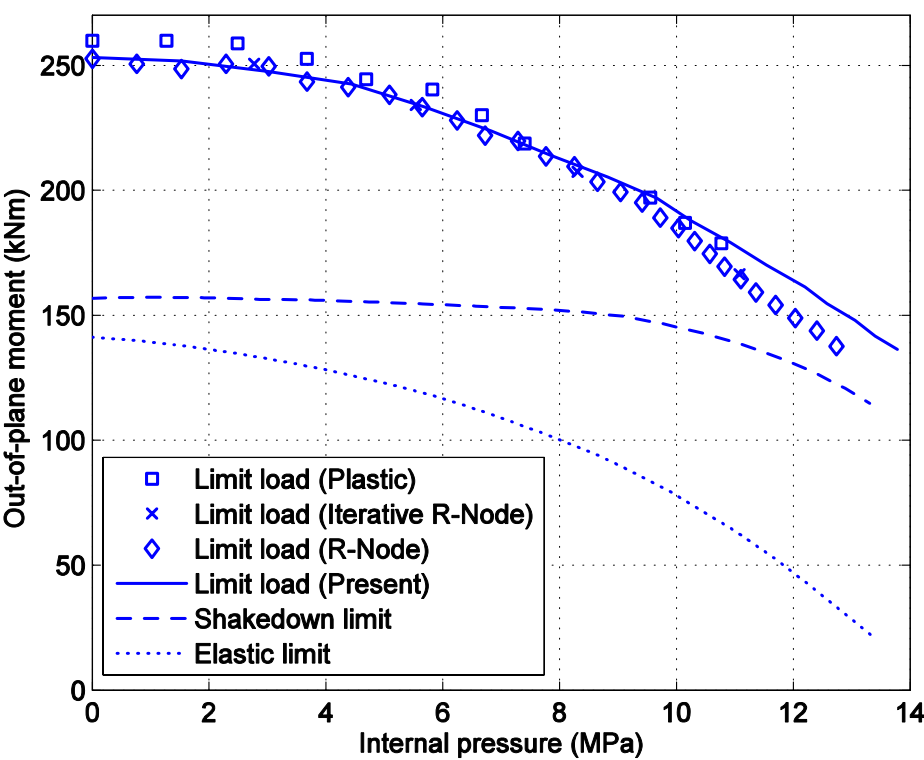


Figure 6.27 Effect of internal pressure on out-of-plane limit moments

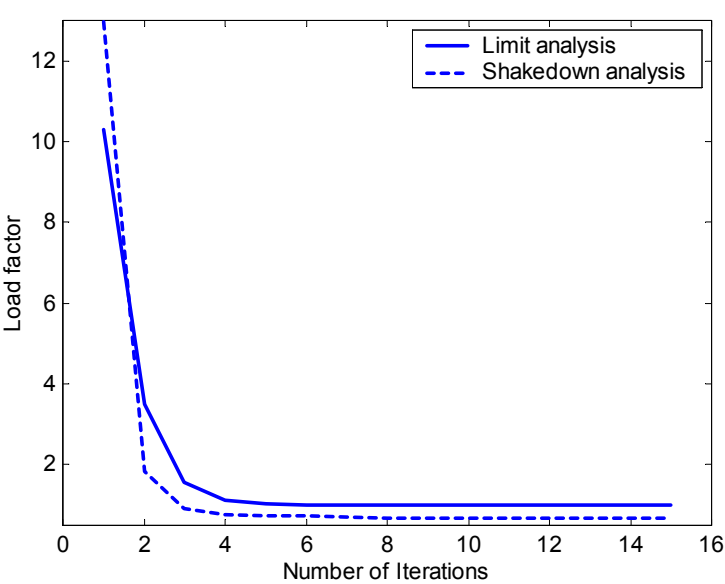


Figure 6.28 Limit load convergence of the pipe bend

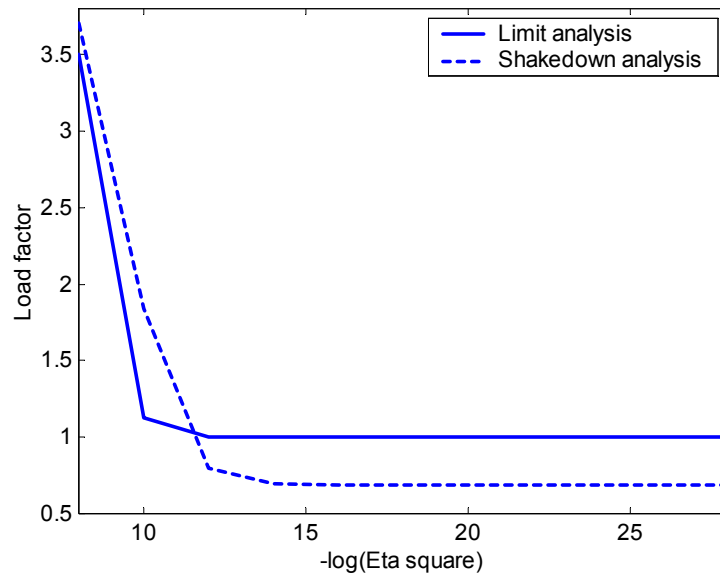


Figure 6.29 Influence of η^2

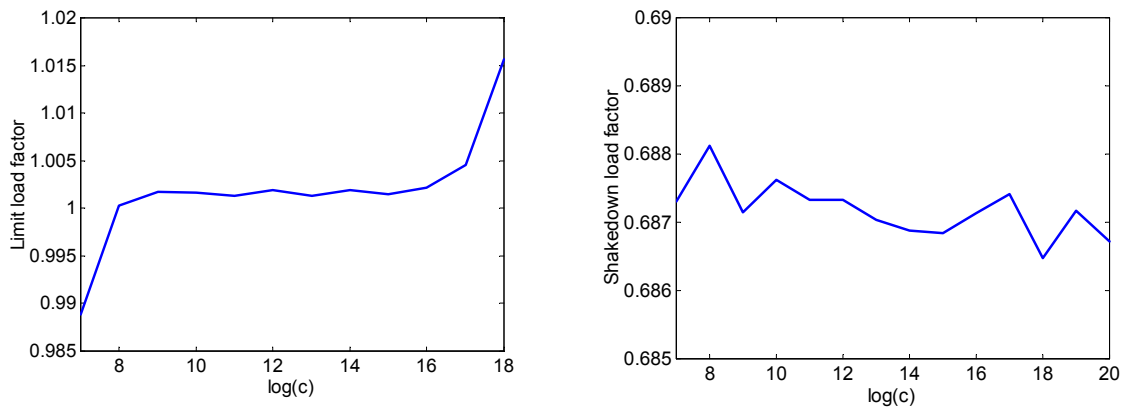


Figure 6.30 Influence of penalty parameter c

6.9 Nozzle in the knuckle region of a torispherical head

Torispherical drumheads under internal pressure loading are known to have high stresses in the ‘knuckle region’ due to the change of the curvature of the shell. In designing such vessels it is usually necessary to have piping nozzle connections welded in the head. To assess the plastic collapse limit and shakedown limit of such structures is of great interest to many designers and has been included in some design code rules, e.g. the UK pressure vessel design code BS 5500, the German pressure vessel design code AD-Merkblatt B3 and the European standard for unfired pressure vessels CEN. But they are still limited to some specific head shapes and loadings and not applicable for nozzles

particularly for nozzle encroaching in the knuckle region [Hsieh et al., 2000]. Recently, a parametric study of the knuckle-encroaching nozzles was conducted by Bauer and Saal [1997] by using finite element analysis. Using the von Mises yield criterion and 15-times the elastic slope method, that is by drawing a line at a slope 15 times that of the elastic portion of the relevant load versus deformation curve, Hsieh et al. [2000] investigated a series of knuckle-encroaching nozzles for both internal pressure and nozzle loads. A study of both individually and combined limit loads has also been undertaken. However, in the above studies, the cyclic loads were not considered.

In the present example, a single nozzle on a Klöpperboden head has been selected for investigation. Both internal pressure p and nozzle loads including axial force F , in-plane bending moment M_I , out-of-plane bending moment M_o , and twisting moment M_t were considered. The loads may be constant or vary independently from zero to the maximum value. The nozzle axis is parallel to the vessel axis as presented in the figure 6.31a. The dimensions are selected from the study in [Hsieh et al., 2000],[Bauer and Saal, 1997], [Tran et al., 2007c].

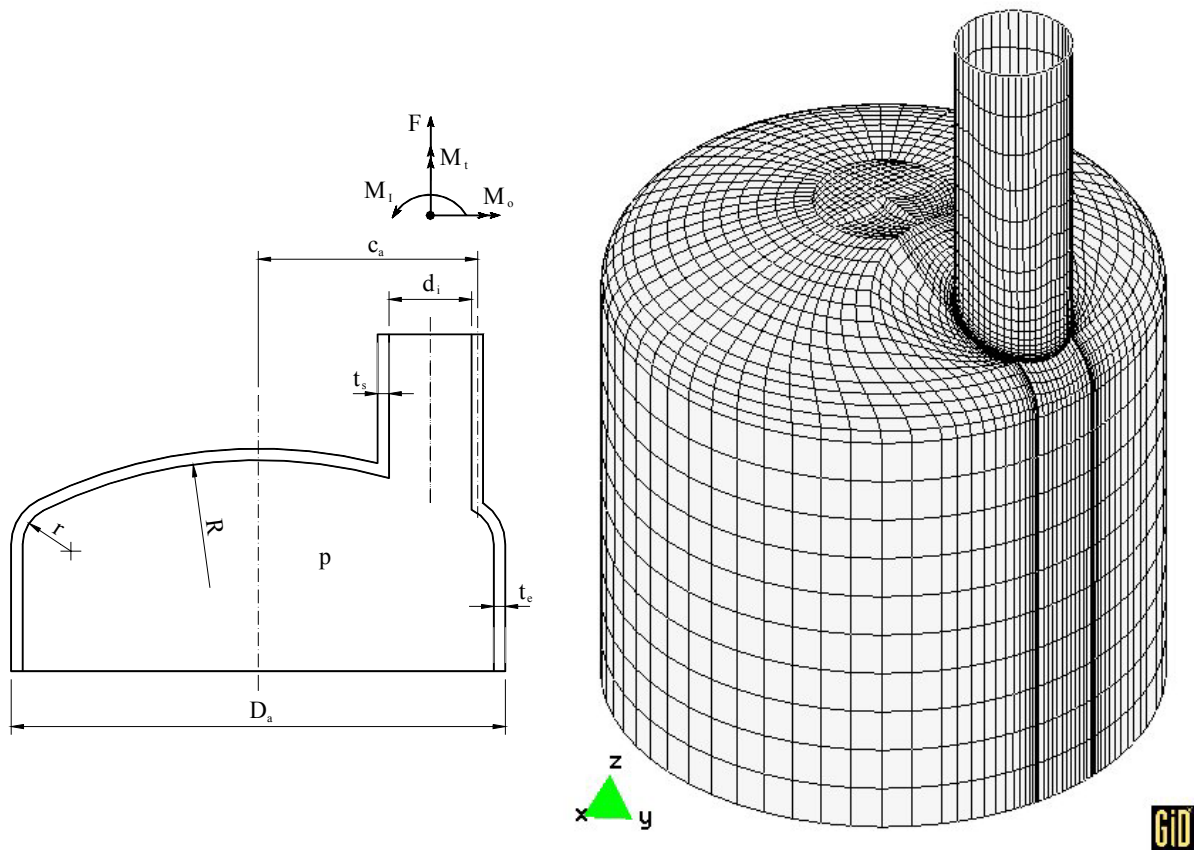


Figure 6.31 Geometrical dimensions of nozzle and FE-mesh

Vessel outer diameter and thickness $D_a = 2000$ mm, $t_e = 17$ mm

Head crown and knuckle radii $R = 2000$ mm, $r = 200$ mm

Nozzle inner diameter and thickness $d_i = 400$ mm, $t_s = 13.6$ mm

Nozzle offset $c_a = 910$ mm

The elastic-perfectly plastic material model was assumed with yield stress $\sigma_y = 340$ MPa. In order to ensure that the boundary condition effects do not influence the nozzle junction behaviour, the vessel cylinder length and nozzle length were chosen as D_a and $3d_i$, respectively. For all load cases the end of the main vessel is fully clamped. In our numerical analysis the full model was meshed by using 3032 quadrangular 4-noded flat shell elements as shown in figure 6.31b.

Numerical results for individual loads are introduced in table 6.10. Together with the first yield loads and limit loads, shakedown limits are also presented. It is seen that in all cases the results obtained with the present shell model compare very well with those gained by Hsieh et al. [2000] with 20-noded volume elements. The maximum difference of the limit analyses is 2.7% appearing in the case of internal pressure. It is noted by Hsieh et al. [2000] in this case that the limit load of using linear finite elements, i.e. the 8-noded brick finite elements, is 29% higher than that of using 20-noded elements.

Table 6.10: Elastic limit, limit and shakedown loads of the nozzle

Source, type of element	Limit criterion	Pressure [MPa]	Axial force [MN]	In-plane moment [kNm]	Out-of-plane moment [kNm]	Torsion [kNm]
Hsieh et al. [2000], volume elements	Elastic limit	1.37	0.45	64.7	66.5	193.8
	Plastic collapse limit	3.54	1.63	282.6	265.8	625
Present, shell elements	Elastic limit	1.439	0.391	64.4	68.2	193.3
	Plastic collapse limit	3.636	1.669	284	270.8	635
	Shakedown limit	2.878	0.783	128.8	136.4	386.6

The elastic analysis of the load case of axial force shows the exceptionally large difference of 13.1%. Therefore two mesh convergence analyses have been performed. First local mesh refinements with nearly square finite elements have been made around the intersection of the nozzle with the vessel head (figure 6.32a). Next the local refinement has been achieved by changing the shell elements from squares to bad shaped rectangular elements with aspect ratio 12 (figure 6.32b). The size of the elements in the refinement region has been changed by a factor 12 from the locally coarse mesh to the fine one. Figure 6.32 shows that even bad shaped shell elements do not cause convergence problems. Only very coarse meshes cause convergence problems for linearly elastic analyses. In the case of

alternating plasticity these problems carry over to shakedown analyses. The plastic collapse limit is virtually independent on the mesh. Obviously limit analysis is very robust.

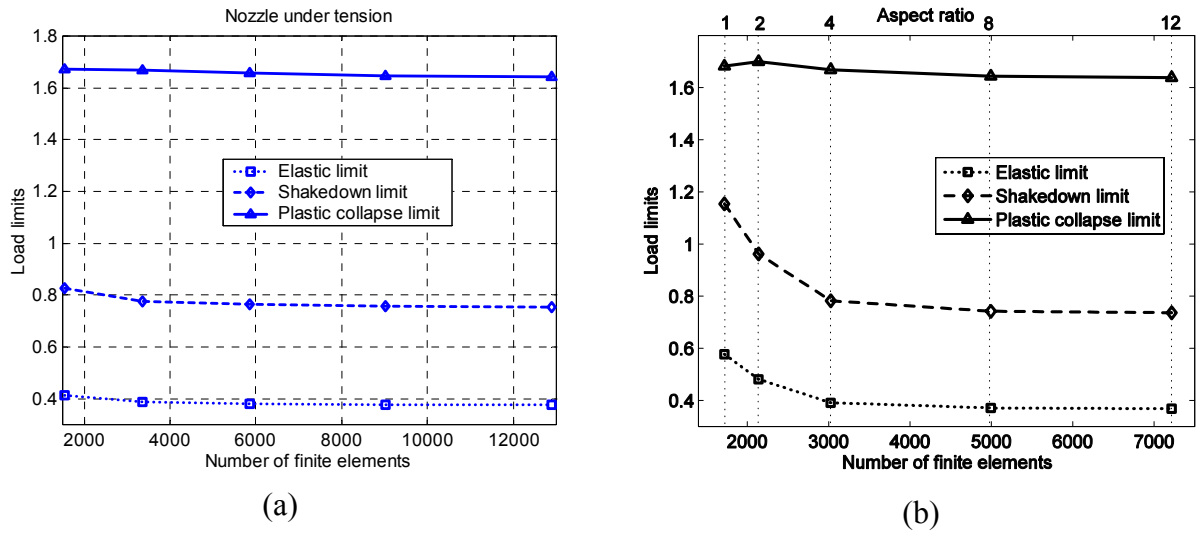


Figure 6.32 Mesh convergence analyses for the case of axial force

The interaction diagrams for load combinations between internal pressure and nozzle loads are presented in figures 6.33-6.36. In all cases the loads are normalized with the respective plastic collapse limit. These figures illustrate clearly the need to consider shakedown as a design criterion for knuckle-encroaching nozzles since the shakedown limits are considerably smaller than 57.7% of the plastic collapse limits in a wide range of parameters. On the other hand, in almost all cases it is twice the elastic limit which indicates that inadaptation will occur due to alternating plasticity. In this case the shakedown check is not mandatory although this leads to a design which is prone to LCF.

In the case of internal pressure and axial force (figure 6.33), the behaviour is of course sign-dependent. For compressive nozzle loading, a strengthening effect on plastic collapse limit appears as presented in Hsieh et al. [2000]. Contrarily, as would not be expected, there is a weakening effect on the shakedown limit in this case.

Figure 6.34 presents the interaction between internal pressure and in-plane bending moment. There is also a strengthening effect on plastic collapse limit in the case of positive bending moment (nozzle rotated inwards) as mentioned by Hsieh et al. It is observed that for this case while in-plane moment plays an important role, internal pressure has a small influence on the shakedown limit.

Figures 6.35 and 6.36 show the interactions of pressure versus out-of-plane bending and torsion moments. For both cases the behaviours of plastic collapse limits can be considered to be bilinear. A topologically different mesh has been used in Tran et al. [2007c] which exhibited sensitivity.

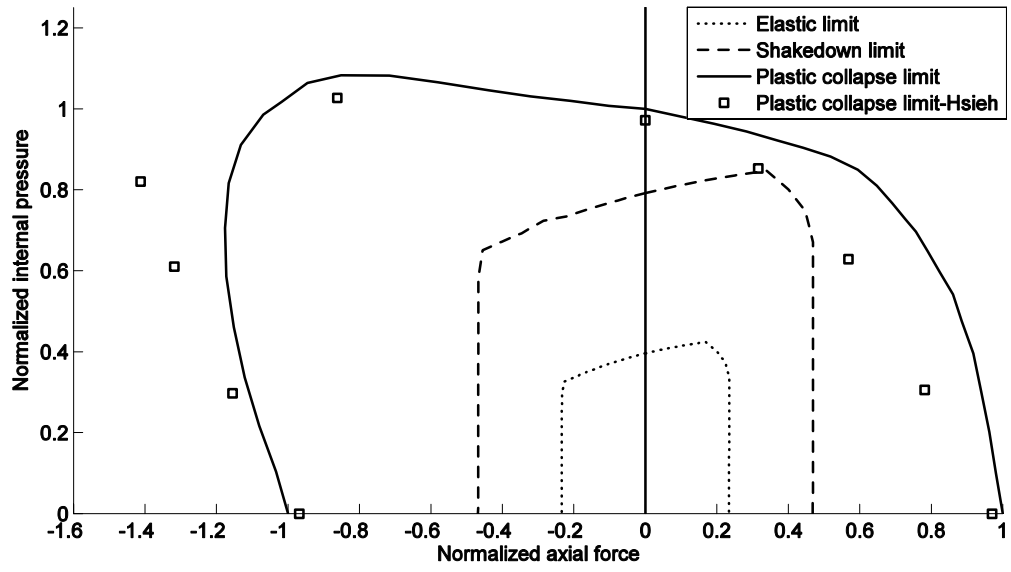


Figure 6.33 Pressure versus axial force interaction

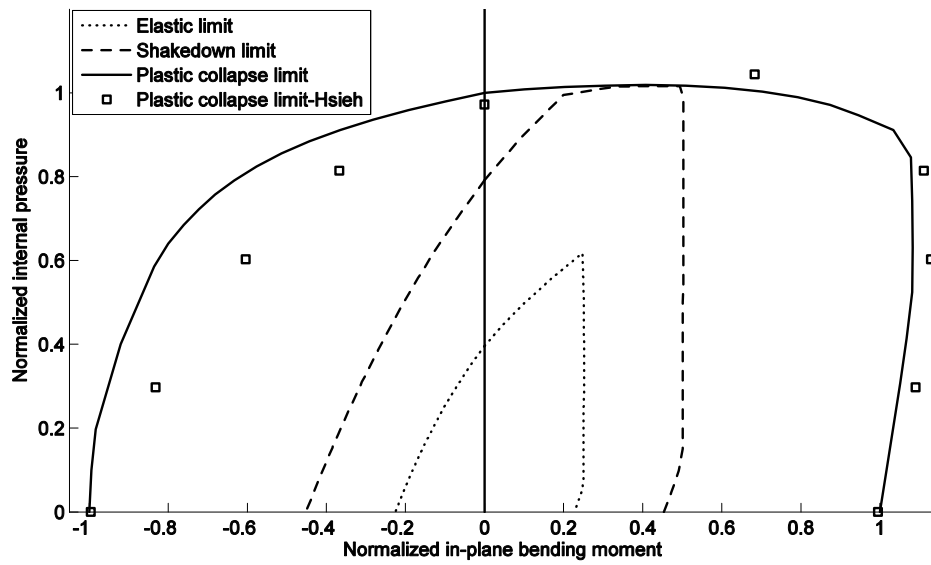


Figure 6.34 Pressure versus in-plane bending moment interaction

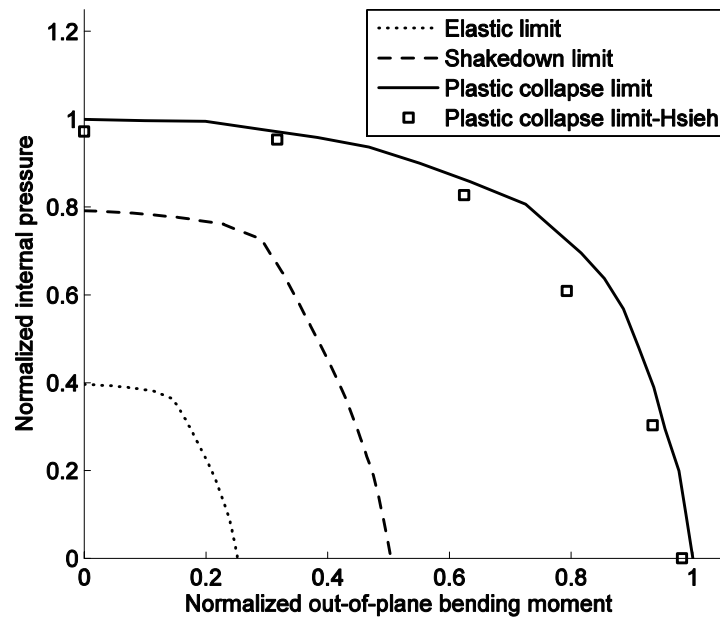


Figure 6.35 Pressure versus out-of-plane bending moment interaction

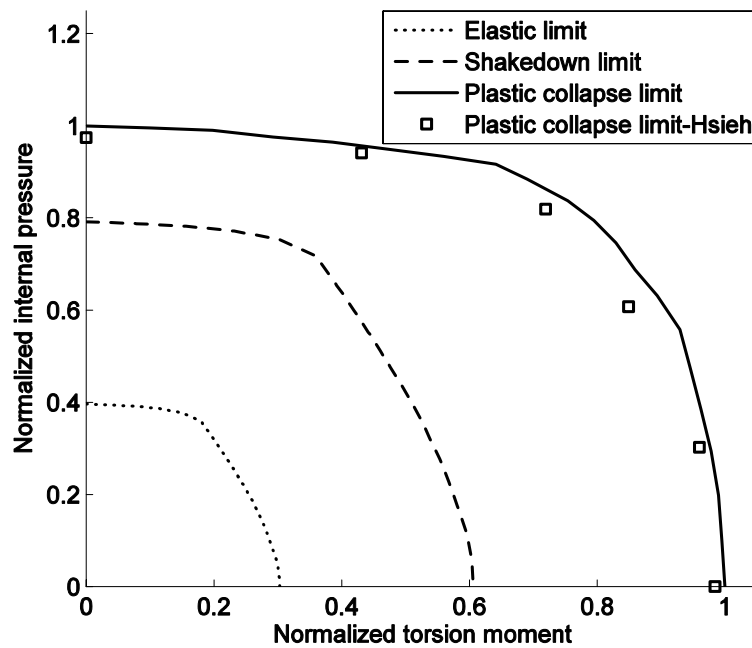


Figure 6.36 Pressure versus torsion moment interaction

7 PROBABILISTIC LIMIT AND SHAKEDOWN ANALYSIS OF STRUCTURES

In this chapter numerical applications of the probabilistic limit and shakedown programming are introduced. Four examples are presented below for the sake of evaluation of the algorithm, including both plate and shell structures. The first two examples illustrate the FORM/SORM calculations for structures in which the loads and yield stress are considered as random variables. In the third example the effect of the thickness imperfection on the limit load of a shell is studied by considering the thickness as another stochastic variable. The fourth example presents the estimation of the system failure probability of a frame formed of three plates subjected to vertical and horizontal loads. In each numerical test, some existing analytical and numerical solutions found in literature are briefly represented and compared.

7.1 Square plate with a central circular hole

In this example a square plate with central circular hole which was investigated in section 6.6 and in [Tran et al., 2007b] is considered. It has the ratio $R/L=0.2$ and is subjected to a uniaxial tension p_1 which can be constant or can vary within the range $[0, p_{\max}]$. Both yield limit σ_y and load p_1 are supposed to be random variables. This structure was also studied analytically and numerically by Staat and Heitzer [2003b] using FORM and volume element. The following two cases are examined.

Limit load analysis

For this case the exact plastic collapse limit is given by $p_{\lim} = (1 - R/L)\sigma_y$ in the range $R/L \leq 0.2$, since the lower and upper bound are coincident. If both material and load random variables are supposed to be normally distributed with means μ_r, μ_s and standard deviations σ_r, σ_s respectively, then the reliability index may be given [Staat and Heitzer, 2003]

$$\beta_{HL} = \frac{(1 - R/L)\mu_r - \mu_s}{\sqrt{(1 - R/L)^2 \sigma_r^2 + \sigma_s^2}} = \frac{0.8\mu_r - \mu_s}{\sqrt{0.64\sigma_r^2 + \sigma_s^2}}. \quad (7.1)$$

If both random variables are log-normally distributed, Staat and Heitzer also introduced the analytical expression

$$\beta_{HL} = \frac{\log((1-R/L)m_r) - \log(m_s)}{\sqrt{\delta_r^2 + \delta_s^2}} \quad (7.2)$$

where m_r, m_s and δ_r, δ_s are calculated as follows

$$m_{r,s} = \mu_{r,s} e^{-\delta_{r,s}^2/2} = \frac{\mu_{r,s}}{\sqrt{\left(\frac{\sigma_{r,s}^2}{\mu_{r,s}^2} + 1\right)}}, \quad \delta_{r,s} = \sqrt{\log\left(\frac{\sigma_{r,s}^2}{\mu_{r,s}^2} + 1\right)}. \quad (7.3)$$

In our numerical analysis, both kinds of random variables above were tested. Numerical results of failure probability P_f for both normal and log-normal distributions are introduced in tables 7.1-7.7, compared with the exact solutions and numerical solutions of Staat and Heitzer. The numerical error involves both deterministic shakedown analysis and reliability analysis is very small and acceptable. It is shown that SORM solutions are almost the same of FORM due to weak non-linearity of the limit state function. The weak non-linearity may be lost in the case of multi-parameter loads or by an extreme value distribution of the random variables. Figure 7.1 presents the failure probabilities versus μ_s / μ_r for the case of log-normal distributions, which are obtained by SORM.

Table 7.1: Numerical results and comparison for normal distributions

Limit analysis $\sigma_{r,s} = 0.1\mu_{r,s}$				
μ_s / μ_r	P_f (anal.)	P_f (FORM)	P_f (SORM)	P_f (num.) [Staat et al., 2003b]
0.2	1.718E-13	1.880E-13	1.878E-13	2.643E-13
0.3	2.426E-09	2.720E-09	2.716E-09	3.843E-09
0.4	3.872E-06	3.872E-06	3.872E-06	6.112E-06
0.5	7.364E-04	7.424E-04	7.421E-04	1.093E-03
0.6	2.275E-02	2.050E-02	2.140E-02	3.049E-02
0.7	1.734E-01	1.606E-01	1.606E-01	2.067E-01
0.8	5.000E-01	4.835E-01	4.835E-01	5.550E-01
0.9	7.969E-01	7.981E-01	7.986E-01	8.305E-01
1.0	9.408E-01	9.419E-01	9.419E-01	9.544E-01
1.1	9.863E-01	9.848E-01	9.848E-01	9.900E-01
1.2	9.972E-01	9.973E-01	9.973E-01	9.981E-01
1.3	9.995E-01	9.996E-01	9.996E-01	9.996E-01
1.4	9.999E-01	9.999E-01	9.999E-01	9.999E-01

Table 7.2: Numerical results and comparison for normal distributions

Limit analysis $\sigma_r = 0.2\mu_r$, $\sigma_s = 0.1\mu_s$				
μ_s / μ_r	P_f (anal.)	P_f (FORM)	P_f (SORM)	P_f (num.) [Staat et al., 2003b]
0.1	6.313E-06	5.901E-06	5.902E-06	6.455E-06
0.2	9.919E-04	9.436E-04	9.437E-04	1.085E-04
0.3	1.065E-03	1.045E-03	1.046E-03	1.205E-03
0.4	7.646E-03	7.494E-03	7.496E-03	8.763E-03
0.5	3.675E-02	4.053E-02	4.052E-02	4.163E-02
0.6	1.209E-01	1.318E-01	1.318E-01	1.361E-01
0.7	2.835E-01	3.028E-01	3.028E-01	3.103E-01
0.8	5.000E-01	5.314E-01	5.314E-01	5.319E-01
0.9	7.070E-01	7.042E-01	7.042E-01	7.397E-01
1.0	8.554E-01	8.621E-01	8.621E-01	8.765E-01
1.1	9.388E-01	9.451E-01	9.451E-01	9.499E-01
1.2	9.772E-01	9.850E-01	9.850E-01	9.821E-01
1.3	9.925E-01	9.955E-01	9.955E-01	9.943E-01
1.4	9.976E-01	9.987E-01	9.987E-01	9.983E-01
1.5	9.993E-01	9.995E-01	9.995E-01	9.995E-01
1.6	9.998E-01	9.999E-01	9.999E-01	9.999E-01

Table 7.3: Numerical results and comparison for normal distributions

Limit analysis $\sigma_r = 0.2\mu_r$, $\sigma_s = 0.2\mu_s$				
μ_s / μ_r	P_f (anal.)	P_f (FORM)	P_f (SORM)	P_f (num.) [Staat et al., 2003b]
0.1	7.085E-06	6.866E-06	6.866E-06	7.271E-06
0.2	1.374E-04	1.312E-04	1.312E-04	1.514E-04
0.3	1.717E-03	1.887E-03	1.887E-03	1.948E-03
0.4	1.267E-02	1.247E-02	1.248E-02	1.437E-02
0.5	5.590E-02	6.252E-02	6.250E-02	6.271E-02
0.6	1.587E-01	1.723E-01	1.723E-01	1.742E-01
0.7	3.190E-01	3.366E-01	3.366E-01	3.427E-01
0.8	5.000E-01	5.240E-01	5.239E-01	5.256E-01
0.9	6.610E-01	6.851E-01	6.850E-01	6.843E-01
1.0	7.826E-01	8.019E-01	8.018E-01	8.021E-01
1.1	8.649E-01	8.795E-01	8.794E-01	8.775E-01
1.2	9.172E-01	9.277E-01	9.276E-01	9.258E-01
1.3	9.493E-01	9.563E-01	9.562E-01	9.550E-01
1.4	9.686E-01	9.730E-01	9.730E-01	9.729E-01
1.5	9.802E-01	9.831E-01	9.831E-01	9.823E-01
1.6	9.873E-01	9.892E-01	9.892E-01	9.882E-01

Table 7.4: Numerical results and comparison for log-normal distributions

Limit analysis $\sigma_r = 0.1\mu_r$, $\sigma_s = 0.1\mu_s$				
μ_s / μ_r	P_f (anal.)	P_f (FORM)	P_f (SORM)	P_f (num.) [Staat et al., 2003b]
0.3	1.790E-12	1.704E-12	1.704E-12	9.593E-12
0.4	4.473E-07	5.097E-07	5.097E-07	1.409E-06
0.5	4.315E-04	5.205E-04	5.205E-04	1.009E-03
0.6	2.071E-02	1.814E-02	1.814E-02	3.485E-02
0.7	1.719E-01	1.604E-01	1.604E-01	2.409E-01
0.8	5.000E-01	4.794E-01	4.794E-01	5.396E-01
0.9	7.981E-01	7.839E-01	7.839E-01	8.575E-01
1.0	9.431E-01	9.373E-01	9.373E-01	9.648E-01
1.1	9.880E-01	9.867E-01	9.867E-01	9.935E-01
1.2	9.979E-01	9.976E-01	9.976E-01	9.990E-01
1.3	9.997E-01	9.997E-01	9.997E-01	9.998E-01
1.4	9.999E-01	9.999E-01	9.999E-01	9.999E-01

Table 7.5: Numerical results and comparison for log-normal distributions

Limit analysis $\sigma_r = 0.1\mu_r$, $\sigma_s = 0.2\mu_s$				
μ_s / μ_r	P_f (anal.)	P_f (FORM)	P_f (SORM)	P_f (num.) [Staat et al., 2003b]
0.2	3.090E-10	2.146E-10	2.152E-10	3.566E-10
0.3	6.586E-06	4.490E-06	4.497E-06	6.861E-06
0.4	1.107E-03	8.235E-04	8.235E-04	1.168E-03
0.5	2.000E-02	1.645E-02	1.645E-02	2.114E-02
0.6	1.090E-01	1.011E-01	1.011E-01	1.115E-01
0.7	2.959E-01	2.738E-01	2.738E-01	2.981E-01
0.8	5.263E-01	5.024E-01	5.024E-01	5.338E-01
0.9	7.248E-01	7.061E-01	7.061E-01	7.337E-01
1.0	8.582E-01	8.472E-01	8.472E-01	8.635E-01
1.1	9.334E-01	9.269E-01	9.269E-01	9.353E-01
1.2	9.709E-01	9.676E-01	9.676E-01	9.715E-01
1.3	9.879E-01	9.866E-01	9.866E-01	9.884E-01
1.4	9.951E-01	9.947E-01	9.947E-01	9.954E-01
1.5	9.981E-01	9.979E-01	9.979E-01	9.982E-01

Table 7.6: Numerical results and comparison for log-normal distributions

Limit analysis $\sigma_r = 0.2\mu_r$, $\sigma_s = 0.1\mu_s$				
μ_s / μ_r	P_f (anal.)	P_f (FORM)	P_f (SORM)	P_f (num.) [Staat et al., 2003b]
0.2	1.327E-10	1.678E-10	1.678E-10	8.296E-10
0.3	3.574E-06	7.072E-06	7.050E-06	1.303E-05
0.4	7.067E-04	1.062E-03	1.060E-03	1.807E-03
0.5	1.442E-02	1.782E-02	1.781E-02	2.848E-02
0.6	8.638E-02	1.078E-01	1.077E-01	1.407E-01
0.7	2.520E-01	2.873E-01	2.872E-01	3.518E-01
0.8	4.736E-01	5.121E-01	5.121E-01	5.860E-01
0.9	6.790E-01	7.124E-01	7.124E-01	7.744E-01
1.0	8.264E-01	8.510E-01	8.509E-01	8.884E-01
1.1	9.146E-01	9.297E-01	9.296E-01	9.509E-01
1.2	9.610E-01	9.689E-01	9.689E-01	9.796E-01
1.3	9.831E-01	9.870E-01	9.870E-01	9.918E-01
1.4	9.930E-01	9.947E-01	9.947E-01	9.969E-01
1.5	9.971E-01	9.979E-01	9.979E-01	9.988E-01

Table 7.7: Numerical results and comparison for log-normal distributions

Limit analysis $\sigma_r = 0.2\mu_r$, $\sigma_s = 0.2\mu_s$				
μ_s / μ_r	P_f (anal.)	P_f (FORM)	P_f (SORM)	P_f (num.) [Staat et al., 2003b]
0.1	5.655E-14	3.885E-14	3.887E-14	1.337E-13
0.2	3.715E-07	4.828E-07	4.820E-07	6.786E-07
0.3	2.308E-04	2.458E-04	2.451E-04	4.601E-03
0.4	6.664E-03	6.485E-03	6.500E-03	9.443E-03
0.5	4.665E-02	4.363E-02	4.363E-02	5.864E-02
0.6	1.521E-01	1.497E-01	1.497E-01	1.816E-01
0.7	3.167E-01	3.120E-01	3.121E-01	3.601E-01
0.8	5.000E-01	4.899E-01	4.908E-01	5.458E-01
0.9	6.629E-01	6.541E-01	6.541E-01	7.046E-01
1.0	7.871E-01	7.786E-01	7.786E-01	8.213E-01
1.1	8.722E-01	8.665E-01	8.665E-01	8.959E-01
1.2	9.261E-01	9.225E-01	9.225E-01	9.414E-01
1.3	9.584E-01	9.562E-01	9.562E-01	9.674E-01
1.4	9.771E-01	9.762E-01	9.763E-01	9.828E-01
1.5	9.875E-01	9.868E-01	9.868E-01	9.907E-01

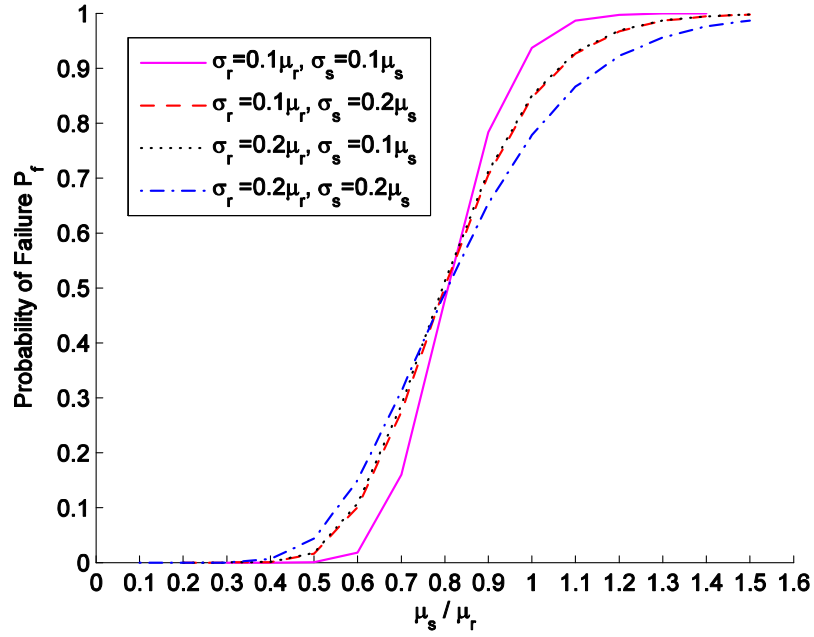


Figure 7.1 Probability of failure versus μ_s / μ_r for log-normally distributed variables

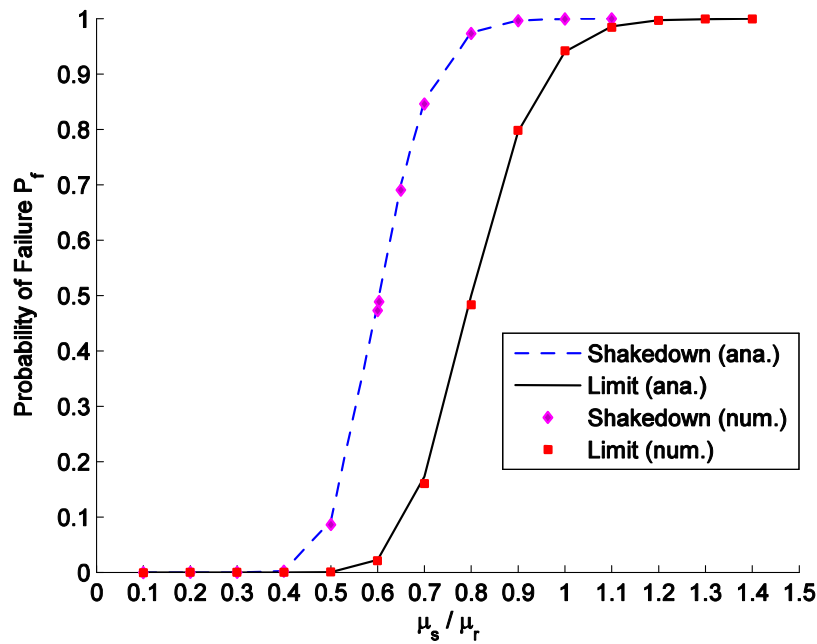


Figure 7.2 Comparison of the results for probability of failure for normally distributed variables

Shakedown load analysis

For this case, the tension p varies within the range $[0, p_{\max}]$ and only the amplitudes but not the uncertain complete load history influences the solution. Consider the case where the maximal magnitude p_{\max} is a random variable and the minimal magnitude is held zero.

From the deterministic analysis we got the shakedown load $p_{sh} = 0.60332\sigma_y$. The numerical probability of failure for normally distributed variables are presented in table 7.8, compared with the analytical solutions, which are calculated by (7.1). In figure 7.2 the failure probabilities (SORM approximations) are shown versus μ_s / μ_r for both two cases limit and shakedown analysis and for the case of normal distributions with $\sigma_{r,s} = 0.1\mu_{r,s}$. It is worth to note that the shakedown probabilities of failure are considerably smaller than those of limit analysis. Thus, the loading conditions should be considered carefully when assessing the load carrying capacity of the structure.

Table 7.8: Numerical results and comparison for normal distributions

Shakedown analysis $\sigma_{r,s} = 0.1\mu_{r,s}$			
μ_s / μ_r	P_f (anal.)	P_f (FORM)	P_f (SORM)
0.2	1.109E-10	9.333E-11	9.333E-11
0.3	3.371E-06	2.833E-06	2.833E-06
0.4	2.486E-03	2.168E-03	2.168E-03
0.5	9.366E-02	8.644E-02	8.648E-02
0.6	4.844E-01	4.732E-01	4.732E-01
0.60332	5.000E-01	4.891E-01	4.891E-01
0.65	7.007E-01	6.906E-01	6.906E-01
0.7	8.523E-01	8.464E-01	8.464E-01
0.8	9.752E-01	9.735E-01	9.735E-01
0.9	9.969E-01	9.967E-01	9.967E-01
1.0	9.996E-01	9.996E-01	9.996E-01
1.1	9.999E-01	9.999E-01	9.999E-01

7.2 Pipe-junction subjected to internal pressure

In this example, the pipe-junction which was investigated in section 6.3 and in [Tran et al., 2007d] is considered. It is subjected to internal pressure p which can be constant or vary within the range $[0, p_{\max}]$. Both yield limit σ_y and load p are considered as random variables. Numerical deterministic analyses lead to a collapse pressure $p_{\lim} = 0.145\sigma_y$ and shakedown limit $p_{sh} = 0.10267\sigma_y$. If both material and load random variables are supposed to be normally distributed with means μ_r, μ_s and standard deviations σ_r, σ_s respectively, then the reliability index may be given [Staat and Heitzer, 2003b]

$$\beta_{HL} = \frac{0.145\mu_r - \mu_s}{\sqrt{0.021\sigma_r^2 + \sigma_s^2}} \quad \text{for limit analysis} \quad (7.4a)$$

Table 7.9: Numerical results and comparison for normal distributions, $\sigma_{r,s} = 0.1\mu_{r,s}$

Limit analysis				Shakedown analysis			
μ_s / μ_r	P_f (anal.)	P_f (FORM)	P_f (SORM)	μ_s / μ_r	P_f (anal.)	P_f (FORM)	P_f (SORM)
0.04	1.469E-12	1.239E-12	1.345E-12	0.03	5.456E-12	4.349E-12	4.352E-12
0.06	3.036E-08	2.764E-08	2.976E-08	0.04	6.441E-09	9.304E-09	9.302E-09
0.08	4.336E-05	4.225E-05	4.474E-05	0.05	1.992E-06	1.758E-06	1.804E-06
0.10	5.312E-03	5.108E-03	5.312E-03	0.06	1.665E-04	1.423E-04	1.433E-04
0.12	9.204E-02	8.946E-02	9.157E-02	0.07	4.280E-03	3.391E-03	3.401E-03
0.14	4.020E-01	3.953E-01	4.000E-01	0.08	4.078E-02	3.761E-02	3.783E-02
0.145	5.000E-01	4.934E-01	4.983E-01	0.09	1.767E-01	1.648E-01	1.663E-01
0.15	5.947E-01	5.890E-01	5.890E-01	0.10	4.261E-01	4.180E-01	4.182E-01
0.16	7.564E-01	7.537E-01	7.537E-01	0.10267	5.000E-01	4.869E-01	4.873E-01
0.18	9.350E-01	9.346E-01	9.346E-01	0.11	6.869E-01	6.698E-01	6.698E-01
0.20	9.870E-01	9.869E-01	9.869E-01	0.12	8.637E-01	8.683E-01	8.677E-01
0.22	9.978E-01	9.978E-01	9.978E-01	0.14	9.842E-01	9.866E-01	9.865E-01
0.24	9.997E-01	9.997E-01	9.997E-01	0.16	9.987E-01	9.986E-01	9.986E-01
0.26	9.999E-01	9.999E-01	9.999E-01	0.18	9.999E-01	9.999E-01	9.999E-01

Table 7.10: Numerical results for Weibull distributions, $\sigma_{r,s} = 0.1\mu_{r,s}$

Limit analysis			Shakedown analysis		
μ_s / μ_r	P_f (FORM)	P_f (SORM)	μ_s / μ_r	P_f (FORM)	P_f (SORM)
0.04	7.238E-08	6.504E-08	0.03	6.945E-07	6.242E-07
0.06	9.514E-06	8.580E-06	0.04	2.448E-05	2.212E-05
0.08	3.280E-04	2.982E-04	0.05	3.818E-04	3.473E-04
0.10	4.807E-03	4.437E-03	0.06	3.152E-03	2.897E-03
0.12	3.955E-02	3.734E-02	0.07	1.975E-02	1.846E-02
0.14	2.051E-01	2.005E-01	0.08	8.956E-02	8.581E-02
0.145	2.812E-01	2.775E-01	0.09	2.836E-01	2.798E-01
0.15	3.689E-01	3.663E-01	0.10	5.798E-01	5.782E-01
0.16	5.567E-01	5.556E-01	0.10267	6.538E-01	6.508E-01
0.18	8.367E-01	8.326E-01	0.11	8.120E-01	8.074E-01
0.20	9.476E-01	9.449E-01	0.12	9.236E-01	9.200E-01
0.22	9.827E-01	9.819E-01	0.14	9.873E-01	9.870E-01
0.24	9.937E-01	9.945E-01	0.16	9.974E-01	9.990E-01
0.26	9.977E-01	9.993E-01	0.18	9.994E-01	9.999E-01

$$\beta_{HL} = \frac{0.10267\mu_r - \mu_s}{\sqrt{0.01054\sigma_r^2 + \sigma_s^2}} \quad \text{for shakedown analysis} \quad (7.4b)$$

Numerical probabilities of failure for limit and shakedown analyses for normal distribution are presented in table 7.9, compared with corresponding analytical solutions. Both random variables have standard deviations $\sigma_{r,s} = 0.1\mu_{r,s}$. The numerical error now comes only from reliability analysis. It is shown that numerical results of FORM and SORM are very close to the exact ones, especially for the case of limit analysis. Otherwise SORM gives slightly better results compared with FORM.

Besides normal and log-normal distributions, the Weibull distribution is frequently used for modelling loads and resistance. Table 7.10 shows the numerical results of FORM/SORM for the case that both random variables have Weibull distribution. The Weibull distribution leads to much larger failure probabilities in shakedown analysis but to much smaller ones in limit analysis (figure 7.3). No analytical results are known. The limit state function is non-linear after the transformation into the \mathbf{u} space. In this case SORM would give improved results.

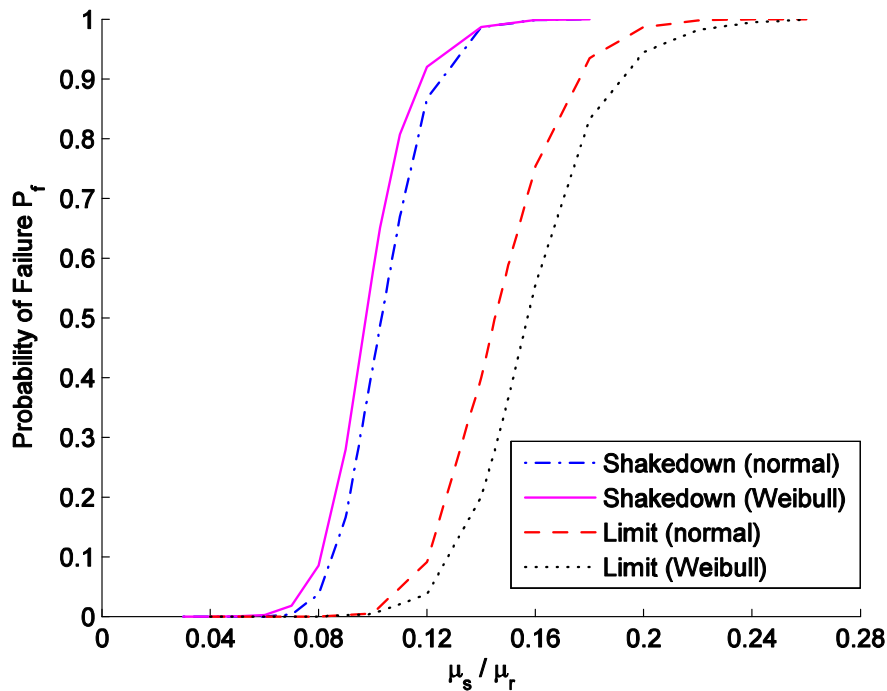


Figure 7.3 Probabilities of failure for normally and Weibull distributed variables

7.3 Limit analysis of cylindrical pipe under complex loading

Beside the loading and material strength, it is well known that the load carrying capacity of shell structures is generally influenced by their initial imperfections which occurs during the manufacturing and construction stages such as variability of thickness. In this example, the effect of thickness imperfection on the limit loads of a shell structure is examined. The cylindrical pipe subjected to complex loading which was investigated in

section 6.1 is considered here. The following geometrical and physical parameters are adopted: $L = 2700\text{mm}$, $r = 300\text{mm}$, $\sigma_y = 120\text{MPa}$. For this purpose, only the loading and the thickness h of the pipe are modelled as random variables. The following loading cases are examined

Internal pressure

For this case, the exact plastic collapse limit pressure is given by $p_{\text{lim}} = \sigma_y h / r$. Thus, the resistance R depends linearly on the realization h of the thickness basic variable Z . The magnitude of the internal pressure is the second basic variable X . The limit state function is defined by

$$g(X, Z) = \frac{\sigma_y}{r} Z - X. \quad (7.5)$$

If both thickness and load random variables are supposed to be normally distributed with means μ_t , μ_s and standard deviations σ_t , σ_s respectively, then the limit state function $g(\mathbf{U})$ in the standard Gaussian space is a linear function. Note that σ_y is the yield stress and not a standard deviation here. The mean and standard deviation of the limit state function can be calculated as follows

$$\mu_g = \frac{\sigma_y}{r} \mu_t - \mu_s, \quad \sigma_g = \sqrt{\left(\frac{\sigma_y}{r}\right)^2 \sigma_t^2 + \sigma_s^2} \quad (7.6)$$

from which, the reliability index becomes

$$\beta_{HL} = \frac{\mu_g}{\sigma_g} = \frac{(\sigma_y / r) \mu_t - \mu_s}{\sqrt{(\sigma_y / r)^2 \sigma_t^2 + \sigma_s^2}}. \quad (7.7a)$$

The limit state function becomes non-linear if both basic variables are log-normally distributed. Analogously with (7.2), we obtain the exact reliability index for FORM

$$\beta_{HL} = \frac{\log((\sigma_y / r) m_t) - \log(m_s)}{\sqrt{\delta_t^2 + \delta_s^2}} \quad (7.7b)$$

where m_t , m_s and δ_t , δ_s are calculated as in (7.3).

Bending moment

The exact plastic collapse limit moment is linearised by $M_b^{\text{lim}} = 4r^2 \sigma_y h$ (see (6.1)). The limit state function is a linear function of basic variables X, Z and defined by

$$g(X, Z) = 4r^2 \sigma_y Z - X. \quad (7.8)$$

The reliability indexes for both cases of normally and log-normally distributed random variables are obtained, respectively

$$\beta_{HL} = \frac{4r^2\sigma_y\mu_t - \mu_s}{\sqrt{(4r^2\sigma_y)^2\sigma_t^2 + \sigma_s^2}} \quad (7.9a)$$

$$\beta_{HL} = \frac{\log(4r^2\sigma_y m_t) - \log(m_s)}{\sqrt{\delta_t^2 + \delta_s^2}}. \quad (7.9b)$$

Torsion moment

In this case the exact plastic collapse limit moment is given by $M_t^{\lim} = 2\pi r^2\sigma_y h / \sqrt{3}$. The limit state function is a linear function of basic variables X, Z and defined by

$$g(X, Z) = \frac{2}{\sqrt{3}}\pi r^2\sigma_y Z - X. \quad (7.10)$$

The reliability indexes for both cases of normally and log-normally distributed random variables are obtained, respectively

$$\beta_{HL} = \frac{\frac{2}{\sqrt{3}}\pi r^2\sigma_y\mu_t - \mu_s}{\sqrt{\left(\frac{2}{\sqrt{3}}\pi r^2\sigma_y\right)^2\sigma_t^2 + \sigma_s^2}} \quad (7.11a)$$

$$\beta_{HL} = \frac{\log\left(\frac{2}{\sqrt{3}}\pi r^2\sigma_y m_t\right) - \log(m_s)}{\sqrt{\delta_t^2 + \delta_s^2}}. \quad (7.11b)$$

Axial load

The exact plastic collapse limit load is given by $F_{\lim} = 2\pi r\sigma_y h$. The limit state function is a linear function of the basic variables X, Z and defined by

$$g(X, Z) = 2\pi r\sigma_y Z - X. \quad (7.12)$$

The reliability indexes for both cases of normally and log-normally distributed random variables are obtained, respectively

$$\beta_{HL} = \frac{2\pi r\sigma_y\mu_t - \mu_s}{\sqrt{(2\pi r\sigma_y)^2\sigma_t^2 + \sigma_s^2}} \quad (7.13a)$$

$$\beta_{HL} = \frac{\log(2\pi r\sigma_y m_t) - \log(m_s)}{\sqrt{\delta_t^2 + \delta_s^2}}. \quad (7.13b)$$

Table 7.11: Numerical results and comparison for pressure case

Normal distributions: $\sigma_{t,s} = 0.1\mu_{t,s}$				Log-normal distributions: $\sigma_{t,s} = 0.1\mu_{t,s}$			
μ_s / μ_t $\times 10^{-6} \frac{m^3}{kN}$	P_f (anal.)	P_f (FORM)	P_f (SORM)	μ_s / μ_t $\times 10^{-6} \frac{m^3}{kN}$	P_f (anal.)	P_f (FORM)	P_f (SORM)
0.10	1.718E-13	1.720E-13	1.724E-13	0.14	4.964E-14	3.160E-14	3.179E-14
0.15	2.428E-09	1.935E-09	1.935E-09	0.15	1.791E-12	1.175E-12	1.175E-12
0.20	3.872E-06	3.651E-06	3.700E-06	0.20	4.473E-07	3.277E-07	3.274E-07
0.25	7.364E-04	6.117E-04	6.117E-04	0.25	4.316E-04	3.522E-04	3.524E-04
0.30	2.275E-02	1.976E-02	2.017E-02	0.30	2.071E-02	1.844E-02	1.849E-02
0.35	1.734E-01	1.580E-01	1.582E-01	0.35	1.719E-01	1.596E-01	1.596E-01
0.40	5.000E-01	4.740E-01	4.741E-01	0.40	5.000E-01	4.752E-01	4.753E-01
0.45	7.969E-01	7.787E-01	7.792E-01	0.45	7.981E-01	7.798E-01	7.799E-01
0.50	9.408E-01	9.332E-01	9.333E-01	0.50	9.432E-01	9.356E-01	9.356E-01
0.55	9.863E-01	9.840E-01	9.840E-01	0.55	9.880E-01	9.859E-01	9.860E-01
0.60	9.972E-01	9.967E-01	9.967E-01	0.60	9.980E-01	9.975E-01	9.975E-01
0.65	9.995E-01	9.994E-01	9.994E-01	0.65	9.997E-01	9.996E-01	9.996E-01
0.70	9.999E-01	9.999E-01	9.999E-01	0.70	9.999E-01	9.999E-01	9.999E-01

Table 7.12: Numerical results and comparison for bending moment case

Normal distributions: $\sigma_{t,s} = 0.1\mu_{t,s}$				Log-normal distributions: $\sigma_{t,s} = 0.1\mu_{t,s}$			
μ_s / μ_t $\times 10^{-5} \frac{1}{kN}$	P_f (anal.)	P_f (FORM)	P_f (SORM)	μ_s / μ_t $\times 10^{-5} \frac{1}{kN}$	P_f (anal.)	P_f (FORM)	P_f (SORM)
0.15	3.488E-10	3.360E-10	3.378E-10	0.15	3.231E-14	3.030E-14	3.075E-14
0.20	5.484E-07	5.284E-07	5.324E-07	0.20	2.393E-08	2.257E-08	2.279E-08
0.25	1.330E-04	1.284E-04	1.292E-04	0.25	5.282E-05	5.039E-05	5.076E-05
0.30	6.041E-03	5.859E-03	5.886E-03	0.30	4.871E-03	4.704E-03	4.729E-03
0.35	7.013E-02	6.849E-02	6.869E-02	0.35	6.783E-02	6.629E-02	6.649E-02
0.40	2.934E-01	2.888E-01	2.893E-01	0.40	2.927E-01	2.891E-01	2.895E-01
0.432	5.000E-01	4.945E-01	4.949E-01	0.432	5.000E-01	4.946E-01	4.950E-01
0.45	6.135E-01	6.083E-01	6.079E-01	0.45	6.139E-01	6.085E-01	6.081E-01
0.50	8.483E-01	8.449E-01	8.447E-01	0.50	8.500E-01	8.466E-01	8.463E-01
0.55	9.542E-01	9.528E-01	9.528E-01	0.55	9.565E-01	9.552E-01	9.551E-01
0.60	9.885E-01	9.880E-01	9.880E-01	0.60	9.901E-01	9.897E-01	9.896E-01
0.65	9.974E-01	9.973E-01	9.973E-01	0.65	9.981E-01	9.980E-01	9.980E-01
0.70	9.994E-01	9.994E-01	9.994E-01	0.70	9.997E-01	9.997E-01	9.997E-01
0.75	9.999E-01	9.999E-01	9.999E-01	0.75	9.999E-01	9.999E-01	9.999E-01

Table 7.13: Numerical results and comparison for torsion moment case

Normal distributions: $\sigma_{t,s} = 0.1\mu_{t,s}$				Log-normal distributions: $\sigma_{t,s} = 0.1\mu_{t,s}$			
μ_s / μ_t $\times 10^{-5} \frac{1}{kN}$	P_f (anal.)	P_f (FORM)	P_f (SORM)	μ_s / μ_t $\times 10^{-5} \frac{1}{kN}$	P_f (anal.)	P_f (FORM)	P_f (SORM)
0.10	2.673E-13	2.811E-13	2.803E-13	0.14	1.497E-13	1.127E-13	1.127E-13
0.15	4.123E-09	3.585E-09	3.585E-09	0.15	5.031E-12	3.832E-12	3.832E-12
0.20	6.507E-06	5.670E-06	5.670E-06	0.20	9.381E-07	7.756E-07	7.756E-07
0.25	1.142E-03	1.017E-03	1.017E-03	0.25	7.250E-04	6.584E-04	6.584E-04
0.30	3.145E-02	2.889E-02	2.889E-02	0.30	2.924E-02	2.821E-02	2.821E-02
0.35	2.132E-01	2.021E-01	2.021E-01	0.35	2.120E-01	2.009E-01	2.009E-01
0.39178	5.000E-01	4.845E-01	4.845E-01	0.39178	5.000E-01	4.846E-01	4.846E-01
0.40	5.584E-01	5.429E-01	5.429E-01	0.40	5.585E-01	5.431E-01	5.431E-01
0.45	8.354E-01	8.257E-01	8.257E-01	0.45	8.370E-01	8.272E-01	8.272E-01
0.50	9.558E-01	9.521E-01	9.522E-01	0.50	9.581E-01	9.545E-01	9.545E-01
0.55	9.904E-01	9.895E-01	9.895E-01	0.55	9.919E-01	9.910E-01	9.910E-01
0.60	9.982E-01	9.980E-01	9.980E-01	0.60	9.987E-01	9.986E-01	9.986E-01
0.65	9.997E-01	9.996E-01	9.996E-01	0.65	9.998E-01	9.998E-01	9.998E-01
0.70	9.999E-01	9.999E-01	9.999E-01	0.70	9.999E-01	9.999E-01	9.999E-01

Table 7.14: Numerical results and comparison for tension case

Normal distributions: $\sigma_{t,s} = 0.1\mu_{t,s}$				Log-normal distributions: $\sigma_{t,s} = 0.1\mu_{t,s}$			
μ_s / μ_t $\times 10^{-6} \frac{m}{kN}$	P_f (anal.)	P_f (FORM)	P_f (SORM)	μ_s / μ_t $\times 10^{-6} \frac{m}{kN}$	P_f (anal.)	P_f (FORM)	P_f (SORM)
0.05	1.414E-14	1.385E-14	1.383E-14	0.10	3.601E-09	4.715E-09	4.790E-09
0.06	6.153E-13	5.718E-13	5.752E-13	0.125	1.309E-05	1.427E-05	1.427E-05
0.07	2.102E-11	1.909E-11	1.913E-11	0.15	1.796E-03	1.729E-03	1.730E-03
0.08	5.525E-10	4.999E-10	5.000E-10	0.175	3.444E-02	3.421E-02	3.427E-02
0.09	1.105E-08	9.983E-09	9.991E-09	0.20	1.914E-01	1.866E-01	1.884E-01
0.10	1.674E-07	1.516E-07	1.530E-07	0.2262	5.000E-01	4.890E-01	4.869E-01
0.15	2.496E-03	2.312E-03	2.313E-03	0.25	7.609E-01	7.522E-01	7.522E-01
0.20	1.928E-01	1.854E-01	1.850E-01	0.275	9.169E-01	9.126E-01	9.126E-01
0.2262	5.000E-01	4.890E-01	4.882E-01	0.30	9.773E-01	9.758E-01	9.758E-01
0.25	7.599E-01	7.512E-01	7.512E-01	0.325	9.949E-01	9.945E-01	9.945E-01
0.30	9.753E-01	9.737E-01	9.737E-01	0.35	9.990E-01	9.989E-01	9.989E-01
0.35	9.985E-01	9.984E-01	9.984E-01	0.375	9.998E-01	9.998E-01	9.998E-01
0.40	9.999E-01	9.999E-01	9.999E-01	0.40	9.999E-01	9.999E-01	9.999E-01

The probabilities of failure P_f are presented in tables 7.11-7.14 for both distributions and in figures 7.4-7.5 for log-normal distributed variables. Numerical solutions of the limit analyses are compared with the analytical ones resulting from exact solutions. For each loading case, both random variables are normally or log-normally distributed with standard deviations $\sigma_{t,s} = 0.1\mu_{t,s}$. It is shown that our results compare well with the analytical ones for all cases.

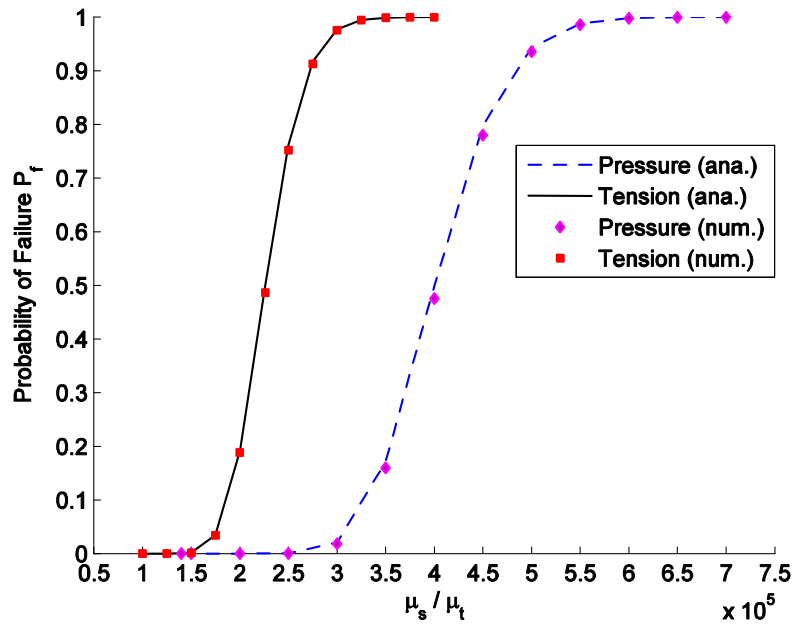


Figure 7.4 Comparison of the results for log-normally distributed variables

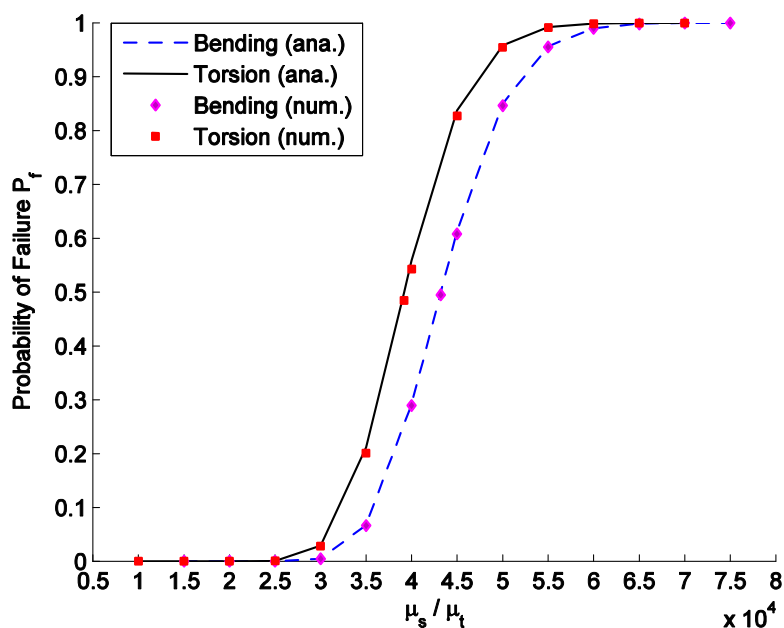


Figure 7.5 Comparison of the results for log-normally distributed variables

7.4 Folding shell subjected to horizontal and vertical loads

In this example, a well-known problem of having several failure modes is investigated. Consider the frame formed of three plates of figure 7.6a which is generated by prolonging a plane frame in the third direction. It is made of elastic-perfectly plastic material and subjected to two uniform horizontal and vertical loads H , V . The loading and geometrical data were selected to match those of the plane frame included in the book of Madsen et al. [1986]. Loads and limit plastic bending moment (material strength) are random variables which are assumed mutually independent and log-normally distributed. There are three basic variables and their mean values and standard deviations are given by

$$\text{Horizontal load } H \quad \mu_H = 50 \text{ kNm}, \sigma_H = 15 \text{ kNm}$$

$$\text{Vertical load } V \quad \mu_V = 40 \text{ kNm}, \sigma_V = 12 \text{ kNm}$$

$$\text{Material strength } \sigma_y \quad \mu_{\sigma_y} = 3372.5 \text{ kN/m}^2, \sigma_{\sigma_y} = 337.25 \text{ kN/m}^2$$

The thickness of the shell is supposed to be constant $h=0.4 \text{ m}$. The plastic moment capacity M_p at each section is then a random variable with mean value and standard deviation as follows

$$\mu_{M_p} = \frac{bh^2}{4} \mu_{\sigma_y} = 134.9 \text{ kNm}$$

$$\sigma_{M_p} = \frac{bh^2}{4} \sigma_{\sigma_y} = 13.49 \text{ kNm}$$

Hinge lines are thought to form at the end of elements (beam and columns) or at lines of load application. As in the original plane frame, three failure modes caused by plastic hinge mechanisms are expected to occur, those are sway mode, frame mode and beam mode (figure 7.7).

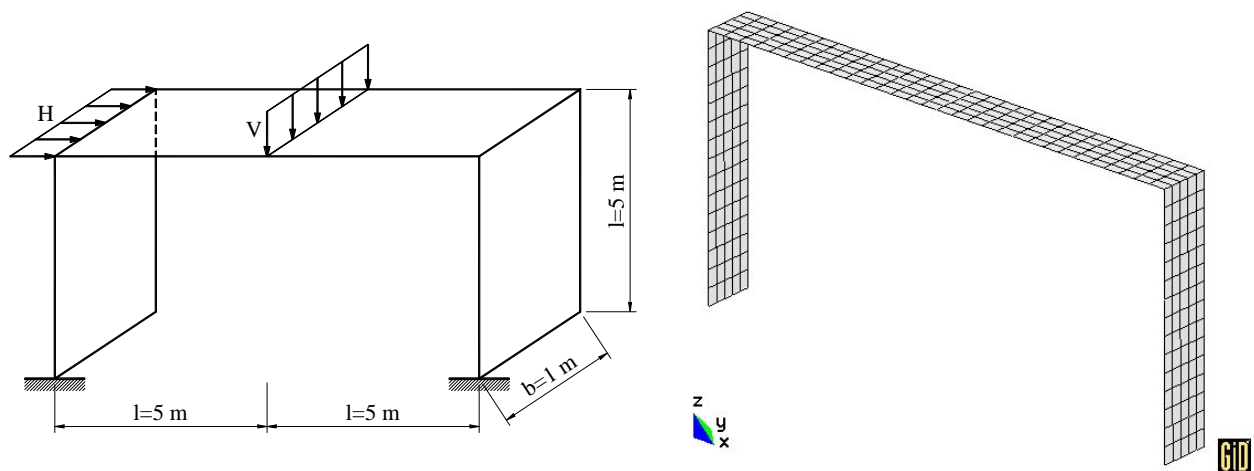


Figure 7.6 Geometrical dimensions and FE-mesh of the frame

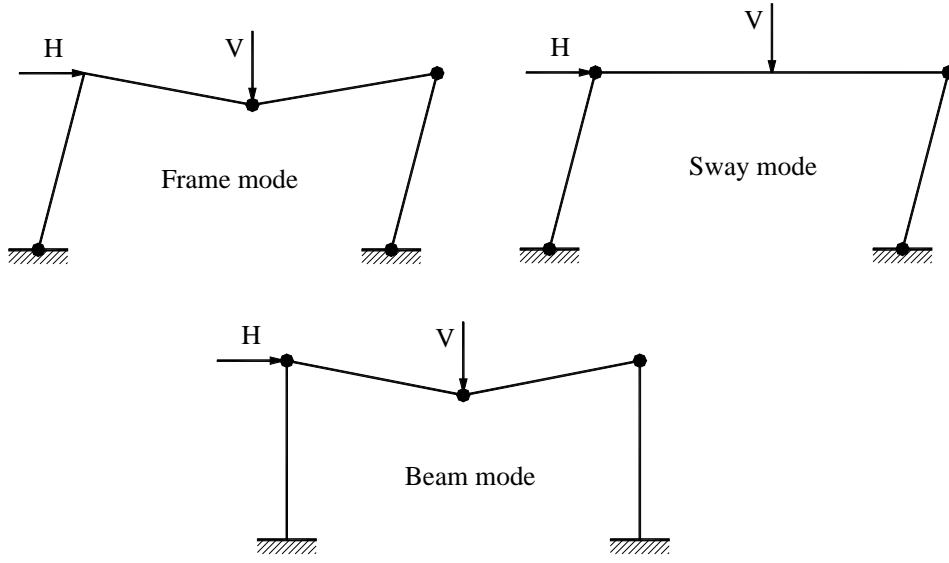


Figure 7.7 Three failure modes of the frame

Numerical computation is carried out by using 300 quadrangular flat 4-node shell elements as shown in figure 7.6b. The ‘barriers’ technique developed by Der Kiureghian and Dakessian is performed with $\gamma = 0.4$, $\delta = 0.3$ in order to find all the three design points as expected. Our numerical results of design points are presented in table 7.15. The global design point $\mathbf{u}_1^* = 3.083[0.944 \ 0.024 \ -0.329]^T$ with $\beta_{HL1} = 3.083$ was found firstly. This design point corresponds to the Sway mode since the effect of the horizontal load H is dominant. After adding a bulge $B_1(\mathbf{u})$ at \mathbf{u}_1^* , the algorithm converges to the second design point $\mathbf{u}_2^* = 3.24[0.776 \ 0.47 \ -0.422]^T$ with $\beta_{HL2} = 3.240$. This design point corresponds clearly to the Frame mode because both of loads have big contributions to the failure of the structure. We continuously added a bulge $B_2(\mathbf{u})$ at \mathbf{u}_2^* and found the third design point $\mathbf{u}_3^* = 3.461[0.457 \ 0.783 \ -0.421]^T$ with $\beta_{HL3} = 3.461$ which corresponds to the Beam mode. Now we suppose to proceed further and place a bulge $B_3(\mathbf{u})$ at \mathbf{u}_3^* . Our search algorithm now converges to $\mathbf{u}_4^* = 3.307[0.925 \ -0.325 \ -0.194]^T$ with $\beta_{HL4} = 3.307$. The distance $\|\mathbf{u}_4^* - \mathbf{u}_1^*\| = 1.218$ between the two design points is less than but close to the radius $r_1 = 0.4 \times 3.083 = 1.233$ of the bulge, thus confirming that \mathbf{u}_4^* is a spurious design point. If we further place a bulge $B_4(\mathbf{u})$ at \mathbf{u}_4^* and continue the algorithm, the point $\mathbf{u}_5^* = 4.07[0.667 \ 0.59 \ -0.454]^T$ with $\beta_{HL5} = 4.070$ is found. Obviously it is also a spurious design point since the distances $\|\mathbf{u}_5^* - \mathbf{u}_3^*\| = 1.24$ between the two design points \mathbf{u}_3^* , \mathbf{u}_5^* and $\|\mathbf{u}_5^* - \mathbf{u}_2^*\| = 1.028$ between the two design points \mathbf{u}_2^* , \mathbf{u}_5^* are less than the radius $r_3 = 0.4 \times 3.461 = 1.384$ and $r_2 = 0.4 \times 3.24 = 1.296$ of the bulges. Thus, at this stage, we stop

to search and assume that there are only three design points for this problem. It should be noted here that, the SQP algorithm worked well in this case to seek all the optimal points. Conversely, the simple gradient search algorithm failed after adding the first bulge. It oscillates around a foot of the bulge unstoppably.

Table 7.15: Multiple design points and search steps

Step	a_1	a_2	a_3	β_{HL}	Nature	Mode
1	0.944	0.024	-0.329	3.083	global design point	Sway mode
2	0.776	0.470	-0.422	3.240	local design point	Frame mode
3	0.457	0.783	-0.421	3.461	local design point	Beam mode
4	0.925	-0.325	-0.194	3.307	spurious design point	-
5	0.667	0.590	-0.454	4.070	spurious design point	-

The linear approximation of the failure set is now constructed by the tangent hyperplanes at the three design points. The corresponding approximations of failure mode correlations and joint failure mode probabilities are listed in table 7.16. The single and system failure probability and reliability indices are presented in table 7.17 and in table 7.18, respectively, compared with those of the original plane frame obtained by Madsen et al. It is shown that our two first failure probabilities of sway and frame modes are smaller than those of plane frame while the last one compares well with the solution of Madsen et al. leading to a smaller failure probability of the system. It is understandable since the stress state is now three-dimensional, not only the bending moment but also the compression force has an influence on the load-carrying capacity of the structure. By comparing the differences between present results and those of Madsen et al. in the tables 7.17 and 7.18, one can easily observe the sensitivity of the failure probability P_f as discussed previously. It is shown that about 10% difference in the reliability indices β_{HL} leads to about 330% difference in the failure probabilities P_f . This sensitivity even increases very fast in the case of small probabilities of failure.

Table 7.16: Failure mode correlations and joint failure mode probabilities (first order)

	Failure mode correlations ρ_{ij}			Joint failure probabilities $P_{ij} \times 10^2$		
	1	2	3	1	2	3
1	1.0	0.883	0.589	0.1023	0.0301	0.0037
2	0.883	1.0	0.899	0.0301	0.0598	0.0155
3	0.589	0.899	1.0	0.0037	0.0155	0.0269

Table 7.17: Failure probability of the frame ($P_f \times 10^2$)

Method	\mathbf{u}_1^* alone (sway)		\mathbf{u}_2^* alone (frame)		\mathbf{u}_3^* alone (beam)		\mathbf{u}_1^* , \mathbf{u}_2^* and \mathbf{u}_3^*
	FORM	SORM	FORM	SORM	FORM	SORM	
Present	0.1023	0.1026	0.0598	0.110	0.0269	0.0166	0.14-0.155
Madsen et al.	0.336	0.322	0.199	0.267	0.0291	0.0283	0.467

Table 7.18: Reliability indices of the frame β_{HL}

Method	\mathbf{u}_1^* alone (sway)		\mathbf{u}_2^* alone (frame)		\mathbf{u}_3^* alone (beam)		\mathbf{u}_1^* , \mathbf{u}_2^* and \mathbf{u}_3^*
	FORM	SORM	FORM	SORM	FORM	SORM	
Present	3.083	3.082	3.240	3.062	3.461	3.589	2.958-2.989
Madsen et al.	2.710	2.725	2.880	2.786	3.440	3.447	2.600

8 SUMMARY

Integrity assessment of pressure vessels and piping by means of direct plasticity methods has been a problem of great interest to many designers, especially in the design of industrial and nuclear power plants. The new European pressure vessel standard EN 13445-3 is based on perfectly plastic limit and shakedown analysis (LISA) [European standard, 2005-06] thus indicating the industrial need for LISA software for safe and reliable design of such structures. Additionally, practical design codes often prescribe what kind of values to choose for the safety factor of the resistance and of the loads for a given problem since all resistance and loading variables are generally random. To this purpose, the present thesis provides an effectively plastic analysis method for the integrity assessment of general shells. Besides a deterministic LISA algorithm, structural reliability analysis based on probabilistic LISA is also performed to establish a rational basis for the choice of safety factors.

In the deterministic LISA procedure three failure modes of structures such as plastic collapse, low cycle fatigue and ratchetting are analyzed based upon an upper bound approach. The direct method involves the use of the exact Ilyushin yield surface and the solution of the non-linear constraint optimization problems is solved by Newton's method in conjunction with a penalty method and the Lagrange dual method. Line search is performed to improve the current kinematic solution. A special "smooth regularization method" was also used for overcoming the non-differentiability of the objective function. The actual Newton directions are updated at each iteration by solving a purely-elastic-like system of linear equations which ensures automatically the kinematical condition of the displacements.

The proposed method appears to be capable of identifying reasonable estimates of the limit and shakedown load factors for a wide range of thin shell problems. It has been tested against experiments and several load limits which have been calculated in literature with different numerical methods using shell or volume elements. The load limits are obtained here together with tests of mesh convergence and robustness. Some of them could be checked against twice the elastic limit because they appear to represent the alternating plasticity limit under the considered loading conditions. A numerically very effective method is achieved from the lesser computational cost by using shell elements compared with volume elements and by direct plasticity methods which achieve plastic solutions in the computing time of only several linear elastic steps. Parametric studies carried out in

some examples show that different choices of optimization parameters have quite different effects on the behaviour of the algorithm.

In the probabilistic LISA, the loading and strength of the material as well as the thickness of the shell are considered as random variables. The procedure involves a deterministic limit and shakedown analysis for each probabilistic iteration. Different kinds of distribution of basic variables are taken into consideration and performed with FORM/SORM for the calculation of the failure probability of the structure. A non-linear optimization was implemented, which is based on the Sequential Quadratic Programming for finding the design point. Non-linear sensitivity analyses are also performed for computing the Jacobian and the Hessian of the limit state function.

The advantage of the method in structural reliability analysis is that the failure under cyclic loading is treated as a time-invariant problem and it is applicable with incomplete data. On the other hand, sensitivity analyses are obtained directly from a mathematical optimization with no extra computational cost. Numerical examples were tested against literature with analytical methods and with a numerical method using volume elements. It is shown that the proposed method is capable of identifying good estimates of the failure probability, even in the case of very small probabilities. The results are achieved just after several deterministic steps even if the starting points are chosen far from the actual design point. If the limit state function is linear with the limit and shakedown analysis, then the use of FORM is sufficient and SORM is only necessary if the linearity is lost after the transformation into the \mathbf{u} space.

Practical experience showed that the existence of multimode failure (multiple design points) in component reliability analysis could give rise to large errors in FORM/SORM approximations of the failure probability. In this thesis, a technique which was developed by [Der Kiureghian and Dakessian, 1998] has been performed to successively find the multiple design points of a reliability problem, when they exist on the limit state surface. This technique is based upon a ‘barrier’ method by constructing a bulge around previous found design points, thus forcing the algorithm to seek a new design point. Second-order bounds of the reliability of series system are then calculated based on the first-order system reliability analysis. Numerical example of a frame made of plates showed that it improves considerably the estimates of the system failure probability.

To the author’s knowledge the above mentioned results contain the following new contributions which have never been published elsewhere:

- The development of a kinematic algorithm of deterministic limit and shakedown analysis for general plate and shell structures using the exact Ilyushin yield surface. The exact Ilyushin yield surface has not been used so far in LISA.
- The development of a kinematic algorithm of probabilistic limit and shakedown analysis for general plate and shell structures using the First and Second Order Reliability Methods. The present thesis is the first one dealing with reliability-based LISA for shells and using SORM.

- The introduction and formulation of the probabilistic LISA in which the thickness is considered as a random variable. Analytical solutions for a simple problem were derived in order to compare with the numerical solutions.
- The sensitivity analysis of the limit state function versus load, material strength and shell thickness variables.
- The introduction and formulation of the reliability problem for the structural systems (series systems). The implementation of a special technique to successively find all the multiple design points on the limit state surface allows to calculate the second-order bounds of the reliability for series systems.

It should be noted that in the present work we accepted some simplified hypotheses, such as perfectly plastic material, small deformation and displacement models. The perfectly plastic material is sufficient with respect to the design codes. However, the present results may be safe to be applied in some practical engineering since some practical materials often exhibit strain hardening. In this meaning limit and shakedown analysis based on the kinematic hardening may improve the present design procedures. On the other hand, the geometrically non-linear effects may become important to very thin-walled structures. On this basis, we would propose here some possibilities for future work:

- Extend the present work for both deterministic and probabilistic LISA to the real materials in which we take into account the bounded kinematic hardening of the material.
- Extend the present work for both deterministic and probabilistic LISA to the real behaviour of thin shell structures in which we consider the large deformation and large displacement hypotheses.
- Perform the deterministic and probabilistic LISA by the application of the primal-dual theory, in which both lower and upper bounds are obtained at each iteration.
- Extend the present work for probabilistic LISA to the real shell structures in which the thickness of the shell is considered a random field, i.e. the random thickness is a function in space. In a similar way temperature fields and temperature dependent material strength can be considered.

REFERENCES

- Abdalla H. F., Megahed M. M. and Younan M. Y. A. (2006). Determination of Shakedown Limit Load for a 90-Degree Pipe Bend Using a Simplified Technique. *ASME J. Pressure Vessel Technol.*, **128** (4), pp. 618-624.
- Andersen K. D. and Christiansen E. (1995). *A Newton barrier method for minimizing a sum of Euclidean norms subject to linear equality constraints*. IMADA preprint PP-1995-07. Department of Mathematics and Computer Science at SDU, Odense University, Denmark.
- Andersen K. D. and Christiansen E. (1998a). Minimizing a sum of norms subject to linear equality constraints. *Comput. Optim. Appl.*, **11**, pp. 65-79.
- Andersen K. D., Christiansen E. M. and Overton, L. (1998b). Computing limit loads by minimizing a sum of norms. *SIAM J. Sci. Comput.* **19**, pp. 1046-1062.
- Andersen K. D., Christiansen E., Conn A. R., Overton M. L. (2000). An efficient primal-dual interior-point method for minimizing a sum of Euclidean norms. *SIAM J. Sci. Comput.*, **22**, pp. 243-262.
- Augusti G., Baratta A., Casciati F. (1984). *Probabilistic Method in Structural Engineering*. Chapman and Hall, London.
- Bauer H., Saal H. (1997). *Nozzles in the knuckle region of pressure vessels heads – strength and stiffness under various loading conditions*. In Proc. Int. Conf. Carrying capacity of steel shell structures, Brno, pp. 138-144.
- Bazaraa M. S., Sherali H. D., Shetty C. M. (1993). *Nonlinear programming Theory and Algorithms*. John Wiley & Sons, Inc., New York.
- Bisbos C. D. and Papaioannou G. (2006). *Shakedown analysis of FEM-discretized steel shell structures under the Ilyushin yield criterion*. In Baniotopoulos C. C. (ed.): II. Int. Conference on Nonsmooth Nonconvex Mechanics with Applications in Engineering (II. NNMAE), Thessaloniki, Juli 7-8, pp. 197-204.
- Bisbos C. D., Pardalos P. M. (2007). Second-order cone and semidefinite representations of material failure criteria. *Journal of Optimization Theory and Applications*, **134** (2), pp. 275-301. <http://dx.doi.org/10.1007/s10957-007-9243-8>
- Bjerager P. (1989). Plastic systems reliability by LP and FORM. *Computers and Structures*, **31**, pp. 187-196.
- Bjerager P. (1991). *Methods for structural reliability computations*. In Course on Reliability Problems: General Principles and Applications of Solids and Structures, International Center for Mechanical Sciences, Udine, Italy, 1990. CISM lecture notes, Springer, Wien.
- Bleich H. (1932). Über die Bemessung statisch unbestimmter Stahlwerke unter der Berücksichtigung des elastisch-plastischen Verhaltens des Baustoffes. *Bauingenieur*, **13**, pp. 261-267.
- Bolt S. E. and Greenstreet W. L. (1971). *Experimental determination of plastic collapse loads for pipe elbows*. ASME paper 71-PVP-37.

- Borkowski A. and Kleiber M. (1980). On a numerical approach to shakedown analysis of structures. *Computer methods in applied mechanics and engineering*, **22**, pp. 110-119.
- Bree J (1967). Elastic-plastic behaviour of thin tubes subjected to internal pressure and intermittent high-heat fluxes with applications to fast-nuclear-reactor fuel elements. *Journal of Strain Analysis*, **2**, pp. 226-238.
- Bridgman P. W. (1923), The compressibility of thirty metals as a function of pressure and temperature. *Proc. Am. Acad. Arts Sci.*, **58**, pp. 163-242.
- Bridgman P. W. (1952). *Studies in Large Plastic Flow and Fracture*. McGraw-Hill, New York.
- Burgoyne C. J. and Brennan M. G. (1993a). Calculation of elasto-plastic rigidities using the exact Ilyushin yield surface. *Int. J. Sol. Struct.*, **30** (8), pp. 1133-1145.
- Burgoyne C. J. and Brennan M. G. (1993b). Exact Ilyushin yield surface. *Int. J. Sol. Struct.*, **30** (8), pp. 1113-1131.
- Calladine C. R. (1974). Limit analysis of curved tubes. *J. Mech. Eng. Science*, **16**, pp. 85-87.
- Capsoni A. and Corradi L. (1997). A finite element formulation of the rigid-plastic limit analysis problem. *Int. J. Num. Meth. Eng.*, **40**, pp. 2063-2086.
- Carvelli V., Cen Z. Z., Liu Y., Maier G. (1999). Shakedown analysis of defective pressure vessels by a kinematic approach. *Archive of Applied Mechanics*, **69**, pp. 751-764.
- Casciaro R. and Cascini L. (1982). A mixed formulation and mixed finite elements for limit analysis. *Int. J. Num. Meth. in Eng.*, **18**, pp. 211-243.
- Chapelle D., Bathe K. J. (2003). *The finite element analysis of shells – fundamentals*. Berlin: Springer.
- Chattopadhyay J., Venkatramana W., Dutta B. K. and Kushwaha H.S. (1999). *Limit Load of Elbows Under Combined Internal Pressure and Bending Moment*. Proceedings of the 15th International Conference on Structural Mechanics in Reactor Technology, SMiRT, Vol. V, Korea, pp. 281-288.
- Chattopadhyay J., Nathani D. K., Dutta B. K. and Kushwaha H. S. (2000). Closed-Form collapse moment equations of Elbows under combined internal pressure and in-plane bending moment. *ASME J. Pressure Vessel Technol.*, **122**, pp. 431-436.
- Clark R. A. and Reissner E. (1951). Bending of curved tubes. *Advances in Applied Mechanics*, **2**, pp. 93-122.
- Cocks A. C. F. and Leckie F. A. (1988). Deformation bounds for cyclically loaded shell structures operating under creep condition. *Journal of Applied Mechanics, Transactions of the ASME*, **55**, pp. 509-516.
- Code_Aster 7.3 (2003). *User's manual*. A product of EDF R&D, Clamart, France. <http://www.code-aster.org>
- Cornell C. A. (1967). Bounds on the Reliability of structural systems. *Journal of the Structural Division, ASCE*, **93**, ST1, Feb., pp. 171-200.
- Crisfield M. A. (1973). *Large deflection elasto-plastic buckling analysis of plates using finite elements*. Transport and Road Research Lab. Report 51UC.
- Der Kiureghian A., Dakessian T. (1998). Multiple design points in first and second-order reliability. *Structural Safety*, **20**, pp. 37-49.
- Desquines J., Plancq D. and Wielgosz C. (1997). In-plane limit moment for an elbow lower bound analytical solution and finite element processing by elastic compensation method. *Int. J. Pres. Ves. & Piping*, **71**, pp. 29-34.

- Diem H. (1994). *Untersuchungen zum Geometrieinfluß auf das Verformungs- und Versagensverhalten von Rohrbogen*. Dissertation, Universität Stuttgart.
- Ditlevsen O. (1979). Narrow reliability bounds for structural systems. *Journal of Structural Mechanics*, **7** (4), pp. 453-472.
- Ditlevsen O. and Bjerager P. (1986). Methods of structural system reliability. *Structural Safety*, **3**, pp. 195-229.
- Dronia S. (2005). *Sequentielle Quadratische Programmierung für effektive Zuverlässigkeitsanalyse mit der Finite Element Methode*. Diplomarbeit, Labor für Biomechanik, Fachhochschule Aachen Campus Jülich, Germany.
- Drubay B., et al. (1995). *A16: Guide for Defect Assessment and Leak-Before-Break Analysis*. Third Draft, Commissariat A L'energie Atomique, Rapport DMT 96.096, France.
- Dunny C. W., Sobel M. (1955). Approximations to the probability integral and certain percentage points of multivariate analogue of Student's t-distribution. *Biometrika*, **42**, pp. 258-260.
- European Standard (2005-06). *Unfired pressure vessels - Part 3: Design, Annex 2: Annex B Direct route for design by analysis and Annex C Stress categorisation route for design by analysis*. CEN European Committee for Standardization, EN 13445-3:2002, Issue 14.
- Fanous I. F. Z., Adibi-Asl R. and Seshadri R. (2005). Limit load analysis of pipe bends using the R-node method. *ASME J. Pressure Vessel Technol.*, **127**, pp. 443-448.
- Fiacco A. (1983). *Introduction to Sensitivity and Stability Analysis in Nonlinear Programming*. Academic Press, New York.
- Fiessler B., Neumann H. J., Rackwitz R. (1979). Quadratic Limit States in Structural Reliability Theory. *ASCE, Journal of Engineering Mechanics*, **105**, pp. 661-676.
- Franco J. R. Q., Ponter A. R. S. (1997.a). A general approximate technique for the finite element shakedown and limit analysis of axisymmetrical shells. Part 1: Theory and fundamental relations. *Int. J. for Num. Meth. in Engng.*, **40** (19) pp. 3495-3513.
- Franco J. R. Q., Ponter A. R. S. (1997.b). A general approximate technique for the finite element shakedown and limit analysis of axisymmetrical shells. Part 2: Numerical applications. *Int. J. for Num. Meth. in Engng.*, **40** (19) pp. 3515-3536.
- Frieze P. A. (1975). *Ultimate load behaviour of steel box girders and their components*. PhD Thesis, University of London.
- Gaydon F. A., McCrum A. W. (1954). A theoretical investigation of the yield point loading of a square plate with a central circular hole. *Journal of the Mechanics and Physics of Solids*, **2**, pp. 156-169.
- GiD 7.2 (2002). *User's manual*. A product of Center for Numerical Methods in Engineering (CIMNE), Barcelona. <http://www.gid.cimne.upc.es>
- Gollwitzer S., Abdo T., Rackwitz R. (1988). *FORM Manual*. RCP GmbH, München.
- Gokhfeld D. A. and Cherniavsky O. F. (1980). *Limit analysis of structures at thermal cycling*. Sijthoff & Noordhoff, The Netherlands.
- Goodall I. M. (1978a). *Large deformations in plastically deformed curved tubes subjected to in-plane bending*. Research Division Report CEGB-RD/B/N4312, Central electricity generating board, UK.

- Goodall I. W. (1978b). *Lower Bound Limit Analysis of Curved Tubes Loaded by Combined Internal Pressure and In-plane Bending Moment*. Research Division Report RD/B/N4360, Central electricity generating board, UK.
- Gorman M. R. (1981). Automatic generation of collapse mode equations. *J. Struct. Div., ASCE*, Vol. **107**, No. ST7, July, pp. 1350-1354.
- Griffiths J. E. (1979). The effect of cracks on the limit load of pipe bends under in-plane bending experimental study. *Int. J. Sci.*, **21**, pp. 119-130.
- Grimmelt M. J., Schuëller G. I. (1982). Benchmark Study on methods to determine collapse failure probabilities of redundant structures. *Structural Safety*, **1**, pp. 93-106.
- Hasofer A. M., Lind N. C. (1974). An exact and Invariant First Order Reliability Format. *ASCE, Journal of Engineering Mechanics Division*, Vol. **100**, No. EM1, pp. 111-121.
- Heitzer M. (1999). *Traglast- und Einspielanalyse zur Bewertung der Sicherheit passiver Komponenten*. Berichte des Forschungszentrums Jülich, Jül-3704, Dr.-Ing. Thesis, RWTH Aachen.
- Heitzer M. and Staat M. (1999). FEM-computation of load carrying capacity of highly loaded passive components by direct methods. *Nuclear Engineering and Design*, **193** (3), pp. 349-358. [http://dx.doi.org/10.1016/S0029-5493\(99\)00190-9](http://dx.doi.org/10.1016/S0029-5493(99)00190-9)
- Heitzer M., Staat M. (2000). Reliability Analysis of Elasto-Plastic Structures under Variable Loads. In: *Inelastic Analysis of Structures under Variable Loads: Theory and Engineering Applications* (edited by Weichert D., Maier G.) Kluwer, Academic Press, Dordrecht, pp. 269-288.
- Heitzer M., Staat M. (2002). Limit and Shakedown Analysis with Uncertain Data. In: *Stochastic Optimization Techniques, Numerical Methods and Technical Applications* (edited by Marti K.), Lecture Notes in Economics and Mathematical Systems, Vol. **513**, Springer Heidelberg, pp. 253-267.
- Hilsenkopf P. et al. (1988). Experimental Study of Behavior and Functional Capability of Ferritic Steel Elbows and Austenitic Stainless Steel Thin-Walled Elbows. *Int. J. Pres. Vessels and Piping*, **33** (2), pp. 111-128.
- Hodge P. G. Jr. (1954). The Rigid-plastic analysis of symmetrically loaded cylindrical shells. *J. App. Mech.*, **21**, pp. 336-442.
- Hodge P. G. Jr. (1959). *Plastic analysis of structures*. McGraw-Hill, New York.
- Hodge P. G. Jr. (1961). The Mises yield condition for rotationally symmetric shells. *Quarterly of Applied Mathematics*, Vol. **XVIII**, No. 4, 305-311.
- Hodge P. G. Jr. (1963). *Limit analysis of rotationally symmetric plates and shells*. Prentice Hall, Englewood, New Jersey.
- Hohenbichler M. (1981). *Approximate evaluation of the multinormal distribution function*. Berichte zur Zuverlässigkeitstheorie der Bauwerke, Tech. Univ. München, Heft **58**.
- Hohenbichler M., Rackwitz R. (1983). First-order concepts in system reliability. *Structural Safety*, **1**, pp. 177-188.
- Hohenbichler M., Gollwitzer S., Kruse W., Rackwitz R. (1987). New light on first- and second-order reliability methods. *Structural Safety*, **4**, pp. 267-284.

- Hsieh M. F., Moffat D. G., Mistry J. (2000). Nozzles in the knuckle region of a torispherical head: limit load interaction under combined pressure and piping loads. *Int. J. Pres. Vessels and Piping*, **77**, pp. 807-815.
- Ilyushin A. A. (1948). *Plasticity*. Gostekhizdat, Moscow. In Russian.
- Ivanov G. V. (1967). Approximating the final relationship between the forces and moments of shell under the Mises plasticity condition. *Inzhenernyi Zhurnal Mekhanika Tverdogo Tela*, **6**, pp. 74-75. In Russian.
- Jospin R. J. (1992). *Etats limites des tuyauteries par la méthode des éléments finis et la programmation mathématique*. Thèse de doctorat, Université de Liège.
- Kalisky S. (1985). *Plasticity, Theory and Engineering Applications*. Elsevier, Amsterdam.
- Klingmüller O. (1979). *Anwendung der Traglastberechnung für die Beurteilung der Sicherheit von Konstruktionen*. Thesis Forschungsberichte aus dem Fachbereich Bauwesen **9**, Universität Essen Gesamthochschule.
- Koiter W. T. (1960). General theorems for elastic plastic solids. In: *Progress in Solid Mechanics* (edited by Sneddon I. N. and Hill R.), pp. 165-221, Nord-Holland, Amsterdam.
- König J. A. (1966). Theory of shakedown of elastic-plastic structures. *Arch. Mech. Stos.*, **18**, pp. 227-238.
- König J. A. (1969). A shakedown theorem for temperature dependent elastic moduli. *Bull. Acad. Pol. Sci., Sér. Sci. Techn.*, Vol. **17**, pp. 161-165.
- König J. A. (1972). *On shakedown criterion*. Proc. Int. Symp. Foundations of Plasticity, Vol. **2**, pp. 56-60, Warsaw.
- König J. A., Kleiber M. (1978). On a new method of shakedown analysis. *Bull. Acad. Pol. Sci., Sér. Sci. Techn.*, **4**, pp. 165-171.
- König J. A. (1987). *Shakedown of elastic-plastic structures*. Elsevier, New York.
- Kussmaul K., Diem H. K., Uhlmann D. and Kobes H. (1995). *Pipe Bend Behaviour at Load Levels Beyond Design*. Proceedings of 13th International Conference on Structural Mechanics in Reactor Technology, SMiRT. Brazil. Vol. **G**., pp. 187-198.
- Larson L.D., Stokey W.F. and Franzen W.E. (1975). An approximate Model for an elastic-plastic pipe element under combined loading. *Journal of Pressure Vessel Technology, Transaction of the ASME*, **97**, pp. 22-28.
- Little G. H. (1977). Rapid analysis of plate collapse by live energy minimization. *Int. J. Mech. Sci.*, **19**, pp. 725-744.
- Liu Y. H., Carvelli V., Maier G. (1997). Integrity assessment of defective pressurized pipelines by direct simplified methods. *Int. J. Pres. Ves. & Piping*, **74**, pp. 49-57.
- Locci J. M. (1995). *Automatization of limit analysis calculations, application to structural reliability problems*. In: Proceedings of the ICASP7 conference, Paris (edited by Lemaire M., Favre J. L., Mébarki A.), Vol. **2**: Applications of Statistics and Probability. A. A. Balkema Rotterdam, Brookfield, pp. 1095-1110.
- Lubliner J. (2005). *Plasticity Theory*. Revised edition, University of California at Berkeley.
- Madsen H.O., Krenk S., Lind N.C. (1986). *Methods of Structural Safety*. Prentice-Hall, Englewood Cliffs.
- Maier G. (1969). Shakedown theory in perfect elastoplasticity with associated flow-laws. *Meccanica*, **4**, pp. 250-260.

- Maier G. (1970). A matrix structural theory of piecewise-linear plasticity with interacting yield planes. *Meccanica*, **7**, pp. 51-66.
- Maier G. (1973). A shakedown matrix theory allowing for work hardening and second-order geometric effects. In: *Foundations of plasticity* (edited by Sawczuk A.), North-Holland, Amsterdam, pp. 417-433.
- Martin J. B. (1975). *Plasticity*. MIT Press, Cambridge.
- Melan E. (1936). Theorie statisch unbestimmter Systeme aus ideal plastischem Baustoff. *Sitzber. Akad. Wiss. Wien IIa* **145**, pp. 195-218.
- Melchers R. E. (1987). *Structural Reliability – Analysis and Prediction*. Ellis Horwood limited, Chichester.
- Morelle P. (1984). Structural shakedown analysis by dual finite-element formulations. *Eng. Struct.*, **6** (1), pp. 70-79.
- Morelle P. (1989). *Analyse duale de l'adaptation plastique des structures par la méthode des éléments finis et la programmation mathématique*. Thèse de Doctorat, Université de Liège, Belgique.
- Mourad H. M. and Younan M. Y. A. (2002). Limit load analysis of pipe bends under out-of-plane moment loading and internal pressure. *ASME J. Pressure Vessel Technol.*, **124**, pp. 32–37.
- Moxham K. E. (1971). *Theoretical prediction of the strength of welded steel plates in compression*. Cambridge University Report No CUED/C-Struct/TR2.
- Nguyen Dang H., König J. A. (1976). A finite element formulation for shakedown problems using a yield criterion of the mean. *Comp. Meth. Appl. Mech. Eng.*, **8**, 179-192.
- Nguyen Dang H., Morelle P. (1990). Plastic shakedown analysis. In: *Mathematical programming methods in structural plasticity*. (edited by Smith, D. L.), pp. 183-205.
- Nguyen Dang H., Tran T. N. (2004). Analysis of cracked plates and shells using “metis” finite element model. *Finite Element in Analysis and Design*, Vol. **40** (8), pp. 855-878. [http://dx.doi.org/10.1016/S0168-874X\(03\)00117-3](http://dx.doi.org/10.1016/S0168-874X(03)00117-3).
- Panagiotopoulos P. D. (1985). *Inequality problems in Mechanics and Applications, Convex and Nonconvex Energy Functions*. Birkhäuser, Boston.
- Polizzotto C., Borino G., Caddemi S., Fuschi P. (1991). Shakedown problems for material with internal variables. *Eur. J. Mech. A/Solids*, **10**, (6), pp. 621-639.
- Polizzotto C. (1993.a). On the condition to prevent plastic shakedown of structures: Part I – Theory. *J. Appl. Mech. ASME*, **60**, pp. 15-19.
- Polizzotto C. (1993.b). On the condition to prevent plastic shakedown of structures: Part II – The plastic shakedown limit load. *J. Appl. Mech. ASME*, **60**, pp. 20-25.
- Ponter A. R. S., Carter K. F. (1997.a). Shakedown state simulation techniques based on linear elastic solution. *Comput. Methods Appl. Mech. Engrg.*, **140**, pp. 259-279.
- Ponter A. R. S., Carter K. F. (1997.b). *The calculation of limit load and shakedown boundaries by effective modulus method*. Transactions of the 14th International Conference on Structural Mechanics in Reactor Technology (SmiRT 14), Lyon, France, August 17-22.
- Ponter A. R. S., Fuschi P., Engelhardt M. (2000). Shakedown limits for a general yield condition: implementation and application for a Von Mises yield condition. *European Journal of Mechanics - A/Solids*, **19** (3), pp. 423-445.

- Powell M. J. D. (1978). Algorithms for Nonlinear Constraints that Use Lagrangian Functions. *Mathematical Programming*, **14**, pp. 224-248.
- Prager W., Hodge P.G.Jr. (1951). *Theory of perfectly plastic solids*. Wiley, New York.
- Prager W. (1959). *Probleme der Plastizitätstheorie*. Birkhäuser, Basel 1955; English edition: *Introduction to plasticity*, Addison-Wesley, Boston.
- Prager W. (1972). Limit analysis: The development of a concept. In: *Foundation of plasticity 2* (edited by Sawczuk A.), Noordhoff, Groningen.
- Preiss R. (2000). *Ratcheting and shakedown analysis of pressure equipment using elasto-plastic Finite-Element-Analysis*. PhD Thesis, TU Wien.
- Rackwitz R. (1978). *Close bounds for the reliability of structural systems*. Berichte zur Zuverlässigkeitstheorie der Bauwerke, Tech. Univ. München, Heft **29**.
- Rackwitz R. (1993-2004). *Zuverlässigkeit und Lasten im konstruktiven Ingenieurbau*. Lecture Notes, Technische Universität München.
- Rahman S.M. (2006). *Finite element analysis and related numerical schemes for ratchetting simulation*. Dissertation, North Carolina State University, Raleigh.
- Ramachandran K. (1984). Systems Bounds: A critical study. *Civil Engineering Systems*, **1**, March, pp. 123-128.
- Rashedi M. R., Moses F. (1983). *Studies on reliability of structural systems*. Report No. R83-3, Department of Civil Engineering, Case Western Reserve University, Cleveland, Ohio.
- Robinson M. (1971). A comparison of yield surfaces for thin shells. *Int. J. Mech. Sci.*, **13**, pp. 345-354.
- Sawczuk A. (1969a). On incremental collapse of shells under cyclic loading. In: *Theory of the Thin Shells* (edited by Niordson F. I.), Springer-Verlag, Berlin, pp. 328-340.
- Sawczuk A. (1969b). Evaluation of upper bounds to shakedown loads for shells. *J. Mech. Phys. Solids*, **17**, pp. 291-301.
- Schittkowski K. (1983a). Theory, implementation and test of a nonlinear programming algorithm. In: *Optimization Methods in Structural Design* (edited by Eschenauer H., Olho N.), BI Wissenschaftsverlag, Mannheim.
- Schittkowski K. (1983b). On the convergence of a sequential quadratic programming method with an augmented Lagrangian search direction. *Optimization*, **14**, pp. 197-216.
- Schittkowski K. (1988). Solving nonlinear least squares problems by a general purpose SQP-method. In: *Trends in Mathematical Optimization* (edited by Hoffmann K.-H., Hiriart-Urruty J.-B., Lemarechal C., Zowe J.), International Series of Numerical Mathematics, Vol. **84**, Birkhäuser, pp. 295-309.
- Schittkowski K. (2004). *NLPQLP20: A Fortran implementation of a sequential quadratic programming algorithm with distributed and non-monotone line search - user's guide*. Report, Department of Computer Science, University of Bayreuth.
- Seitzberger M. (2000). *Contributions to an Efficient Numerical Analysis of the Plastic Behaviour of Thin-Walled Structures*. Fortschritt-Berichte VDI, Reihe 18, Nr. 247, VDI-Verlag, Düsseldorf.
- Shalaby M. A. and Younan M. Y. A. (1998a). Limit loads for pipe elbows with internal pressure under in-plane closing bending moment. *ASME J. Pressure Vessel Technol.*, **120**, pp. 35-42.

- Shalaby M. A. and Younan M. Y. A. (1998b). *Limit Loads for Pipe Elbows Subjected to In-plane Opening Moment and Internal Pressure*. Paper Presented at the 1998 ASME/JSME Joint Pressure Vessels and Piping Conference held at San Diego, California, July 26-30, PVP Vol. **368**, 1998, pp. 163-170.
- Siemaszko A., Bielawski G., Knabel J. (2001). *Shakedown and limit reliability-based design*. Transactions SMiRT-16 Structural Mechanics in Reactor Technology, Washington, DC USA, August 12-17.
- Spence J. and Findlay G. E. (1973). *Limit loads for pipe bends under in-plane bending*. Proc. 2nd Int. Conf. on Pressure Vessel Technology, ASME Vol. **1**, pp. 393-399.
- Staat M., Heitzer M. (1997). *Limit and shakedown analysis for plastic safety of complex structures*. Transactions of the 14th International Conference on Structural Mechanics in Reactor Technology (SMiRT 14), Lyon, France, August 17-22. <http://www.iasmirt.org/SMiRT14/B02-2>
- Staat M., Heitzer M. (2001). LISA – a European project for FEM-based limit and shakedown analysis. *Nuclear Engineering and Design*, **206** (2-3), pp. 151-166. [http://dx.doi.org/10.1016/S0029-5493\(00\)00415-5](http://dx.doi.org/10.1016/S0029-5493(00)00415-5)
- Staat M. (2002). Some Achievements of the European Project LISA for FEM Based Limit and Shakedown Analysis. In N. Badie (ed.) *Computational Mechanics: Developments and Applications - 2002*. ASME PVP Vol. **441**, Paper PVP2002-1300, pp.177-185.
- Staat M., Heitzer M. (2002). *The restricted influence of kinematic hardening on shakedown loads*. Proceedings of WCCM V, 5th World Congress on Computational Mechanics, Vienna, Austria, July 7-12. <http://opus.bibliothek.fh-aachen.de/opus/volltexte/2005/79/>
- Staat M. and Heitzer M. (ed.) (2003a). *Numerical Methods for Limit and Shakedown analysis – Deterministic and Probabilistic Problems*. NIC Series Vol. 15, John von Neumann Institute for Computing, Jülich. <http://www.fz-juelich.de/nic-series/volume15/nic-series-band15.pdf>
- Staat M. and Heitzer M. (2003b). Probabilistic limit and shakedown problems. In [Staat and Heitzer (2003a)].
- Staat M., Heitzer M., Lang H., Wirtz K. (2005). Direct Finite Element Route for Design-by-Analysis of Pressure Components. *Int. J. Pressure Vessels Piping*, **82** (1), pp. 61-67. <http://dx.doi.org/10.1016/j.ijpvp.2004.04.006>
- Taylor N. et al. (1999). *The design-by-analysis manual*. Report EUR 19020 EN, European Commission, Joint Research Centre, Petten, The Netherlands. For error corrections and remarks see: http://info.tuwien.ac.at/IAA/news/dba1_engl.htm
- Thoft-Christensen P. and Baker M. J. (1982). *Structural reliability theory and its applications*. Springer-Verlag, Berlin.
- Touboul F., et al. (1989). *Design Criteria for Piping Components Against Plastic Collapse: Application to Pipe Bend Experiments*. Proceedings of 6th International Conference of Pressure Vessel Technology, Beijing, China, September 11-15, eds., Cengdian, Liu, and Nichols, pp. 73-84.
- Tran T. N., Staat M., Kreißig R. (2007a). *Calculation of load carrying capacity of shell structures with elasto-plastic material by direct methods*. Proceedings of the International Conference on Material Theory and Nonlinear Dynamics, Hanoi, Vietnam, September 24-26. <http://opus.bibliothek.fh-aachen.de/opus/volltexte/2007/227/>.
- Tran T. N., Staat M., Kreißig R. (2007b). *Finite element shakedown and limit reliability analysis of thin shells*. Proceedings of 9th International conference on computational plasticity, COMPLAS IX, Barcelona, Spain, September 05-07, eds., Oñate E. and Owen D. R. J. <http://opus.bibliothek.fh-aachen.de/opus/volltexte/2007/233/>

- Tran T. N., Kreißig R., Vu D. K., Staat M. (2007c). Upper bound limit and shakedown analysis of thin shells using the exact Ilyushin yield surface. *Computer & Structures*, in press.
<http://dx.doi.org/10.1016/j.compstruc.2008.02.005>
- Tran T. N., Kreißig R., Staat M. (2007d). Probabilistic limit and shakedown analysis of thin plates and shells. *Structural Safety*, in press. <http://dx.doi.org/10.1016/j.strusafe.2007.10.003>.
- Tran T. N., Kreißig R., Staat M. (2007e). Load bearing capacity of thin shell structures with elasto-plastic material by direct methods. *Technische Mechanik*, in press.
- Tran T. N., Pham P. T., Vu D. K., Staat M. (2008). Reliability analysis of inelastic shell structures under variable loads. In: A.R.S. Ponter, D. Weichert, (eds.) *Limit States of Materials and Structures: Direct Methods*. Springer, Berlin, to appear.
- Tvedt L. (1983). *Two Second-order Approximations to the Failure Probability*. Veritas Report RDIV/20-004-83, Det Norske Veritas, Oslo, Norway.
- Vu D. K. (2001). *Dual Limit and Shakedown analysis of structures*. PhD Thesis, Université de Liège, Belgium.
- Vu D. K., Yan A. M., Nguyen Dang H. (2004). A primal-dual algorithm for shakedown analysis of structure. *Comp. Meth. Appl. Mech. Engng.*, **193**, pp. 4663-4674.
- Vu D. K., Staat M., Tran I. T. (2007). Analysis of pressure equipment by application of the primal-dual theory of shakedown. *Communications in Num. Meth. in Engng.*, **23** (3), pp. 213-225.
<http://dx.doi.org/10.1002/cnm.891>
- Wang, Tsau Yueh, Corotis R. B., Ellingwood B. R. (1990). Limit state sensitivity of structural frames subjected to cyclic forces. *J. Struct. Engng., ASCE*, **116** (10), pp. 2824-2841.
- Weichert D., Gross-Weege J. (1988). The numerical assessment of elastic-plastic sheets under variable mechanical and thermal loads using a simplified tow-surface yield condition. *Int. J. Mech. Sci.*, **30**, pp. 757-767.
- Weichert D., Hachemi A. (2002). Shakedown of thin-walled structures with geometrical non-linear effects. In: *Inelastic behaviour of structures under variable repeated loads: Direct analysis methods* (edited by Weichert D., Maier G.), Springer, Wien NewYork, pp. 229-238.
- Wierskowski C. (2005). *Probabilistische Einspielanalyse mit der Finite Elemente Methode und FORM/SORM*. Diplomarbeit, Labor für Biomechanik, Fachhochschule Aachen Campus Jülich, Germany.
- Yan A. M. (1996). *Limit analysis of general pipe elbow subjected to complex loading*. LTAS-FRAMATOME, Report CL2-6, University of Liege, June.
- Yan A. M. (1997). *Contribution to the direct limit state analysis of plastified and cracked structures*. PhD Thesis, Université de Liège, Belgium.
- Yan A. M., Nguyen Dang H. (2000). Direct finite element kinematical approaches in limit and shakedown analysis of shells and elbows. In: *Inelastic Analysis of Structures under Variable Loads: Theory and Engineering Applications* (edited by Weichert D., Maier G.) Kluwer, Academic Press, Dordrecht, pp. 233-254.
- Yan A. M., Vu D. K., Nguyen D. H. (2003). Kinematical formulation of limit and shakedown analysis. In [Staat and Heitzer (2003a)].

- Yang W. H. (1982). A variational principle and an algorithm for limit analysis of beams and plates. *Comp. Meth. Appl. Mech. Eng.*, **33**, pp. 575-582.
- Zhang Y. G., Lu M. W. (1995a). An algorithm for plastic limit analysis. *Comp. Meth. Appl. Mech. Eng.*, **126**, pp. 333-341.
- Zhang Y. G. (1995b). An iteration algorithm for kinematic shakedown analysis. *Comp. Meth. Appl. Mech. Eng.*, **127**, pp. 217-226.
- Zimmermann J. J. (1991). *Analysis of structural system reliability with stochastic programming*. PhD Thesis, John Hopkins University, Baltimore, Maryland.

Appendix

PROBABILITY DISTRIBUTIONS AND TRANSFORMATION TO THE STANDARD GAUSSIAN SPACE

Let X be a random variable with mean μ , standard deviation σ , variance σ^2 , coefficient of variation $v = \sigma / \mu$ and shift parameter a . This parameter gives the smallest possible value of X . The Probability Density Function (PDF) and Cumulative Distribution Function (CDF) of X are denoted by f and F , respectively.

The mean and variance of X can be calculated from the PDF f or measurements of X . Suppose first, that f is known. Then,

$$\mu = \int_{x^a}^{x^b} xf(x)dx \quad (\text{A.1})$$

and

$$\sigma^2 = \int_{x^a}^{x^b} (x - \mu)^2 f(x)dx \quad (\text{A.2})$$

where the limits of integration x^a and x^b extend over the range of possible values of X . For example, this range is $(-\infty, +\infty)$ when X follows a Gaussian probability. When f is not available, μ and σ^2 can be estimated from a set of m measurements $\{x^{(1)}, x^{(2)}, \dots, x^{(m)}\}$ of random parameter X . The estimates of μ and σ^2 are, respectively,

$$\hat{\mu} = \frac{1}{m} \sum_{k=1}^m x^{(k)} \quad (\text{A.3})$$

and

$$\hat{\sigma}^2 = \frac{1}{m-1} \sum_{k=1}^m (x^{(k)} - \hat{\mu})^2 \quad (\text{A.4})$$

and approach the actual values of the mean and variance of X as m increases indefinitely.

Probabilities and distributions that are available in our code are given in this appendix when available in closed form. Closed form results are also presented for the transformation from the standard Gaussian U with mean zero and unit variance to variable X .

1. Normal distribution, $N(\mu, \sigma^2)$

PDF:

$$f(x) = \frac{1}{\sqrt{2\pi}\sigma} \exp\left\{-0.5\left[\frac{x-\mu}{\sigma}\right]^2\right\}, \quad -\infty \leq x \leq +\infty. \quad (\text{A.5})$$

Parameters: $E(X) = \mu, \text{Var}(X) = \sigma^2$

CDF:

$$F(x) = \int_{-\infty}^x f(t)dt = \Phi\left[\frac{x-\mu}{\sigma}\right] \quad (\text{A.6})$$

where

$$\Phi(x) = \int_{-\infty}^x f(u)du. \quad (\text{A.7})$$

Transformation:

$$X = \mu + \sigma U. \quad (\text{A.8})$$

2. Log-Normal distribution

PDF:

$$f(x) = \frac{1}{\sqrt{2\pi x\tilde{\sigma}}} \exp\left\{-0.5\left[\frac{\ln(x) - \tilde{\mu}}{\tilde{\sigma}}\right]^2\right\}, \quad x \geq a \quad (\text{A.9})$$

Parameters: $E(X) = \mu, \text{Var}(X) = \sigma^2$, shift a and coefficient of variation $v = \sigma/(\mu - a)$

$$\begin{aligned} \tilde{\sigma}^2 &= \ln[1 + v^2] \\ \tilde{\mu} &= \ln(\mu) - 0.5\tilde{\sigma}^2. \end{aligned} \quad (\text{A.10})$$

Transformation:

$$X = a + \exp(\tilde{\mu} + \tilde{\sigma}U). \quad (\text{A.11})$$

3. Exponential distribution, $E(\lambda, a)$

PDF:

$$f(x) = \lambda \exp\{-\lambda(x-a)\}, \quad x \geq a. \quad (\text{A.12})$$

Parameters: $E(X) = a + 1/\lambda, \text{Var}(X) = 1/\lambda^2$.

CDF:

$$F(x) = 1 - \exp\{-\lambda(x-a)\}, \quad x \geq a. \quad (\text{A.13})$$

Transformation:

$$X = a - \frac{1}{\lambda} \Phi(-U). \quad (\text{A.14})$$

4. Uniform distribution, $U[a, b]$

PDF:

$$f(x) = \frac{1}{b-a}, \quad a \leq x \leq b. \quad (\text{A.15})$$

Parameters:

$$E(X) = (a+b)/2, \quad \text{Var}(X) = (b-a)^2/12$$

CDF:

$$F(x) = \frac{x-a}{b-a}, \quad a \leq x \leq b. \quad (\text{A.16})$$

Transformation:

$$X = a + (b-a)\Phi(U). \quad (\text{A.17})$$

5. Gamma distribution, $G(k, vx)$

PDF:

$$f(x) = \frac{v(vx)^{k-1} \exp(-vx)}{\Gamma(k)}, \quad x \geq a. \quad (\text{A.18})$$

where the gamma function

$$\Gamma(k) = \int_0^{\infty} \exp(-u) u^{k-1} du. \quad (\text{A.19})$$

Parameters:

$$E(X) = a + k/v, \quad \text{Var}(X) = k/v^2$$

CDF:

$$F(x) = \frac{\Gamma(k, vx)}{\Gamma(k)}, \quad x \geq 0. \quad (\text{A.20})$$

where

$$\Gamma(k, y) = \int_0^y \exp(-u) u^{k-1} du. \quad (\text{A.21})$$

Transformation: not available in closed form. Therefore a Newton-Raphson iteration scheme can be employed in order to obtain the inverse.

6. Weibull Distribution

PDF:

$$f(x) = \frac{k}{v-a} \left(\frac{x-a}{v-a} \right)^{k-1} \exp \left\{ - \left(\frac{x-a}{v-a} \right)^k \right\}, \quad x \geq a. \quad (\text{A.22})$$

Parameters: $k > 0, E(X) = a + (v-a) \Gamma(1+1/k).$

$$\text{Var}(X) = (v-a)^2 \left[\Gamma(1+2/k) - \Gamma^2(1+1/k) \right]$$

CDF:

$$F(x) = 1 - \exp \left\{ - \left(\frac{x-a}{v-a} \right)^k \right\}, \quad x \geq a. \quad (\text{A.23})$$

Transformation:

$$X = a + (v-a) \left\{ -\ln[\Phi(-U)] \right\}^{1/k}. \quad (\text{A.24})$$

7. Extreme Type I Distribution

PDF:

$$f(x) = \alpha \exp \left\{ -\alpha(x-v) - \exp[-\alpha(x-v)] \right\}, \quad -\infty \leq x \leq +\infty. \quad (\text{A.25})$$

Parameters: $E(X) = v + (0.577/\alpha), \text{Var}(X) = \pi^2/(6\alpha^2).$

CDF:

$$F(x) = \exp \left\{ -\exp[-\alpha(x-v)] \right\}, \quad -\infty \leq x \leq +\infty. \quad (\text{A.26})$$

Transformation:

$$X = v - \frac{1}{\alpha} \ln \left\{ -\ln[\Phi(U)] \right\}. \quad (\text{A.27})$$